Iowa State University
Digital Repository

Retrospective Theses and Dissertations

Iowa State University Capstones, Theses and Dissertations

1989

Selective electrocatalysis of anodic oxygen-transfer reactions at chemically modified, thin-film lead dioxide electrodes

Hsiangpin Chang
Iowa State University

Follow this and additional works at: https://lib.dr.iastate.edu/rtd

Part of the Analytical Chemistry Commons

Recommended Citation

www.manaraa.com

INFORMATION TO USERS

The most advanced technology has been used to photograph and reproduce this manuscript from the microfilm master. UMI films the text directly from the original or copy submitted. Thus, some thesis and dissertation copies are in typewriter face, while others may be from any type of computer printer.

The quality of this reproduction is dependent upon the quality of the copy submitted. Broken or indistinct print, colored or poor quality illustrations and photographs, print bleedthrough, substandard margins, and improper alignment can adversely affect reproduction.

In the unlikely event that the author did not send UMI a complete manuscript and there are missing pages, these will be noted. Also, if unauthorized copyright material had to be removed, a note will indicate the deletion.

Oversize materials (e.g., maps, drawings, charts) are reproduced by sectioning the original, beginning at the upper left-hand corner and continuing from left to right in equal sections with small overlaps. Each original is also photographed in one exposure and is included in reduced form at the back of the book. These are also available as one exposure on a standard 35mm slide or as a 17″ x 23″ black and white photographic print for an additional charge.

Photographs included in the original manuscript have been reproduced xerographically in this copy. Higher quality 6″ x 9″ black and white photographic prints are available for any photographs or illustrations appearing in this copy for an additional charge. Contact UMI directly to order.

Selective electrocatalysis of anodic oxygen-transfer reactions at chemically modified, thin-film lead dioxide electrodes

Chang, Hsiangpin, Ph.D.

Iowa State University, 1989

Selective electrocatalysis of anodic oxygen-transfer reactions

at chemically modified, thin-film lead dioxide electrodes

by

Hsiangpin Chang

A Dissertation Submitted to the

Graduate Faculty in Partial Fulfillment of the

Requirements for the Degree of

DOCTOR OF PHILOSOPHY

Department: Chemistry
Major: Analytical Chemistry

Approved:

In Charge of Major Work

For the Major Department

For the Graduate College

Iowa State University
Ames, Iowa

1989

TABLE OF CONTENTS

LIST OF MAJOR SYMBOLS AND ABBREVIATIONS

$Bi-PbO_2$ - bismuth-doped lead dioxide

Bi^{3+}/PbO_2 - bismuth(III)-adsorbed lead dioxide

DMSO   - dimethyl sulfoxide

$DMSO_2$ - dimethyl sulfone

E°   - standard potential

$E_{1/2}$ - half-wave potential

EDS   - X-ray energy dispersive spectroscopy

e-t   - electron-transfer

FI-EC   - flow injection with electrochemical detector

GC   - glassy carbon

GC/MS   - gas chromatography/mass spectrometry

O-t   - oxygen-transfer

RDE   - rotating disc electrode

RRDE   - rotating ring-disc electrode

SCE   - saturated calomel electrode

SEM   - scanning electron microscope

TMSO   - tetramethyl sulfoxide

TPCA   - 2-thiophene carboxylic acid

XPS   - X-ray photoelectron spectroscopy

XRD   - X-ray diffraction

Ø   - scan rate

w - rotational velocity

v - kinematic viscosity

DEDICATION

To my beloved parents and my dearest wife:

Duan Qiongyin, Chang Qingshu, and Chang S. Suichu

I. GENERAL INTRODUCTION

A. Strategies to Modify Lead Dioxide Electrodes Selectively for Catalysis of Anodic Oxygen-Transfer Reactions

"The last word of 'analytical chemistry' is *chemistry*."

-Dennis C. Johnson

What are anodic oxygen-transfer reactions?

An anodic oxygen-transfer (O-t) reaction is defined as a reaction
that involves the transfer of oxygen from the solvent (H_2O) to the
reactant R, which can be written in general as follows:

$$R + H_2O \xrightarrow{\text{electrode}} RO + 2 H^+ + 2 e \qquad [1]$$
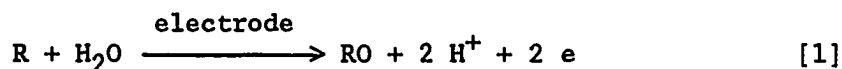
This type of reaction differs from simple electron-transfer (e-t)
reactions, e.g., $Fe^{2+} - Fe^{3+} + e$. The O-t reactions are more complicated
than e-t reactions because of the coupling of proton- and oxygen-transfer
steps with the transfer of electrons. The O-t reactions in acidic media
are usually characterized by slow heterogeneous kinetics at conventional
electrodes because of the additional process of activation of the oxygen
from water. It has been concluded that, generally, anodic O-t reactions
can occur only via chemical participation of some electrode surface
species, e.g., a labile, adsorbed hydroxyl radical generated during
anodic surface oxide formation or water discharge (1). Unfortunately,
these labile surface hydroxyl species are not readily available at the
conventional solid electrodes commonly used as anodes. In order to use
the anodic O-t reactions efficiently for practical applications, e.g., in
electroorganic synthesis, fuel cells, and anodic amperometric detection,
it is necessary to search for new electrode materials with selective,
catalytic activity for O-t reactions.

Some typical anodic O-t reactions of practical importance are listed
in Table 1. The production of perchlorate, benzoquinone, and
anthroquinone are significant for commercial electrosynthesis (2). The

3

Table 1. Examples of Oxygen-Transfer Reactions

$$H_2O + SO_3^{2-} \longrightarrow SO_4^{2-} + 2H^+ + 2e$$

$$CO \longrightarrow CO_2$$

$$Cl^- \longrightarrow ClO_3^- \longrightarrow ClO_4^-$$

$$Cr^{3+} \longrightarrow Cr_2O_7^{2-}$$

$$(CH_3)_2SO \longrightarrow (CH_3)_2SO_2 \quad (E° = 0.0 \text{ V vs. SCE})$$

$$Mn^{2+} \longrightarrow MnO_4^- \quad (E° = 1.3 \text{ V})$$
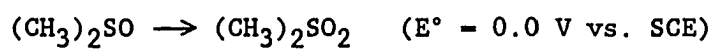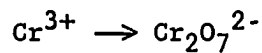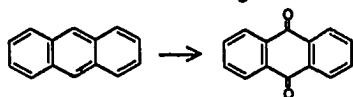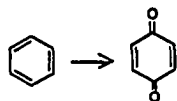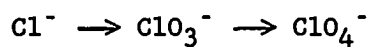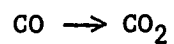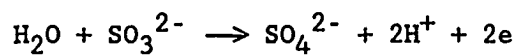
oxidation of Cr(III) to chromic acid, and Mn(II) to permanganate, are used in indirect oxidative electrolyses (3).

Throughout this research, the oxidation of dimethyl sulfoxide (DMSO) to dimethyl sulfone ($DMSO_2$) is used as the primary model O-t reaction. It was chosen because it is a one-oxygen-transfer reaction with a simple oxidation product which is soluble in aqueous solution. The oxidation of Mn(II) to MnO_4^- was chosen as a secondary model reaction because its product has intense color and so can be monitored easily with a spectrophotometric detector. The characteristic slow kinetics of anodic O-t reactions is well represented by these two reactions in spite of their relatively low values of standard potential, 0.0 V and 1.35 V (4), respectively. Additional reactions from Table 1 were also studied. It was hoped that electrodes that tested positive for electrocatalysis with the model reactions would work virtually the same for other O-t reactions because all anodic O-t reactions share the same kinetic barrier.

Why do we need to modify lead dioxide electrodes?

Firstly, it has been a common perception that pure lead dioxide electrode lacks specific catalytic activities despite its wide use for anodic electrosynthesis (5). The common choice of PbO_2 as an anodic material for large-scale anodic electrosynthesis has been based, apparently, on the knowledge of the very large overpotential for oxygen evolution at pure PbO_2 and the impression that the accessibility of a large positive potential with minimal background current can adequately drive slow anodic reactions. Provided the above premise is correct, that anodic O-t reactions are electrocatalyzed by mechanistic coupling

with the process of oxygen evolution, then the common strategy is seen to be without rational foundation. It is believed that properly modified PbO_2 electrodes with specific catalytic activity can play an important role in many practical electrochemical processes.

Secondly, the initial screening of electrode materials indicated that lead dioxide might be particularly appropriate for O-t reactions following modification of the bulk and/or surface structure of the oxide by incorporation of alternate metals for the lead. From previous studies of O-t reactions at noble metal electrodes, e.g., Au and Pt (1), it is known that the surfaces of metal oxides can be active participants in the electrocatalysis of anodic O-t reaction. However, O-t reactions at the noble metal electrodes lack long-term stability under constant-potential or constant-current conditions because of the passivation of the electrode surface which depresses the formation of the surface-bound state of active oxygen. It is anticipated that bulk oxide electrodes, e.g., PbO_2, should be better electrodes for O-transfer than the noble metals, because they are "oxygen-rich" at the surfaces (6). This is proved by the moderate catalytic activity of pure PbO_2 for the oxidation of some sulfur compounds (6a-c) and I^- to IO_4^- (7). It is also predicted that the catalytic activity of PbO_2 will be enhanced by proper chemical modification, specifically incorporation of foreign species as catalysts.

Thirdly, lead dioxide is believed to be readily suitable for chemical modification. It is a non-stoichiometric dioxide, with formulae of PbO_x (x = 1.9 - 2.0) (5). Thus, it should be possible to incorporate foreign ionic species into PbO_2 matrix by electrodeposition (6b-e).

The surface defects of PbO_2 can also contribute to chemisorption and catalysis (8a). In addition, the surface structure of most metal oxides can be considered at atomic level as either terminated OH species or bridged O species (8b-d):
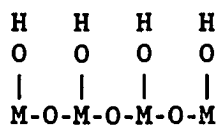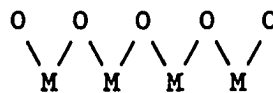
```
H   H   H   H
O   O   O   O              O   O   O   O   O
|   |   |   |               \ / \ / \ / \ /
M-O-M-O-M-O-M               M   M   M   M

   (terminated OH)             (bridiged O)
```

The actual picture undoubtedly is more complex, being some combination of both. In any case, some ion exchange or complexation ability of the oxide surface exists, which can be used to chemisorb ionic species as catalytic agents and thus to modify the surfaces of lead dioxide.

Finally, from practical points of view, lead dioxide was chosen because of its high electric conductivity, ease and low cost of preparation, chemical inertness to both acidic and alkaline media, stability at high temperatures, and high oxygen overpotential. The fundamental research of chemically modified electrodes has received great success in the last decade. However, the electrode materials tested have been mainly organic polymers and have not been accepted in large-scale electrolysis because of their lack of chemical inertness and stability. It is hopeful that the development of inorganic, modified PbO_2 electrodes will change this situation.

How to modify PbO$_2$ electrodes selectively for catalysis of anodic O-transfer reactions?

To answer this question, the mechanism of O-t reaction is considered first in relation with that of anodic oxygen evolution. It is generally believed (9) that the first and rate-limiting step for the anodic evolution of oxygen is the discharge of water to yield the hydroxyl radical ($\cdot$OH) which is adsorbed at the electrode (M), as shown in Figure 1. The adsorbed hydroxyl radicals are further oxidized to give dioxygen and regenerate the M surface. If an oxidizable reactant R is present in the solution, the hydroxyl can be transferred to R to produce the oxidation product RO, which is indicated by the wide arrows in Figure 1.

It is, thus, clear that the electrocatalysis of O-t reactions can be achieved by simultaneous promotion of the rate of hydroxyl generation and depression of the rate of oxygen evolution. This can be done by incorporation onto the PbO$_2$ surface of a material with a low oxygen-evolution overpotential as catalyst in such a way that the catalytic sites are well separated from each other. Therefore, they serve as centers to generate the $\cdot$OH species yet with a relatively low yield of oxygen gas. This strategy is illustrated schematically in Figure 2. Since PbO$_2$ (A) has a high oxygen overpotential and the coverage of the catalyst (B) on PbO$_2$ is low, the modified PbO$_2$ should have a similar, if not the same, low value of oxygen overpotential to that of the pure PbO$_2$. Yet the activity for the anodic O-t reaction at the modified PbO$_2$ should be increased greatly without losing the advantages, e.g., low background signal, of the pure PbO$_2$ electrode. The resultant chemically modified

PbO_2 electrode can be regarded as a partially covered or a so-called "array" electrode (10). With appropriate surface coverage of the catalyst, the O-t reaction at these electrodes should proceed quickly and under mass-transport control. However, it is expected that if the coverage is too high, the catalytic activity for the O-t reaction will decrease because the catalysts at the electrode surface will no longer be separated from each other, so a high background signal for oxygen evolution will arise.

Selection of catalysts

The potential catalysts for PbO_2 modification should be the ones that have low values of oxygen overpotential. There has been a large body of literature on the studies of oxygen-evolution as a function of electrode materials. Most important to the present study is the work by Trassatti (11) and other workers who tried to correlate the oxygen overpotential to the enthalpy of the oxide transition. The corresponding plots have a peaked shape, with large overpotential for both small and large transition enthalpy, and a minimum overpotential for an intermediate transition enthalphy. Because of their cone shape, the plots have been referred to as "volcano plots." Based on this correlation, some doping agents can be selected initially to test (6d,e). However, the use of the volcano plot to anticipate potential catalysts has limitations. For instance, the values of heat of formation used for the plots are only for oxides of two oxidation states. Nevertheless, the catalysts incorporated into the PbO_2 may not necessarily exist in a pure oxide form or may not easily change in oxidation state. An additional

difficulty is that the metal ions chosen from the volcano plots might not be incorporated readily into or onto the PbO_2 surface. Therefore, the selection of the catalysts in this study was done empirically. Attention was, however, paid to develop techniques to reduce the burden of repetitive work for the screening of catalysts out of a large number of candidates.

It was also hoped that more than one catalyst can be found, so the identity of the catalysts can be varied to yield information pertaining to the mechanism of the electrocatalysis.

Scope of research

The scope of this research is summarized as follows:

(1) Development of efficient methods for chemical modification of lead dioxide electrodes and selection of catalysts for electrocatalysis of anodic O-t reactions;

(2) Characterization of the resultant catalytic electrode materials;

(3) Understanding of the kinetics and mechanism of the electrocatalysis.

Experimental configurations

Thin-film PbO_2 electrodes (ca. 10 - 50 µm) electrodeposited on Au or other substrates were used throughout this study, primarily because of the convenience in electrode preparation. It will be proved that the actual behavior of the modified PbO_2 electrodes does not change with the thickness of the oxide films.

Most of the studies were done in acidic media, specifically

$HClO_4$ solutions, because $HClO_4$ is a non-chelating acid.

The basic electrochemical techniques used are hydrodynamic voltammetry and chronoamperometry in conventional electrolysis cells. Exhaustive electrolysis at large-area screen electrodes was used for experimental upgrading. Flow-through systems, visible spectrophotometry, and gas chromatography with mass spectrometric detection were also used for special purposes. Some techniques for surface and structure analysis, e.g., X-ray diffraction (XRD), X-ray photoelectron spectroscopy (XPS), scanning electron microscopy (SEM), and X-ray energy-dispersive spectroscopy (EDS), were used to characterize the morphology, composition, and structure of the modified PbO_2 films.

References

1. (a) Johnson, D. C. J. Electrochem. Soc. 1972, 119, 331. (b) Austin, D. S.; Johnson, D. C.; Hines, T. G.; Berti, E. T. Anal. Chem. 1983, 55, 2222. (c) Cabelka, T. D.; Austin, D. S.; Johnson, D. C. J. Electrochem. Soc. 1984, 131, 1596; 1985, 132, 359.

2. (a) Seltzer, R. J. C&EN, August 8, 1988; p. 13. (b) Aprem, M. M.; Unnikrishnan, K.; Sukumaran, K. M.; Nair, K. S. Trans. SAEST, 1985, 20, 201.

3. (a) Steckhan, E. Top. Curr. Chem. Electrochemistry, Volume 1; Stechhan, E., Ed.; Springer-Verlag: Berlin, 1987. (b) Ibl, N.; Kramer, K.; Ponto, L.; Robertson, P. In "Electro-organic Synthesis Technology"; Krumpelt, M; Weissman, E. V.; Alkire, R. C., Eds.; AIChE Symposium Series, Vol. 75, No. 185, New York, 1979.

4. "Standard Potentials in Aqueous Solutions"; Bard, A. J.; Parson, R.; Jordan, J., Eds.; M. Dekker: New York, 1985.

5. Carr, J. P.; Hampson, N. A. Chem. Rev. 1972, 72, 679.

6. (a) Tang, A. P.-C.; Johnson, D. C. Anal. Chim. Acta In press. (b) Austin, D. S.; Polta, J. A.; Polta, T. Z.; Tang, A. P.-C.; Cabelka, T. P.; Johnson, D. C. J. Electroanal. Chem. 1984, 168, 227. (c) Johnson, D. C.; Polta, J. A.; Polta, T. Z.; Neuburger, G. G.; Johnson, J.; Tang, A. P.-C.; Yeo, I.-H.; Baur, J. J. Chem. Soc.,

Faraday Trans. 1, 1986, 82, 1081. (d) Yeo, I.-H.; Johnson, D. C. J. Electrochem. Soc. 1987, 134, 1973. (e) Yeo, I.-H. Ph.D. Dissertation, Iowa State University, Ames, Iowa, 1987.

7. Hampel, C. A. "The Encyclopedia of Electrochemistry"; Chapman & Hall: London, 1964; p. 763.

8. (a) Henrich, V. E. In "Surface and Near-Surface Chemistry of Oxide Mateirals"; Nowotny, J.; Dufour, L.-C., Eds.; Elsevier: Amsterdam, 1988; Chapter 2, p. 23. (b) Hall, W. K. In "Chemistry and Physics of Solid Surfaces VI"; Vanselow, R.; Howe, R., Eds.; Springer-Verlag: Berlin, 1986; Chapter 5, p. 73. (c) Ruvarac, A. In "Inorganic Ion Exchange Materials"; Clearfield, A., Ed.; CRC Press: Boca Raton, 1982; Chapter 5, p. 141. (d) Abe, M. In "Inorganic Ion Exchange Materials"; Clearfield, A., Ed.; CRC Press: Boca Raton, 1982; Chapter 6, p. 275.

9. (a) Tarasevich, M. R.; Sadkowski, A.; Yeager, E. In "Comprehensive Treatise of Electrochemistry," Conway, B. E.; Bockris, J. O'M.; Yeager, E.; Khan, S. U. M.; White, R. E., Eds.; Plenum Press: New York, 1983; Volume 7, p. 301. (b) O'Sullivan, E. J. O'M.; Calvo, E. J. In "Comprehensive Chemical Kinetics," Compton, R. G., Ed.; Elsevier: Amsterdam, 1987; Volume 27, p. 247.

10. (a) Caprani, A.; Deslouis, C.; Robin, S.; Tribollet, B. J. Electroanal. Chem. 1987, 238, 67. (b) Levart, E. J. Electroanal. Chem. 1985, 187, 247. (c) Amatore, C.; Saveant, J. M.; Tessier, D. J. Electroanal. Chem. 1983, 147, 39. (d) Contamin, O.; Levart, E. J. Electroanal. Chem. 1982, 136, 259. (e) Gueshi, T.; Tokuda, K.; Matsuda, H. J. Electroanal. Chem. 1979, 101, 29; 1978, 89, 247. (f) Tokuda, K.; Gueshi, T.; Matsuda, H. J. Electroanal. Chem. 1979, 102, 41. (g) Filinovsk, V. Yu. Electrochim. Acta 1979, 25, 309.

11. Trasatti, S. J. Electroanal. Chem. 1980, 111, 125.
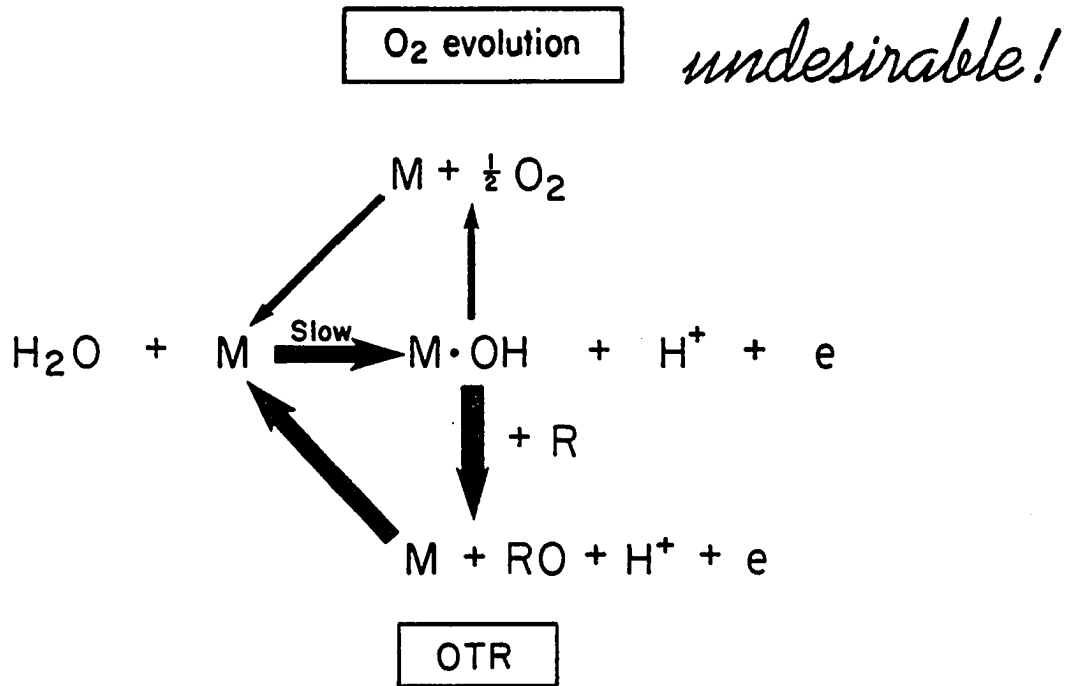
Figure 1. Schematic diagram for the mechanism of oxygen evolution
and oxygen-transfer mediation

Figure 2. Schematic illustration for the strategy to modify PbO_2
electrode for selective electrocatalysis of
oxygen-transfer reactions

Region: (A) inert electrode material with high
oxygen-evolution overpotential,
(B) active electrode material with low
oxygen-evolution overpotential

II. KINETICS AND MECHANISM OF ELECTRODEPOSITION

OF LEAD DIOXIDE IN ACIDIC MEDIA

A. Chronoamperometric and Voltammetric Studies of the

Nucleation and Electrodeposition of ß-Lead Dioxide

at a Rotated Gold Disc Electrode[1]

"If it is possible to cut out a word, then always cut
it out."
                    -George Orwell,
                    "Politics and the English Language"

Abstract

The electrodeposition of ß-PbO$_2$ from HClO$_4$ solutions of Pb(II) at a Au rotated disc electrode (RDE) was studied as a function of applied potential, rotational velocity, and the concentrations of HClO$_4$ and Pb(II). A long induction period (i.e., i $\simeq$ 0) is associated with high acidity, low concentration of Pb(II), and high rotational velocity. Following the induction period, the current rises to a steady-state value which is significantly lower than the mass transport-limited value for Pb(II). The steady-state value of electrode current decreases as rotational velocity is increased, contrary to expectations for a mass transport-controlled process at a RDE. The generation of a soluble intermediate species is proposed to account for these observations.

Repeated cycles of deposition and stripping of PbO$_2$ at the Au RDE results in a decreasing induction period for subsequent PbO$_2$ deposition. This is concluded to result because an ultra-thin Pb(II) film (possibly PbO) is formed which is stabilized by interaction with the Au substrate and is not dissolved following the negative potential scan to 0.3 V. The original state of the clean Au surface is regenerated by cathodic H$_2$(g) evolution, chemical stripping with H$_2$O$_2$ or KMnO$_4$, or by mechanical abrasion.

Introduction

Recently in this laboratory, pure and extensively doped ß-PbO$_2$ electrodes have been studied for their electrocatalytic properties in support of anodic oxidation reactions involving simultaneous transfer of oxygen from the H$_2$O solvent to the reaction products (1). These oxide

materials are electrochemically deposited onto Au or Pt rotated disc electrodes (RDEs) in acidic media (pH < 1). This work is part of a general search for unique anode materials with catalytic properties surpassing those of the more traditional anodes (i.e., C, Pt and Au) for use as amperometric transducers. Significance is projected also for larger-scale industrial processes. Lead dioxide was chosen as the host oxide in these experiments because of its relatively high electrical conductivity, low cost, ease of preparation, inertness in both acidic and alkaline solutions, and stability at high temperatures. Furthermore, this oxide is not a stoichiometric dioxide (i.e., PbO_x, $1.9 < x < 2.0$) (2) and it was suspected that defect sites might exist on the electrode surface which can participate catalytically in anodic O-transfer reactions.

Pure electrodeposited ß-PbO_2 was demonstrated to exhibit a moderate electrocatalytic activity for supporting various anodic reactions in acidic media, especially for sulfur compounds. However, that activity can be increased greatly for numerous reactions by incorporation of group VA metals, especially bismuth, to form the mixed oxides (1b-e). Since the anodic electrodeposition of PbO_2 from aqueous solutions of Pb(II) requires oxygen transfer, a clearer understanding of the deposition mechanism could provide valuable insight into the mechanisms of anodic O-transfer reactions at the pure and mixed-oxide electrodes.

An intense interest in the PbO_2-Pb(II) redox couple has existed because of the use of PbO_2 in lead-acid batteries (2,3), as well as for anodes in electrosynthesis (4). Secondary interest in the redox couple

has resulted because the deposition of PbO_2 is a unique model for testing electrocrystallization theories (5,6). Summaries of the literature are cited (7). Most published studies of PbO_2 have focused on physical properties (morphology, density, porosity, durability, and surface area) of the oxide deposited at high current densities and pH 3 - 7, and the discharge/recharge kinetics in H_2SO_4 media. Little work has been concerned with kinetics and mechanisms in acidic media other than H_2SO_4. The anodic reaction has served also for preconcentration of Pb(II) in the electrogravimetric (8) and cathodic stripping determinations of trace levels of the metal ion in water (9).

Fleischman et al. (5) were the first to consider in depth the complexity of the mechanism for electrodeposition of PbO_2 from aqueous solutions of Pb(II). Their mechanism, summarized by [1-4], has received wide support (4a,9b,10).

$$OH^- \longleftrightarrow OH_{ads} + e \qquad\qquad [1]$$

$$Pb^{2+} + (OH)_{ads} + OH^- \longrightarrow Pb(OH)^+_{2,ads} \qquad (slow) \qquad [2]$$

$$Pb^{2+} + (OH)_{ads} + OH^- \longrightarrow Pb(OH)^{2+}_{2,ads} + e \quad (slow) \qquad [3]$$

$$Pb(OH)^{2+}_{2,ads} \longleftrightarrow PbO_2(s) + 2H^+ \qquad\qquad [4]$$
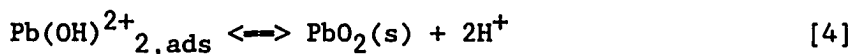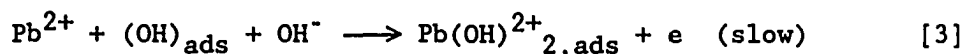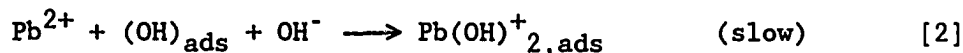
Alternately, the production of $Pb(OH)^{2+}_{2,ads}$ in [3] can be written based on the oxidation of $Pb(OH)^+_{2,ads}$ from [2]. The products of [2] and [3] were postulated to be insoluble and adsorbed on the substrate.

The majority of studies of PbO_2 electrodeposition have been

performed in unstirred solutions, with only a few at hydrodynamic electrodes (9b,11). Application of the rotated disc electrode (RDE) is appropriate for mechanistic studies of multi-electron processes with coupled chemical reactions because of the large dynamic range for mass transfer available at this electrode. Here we describe chronoamperometric and voltammetric data for a Au RDE as a function of rotational velocity, deposition potential, and the concentrations of $HClO_4$ and Pb(II). We propose that a significant solubility exists for the intermediate products of the PbO_2 deposition process.

Experimental

Reagents   Chemicals were Reagent Grade and water was distilled followed by purification in a Barnstead NANOpure-II system (Boston, MA). Lead(II) solutions were prepared by dissolution of PbO in $HClO_4$. In studies of the effect of $HClO_4$ concentration, $NaClO_4$ was added to maintain constant ionic strength. The Cl⁻ impurity in all solutions was < 1 μM, as calculated from impurity levels specified on the reagent bottles.

Instrumentation   Disc electrodes were constructed from gold (44.7 mm^2), platinum (45.6 mm^2) and glassy carbon (19.1 mm^2) by Pine Instrument Co. (Grove City, PA). A PIR rotator and RDE4 potentiostat (Pine Instrument Co.) also were used. Electrode potentials were controlled vs. a saturated calomel electrode (SCE; Fischer Scientific, Inc.) contacting the electrolysis solution through a Luggin capillary. The Pt-wire counter electrode was located in a separate chamber filled with the

supporting electrolyte and contacting the electrolysis solution through a fritted glass membrane.

Procedures   Disc electrodes were polished prior to every experiment with 0.05-μm alumina on microcloth (Buehler, Ltd.), except as noted.   Solid PbO_2 deposits were removed electrolytically at 0.2 V, prior to removal of the RDE from the electrolysis solution, followed by chemical stripping of any oxide residue in a 1:1 mixture of acetic acid and hydrogen peroxide (30%).   Amperometric data were obtained in triplicate and average values are reported.

Results and discussions

Analysis of transient current-time curves   A typical chronoamperometric response (i-t) for PbO_2 deposition at the Au RDE in $HClO_4$ solution is shown in Figure 1.   Recording of the i-t curve was started for the freshly polished RDE immediately following the first potential step from 0.2 V to 1.6 V.   The transient curve shown is divided into four regions to facilitate discussion.   The induction period (A), with a time period t_0, corresponds to a relatively small electrode current ($i \simeq 0$).   Previous designations of t_0 have been based on the first apparent departure of current from zero (4a,5,6).   That is a rather arbitrary and subjective definition depending on the current sensitivity of the recorder.   Our designation of t_0 is applied easily.   The value of t_0 shown in Figure 1 is significantly longer than reported previously (4a,5a-b) for pH 2 - 5.   This will be demonstrated to be the consequence of rotation of the RDE and lower pH.

Region B (Figure 1), with a time period designated t_1, corresponds to rapid growth of PbO_2 nuclei with a corresponding transition of the electrode current from virtually zero to a steady-state value (i_{ss}). Historically, it is the early part of Region B (i.e., $0 < i \ll i_{ss}$) which has received the greatest attention in electrocrystallization studies (4a,5a,6,9-12). For two dimensional growth, which is assumed for the initial monolayer of oxide, the value of i is predicted to be proportional to $(t-t_0)^2$, whereas for three-dimensional growth, i.e., bulk deposition, i is predicted to be proportional to $(t-t_0)^3$ (12). However, for $t-t_0 \simeq 0$, it is difficult to discern between the second and third order dependencies, and a clear transition from two-dimensional to three-dimensional growth kinetics is difficult to determine. We shall use the value of t_1 and the estimated slope (S) of the i-t curve at $i = 0.5i_{ss}$ (i.e., $S = i_{ss}/t_1$) to characterize Region B.

Region C (Figure 2-1) corresponds to the observation of a steady-state value of electrode current (i_{ss}). The steady-state current has been proposed to be the mass-transport limited value (10); however, this clearly is not the case here. For $C_{Pb(II)}^b = 0.2$ M, the transport-limited steady-state current would be much in excess of values shown in Figure 1. Hence, the reaction is concluded to be under kinetic control.

Results of a typical study of the steady-state current as a function of rotational velocity (w) are shown as Region D of Figure 1. For a mass-transport limited, steady-state reaction, values of i_{ss} are expected to increase proportionally to $w^{1/2}$. Hence, the decrease of i_{ss} with increasing $w^{1/2}$ is concluded to be a significant indicator of the

mechanistic complexity of the deposition reaction. Observations in
Region D are discussed further in a later section.

Variation of Pb(II) and $HClO_4$ concentrations   The dependence of
of t_o, t_1, S, and i_{ss} on $C_{Pb(II)}^b$ was studied for 1.70 M $HClO_4$ at a
rotation speed of 0 rev min^{-1}. Clearly, t_o decreased with increasing
$C_{Pb(II)}^b$, which is in agreement with the mechanism of [1-4]. The value of
i_{ss} increased as a linear function of $C_{Pb(II)}^b$, which also is consistent
with the pseudo-first order dependence of the deposition rate on $C_{Pb(II)}^b$
for the mechanism under consideration. It should be noted that for 0 rev
min^{-1}, a steady-state current was observed. This value of i_{ss} was much
lower than the diffusion-limited current, i.e., the Cottrell current,
which is, along with the observed absence of a time dependence in Region
C, further evidence for the designation of total control of electrode
current by the deposition kinetics. Hence, there is virtually no
concentration polarization, and $C_{Pb(II)}^s \simeq C_{Pb(II)}^b$. The value of S
increased with increasing $C_{Pb(II)}^b$ both because of the increase in i_{ss} and
the decrease in t_1.

The dependence of t_o, t_1, S and i_{ss} on C_{HClO4}^b also was studied at 0
rev min^{-1}. Values of i_{ss} and S decreased substantially, and t_o and t_1
increased, as C_{HClO4}^b was increased (pH decreased). This is consistent
with the mechanism in [1-4], since higher H^+ concentration should
decrease the equilibrium surface activity of OH_{ads} in [1] for a constant
electrode potential. However, the dependencies could not be linearized
by resorting to customary plotting strategies, i.e., log-log, etc.
Hence, estimation of reaction order was not possible.

<u>Variation</u> <u>of</u> <u>rotational</u> <u>velocity</u>   Changes in t_o, t_1 and S with

increasing values of $w^{1/2}$ are shown in Figure 2. The positive linear t_o-

$w^{1/2}$ dependence is concluded to be the result of the solubility of one or

both of the intermediate products of the induction period proposed in

[2,3], i.e., $Pb(OH)_2^+$ and/or $Pb(OH)_2^{2+}$. These soluble intermediate

products are transported away from the electrode, by the convective-

diffusion mechanism, and nucleation as well as growth of existing nuclei

is defeated in [4]. The decrease in S shown in Figure 2 is a result

largely of the decrease in i_{ss} with increased $w^{1/2}$.

Further study of the dependence of i_{ss} on $w^{1/2}$ was made using two

strategies. Method A: The value of $w^{1/2}$ desired for the measurement of

i_{ss} in Period C - D was used also for Periods A and B. According to the

standard procedure, the electrode surface was also cathodically stripped

and mechanically polished preliminary to the application of each new

value of w. Method B: A single low value of w was used for Periods A

and B, and then the measurement of i_{ss} vs. w was performed in Periods C -

D exactly as shown in Figure 1. This procedure was very rapid in

comparison to Method A. Values of current from the two methods ($i_{ss,A}$

and $i_{ss,B}$) are shown in Figure 3. For fixed values of c_{HClO4}^b and $w^{1/2}$,

i_{ss} increases with increasing $c_{Pb(II)}^b$, which is consistent with results

of the study of $c_{Pb(II)}^b$ dependence. From Figure 3 it can be seen that

$i_{ss,A}$ and $i_{ss,B}$ are very similar, provided that other conditions are the

same. Whereas some increase in i_{ss} was seen for a slight increase of w

above 0 rev min^{-1} (Figure 3), generally the increase in $w^{1/2} > 20$ (rev

$min^{-1})^{1/2}$ resulted in no change of $i_{ss,A,B}$ values for small c_{HClO4}^b.

However, a definite inverse dependence on $w^{1/2}$ was observed for large values of c_{HClO4}^b and $c_{Pb(II)}^b$. A similar phenomenon has been described briefly using electrogravimetry for a rotated Pt gauze electrode (8). However, the extent of the study apparently was limited and a detailed mechanistic interpretation of the observation was not offered. The decrease in i_{ss} for increasing $w^{1/2}$ is consistent with the conclusion of the finite solubility of the intermediate products during Periods C - D. We conclude the soluble products are generated throughout Regions A - D.

To minimize the number of figures showing i_{ss}-$w^{1/2}$ plots, the dependencies of the i_{ss}-$w^{1/2}$ relationship on $c_{Pb(II)}^b$ and c_{HClO4}^b are summarized further in Figure 4 for E_{dep} - 1.48 V. Three distinct regions denoting the different characteristics of the deposition kinetics can be designated on the $c_{Pb(II)}^b$-c_{HClO4}^b plane. A linear dependence of i_{ss} on $w^{1/2}$ characteristic of a transport-limited process was observed only in Region A (Figure 4). The value of i_{ss} decreases linearly with increasing $w^{1/2}$ in Region B (Figure 4). For the boundary region between A and B, the i_{ss}-$w^{1/2}$ dependence is irregular. For example, with $c_{Pb(II)}^b$ - 0.05 M and c_{HClO4}^b - 0.4 M, i_{ss} increases with $w^{1/2}$ at low w values but decreases at higher $w^{1/2}$ values. This result is consistent with the conclusion of mixed kinetics-transport control.

<u>Variation of deposition potential</u>   The dependencies of t_o, t_1, S and i_{ss} on E_{dep} are shown in Figure 5. These results are similar to others which are not shown which were obtained as a function of $c_{Pb(II)}^b$ and c_{HClO4}^b. The values of t_o and t_1 decrease and values of S and i_{ss} increase with increasing E_{dep}. The primary influence of E_{dep} on the

deposition kinetics is expected to come by way of [1] which controls the surface activity of OH_{ads} in [2]. The tendency for i_{ss} values to decrease with increasing $w^{1/2}$ was observed for all values E_{dep} - 1.440 - 1.560 V. For the values of E_{dep} used to obtain data in Figures 1 - 5, the contribution of O_2 production to i_{ss} was negligible.

Correlation between PbO_2 deposition and O_2 evolution   It is noted that the initial step [1] in the PbO_2 deposition mechanism is also the first step for the anodic evolution of O_2 at most metal-oxide electrodes (12). It has been proposed also that this is the first step in anodic surface-catalyzed O-transfer reactions (5). It was expected, therefore, that a perceptible rate of nucleation and deposition of PbO_2 on the Au RDE, as well as for Pt and GC, might be observed only when there is a small simultaneous anodic generation of O_2. This is proved to be the case by the voltammetric data in Figure 6. The activation overpotential for O_2 evolution (η) is significantly different for Au, Pt and GC ($\eta_{GC} > \eta_{Au} > \eta_{Pt}$). Hence, the minimum potential value appropriate to initiate an observable rate of PbO_2 deposition is different for the three materials ($E_{dep,GC} > E_{dep,Au} > E_{dep,Pt}$).

The observed differences in O_2-evolution potential became negligible for the three substrates when their respective surfaces were covered with PbO_2. Hence, for the negative potential scans in Figure 6, the apparent half-wave potential values are approximately the same for each curve. When the substrate of any individual electrode becomes covered with PbO_2, continued deposition of PbO_2 occurs only if E_{dep} is appropriate for an appreciable rate of O_2 evolution on the PbO_2 deposit. Consequently for

Pt, since η_{Pt} is slightly less than for η_{PbO2}, the minimal potential required to initiate PbO_2 deposition on Pt is slightly less than is sufficient to maintain a significant rate of continued PbO_2 growth.

The relationship between O_2 evolution and PbO_2 deposition was studied further by constant-potential chronoamperometry. The induction time (t_o) was determined as a function of E_{dep} for the different electrodes. The value of t_o was determined to be approximately inversely related to the residual current for O_2 evolution observed at that value of E_{dep}. Since the O_2 evolution rate is an exponential function of potential, the plot of log t_o vs. E_{dep} was expected to be linear. Furthermore, for any given value of E_{dep} for the three electrodes, it was expected that $t_{o,GC} > t_{o,Au} > t_{o,Pt}$ since $\eta_{GC} > \eta_{Au} > \eta_{Pt}$. A plot of log t_o vs. E_{dep} is shown in Figure 7. We propose that the induction time (t_o) is inversely related to the nucleation rate at the clean electrode surfaces and, therefore, the plot of log t_o vs. E_{dep} corresponds to a Tafel plot for the deposition process. The slopes of these plots are approximately equivalent; however, the differences in intercept are large and are consistent with the difference in η for O_2 evolution at the three electrode materials. A linear plot of log t_o vs. E_{dep} also was presented by Ramamurthy and Kuwana (4a), but without explanation.

<u>Effects</u> <u>of</u> <u>added</u> <u>foreign</u> <u>anions</u>   The rate of electrodeposition of ß-PbO_2 is maximized, in general, by use of small w, low c^b_{HClO4} and large $c^b_{Pb(II)}$. The effect of added inert anions also was considered. Results show that co-existing NO_3^- and ClO_4^- of varied concentration and small amounts of SO_4^{2-}, held to less than 10^{-5} M to prevent precipitation of

26

PbSO$_4$(s), do not have a significant effect on t$_o$. However, NO$_3^-$ tends to increase and ClO$_4^-$ slightly decreases the value of i$_{ss}$. It had been shown (1e) that if the SO$_4^{2-}$ concentration is comparable to $c_{Pb(II)}^b$, t$_o$ is shortened significantly and i$_{ss}$ is increased. Since the standard potential of the PbO$_2$-PbSO$_4$ couple (1.69 V) is higher than that of the PbO$_2$-Pb(II) couple (1.47 V) (13), it does not appear likely that this effect can be explained well by the stabilization by SO$_4^{2-}$ of soluble intermediates generated during the nucleation process. It was determined that addition of Cl$^-$ impurity to ca. 10 M did not change the results reported here. The influence of high levels of Cl$^-$ (> 100 µM) is under study.

Effects of voltammetric electrode pretreatment   Multiple cyclic scans of applied potential at noble metal electrodes have been demonstrated to cause enhancement of some electrode reactions, especially when the potential scans result in the alternate anodic/cathodic formation/dissolution of surface oxide. The observed effect has been attributed to the benefits of oxide-catalyzed oxidative removal of adsorbed impurities (1b), as well as to the increase of surface area by way of surface reconstruction (14).

The alternate anodic deposition and cathodic stripping of PbO$_2$ at Au and Pt RDEs was observed to decrease substantially the induction period (t$_o$) for the subsequent deposition. The phenomenon is demonstrated by changes in voltammetric response (i-E) shown in Figure 8 as a function of scan number. The rate of anodic PbO$_2$ deposition at E$_{dep}$ > ca. 1.5 V increases significantly with scan number for cyclic scans between the

limits 0.3 V and 1.8 V. The anodic current (i_a) at 1.8 V is shown plotted vs. scan number in the figure inset. The cathodic peak ($i_{p,c}$) for stripping of PbO_2 on the negative scan at ca. 1.2 V increases in height and area with scan number, as expected when larger quantities of PbO_2 are deposited in the region 1.55 - 1.80 V due to the decrease of t_o with increasing cycle number. The cathodic peak at ca. 0.9 V corresponds to the reduction of gold oxide formed for E > ca. 1.0 V and remains relatively unchanged with cycle number.

On the basis of Figure 8, it is concluded that the increases in i_a and $i_{p,c}$ are the direct result of an increased number of nucleation sites at the electrode surface. This increase cannot possibly be explained as the result of surface reconstruction (roughening) which might occur with repeated formation/dissolution of gold oxide because the area of the peak for gold oxide reduction remained unchanged. Furthermore, numerous cyclic scans between 0.3 V and 1.8 V prior to addition of Pb(II) to the electrolyte failed to produce the enhancement of deposition rates demonstrated in Figure 8. The return of i-E response from that for the 10th scan to that for the first scan in Figure 8 was achieved by any of the following processes: mechanical abrasion (0.05 μm alumina), chemical treatment with H_2O_2 or $KMnO_4$, or cathodic evolution of $H_2(g)$ at E << -0.3 V. It is concluded that an ultra-thin film of adsorbed Pb(II) is formed by the plating/stripping process and the adsorbed metal ions are rapidly oxidized to adsorbed PbO_2 which serve as nucleation sites for the subsequent deposition of bulk $PbO_2(s)$. The fractional surface coverage by adsorbed Pb(II) increases with cycle number and becomes constant only

when a complete film is formed (e.g., cycle number > 9). The presence of an adsorbed lead species on the Au surface following the voltammetric stripping of $PbO_2(s)$ at 0.3 V was verified by X-ray photoelectron spectroscopy (XPS).

The peak areas in Figure 8 corresponding to the cathodic and anodic current were measured by the "cut-and-weigh" method. It was found that the stripping peak area was virtually the same (ca. 0.1%) as the anodic area and we conclude that all Pb(IV) formed during the anodic process is converted to Pb(II) during cathodic stripping. Therefore the adsorbed lead species cannot be Pb(IV). Following the experiment shown in Figure 8, the Au electrode was rinsed and put in a 1.0 M $HClO_4$ blank solution and the potential was scanned from 1.3 to 1.8 and back to 1.3 V. A small but distinct PbO_2 deposition peak was observed which corresponded to the oxidation of the ultra-thin Pb(II) film at the anodic region. Hence, it can be concluded from Figure 8 that the number of nucleation sites increases with each cycle of $PbO_2(s)$ deposition/stripping. Chemical (H_2O_2 and $KMnO_4$) and electrochemical (H_2 evolution) removal of residual nucleation sites is very efficient. Although the ultra-thin film is stable in the region 1.1 > E > 0.3 V, there was no evidence for underpotential deposition of lead at a clean Au surface during the positive scan for 0.3 < E < 1.1 V.

The effect of the ultra-thin Pb(II) film on PbO_2 deposition also is demonstrated by the chronoamperometric curves shown in Figure 9. After the formation of a substantial deposit of PbO_2 at 1.48 V, the PbO_2 was stripped cathodically at 0.3 V. Then, PbO_2 was redeposited at 1.48 V

without further treatment of the electrode surface. From the redeposition current, it can be seen that t_o has decreased nearly to zero and i_{ss} for deposition of PbO_2 is achieved quickly.

The effect of variation of c^b_{HClO4} on the first (A) and reproducible (B) i-E curves is shown in Figure 10 for potential scans in the range 0.3 - 1.8 V. As c^b_{HClO4} is decreased, the anodic current at 1.7 V and anodic area of the wave for E > 1.5 V increases and, correspondingly, the height and area of the cathodic stripping peak in the region 1.3 - 1.1 V are increased. It is concluded that the number of nucleation sites generated on the first scan is inversely related to c^b_{HClO4}. Both the area and height of the deposition wave and stripping peak for curve d in Figures 10A & B (0.40 M $HClO_4$) change only slightly with cycle number. This is because for this pH, the entire surface of Au is covered by the ultra-thin Pb(II) film after a single cycle of deposition and stripping. These observations and conclusions are consistent with chronoamperometric data in Figures 2 - 5. For the reproducible i-E curve (Figure 10B), the anodic current at 1.7 - 1.8 V is relatively independent of c^b_{HClO4}, as compared to the first scan (Figure 10A). Hence, the maximum number of nuclei which can be formed apparently is relatively independent of c^b_{HClO4}. The shift of peak potential for the stripping process with change in pH (Figures 10A&B) indicates involvement of H^+ in the stripping process.

Optimization of electrodeposition conditions   One purpose of this research was the determination of optimal conditions for PbO_2 deposition. Based on the results of the kinetic and mechanistic studies of PbO_2

deposition at varied conditions as shown above, the following optimal conditions were chosen: 20 mM Pb(II), 0.1 M $HClO_4$, 400 rev min^{-1}, and an initial value E_{dep} = 1.6 V vs. SCE. When the current has reached its maximum value, e.g., ca. 5 sec, E_{dep} is decreased to 1.5 V for the remaining deposition period of 60 - 90 sec. The PbO_2 film prepared in this way is smooth, very adhesive, and highly reflective.

Conclusions

The mechanism of PbO_2 electrodeposition is concluded to involve the generation of a soluble intermediate product which can be transported away from the electrode surface by convective-diffusional processes. Hence, solution agitation can result in a significant barrier for deposition.

When $c^b_{Pb(II)}$ and c^b_{HClO4} are large, deposition is under kinetic control and the rate of deposition decreases with increased rotation rate. Furthermore, the steady-state current for deposition is much less than the mass-transport limited value. The reaction is under mass-transport control only when both $c^b_{Pb(II)}$ and c^b_{HClO4} are low. In this case, the rate of deposition increases with increased rotational velocity. For medium values of $c^b_{Pb(II)}$ and c^b_{HClO4}, the deposition is under mixed control by kinetics and mass-transport. The rate of deposition is relatively independent of rotation rate at the RDE.

It is observed that, in general, the electrodeposition of PbO_2 on Au, Pt, GC, and on PbO_2 itself, occurs at a significant rate only for potential values corresponding to a finite rate for the simultaneous evolution of O_2. The mechanism of O_2 evolution (12d) on oxides is

proposed to correspond to the rapid initial reaction

$$H_2O \longrightarrow OH_{ads} + H^+ + e \quad (\text{fast}) \qquad [5]$$
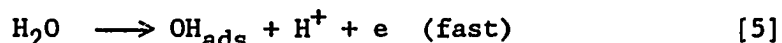
Hence, the OH_{ads} generated by the O_2-evolution reaction [5] can be consumed within the PbO_2 deposition mechanism, as shown in [2]. The rate of O_2 evolution for low anodic current densities at oxide-covered Pt, Au and Pb anodes increases with increase in pH by the amount 0.0591 pH and as an exponential function of applied potential (12d). Accordingly, it is observed that the rate of PbO_2 deposition increases as the values of pH and E_{dep} are increased.

Formation and stripping of PbO_2 during potential cycling produces an electrode surface bearing an ultra-thin film of a Pb(II). This ultra-thin film is stable to 0.3 V vs. SCE, but can be stripped from the electrode by cathodic evolution of H_2 or chemical treatment with H_2O_2 or $KMnO_4$. The ultra-thin Pb(II) film is rapidly oxidized to PbO_2 at E > 1.3 V and serves to nucleate the further deposition of bulk $PbO_2(s)$. Further studies of the mechanism of ultra-thin film formation will be published elsewhere.

References

1. (a) Austin, D. S.; Polta, J. A.; Polta, T. Z.; Tang, A. P.-C.; Cabelka, T. P.; Johnson, D. C. J. Electroanal. Chem. 1984, 168, 227. (b) Johnson, D. C.; Polta, J. A.; Polta, T. Z.; Neuburger, G. G.; Johnson, J.; Tang, A. P.-C.; Yeo, I.-H.; Baur, J. J. Chem. Soc., Faraday Trans. 1 1986, 82, 1081. (c) Tang, A. P.-C.; Johnson, D. C. Anal. Chim. Acta in press. (d) Yeo, I.-H.; Johnson, D. C. J. Electrochem. Soc. 1987, 134, 1973. (e) Yeo, I.-H. Ph.D. Dissertation, Iowa State University, Ames, Iowa, 1987. (f) Wels, B.; Johnson, D. C. not published.

2. Carr, J. P.; Hampson, N. A. Chem. Rev. 1972, 72, 679.

3. (a) Lazarides, C.; Hampson, N. A.; Henderson, M. J. Appl. Electrochem. 1981, 11, 605. (b) "Batteries"; Vol. 2, Kordesch, K. V., Ed.; M. Dekker: New York, 1977.

4. (a) Ramamurthy, A. C.; Kuwana, T. J. Electroanal. Chem. 1982, 135, 243. (b) Narasimham, K. C.; Gomathi, P. S.; Udupa, H. V. K. J. Appl. Electrochem. 1976, 6, 397. (c) Gnanasekaran, K. S. A.; Narasimham, K. C.; Udupa, H. V. K. J. Appl. Electrochem. 1976, 6, 189. (d) Hampel, C. A. "The Encyclopedia of Electrochemistry"; Chapman and Hall: London, 1964; p. 762.

5. (a) Fleischmann, M.; Liler, M. Trans. Faraday Soc. 1958, 54, 1370. (b) Fleischmann, M.; Thirsk, H. R. Electrochim. Acta 1959, 1, 146. (c) Fleischmann, M.; Thirsk, H. R. Electrochim. Acta 1960, 2, 22. (d) Fleischmann, M.; Mansfield, J. R.; Thirsk, H. K.; Wilson, H. G. E.; Wynne-Jones, L. Electrochim. Acta 1967, 12, 967.

6. (a) Barradas, R. G.; Contractor, A. Q. J. Electroanal. Chem. 1982, 138, 425. (b) Barradas, R. G.; Contractor, A. Q. J. Electroanal. Chem. 1981, 129, 327. (c) Stevens, R.; Gilroy, D. J. Microscopy 1981, 124, 265. (d) Gilroy, D.; Stevens, R. J. App. Electrochem. 1980, 10, 51.

7. (a) "The Electrochemistry of Lead"; Kuhn, A. T., Ed.; Academic Press: London, 1979. (b) Pohl, J. P.; Richert, H. In "Electrodes of Conductive Metallic Oxides"; Trasatti, S., Ed.; Elsevier: Amsterdam, 1980. (c) Nagy, Z. "Electrochemical Synthesis of Inorganic Compounds: A Bibliography"; Plenum Press: New York, 1985.

8. (a) Nichols, M. L. Ind. Eng. Chem., Anal. Ed. 1931, 3, 384. (b) Day, T. G.; Delano, P. H.; Schrenk, W. T. Bulletin-Missouri School of Mines and Metallurgy, U. Missouri-Rolla, 1935, 12, No. 1, 1. (c) Lingane, J. J. "Electroanalytical Chemistry"; 2nd edition, Interscience: New York, 1958; p. 374

9. (a) Laitinen, H. A.; Watkins, N. H. Anal. Chem. 1975, 47, 1352. (b) Laitinen, H. A.; Watkins, N. H. J. Electrochem. Soc. 1976, 123, 804. (c) Kinard, J. T.; Propst, R. C. Anal. Chem. 1974, 46, 1106.

10. (a) Beck, F. J. Electroanal Chem. 1975, 65, 231. (b) Beck, F.; Boh, H. Ber. Bunsenges. Phys. Chem. 1975, 79, 233. (c) Hampson, N. A.; Jones, P. C.; Phillips, R. F. Can. J. Chem. 1968, 46, 1325. (d) Hampson, N. A.; Jones, P. C.; Phillips, R. F. Can. J. Chem. 1967, 45, 2039. (e) Hampson, N. A.; Jones, P. C.; Phillips, R. F. Can. J. Chem. 1967, 45, 2045.

11. Nishibe, K. Denki Kagaku 1984, 52, 614; Chem. Abstr. 102, 13988c.

12. (a) Fleischmann, M.; Thirsk, H. R. In "Advances in Electrochemistry and Electrochemical Engineering"; Delahay, P.; Tobias, C. W., Eds.; Interscience: New York, 1963; Volume 3; J. Electrochem. Soc., Japan (overseas suppl. ed.) 1960, 28, E175. (b) Dignam, M. J. In "Comprehensive Treatise of Electrochemistry"; Bockris, J. O'M.; Conway, B. E.; Yeager, E.; White, R. E., Eds.; Plenum Press: New York, 1981; Volume 4. (c) Greef, R.; Peat, R.; Peter, L. M.; Pletcher, D.; Robinson, J. "Instrumental Methods in Electrochemistry"; Ellis Horwood: Chichester, 1985; Chapter 9. (d) Tarasevich, M. R.; Sadkowski, A.; Yeager, E. In "Comprehensive Treatise of Electrochemistry," Conway, B. E.; Bockris, J. O'M.; Yeager, E.; Khan, S. U. M.; White, R. E., Eds.; Plenum Press: New York, 1983; Volumne 7.

13. "Standard Potentials in Aqueous Solutions"; Bard, A. J.; Parsons, R.; Jordan, J., Eds.; Marcel Dekker: New York, 1985; p. 220.

14. (a) Chialvo, A. C.; Triaca, W. E.; Arvia, A. J. J. Electroanal. Chem. 1983, 146, 93. (b) Chialvo, A. C.; Triaca, W. E.; Arvia, A. J. J. Electroanal. Chem. 1984, 171, 303. (c) Herman, E. G.; Alonso, C.; Gonzalez-Velasco, J. J. Electroanal. Chem. 1987, 233, 277. (d) Kinoshita, K. In "Modern Aspects in Electrochemistry"; Bockris, J. O'M.; Conway, B. E.; White, R. E., Eds.; Plenum Press: New York, 1982; Volume 14. (e) Kinoshita, K.; Lundquist, J. T.; Stonehart, P. J. Electroanal. Chem. 1973, 48, 157. (f) Bishop, E.; Hitchcock, P. H. Analyst 1973, 98, 475.
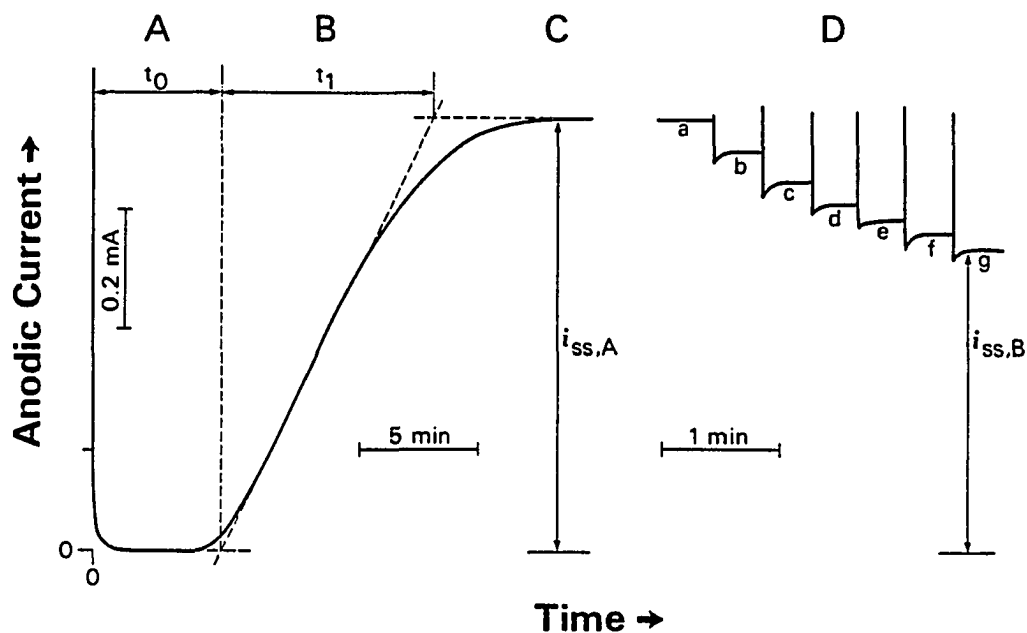
Figure 1. A typical chronomamperometric transient (i-t) for PbO_2
deposition at a Au RDE

Conditions: 0.20 M Pb(II), and 1.70 M $HClO_4$

Regions: (A) induction period (t_0),
           (B) transition period (t_1),
           (C) steady-state period ($t \gg t_0 + t_1$),
           (D) study of rotation speed dependence on i_{ss}

Rotation velocity (rev min^{-1}):   (a) 0, (b) 400, (c) 900,
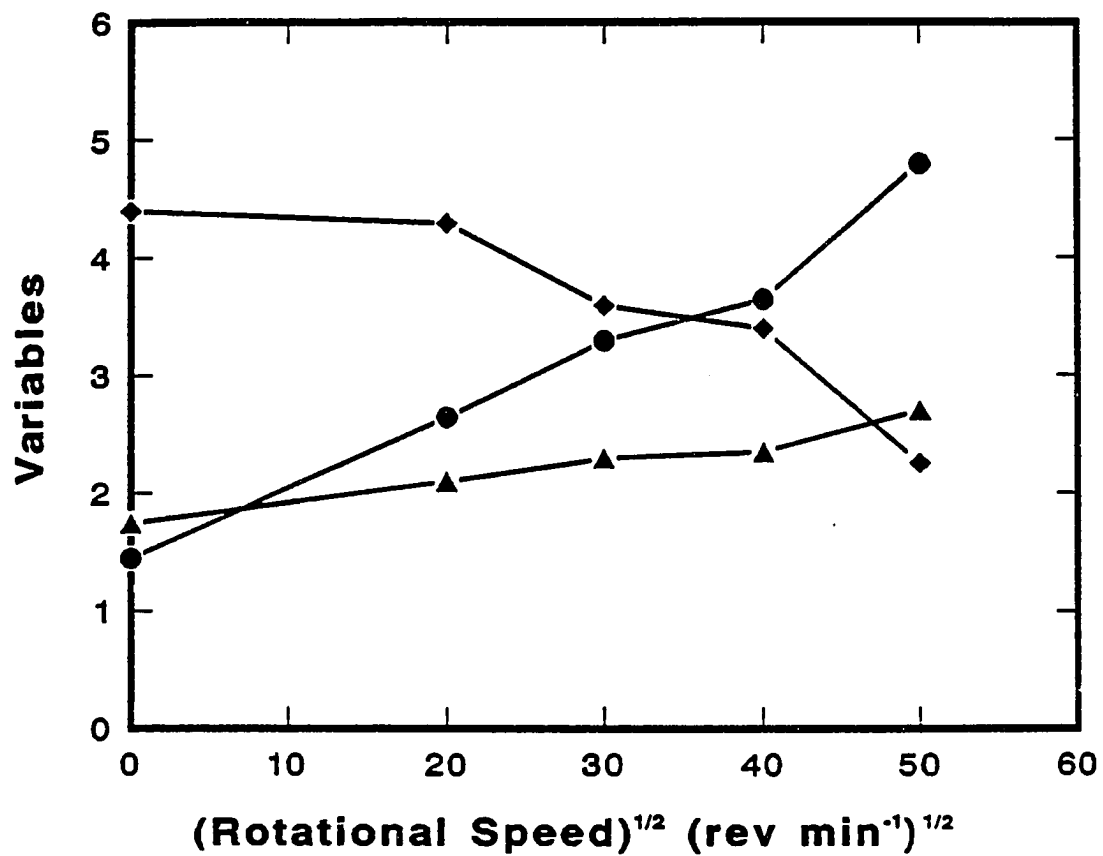   (d) 1600, (e) 2500, (f) 3600, and (g) 4900

Figure 2. Plots of t_0, t_1, and S vs. $w^{1/2}$

Conditions: 0.20 M Pb(II), 1.30 M HClO$_4$,
and 0.40 M NaClO$_4$

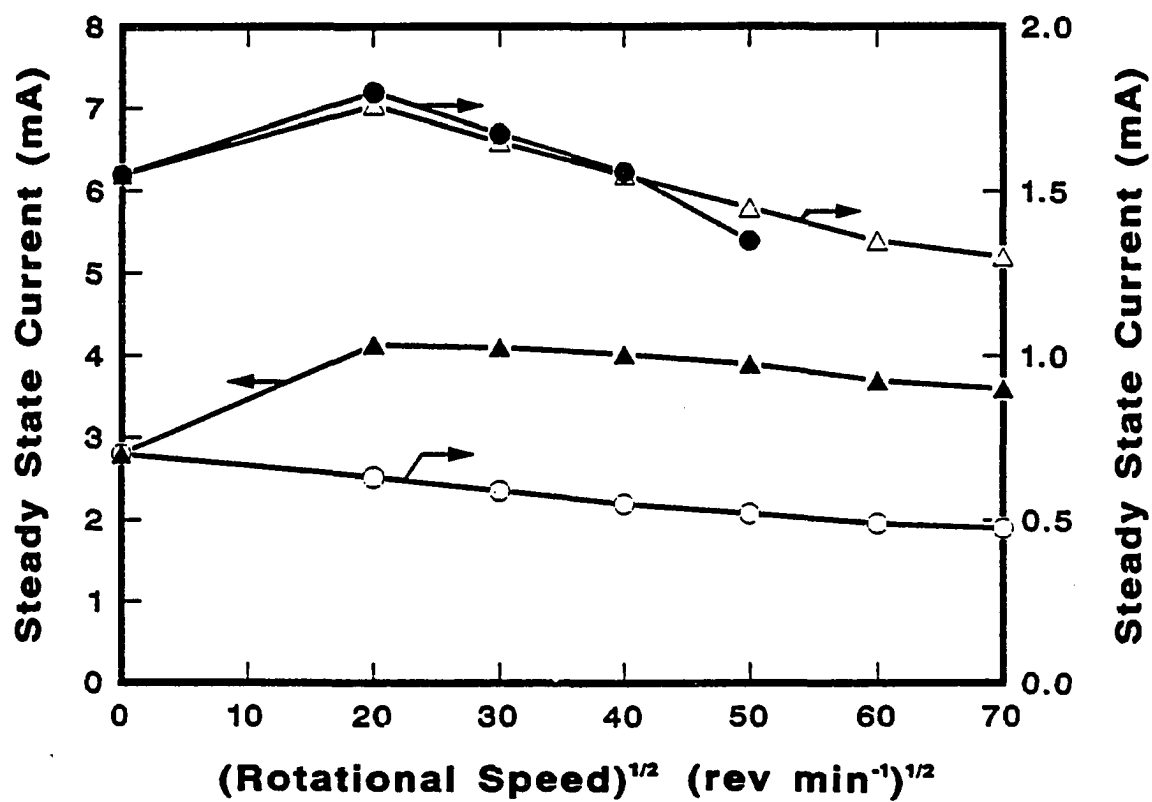Variables: (●) t_0/min, (▲) t_1/min, (◆) S/0.1 mA min^{-1}

Figure 3. Plots of i_{ss} vs. $w^{1/2}$ as a function of C^b_{HClO4}

Conditions: 0.20 M Pb(II)

Variable and C^b_{HClO4}: (●) $i_{ss,A}$ for 1.30 M,
(▲) $i_{ss,A}$ for 0.80 M,
(○) $i_{ss,B}$ for 1.70 M,
(△) $i_{ss,B}$ for 1.30 M
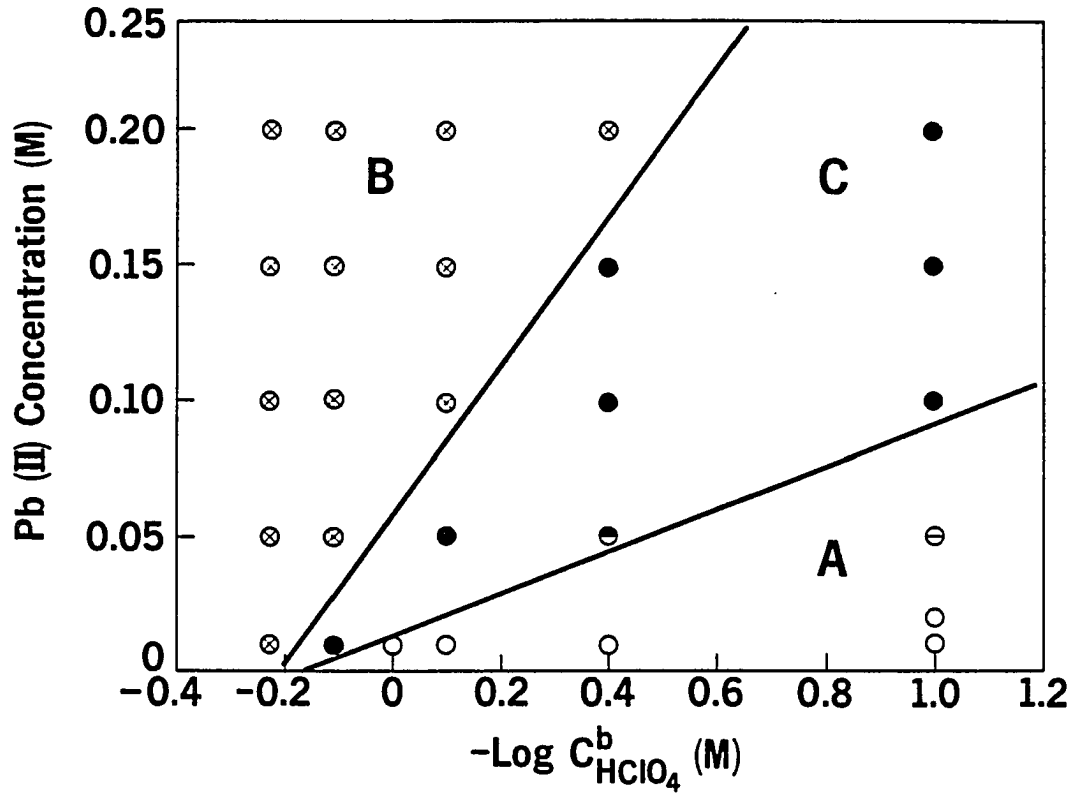
Figure 4. Dependence of the i_{ss}-$w^{1/2}$ relation on $C^b_{Pb(II)}$ and C^b_{HClO4}

If w is increased by 100%:
  (O) i_{ss} increases by 50 - 100%,
  (⊖) i_{ss} increases less than 10%,
  (◑) i_{ss} increases at low w but decreases at high w,
  (●) i_{ss} decreases,
  (⊗) i_{ss} increases by 10 - 50%

Regions: (A) mass transport control,
          (B) kinetic control,
          (C) mixed kinetic-transport control
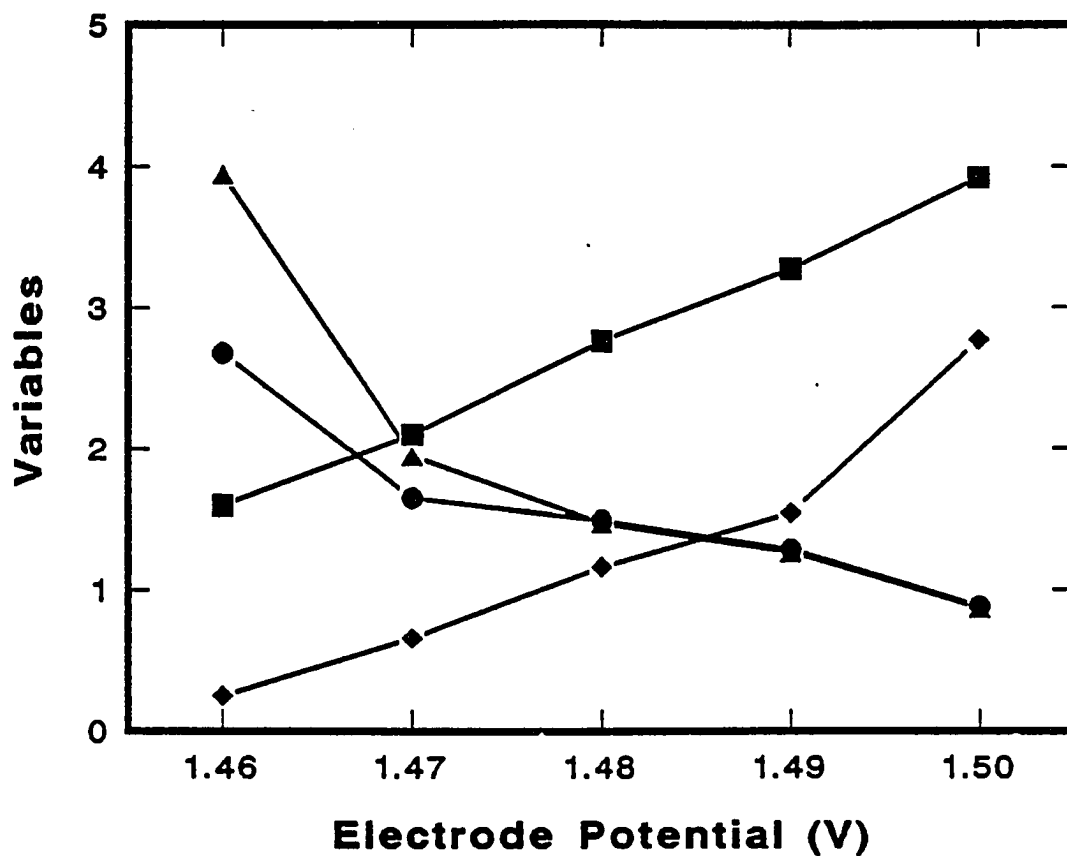
Figure 5. Plots of t_o, t_1, S and i_{ss} vs. E_{dep}

Conditions: 0.20 M Pb(II), 1.30 M $HClO_4$, 0.40 M $NaClO_4$, and 0 rev min^{-1}

Variables: (●) $t_o/2$ min,
(▲) $t_1/2$ min,
(◆) $S/0.4$ mA min^{-1},
(■) $i_{ss}/0.5$ mA
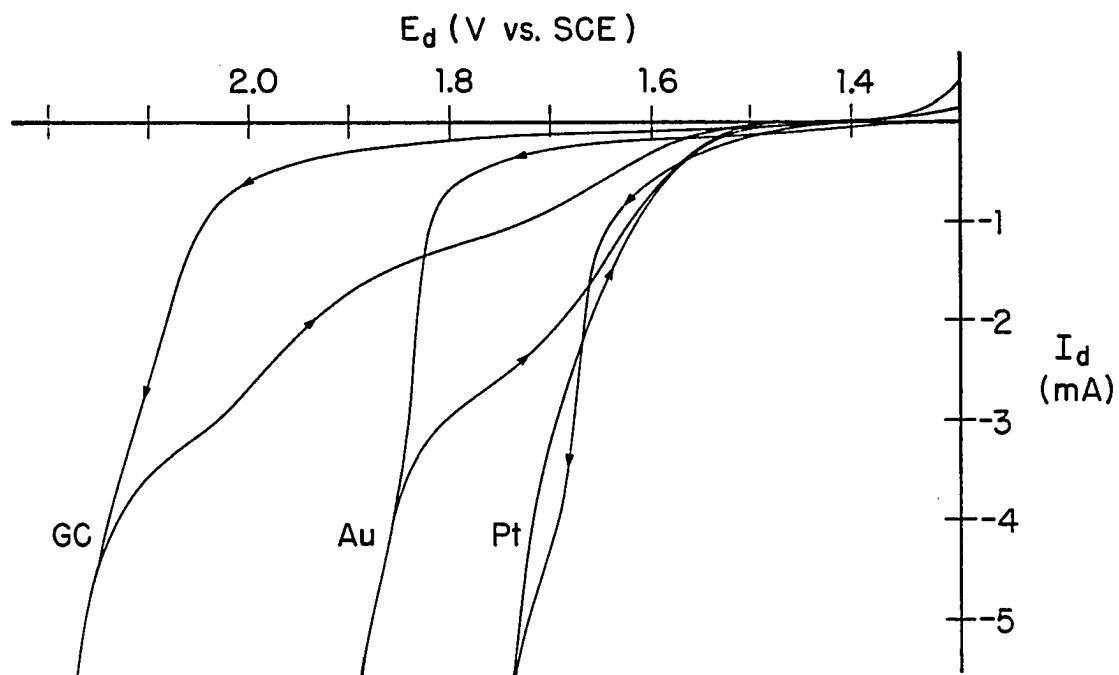
Figure 6. Cyclic voltammograms (i-E) at rotated Au, Pt and GC disc electrodes

Conditions: 10 mM Pb(II), 1.0 M $HClO_4$, 400 rev min^{-1}; scan initiated from E $\ll$ 1.3 V; scan direction indicated by arrows; only first cyclic scan is shown
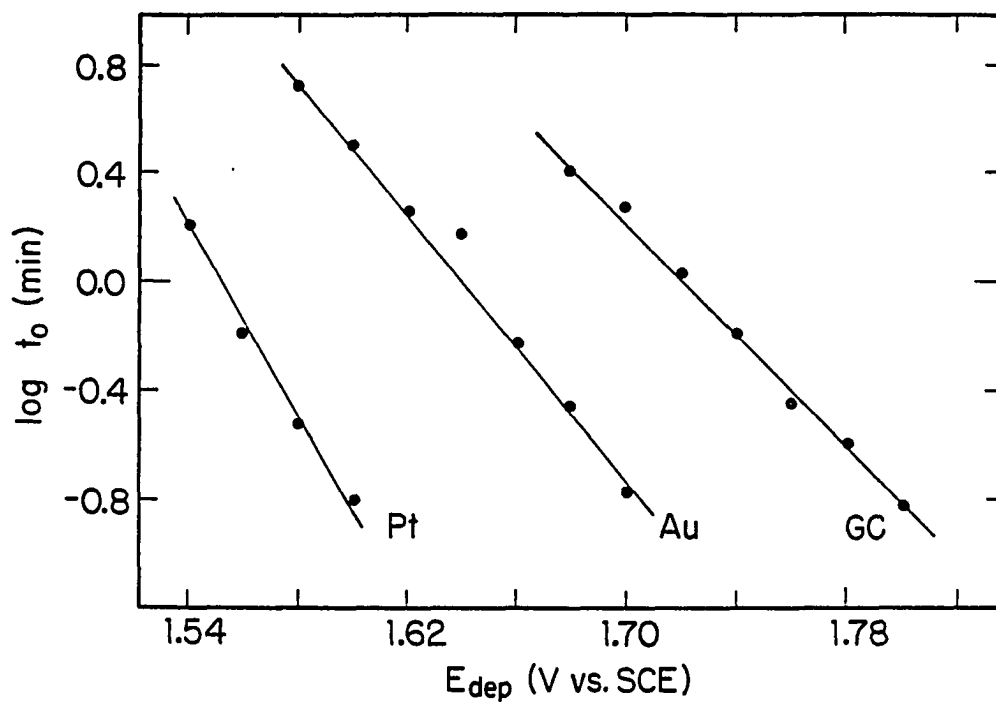
Figure 7. Plot of log t_o vs. E_{dep} for the induction period at rotated
Pt, Au and GC disc electrodes

Conditions: 10 mM Pb(II), 1.0 M $HClO_4$, 400 rev min^{-1};
electrodes freshly polished prior to
experiment
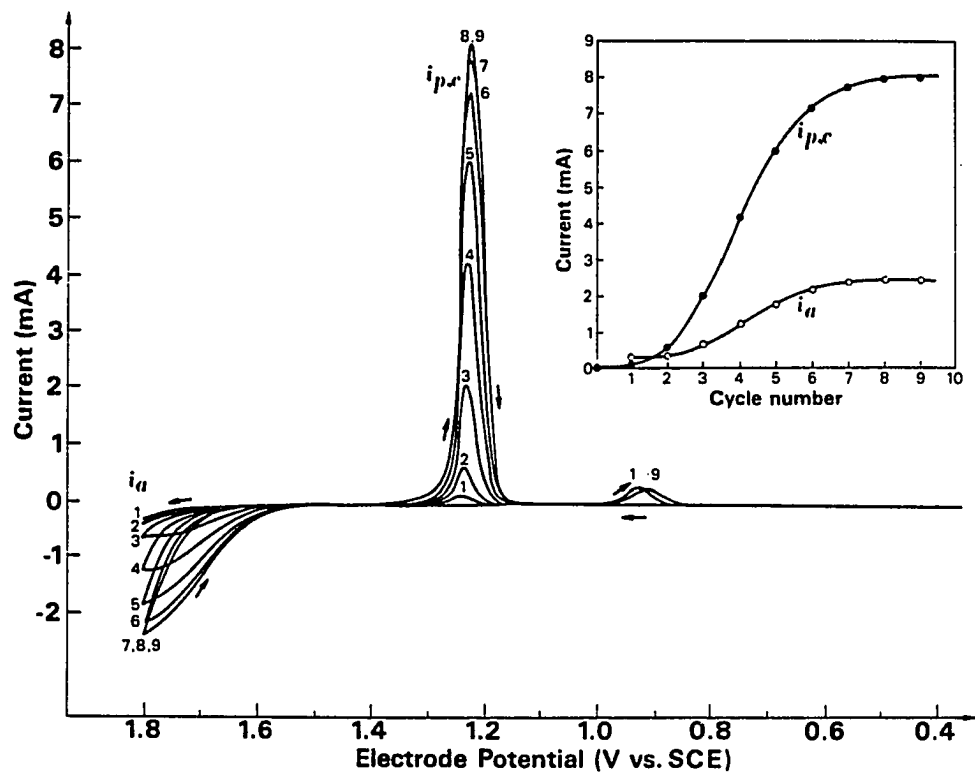
Figure 8. Cyclic voltammograms (i-E) at a rotated Au disc electrode

Conditions: 0.010 M Pb(II), 1.70 M $HClO_4$, 40 mV s^{-1}, and 1000 rev min^{-1}

Curves: cycle number as marked

Inset: i_a and $i_{p,c}$ vs. cycle number
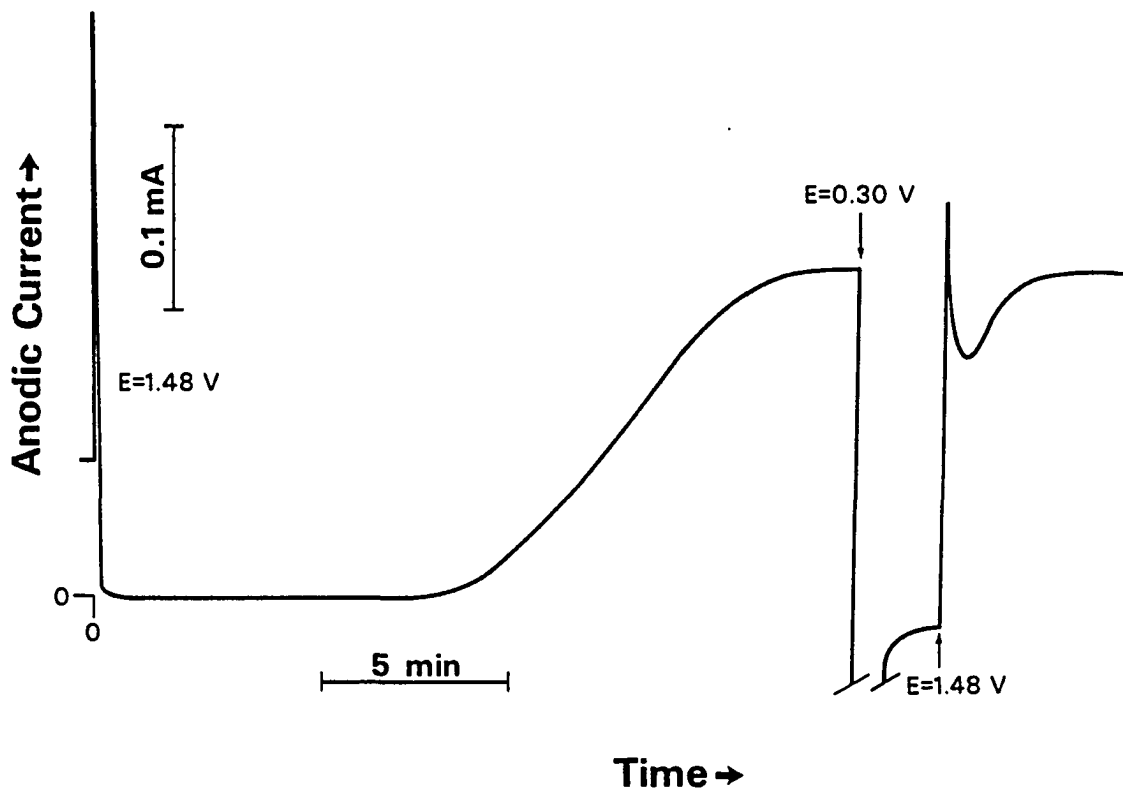
Figure 9. Chronoamperometric transients for PbO_2 deposition, stripping and redeposition

Conditions: $c^b_{Pb(II)}$ = 0.10 M, c^b_{HClO4} = 0.80 M, and 400 rev min^{-1}. E as marked
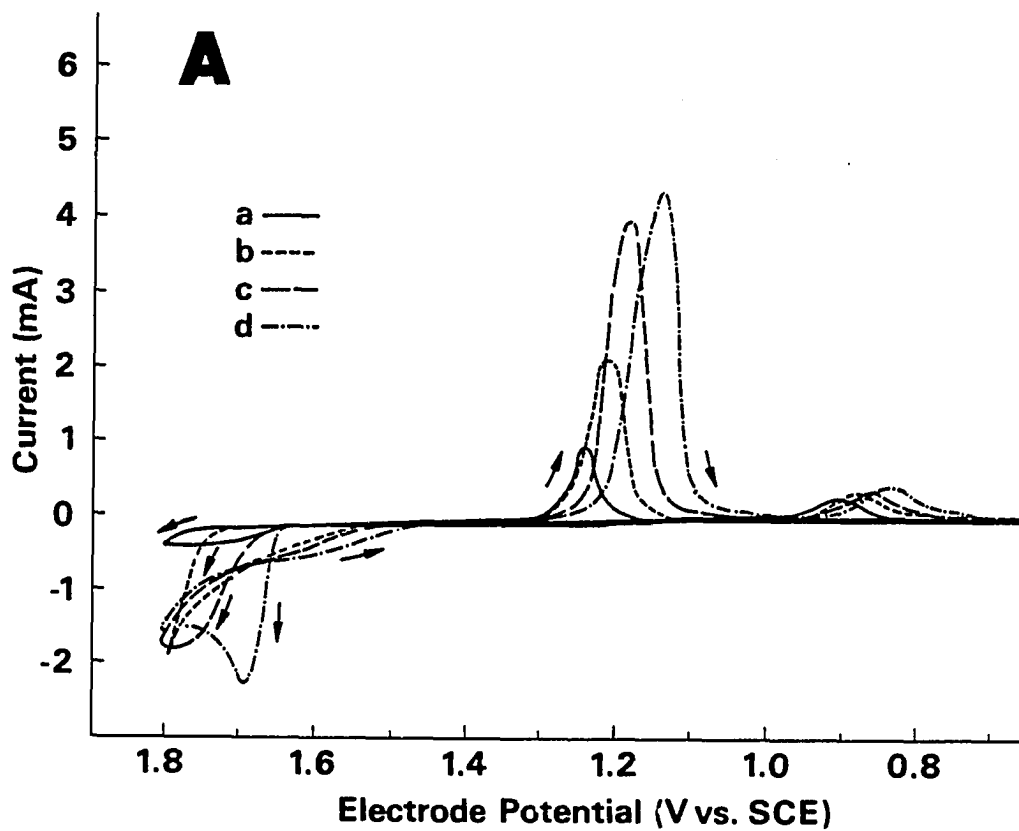
Figure 10A. Effect of pH on cyclic voltammograms: response for
first cycle

Conditions: 0.010 M Pb(II), 40 mV s^{-1}, and 0 rev min^{-1}

c^b_{HClO4} (M): (a) 1.70, (b) 1.40, (c) 0.80, and (d) 0.40
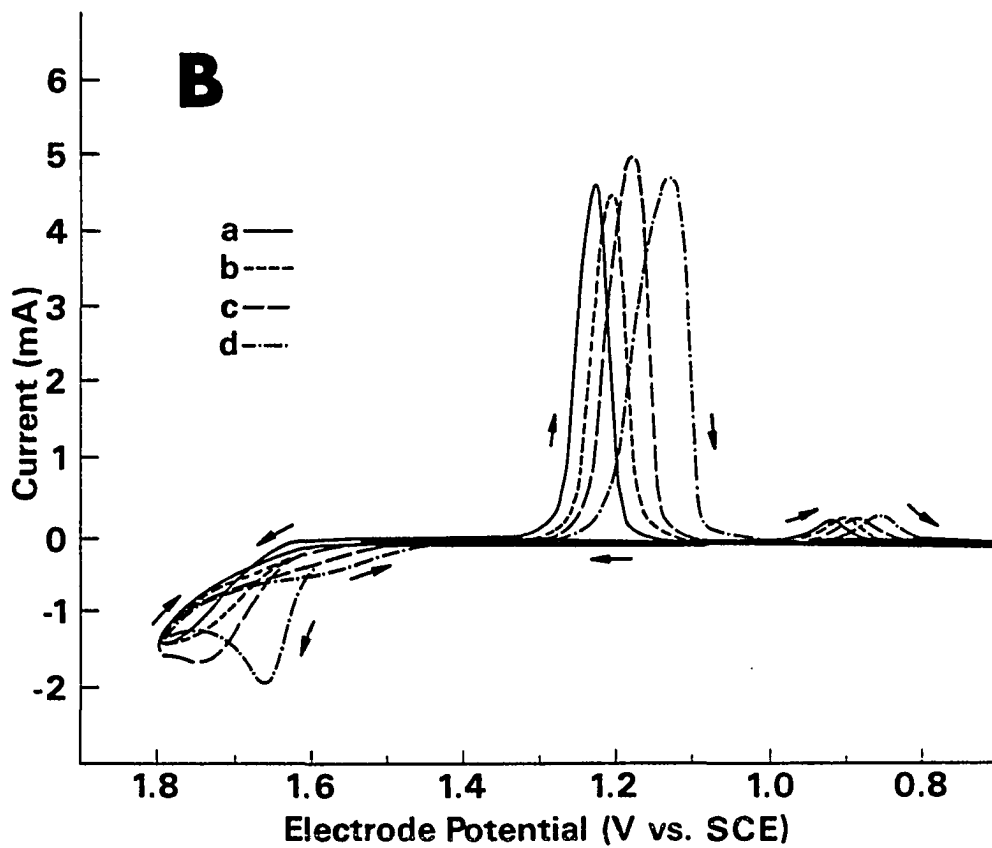
Figure 10B. Effect of pH on cyclic voltammograms: reproducible
response after many cycles

Conditions: as given in Figure 10A

B. Detection of Soluble Intermediate Products during

Electrodeposition and Stripping

of ß-Lead Dioxide at a Gold Electrode[1]

"The search for intermediates in chemical reactions is
like a detective story. The kineticist knows the
actors, present at the beginning, and he sees the
victims. He has to search for witnesses to reconstruct
the course of the events. His witnesses are the
intermediates. If he is lucky he can find some.
Without such witnesses, his reasoning depends on
circumstantial evidence and may often be quite
erroneous. It is obvious, therefore, how important such
intermediates are for the understanding of electrode
reactions and how necessary it is to find the most
direct evidence for their existence."

-Heinz Gerischer,
Farady Soc. Discus. 1973, 56, 7.

---

[1]Published in Chang, H.; Johnson, D. C. J. Electrochem. Soc. 1989,
136, 23-27.

<u>Abstract</u>

A Au rotated ring-disc electrode (RRDE) was applied for the detection of soluble intermediate products during the anodic electrodeposition and cathodic dissolution of ß-PbO$_2$ in solutions of HClO$_4$. A soluble species which can only be reduced at the ring electrode is produced during the anodic nucleation and deposition processes for PbO$_2$(s) at the disc electrode. This soluble intermediate product is concluded to be Pb(IV) which is probably associated with oxygen, e.g., PbO^{2+} or Pb(OH)$_2$$^{2+}$. The cathodic ring current from detection of the soluble Pb(IV) species was studied as a function of the concentrations of Pb(II) and HClO$_4$, and variation of electrode rotational velocity. The results are consistent with chronoamperometric data for PbO$_2$ electrodeposition described previously. Soluble Pb(IV) and Pb(III), as well as Pb(II), are concluded to be products of the cathodic dissolution of PbO$_2$.

<u>Introduction</u>

The deposition of ß-PbO$_2$ from solutions of HClO$_4$ containing Pb(II) is an example of an anodic reaction in which oxygen from H$_2$O is transferred to the reaction product. Recently, strong evidence was presented that this process is electrocatalyzed by the simultaneous evolution of O$_2$ at the electrode surface (1). The deposition mechanism is suspected to involve transfer to Pb(IV) of hydroxyl species which are produced in the O$_2$-evolution reaction. The production of a soluble intermediate species containing lead was suspected on the basis of the inverse dependence of the deposition current on rotational velocity for a

Au disc electrode (1).

The reaction mechanisms of the $PbO_2/PbSO_4$ and $PbSO_4/Pb$ redox couples have long been of interest in H_2SO_4 (2-4), as well as H_3PO_4/H_2SO_4 (5-7), because of their significance for the lead-acid battery. It appears as a frequent assumption that intermediate states of lead produced in these redox processes have virtually no solubility and remain adsorbed at the electrode surface (1,8-10). Laitinen and Watkins (7) described direct evidence for a soluble intermediate in H_3PO_4/H_2SO_4 solutions; the chelating action of the phosphate presumably enhances the stability and solubility of intermediate oxidation states of lead. Others have studied the mechanism for cathodic reduction of PbO_2 in H_2SO_4 with attention given to the detection of soluble Pb(II) (11-14). The search for soluble intermediate products apparently has not been applied to other media.

Here we report on the application of Au rotated ring-disc electrodes (RRDE) to a study of the anodic deposition and cathodic dissolution of ß-PbO_2. Applicability of the RRDE for detection of intermediate products of electrochemical reactions is well known (15-17). To be detected at the ring electrode, the intermediate product of the disc reaction must have a half-life approximately equal to or greater than the average time for convective-diffusional transport from the disc to the ring of the RRDE.

Experimental

Chemicals   All reagents have been described previously (1).

<u>Instrumentation</u>   The Au RRDE was operated with a model PIR rotator, ASR speed controller, and RDE4 dual potentiostat (Pine Instrument, Grove City, PA). The three values of radii characterizing the geometry of the Au RRDE were 3.84, 4.01 and 4.19 mm. The collection efficiency (N) was 0.14, calculated according to (11). Voltammetric (i-E) data were recorded on a model 200 X-Y recorder (Houston Instrument Co.). Chronoamperometric (i-t) data were recorded on a series 5000 two-pen, strip chart recorder (Fischer Scientific).

<u>Procedures</u>   Electrodes were polished before each measurement as in (1), placed in the plating solution, and then connected with the potentiostat with the disc potential (E_d) set at 0.3 V. Scanning of E_d in voltammetric experiments was started from 0.3 V after ca. 30 sec.

<u>Results and discussion</u>

<u>Voltammetry</u>   Current-potential curves obtained at the disc electrode of the Au RRDE $(i_d$-$E_d)$ are shown in Figure 1 for 1.70 M $HClO_4$ before (A) and after (B) addition of 10 mM Pb(II). In the presence or absence of Pb(II), anodic formation of surface gold oxide occurs on the positive scan for $E_d > 1.2$ V (Wave a) and cathodic dissolution of the gold oxide occurs on the negative scan for E_d - 1.0 - 0.9 V (Peak c). Production of O_2 by anodic discharge of H_2O occurs for $E_d > 1.7$ V (Wave b). In the presence of Pb(II), anodic nucleation and deposition of $PbO_2(s)$ occurs for $E_d > 1.6$ V (Wave d) and cathodic dissolution of $PbO_2(s)$ occurs for the negative scan at E_d - ca. 1.0 - 0.85 V (Wave e). Additional description of these processes has been given in (1).

The i_r-E_d curves for the ring electrode at E_r = 0.2 V, obtained

simultaneously with the i_d-E_d curves, are shown in Figure 1 before (B)

and after (D) the addition of 10 mM Pb(II). In the absence of Pb(II),

small anodic signals on the i_r-E_d curves are observed simultaneously with

oxide formation (Peak a') and dissolution (Peak c') at the disc electrode

which are attributed to soluble Au species, in accord with conclusions by

Cadle and Bruckenstein for 0.2 M H_2SO_4 (16). Of major importance to this

study are the additional ring Peaks d' and e' in the i_r-E_d curves in the

presence of Pb(II). At E_r = 0.2 V, there is no reactivity of Pb(II) at

the ring electrode. The possible conclusion that the Peaks d' and e'

might be caused by detection of soluble O_2 is excluded by the fact that

dissolved O_2 in air-saturated solutions is not detected at 0.2 V. Hence,

the cathodic ring currents in Figure 1D corresponding to the disc

electrode processes of anodic nucleation and deposition (ring Peak d'),

and cathodic dissolution of deposited PbO_2(s) (ring Peak e'), are

concluded to be the result of soluble species other than Pb(II) produced

at the disc electrode.

We have reported that the anodic disc current for PbO_2(s) deposition

at E_d = 1.6 V increases with cycle number, see Figure 7 of (1). This

was concluded to be the beneficial effect of surface accumulation of an

ultra-thin film of Pb(II), possibly PbO, which is not stripped from the

electrode surface even for E_d = +0.3 V. Furthermore, this ultra-thin

film is concluded to function as an array of nucleation sites, possibly

in the form of PbO_2 following the change of E_d from 0.3 V to 1.6 V, with

the result of a large decrease in the introduction period for the

subsequent deposition of bulk $PbO_2(s)$. It is noted from Figure 1 (C and D) that Peak d' for the ring electrode first increases and then decreases with scan number, whereas the corresponding disc signal (Wave d) increases steadily with scan number to a reproducible value. Hence, the data in Figure 1D support the conclusion that a soluble intermediate product of the nucleation process at E_d = ca. 1.6 V is produced within the induction period and the amount of this intermediate product decreases substantially when the induction period is completed and the disc current increases to its maximum steady-state value.

Ring Peak d' in Figure 1D increases with increased rotational velocity (w), as illustrated by the nearly linear plots of peak current vs. $w^{1/2}$ in Figure 2. The induction period (t_o) also increases for higher rotational velocity and the increased ring current is consistent with the conclusion that the species detected at the ring electrode is an intermediate product of the nucleation process at the disc. More evidence supporting this conclusion was obtained from chronoamperometric studies which are presented in the next section.

Chronoamperometry   Previous evidence for a soluble intermediate product during $PbO_2(s)$ deposition came from chronoamperometric studies at the Au RDE as a function of rotational velocity for a step of E_d from 0.3 V to 1.48 V, see Figure 1 of (1). Similar i_d-t data are shown in Figure 3a. In Figure 3b is shown i_r-t data obtained simultaneously for E_r = 0.2 V. The cathodic value of i_r is maximum at the start of the induction period ($i_d \ll i_{d,ss}$) for the anodic deposition process at the disc electrode and decreases to a minimum when the induction period is

completed ($i_d - i_{d,ss}$). This is consistent with the voltammetric data for Waves d and d' presented in Figure 1.

Whereas $i_d \ll i_{d,ss}$ during the induction period, i_d is not zero, as is shown by the i_d-t curve in Figure 3c recorded at a high current sensitivity. For increasing small values of rotational velocity, the value of i_r observed during the induction period increases; however, the corresponding value i_d decreases and the induction period (t_o) increases. Hence, further reduction of the intermediate product at the disc surface is necessary to accumulate $PbO_2(s)$. For high rotational velocities, the value of the ratio $-i_r/i_d$ at the start of the induction period was determined to be ca. 0.14, which equals the theoretical collection efficiency (N) for the RRDE. Hence, under these conditions for t $\ll t_o$, $-i_r/Ni_d$ = ca. 1 and it is apparent that the majority of the product of Pb(II) oxidation at the disc electrode is soluble and is transported away from the disc electrode surface.

The rate of $PbO_2(s)$ deposition at the disc electrode increases to a steady-state value at the end of the induction period (i.e., $i_d - i_{d,ss}$) and the value of i_r for detection of the soluble intermediate product decreases to a minimum (see Figure 3). The effect of change of rotational velocity on $i_{d,ss}$ and i_r (E_r = 0.2 V) was studied and typical results are included in Figure 3. The value of $i_{d,ss}$ is a maximum for 0 rev min and i_r = 0 A, as is expected. As the rotational velocity was increased, $i_{d,ss}$ decreased and the concurrent value of i_r increased. These results are consistent with the conclusion of a soluble intermediate product for deposition of $PbO_2(s)$. Plots of i_r/N vs. $w^{1/2}$

are not linear with a zero intercept (Figure 4, Curve b). This is concluded to be indisputable proof of the convective-diffusional loss of a soluble intermediate product of the Pb(II) oxidation at the disc electrode. Note, however, for $i_d = i_{d,ss}$, that values of $-i_r/Ni_d$ are substantially below the unity value which would be expected if all of the product at the disc is soluble and electroactive (17). Hence, for t >> t_o, the majority of the Pb(II) oxidized at the disc is accumulated as $PbO_2(s)$.

Effect of ring potential (E_r)   The oxidation state of the soluble lead species can be deduced from i_r-E_d data obtained as a function of E_r and shown in Figure 5. Peak d' at the ring electrode decreases with increased E_r, and disappears for $E_r > 1.0$ V (see Figure 5A). Hence, the soluble species detected during nucleation and deposition of PbO_2 is reduced but cannot be oxidized and is concluded to be Pb(IV) and not Pb(III).

Peak e' at the ring electrode, obtained concurrently with cathodic dissolution of $PbO_2(s)$ at the disc electrode, is cathodic for $E_r < 1.0$ V and anodic for $E_r > 1.0$ V (Figure 5A). For $E_r >$ ca. 1.0 V, Peak e' appears to be the resultant of superimposed anodic and cathodic peaks; see the illustration of component Peaks e_a' and e_c' in Figure 5C. This is evidence for a mixture of intermediate products and we conclude that both Pb(III) and Pb(IV) are soluble products of the cathodic dissolution of $PbO_2(s)$. The detection of Pb(II) on the negative scan of E_d occurs at slightly more positive values of E_d than that of Pb(IV) when $PbO_2(s)$ just begins to strip from the disc electrode. The cathodic signal for $E_r <$

1.0 V corresponds to reduction of both Pb(II) and Pb(IV) to Pb(II).

Reduction of Pb(II) to Pb^o occurs for $E_r <$ ca. 0.2 V. The peak currents

for Peaks e_a' and e_c' are very small in comparison to Peak e at the disc

electrode, and the amount of Pb(III) and Pb(IV) produced during cathodic

dissolution of $PbO_2(s)$ is very small. This is consistent with the

observation (1) that the areas of Peaks d and e at the disc electrode are

virtually equivalent.

Effect of pH   Depending on the concentrations of Pb(II) and

$HClO_4$, the rate of PbO_2 deposition can be under transport control,

kinetic control, or mixed control, as was illustrated in Figure 4 of

(1). The i_r-E_d response was compared for the extreme conditions of

kinetic and transport control and the results are shown in Figure 5.

For 1.3 M $HClO_4$, (i.e., transport-controlled deposition), the ring

current Peak d' in solution of increased pH (see Figure 5B) becomes peak-

like even at the first scan and the peak height decreases and peak

potential is shifted to slightly more negative potentials as compared

with that in Figure 1. This is because the formation of PbO_2 is faster

at higher pH (1) and the required induction period is completed within

the time spent by E_d in the region 1.6 - 1.7 V during a single potential

scan. Once the Au surface is covered with a $PbO_2(s)$ layer, there is

significantly less soluble Pb(IV) produced and the ring current decreases

to produce a peak-shaped wave. The shape of the ring Peak e' changes

significantly at higher pH. A broad anodic peak appears even at E_r - 0.2

V in 1.30 M $HClO_4$ (see Figure 6B). This indicates that higher pH favors

the formation of Pb(II) during cathodic stripping. We conclude also that

$E^o_{Pb(IV)/Pb(III)} \ll E^o_{Pb(IV)/Pb(II)}$.

Not presented here is i_r-E_d data for 0.4 M and 0.8 M $HClO_4$. The height of ring current Peak d' is even lower and the peak potential is shifted less positive as the $HClO_4$ concentration is decreased. This is consistent with the observation that as pH is increased the deposition kinetics pass from kinetic control to transport control, see data for a Au electrode in Figure 4 of (1).

Effect of Pb(II) concentration   The effects of increasing the Pb(II) concentration in the range 0.01 - 0.15 M on the i_r-E_d curves for E_r = 0.20 V are depicted in Figure 6. The rate of PbO_2 formation is increased for higher $C^b_{Pb(II)}$ (1), so the cathodic ring Peak d' becomes more peak-like and the peak potential shifts to more negative values. Compared with Figure 1D, it is noted for higher values of $C^b_{Pb(II)}$ and pH that the height for Peak d' changes more quickly with scan number. It is noted also that whereas the disc Peak d increases for higher $C^b_{Pb(II)}$, ring Peak d' is virtually unchanged. Thus, the relative amount of soluble Pb(IV) produced decreases with increased $C^b_{Pb(II)}$.

The shape of the ring current Peak e' obtained on the negative scan for E_d from 1.3 V to 1.0 V changes dramatically with a change in $C^b_{Pb(II)}$. The anodic peak component (Peak e_a') becomes higher, broader, and shifted to the negative side with higher concentration of Pb(II), as shown in Figure 7 for E_r = 1.4 V. However, no attempt should be made here to compare the heights of Peaks e_a' in Figure 7 because of the cathodic component e_c'. If Pb(III) is considered as the product of partial reduction of $PbO_2(s)$ at the outermost layer of the oxide film, it

is understandable that for the thicker PbO$_2$(s) film more Pb(III) species

will be produced during stripping, as shown in Figure 7. Since PbO$_2$(s)

deposition occurs faster for higher values of $c^b_{Pb(II)}$ and pH, thicker

PbO$_2$(s) layers are formed for the same time interval of deposition and

more Pb(III) is detected.

Effect of scan interruption   When the scan of E_d was stopped at

1.8 V, it was observed that the ring Peak d' immediately dropped to

virtually zero, see Figure 1. For interruption of the positive scanning

at 1.5 V $<$ E_d $\ll$ 1.8 V, the ring current dropped more slowly.

Conversely, disc Wave d increased when the scan of E_d was interrupted at

1.8 V, which indicates an increasing rate of PbO$_2$(s) formation. These

observations are consistent with the conclusion that lesser quantities of

the soluble intermediate are swept away from the disc electrode when the

rate of PbO$_2$(s) deposition becomes fast under constant potential.

Effect of electrode material and electrode pretreatment   The

above results were all obtained after mechanical polishing of the Au

RRDE. If the electrode was pretreated chemically in a 1:1 H$_2$O$_2$/acetic

acid mixture, or 0.1 M KMnO$_4$ solution, similar i_r-E_d curves were

obtained. This is consistent with the general knowledge that these

pretreatment methods can remove PbO$_2$(s) and the ultra-thin Pb(II) film to

produce a clean Au surface (1).

The existence of soluble Pb(IV) detected during PbO$_2$(s) formation,

and both soluble Pb(III) and Pb(IV) during PbO$_2$(s) stripping, were also

apparent from i_r-E_d curves obtained at Pt ring-disc electrode. These

results were consistent with chronoamperometric data for the Pt-RDE.

Stability of the intermediate products   The soluble Pb(IV)

produced during PbO_2(s) nucleation and deposition is believed to be

unstable in aqueous non-complexing media (5). However, the stability can

be increased by addition of H_3PO_4. This has permitted the direct

detection of electrochemically prepared Pb(IV) species with normal

polarography (5). Similar results were observed in this work. DC

polarography was applied for analysis of acidic solutions of Pb(II)

following 20 - 30 cycles of deposition and dissolution at a large-area

Pt-screen electrode. No polarographic wave for a reducible species other

than Pb(II) was observed in the absence of H_3PO_4. However, a distinct

cathodic wave, concluded to correspond to the result of reduction of

Pb(IV), was observed preceding the cathodic wave for Pb(II) when H_3PO_4

was present in the solution during the deposition/dissolution cycles.

It was of interest then to study the effect of a higher stability of

the intermediate Pb(IV) on the nucleation and deposition of PbO_2(s).

Addition of H_3PO_4 was determined to prevent the further anodic deposition

of PbO_2(s), although already existent deposits were not chemically

dissolved.

Accumulation of dissolution products on Teflon   A dark brown film

accumulated on the Teflon shroud of the electrode during multiple cycles

of deposition (1.48 V) and stripping (0.3 V), as shown in Figure 8. The

film was determined to be an electronic conductor and was found to

contain lead, based on X-ray photoelectron spectroscopy (XPS). The film

appeared to be of approximately uniform thickness growing in a nearly concentric pin-wheel fashion with increasing cycle number. The radius of the accumulated film was increased for the same number of deposition/dissolution cycles by increasing the rotational velocity of the RDE.

Accumulation of the film occurred only with alternate anodic deposition and cathodic dissolution of $PbO_2(s)$ at constant potentials of 1.48 V and 0.3 V, respectively. No film was accumulated for continuous deposition at constant potential or under voltammetric control (i.e., cyclic scans of E_d) (see Figure 8A). There appear to be at least two possible explanations for the appearance of the film: i) Pb(III) and Pb(IV) produced during $PbO_2(s)$ dissolution undergo fast hydrolysis reactions to produce insoluble PbO_2 which then is adsorbed at the Teflon surface, and ii) the rapid dissolution of $PbO_2(s)$ following the potential step to 0.3 V results in undercutting of PbO_2 crystallites which then are transported radially along the surface of the RRDE and can adhere to the Teflon surface.

Conclusions

It is concluded that a soluble form of Pb(IV), probably associated with oxygen (e.g., PbO^{2+} or $Pb(OH)_2^{2+}$), is an intermediate product of the anodic nucleation and deposition of $PbO_2(s)$ from solutions of Pb(II) in $HClO_4$. The quantity of Pb(IV) detected is greatest during the induction period ($t < t_o$), when $i_d \simeq 0$ at freshly polished Au electrodes, and decreases substantially when the rate of deposition reaches a steady-state value ($i_d - i_{d,ss}$).

These observations are consistent with predictions made in (1) of a soluble intermediate to explain the effect of changes in rotational velocity on the induction period (t_o) at clean Au electrodes. Increased rotational velocity causes i_d to decrease, the quantity of soluble Pb(IV) detected to increase, and t_o to be increased. For high rotational velocity in 1.7 M $HClO_4$, virtually all Pb(IV) formed at the disc electrode is lost from the electrode surface by convective-diffusional transport. The long induction period is explained because the residence time of the soluble Pb(IV) at the disc surface is too short. The quantity of Pb(IV) detected is at a minimum for Pb(II) concentrations > ca. 0.1 M and $HClO_4$ concentrations < ca. 1 M, which correlates with conditions for a minimum value of t_o and the maximum rate of the deposition process (i.e., large $i_{d,ss}$).

It has been demonstrated (1) that evolution of O_2 is required to enable the anodic deposition of $PbO_2(s)$. It was demonstrated also that the induction period was short for surfaces at which $PbO_2(s)$ had previously been deposited and then stripped. An ultra-thin film of Pb(II) was concluded (1) to remain at the Au electrode surface following dissolution of $PbO_2(s)$ at 0.3 V which serves as an array of nucleation sites following oxidation to an ultra-thin film of Pb(IV) (probably PbO_2) with the step of potential from 0.3 V to the deposition value. Data obtained with the RRDE demonstrated a significantly lower quantity of soluble Pb(IV) being produced at the start of the induction period when the ultra-thin film was left intact following cathodic dissolution of bulk deposits of $PbO_2(s)$.

It also is concluded that very small quantities of soluble Pb(III) and Pb(IV) are produced with the onset of cathodic dissolution of $PbO_2(s)$ for a negative potential scan. Conditions which favor the rapid deposition of $PbO_2(s)$ favor the production of soluble Pb(III) over Pb(IV) during the dissolution process.

References

1. Chang, H.; Johnson, D.C. J. Electrochem. Soc. 1989, 136, 17; Chapter 2, This Thesis.

2. Hameenoja, E.; Laitinen, T.; Sundholm, G. Electrochim. Acta 1987, 32, 187.

3. Skyllas-Kazacos, M. J. Power Sources 1984, 13, 55.

4. Skyllas-Kazacos, M. J. Electrochem. Soc. 1981, 128, 817.

5. Amile, R. F.; Berger, T. A.; J. Electroanal. Chem. 1972, 36, 427.

6. Bode, H.; Voss, E. Electrochim. Acta 1962, 6, 1.

7. Laitinen, H. A.; Watkins, N. H. J. Electrochem. Soc. 1976, 123, 804.

8. Pohl, J. P.; Scholz, W. J. Power Sources 1985, 16, 293.

9. Volgina, V. A.; Nechaev, E. A.; Bakhchisaraits'yan, N. G. Sov. Electrochem. 1973, 9, 984.

10. Littauer, E. E.; Schreir, L. L. Electrochim. Acta 1967, 12, 465

11. Pohl, J. P.; Rickert, H. Power Sources 1976, 6, 59.

12. Reutschi, P. J. Power Sources 1977/78, 2, 3.

13. Takehara, Z.; Kanamura, K. Electrochim. Acta 1984, 29, 1643.

14. Ellis, S. R.; Hampson, N. A.; Wilkinson, F.; Ball, M. C. J. Electrochem. Soc. 1987, 134, 2388.

15. Albery, W. J.; Bruckenstein, S. Trans. Faraday Soc. 1966, 62, 1920.

16. Cadle, S. H.; Bruckenstein, S. Anal. Chem. 1974, 46, 16.

17. Albery, W. J.; Hitchman, M. L. "Ring-disc Electrodes"; Clarendon Press: Oxford, 1971.

18. Kozawa, A. In "Batteries"; Vol. 1, Kordesch, K. V., Ed.; M. Dekker: New York, 1974; p. 387.

19. Yeo, I.-H. <u>Ph.D.</u> <u>Dissertation</u>, Iowa State University, Ames, Iowa, 1987.
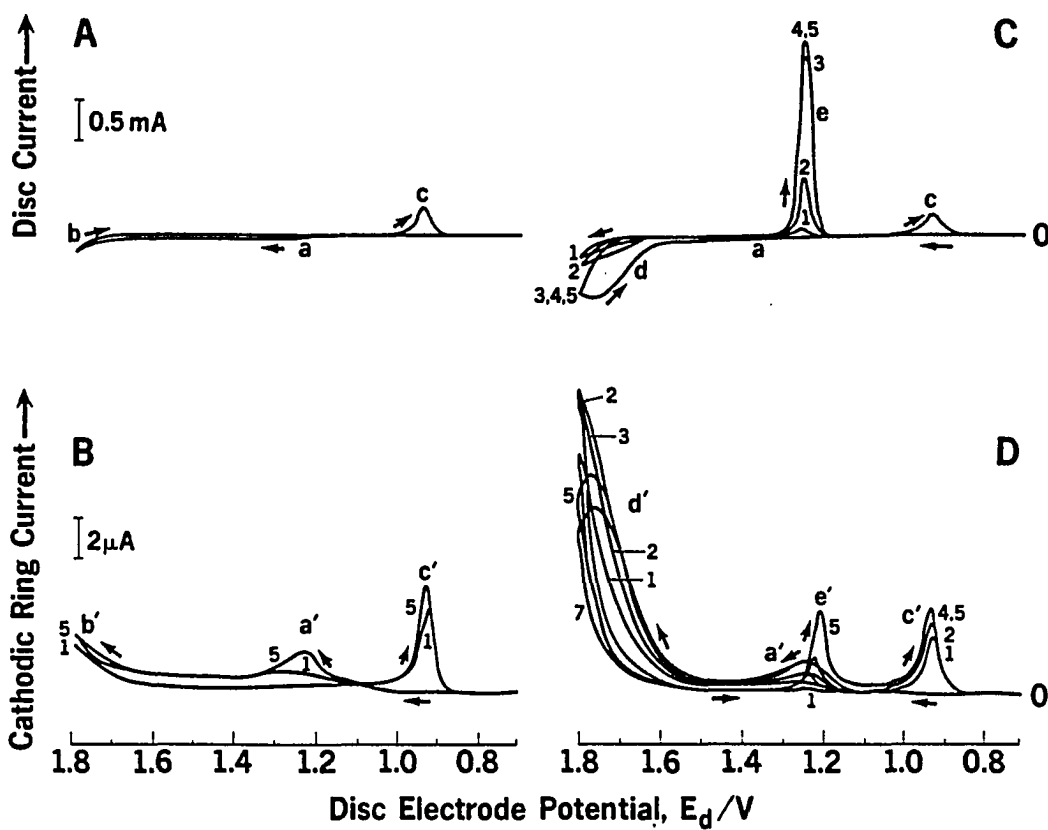
Figure 1. Comparison of Consecutive i_r-E_d and i_d-E_d curves

Conditions: $E_r = 0.2$ V, $\emptyset = 40$ mV s^{-1},
$w = 900$ rev min^{-1}, 1.70 M HClO$_4$

Curves: (A and B) blank solutions,
(C and D) 0.010 M Pb(II);
(A and C) i_d-E_d,
(B and D) i_r-E_d

Scan number: indicated in figure
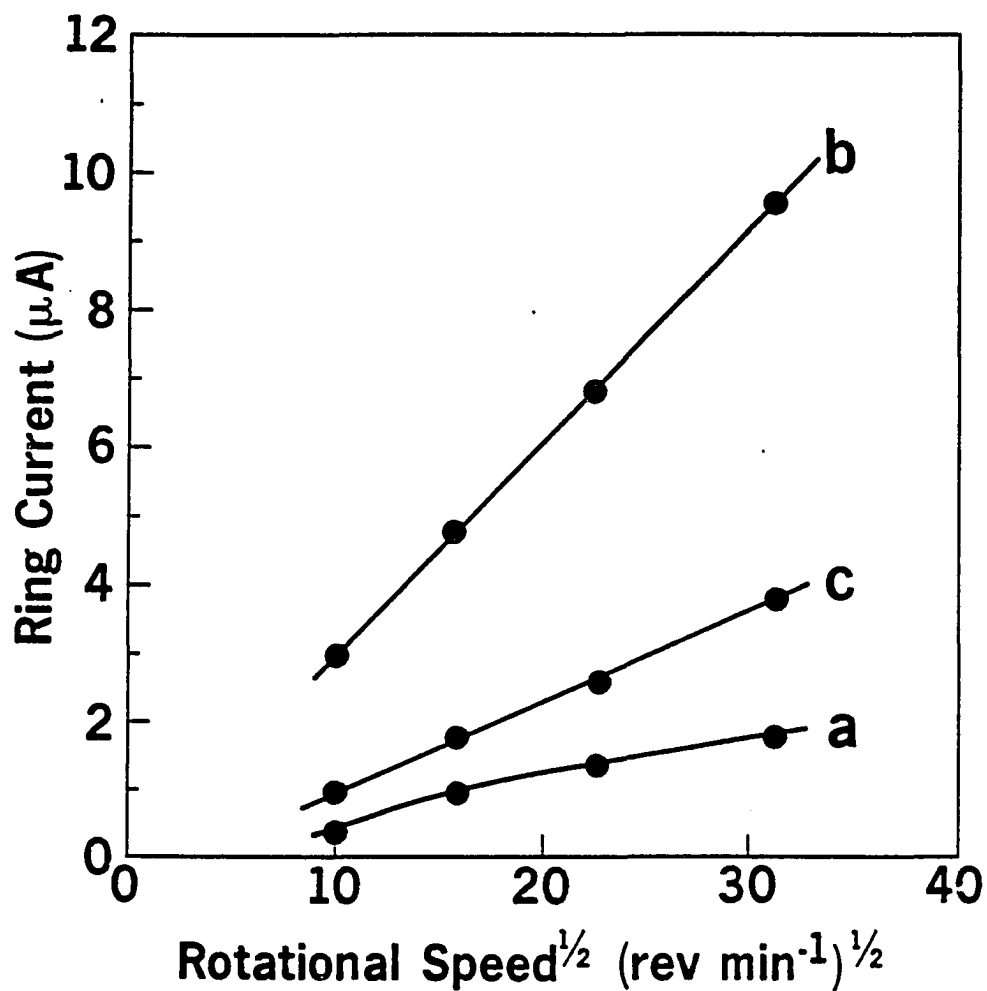
Figure 2. Effect of rotational velocity on the ring current peaks for
Curve D in Figure 1

Conditions: 0.010 M Pb(II), 1.70 M $HClO_4$,
others as given in Figure 1

Curves: (a) Peak a' obtained at E_d - 1.1 - 1.3 V
on positive scan,
(b) Peak d' obtained at E_d - 1.7 - 1.8 V
on positive scan,
(c) Peak e' obtained at E_d - 1.3 - 1.1 V
on negative scan
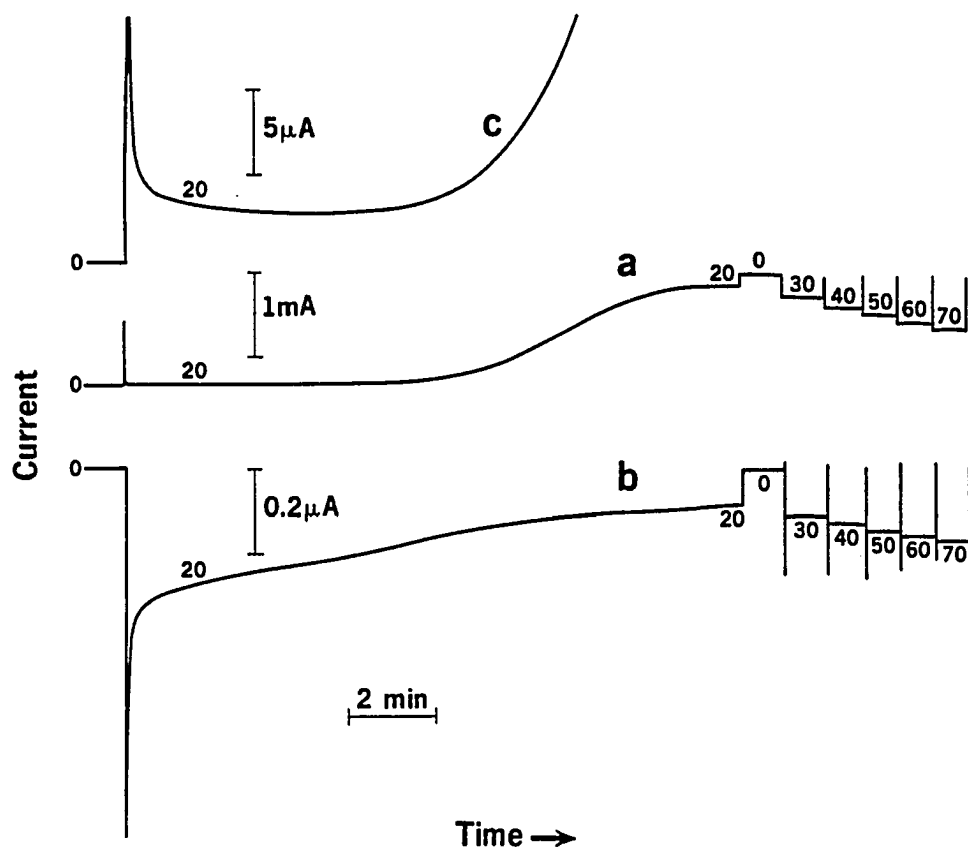
Figure 3. Chronoamperometric response at RRDE

Conditions: 0.20 M Pb(II), 1.40 M $HClO_4$
E_r — 0.20 V, E_d — 1.48 V, $w^{1/2}$
indicated as (rev min^{-1})

Curves: (a) i_d-t, (b) i_r-t, and
(c) i_d-t at higher current sensitivity
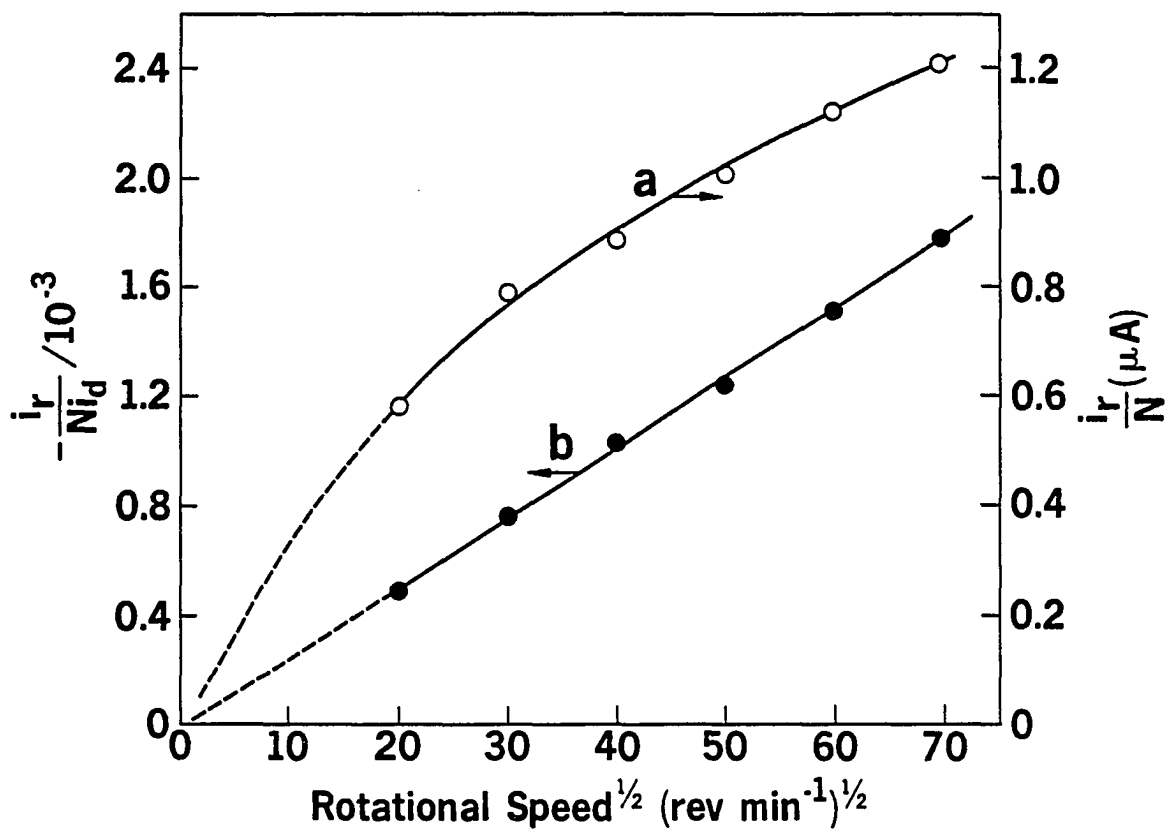
Figure 4. Plots of i_r/N and $-i_r/Ni_d$ vs. $w^{1/2}$

Conditions: as given in Figure 3

Curves: (a) i_r/N, (b) $-i_r/Ni_d$
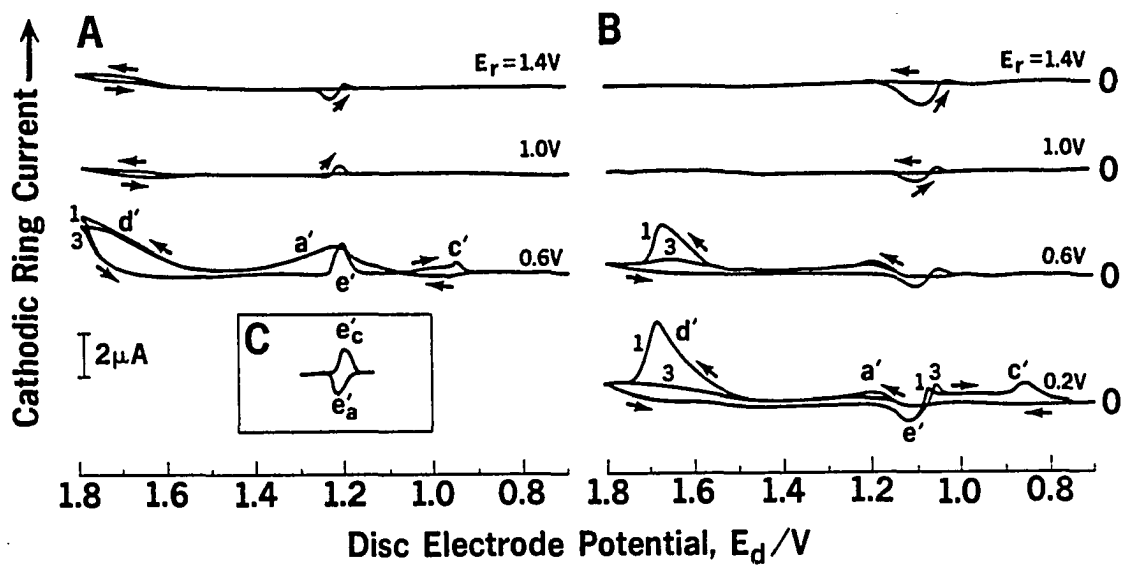
Figure 5. Effect of E_r and $HClO_4$ concentration on i_r-E_d curves

Conditions: E_r as marked (V); others as given in Figure 1

$HClO_4$ concentration (M): (A) 1.70, (B) 1.30

Inset: Estimated components of Peak e'
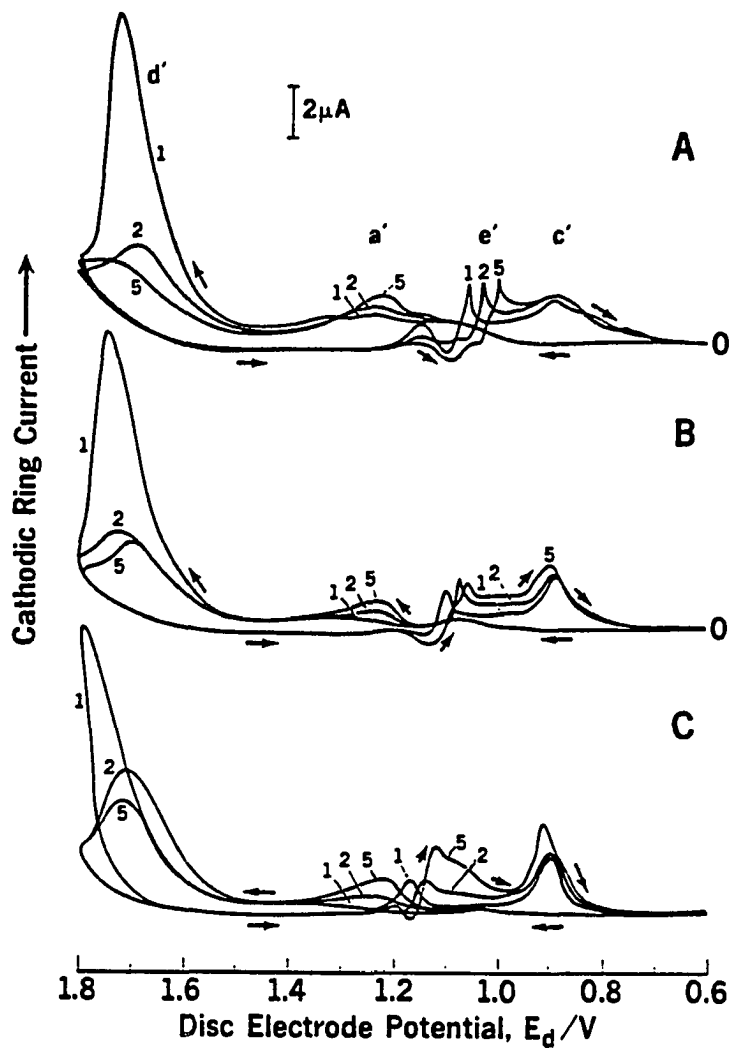
Figure 6. Effect of Pb(II) concentration on i_r-E_d curves at $E_r = 0.2$ V

Conditions: 1.70 M $HClO_4$, other as given in Figure 1

Pb(II) concentration (M): (A) 0.15, (B) 0.10, (C) 0.050
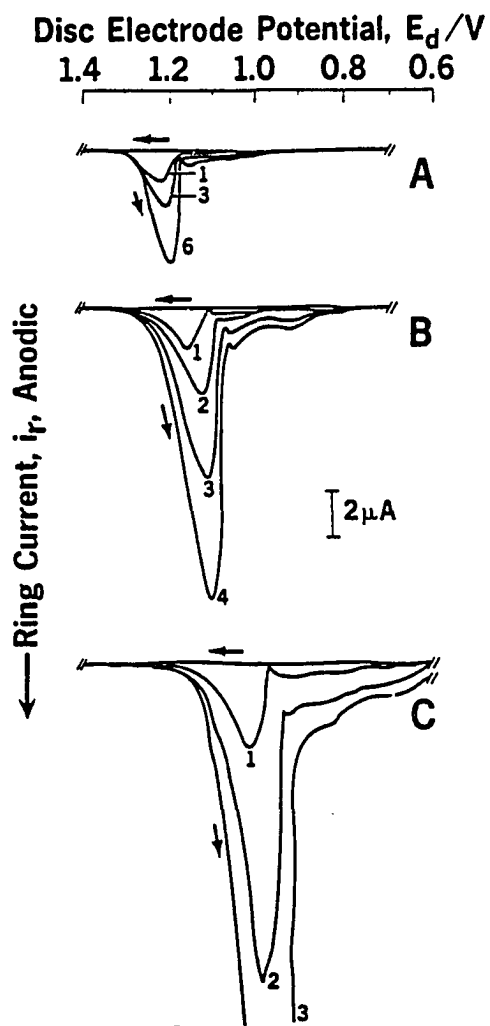
Figure 7. Effect of Pb(II) concentration on i_r-E_d curves
at E_r - 1.4 V for E_d - 1.4 - 0.6 V

Conditions: 1.30 M $HClO_4$, 0.40 M $NaClO_4$,
other as given in Figure 1

Pb(II) concentration (M): (A) 0.050, (B) 0.010, (C) 0.15
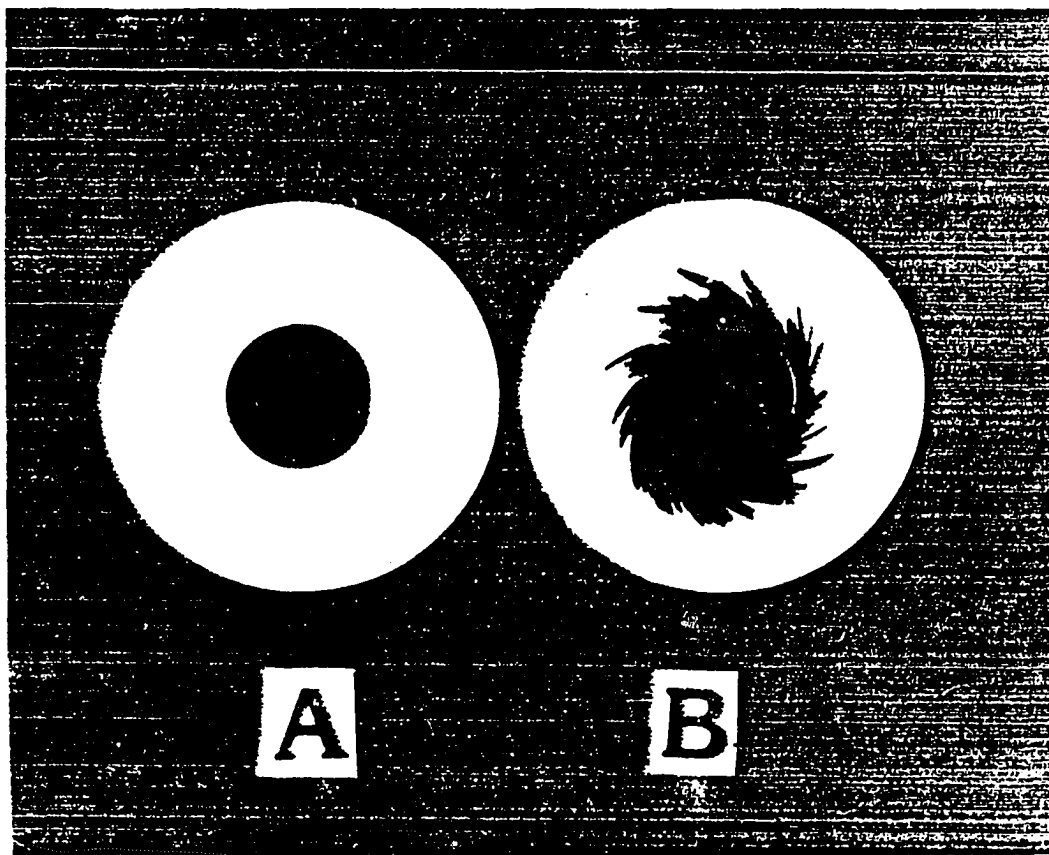
Figure 8. Photograph of PbO_2 film on the Au RDE

Deposition conditions: 0.010 M Pb(II), 0.8 M $HClO_4$,
w = 400 rev min^{-1}

Preparation: (A) continuous deposition,
(B) 15 cycles of deposition/stripping
at constant potentials

III. IN-SITU ELECTROCATALYSIS AND CHARACTERIZATION OF PURE AND BISMUTH-MODIFIED LEAD DIOXIDE

A. Electrocatalysis During in-situ Electrodeposition of Pure and Bismuth-Modified Lead Dioxide in Acidic Media[1]

"The study of chemically modified electrodes has expanded enormously since their disclosure twelve years ago. Despite the fascinating and novel results that have been obtained with them, no practical applications are in sight and will not be until their durability extends beyond the time necessary for writing another research grant application."

-M. M. Baizer,
Pure App. Chem. 1986, 58, 889.

---

[1]To be submitted to J. Electrochem. Soc.

Abstract

Oxidation of Mn^{2+} to MnO_4^- in strongly acidic media does not proceed readily at conventional anodes, e.g., Pt, Au, GC, and PbO_2, apparently due to the deposition of an electroinactive MnO_2 film. However, this reaction can occur under mass-transport control at the PbO_2 deposited in-situ in a solution containing both the Mn^{2+} and Pb^{2+}. The continuous deposition of PbO_2 not only produces an intermediate Pb(IV) species that has strong oxidizing power, but also constantly renews the electrode surface, thereby preventing the accumulation of MnO_2. Many other reactions also are catalyzed during the in-situ deposition of PbO_2. The interactions between the spontaneous electrolysis and electrodeposition also were studied.

Bismuth-doped PbO_2 also can be deposited in-situ in a sample solution containing Bi^{3+} and Pb^{2+}. Pure PbO_2 can be modified in-situ by Bi^{3+} added to the electrolysis solution. In both cases, the existence of Bi^{3+} in the solution prevents the deactivation of the oxide electrode and, thus, ensures the catalytic activity and stability.

Chronoamperometry, voltammetry, flow-injection analysis, visible spectrophotometry, and scanning electron microscopy were used to characterize the in-situ electrodeposited metal oxides and their electrocatalysis.

Introduction

Fouling of solid electrodes occurs frequently due to the adsorption of reactants and/or products, or the self-destruction of the surface-bonded catalysts (1,2). This phenomenon leads to short lifetime and low

reproducibility for the electrodes. Until now, enhancing the stability of the solid electrodes in both electrosynthetic and electroanalytical devices has been an unfinished battle. A recent effort is the so-called "in-situ electrodeposition of catalysts" for some cathodic processes (3-4). By adding Ni^{2+} (3) or Cu^{2+} (4) to the electrolyte, the simultaneous deposition of Ni or Cu "leads to reproducible surfaces of defined structure and properties" (3). This scheme of surface renewal was applied for electrocatalytic hydrogenation of organic molecules at nickel (3), and reduction of carbon dioxide to methane and ethane at copper (4). In-situ deposition of catalyst on mercury by formation of amalgam also has been used for organic electroreduction (5-7). The electroreduction of dimethyl pyrrolidinium at mercury forms an insoluble amalgam which acts as a regenerable catalyst to reduce a variety of organic substances in the solution.

A similar concept has existed for anodic processes. For example, a nickel(III) oxide hydroxide electrode (NiOOH) is spontaneously formed during anodic polarization of a nickel electrode in alkaline media (8-12). This electrode is widely used for many electrooxidation processes as reviewed in (13). It has been concluded that NiOOH is the electrocatalyst which is continuously formed at the electrode surface. The reactivity of the electrode is similar to that of nickel peroxide as a chemical oxidant in homogeneous solutions. Most of the organic oxidation reactions occur at the same potential corresponding to the anodic transition of Ni(II) $\rightarrow$ Ni(III). The same also holds for silver(I/II) oxide (14-16) and cobalt(II/III) oxide electrodes (17). The

in-situ formed nickel oxide electrodes also have been used as detectors for a variety of organic substances, e.g., carbohydrates, amino acids, and proteins (18-22). By adding a small amount of Ni^{2+} to the solution, the continuous deposition of nickel oxide not only renews the catalytic surface but also ensures the existence of high-oxidation-state nickel at the electrode surface. This detection technique has found applications in flow-injection analysis (FIA) and liquid chromatography with electrochemical detection (LC/EC). In-situ anodized PbO_2 formed from a lead electrode in sulfuric acid media also has been used in electrosynthesis (23-24).

In this paper, electrocatalytic phenomena are described for in-situ deposited pure and chemically modified PbO_2 electrodes. The purposes of this study are five-fold:

(1) It has been known from our previous work (25,26) that transient Pb(IV) species (both adsorbed and soluble), possibly associated with oxygen as PbO^{2+} or $Pb(OH)_2^{2+}$, are generated during the nucleation and electrodeposition of PbO_2 from a Pb^{2+} solution. These unstable Pb(IV) species are concluded to have strong oxidizing power. Therefore, as with the other in-situ deposited metal oxide electrodes (8-24), it is interesting and desirable to determine whether there is any catalytic enhancement of activity at in-situ electrodeposited PbO_2 in a solution containing both analyte and Pb^{2+}.

(2) The incorporation of an oxygen-transfer (O-t) mediator, e.g., Bi^{3+}, into electrodeposited PbO_2 results in Bi-doped PbO_2 (Bi-PbO_2) electrodes that selectively catalyze many anodic O-t reactions (27-32). Thus, it is of more importance to test the catalytic activities of in-situ deposited Bi-PbO_2 by the presence of Bi^{3+} and Pb^{2+} simultaneously or Bi^{3+} alone at PbO_2 electrodes.

(3) When the reactant for electrolysis and the metal ion(s) for metal oxide deposition exist in the same solution, two kinds of interactions between their respective electrode processes may occur: the alteration of the rate of the electrodeposition of metal oxides by the co-existing analytes and the enhancement of the oxidation rate of analytes caused by the in-situ electrodeposition of metal oxides. These interactions are also the subjects of study in this paper.

(4) It was observed that the $Bi-PbO_2$ electrode suffered from a short lifetime for the oxidation of Mn^{2+} to MnO_4^- (33). Thus, maintaining the catalytic activity for the electrode becomes the key to its potential applications. It is hoped that the in-situ electrodeposited metal oxide electrodes have higher stability and longer lifetime caused by the continuous renewal of the surface catalytic sites. The cause for the fouling of the pre-deposited $Bi-PbO_2$ electrodes is studied as well.

(5) Flow-injection techniques (34-36) have become very popular in recent years in chemical analysis because of their many unique characteristics, e.g., high sample throughput and small sample volume. Whereas flow-through electrochemical cells have become important to electroanalysis, electrochemical waste treatment, electrosynthesis, and electrowinning of metals (37-40), we have found no reports for application of flow-injection electrochemistry in electrocatalytic research. Here, we describe an example of the application of flow-injection with electrochemical detector (FI-EC) to demonstrate the electrocatalysis for anodic O-t reactions at the in-situ deposited PbO_2.

Experimental

The apparatus for hydrodynamic voltammetry and chronoamperometry was described earlier (25).

The FI-EC system consisted of a model LDC mini-pump (flow rate: 9.6 ml min^{-1}), a 50-μl sample injector, and a home-made flow-through cell with a Au wire electrode (ca. 0.9 mm^2). A model 174A Polarographic Analyzer (EG&G Princeton Applied Research, Princeton, NJ) operated in the sampled dc mode (time constant: 0.5 sec) was used as the potentiostat. The pulsed potential waveform was generated by a model 175 Universal Programmer (EG&G Princeton Applied Research).

The flow-through spectrometric detector for electrolytic products consisted of a 30-ml electrolytic cell with a stirring bar, a Gilson Minipulse 2 peristalic pump, a 1.0-ml Fisher flow-through spectrophoto-metric cell (10 mm pathlength), and a Perkin-Elmer 320 UV-visible spectrophotometer. The dead volume between the two cells was ca. 6 ml. The flow rate was 6 ml min^{-1}. A Pt screen electrode was used as the substrate electrode for this experiment.

The scanning electron microscopy (SEM) and X-ray energy-dispersive spectroscopy (EDS) were taken with a model JSM-U3 microscope (JEOL). Detachable gold RDE for SEM was made by soldering a Au disc sheet onto a stainless steel tip. The deposition of metal oxides was done under the optimal conditions determined previously (25).

All chemicals were reagent grade and dissolved by deionized water. The Pb^{2+} and Bi^{3+} solutions were prepared from their nitrate salts. Solutions were prepared with 1.0 M HClO$_4$.

In-situ electrodeposition of PbO_2

Chronoamperometry   Shown in Figure 1 are chronoamperograms for the oxidation of 10 mM Mn^{2+} at a PbO_2-coated Au RDE (Curve A), the deposition of PbO_2 on a Au RDE from 10 mM Pb^{2+} (Curve B), and the oxidation of 10 mM Mn^{2+} in the presence of 10 mM Pb^{2+} (Curve C). To facilitate the discussion, the values of the steady-state current for Curves A, B, C are symbolized as i_A, i_L, and i_{L+A}, respectively. The symbol i_{L+A} represents the current for the mixture of Pb^{2+} (L), and analyte (A) which is Mn^{2+} in this case; i_L represents the current for Pb^{2+} only; and i_A represents the current for analyte only. Furthermore, $\Delta i = i_{L+A} - i_L$ is defined as the net current for the oxidation of A in the presence of Pb^{2+}, based on the assumption that i_L is not changed by the addition of the analyte. The assumption is reasonable because i_L increases linearly with $w^{1/2}$ (see Figure B). Any additional current resulting from the addition of other substances (i.e., Δi) is concluded to be the result of the oxidation of the analyte.

The value of i_A for Mn^{2+} was virtually zero, as shown in Figure 1A, which means that the oxidation of Mn^{2+} is very slow at the pre-deposited PbO_2 electrode. This observation is consistent with the previous result (31). The addition of Pb^{2+} to the solution greatly enhanced the rate of Mn^{2+} oxidation as shown by $\Delta i \gg i_A$ in Figure 1C. In this case, the solution became pink rapidly due to the color of the oxidation product MnO_4^-. The value of i_{L+A} in Figure 1C increased with increased rotational velocity (w). After the correction for the PbO_2 deposition current, Δi also increased with increased $w^{1/2}$ as shown in Figure 2,

although the Δi-$w^{1/2}$ plot is not as linear as observed for the pre-deposited Bi-PbO_2 electrodes (32). It is concluded that that the oxidation of Mn^{2+} at in-situ deposited PbO_2 is under virtual mass-transport control. The value of Δi also increased with increased Pb^{2+} concentration, i.e., faster rate of PbO_2 deposition, as depicted in Figure 2. It is concluded that the oxidation rate at in-situ deposited PbO_2 is proportional to the rate of PbO_2 deposition.

Also studied were the effects of the co-existing Pb^{2+} ions on the oxidation of other substances. Figure 3 shows the Δi-$w^{1/2}$ plots for some compounds most of which have low reactivities at the pre-deposited PbO_2 electrodes. It is readily apparent that $\Delta i \gg 0$ for all compounds. The value of Δi increased linearly with $w^{1/2}$ for thiourea, thiocyanate, 2-thiophene carboxylic acid (TPCA), and hydroquinone, but not linearly for L-cysteine and 2-mercaptoethanesulfonic anion ($HSCH_2CH_2SO_3^-$). As for L-cystine, Δi decreased slightly with $w^{1/2}$. No effects of co-existing Pb^{2+} were observed on the oxidation of chromium(III) and dimethyl sulfoxide (DMSO), i.e., $\Delta i \simeq 0$.

It is concluded from the above results that the in-situ deposited PbO_2 has higher catalytic activity for some O-transfer reactions than the pre-deposited PbO_2. The catalytic activity of the PbO_2 electrode prepared from an analyte-containing solution, e.g., after the study in Figure 1C, was compared to that of the pre-deposited PbO_2. No difference was observed for a number of reactions, which indicates no activity enhancement at the in-situ deposited PbO_2 without co-existing Pb^{2+}. Therefore, the enhanced catalytic activity as shown in Figure 1C

is not due to a unique surface structure of the in-situ deposited PbO_2. The SEM micrograph also showed that there was little difference in morphology between the pre-deposited PbO_2 and the in-situ deposited PbO_2.

Effects of co-existing analytes on the rate of PbO_2 nucleation and electrodeposition   Listed in Table 1 are the values of t_o, t_1, and S (for definitions, see Ref. 25) for the deposition of PbO_2 at a freshly polished Au RDE from Pb^{2+} solutions with co-existing analytes. The co-existence of organic substances oxidizible at the in-situ deposited PbO_2 greatly increased the values of t_o and t_1, and decreased the values of S (except for hydroquinone), indicating a decreased rate of PbO_2 nucleation and deposition. This is probably due to the consumption of the intermediate Pb(IV) species by the analyte during the nucleation process. A similar effect was observed for increased rates of mass transport at RDE (26). However, the existence of Mn^{2+}, Cr^{3+} or DMSO did not affect the i-t curves for the PbO_2 deposition, as the data for Mn^{2+} is shown in Figure 1C. This is quite understandable for Cr^{3+} and DMSO since they are not readily oxidizable at the in-situ deposited PbO_2.

Cyclic voltammetry   The catalytic activity of the in-situ deposited PbO_2 was demonstrated also by cyclic voltammetry, as shown in Figure 4. Compared with the current for PbO_2 deposition (Curve a), a large net current was observed when TPCA was present (Curve b), while TPCA did not show any i-E wave at the pre-deposited PbO_2. At the same current scale, the anodic current for Curve b in the positive scan arose at less positive potential values than for Curve a, indicating the

Table 1. Effects of Co-existing Analytes on the Kinetics of PbO_2 Deposition at Au RDE

Conditions: 10 mM Pb^{2+} and 10 mM analyte, 1.0 M $HClO_4$; 400 rev min^{-1}; E - 1.7 V

analyte	t_o (min)	t_1 (min)	S (mA/min)
-	0.08	0.16	16.5
thiourea	5.45	1.89	6.77
SCN^-	2.71	2.95	4.41
hydroquinone	0.15	0.25	24.2
TPCA	7.29	2.30	4.52
EDTA	6.23	2.50	4.00
$HSCH_2CH_2SO_3^-$	2.43	2.38	4.23
L-cysteine	3.71	1.93	4.77
L-cystine	1.55	0.81	8.15
Mn^{2+}	0.08	0.18	15
Cr^{3+}	0.07	0.21	12.9
DMSO	0.08	0.17	17

catalytic effect of the initial PbO_2 nuclei. This observation corresponds to the detection of the highest concentration of soluble Pb(IV) species in the induction period (26). In the 2nd scan, the Au RDE had already been covered by PbO_2, so the current for TPCA arose at much less positive potential values and followed the trace for the reverse scan in the 1st cycle. A large difference existed between the steady-state i-E curves in the presence and absence of TPCA.

Also shown in Figure 4 is the i-E for DMSO (Curve c). Only a small current increase was observed at very high potential values (1.75 - 1.85 V), which is consistent with the chronoamperometric data.

Voltammograms similar to those for TPCA were obtained for oxidation of Mn^{2+} to MnO_4^- at the in-situ deposited PbO_2 with different substrates, as shown in Figure 5. The dashed Curves A, B, C represent the deposition of PbO_2 at GC, Au and Pt, respectively (25). The i-E curves shifted to less positive potentials as a result of the addition of Mn^{2+} (solid lines), with generation of MnO_4^- as indicated by the purple color. The magnitude of the shift in potential in the positive scan had the same order of oxygen-evolution overpotential and the potential for PbO_2 deposition at the substrates, i.e., GC > Au > Pt. This result is concluded to be evidence for the correlation between the oxygen evolution and O-transfer reaction (25). The current in the negative scans fell to zero in the same potential range for the three substrates, indicating the coverage of the substrate by PbO_2. It is noticeable that the potential value at the same current in the negative scan for oxidation of Mn^{2+} in Figure 5 is virtually the same as that for TPCA in Figure 4, indicating

the same rate controlling step in the these anodic processes. The large

potential difference between the solid and dashed curve in the positive

scan, especially for GC, demonstrates again the catalytic activities of

the in-situ deposited PbO_2 at a potential region in which no apparent

deposition current is monitored, yet a small amount of soluble

intermediate Pb(IV) species is generated (26). Therefore, it is

concluded that the catalytic activity of the in-situ deposited PbO_2

electrode is the result of the formation of the intermediate Pb(IV)

species.

Deposition of metal oxide-coated Au electrode in the flow-through

system The catalytic activities of the in-situ deposited PbO_2

electrode also can be demonstrated with a FI-EC system. The deposition

of PbO_2 film in a flow-through cell was done either with continuous flow

of a Pb^{2+} solution or with a series of injections of the solution. Both

cases are illustrated by the i-t curves in Figure 6. The shape of the i-

t Curve A for continuous flow and the shape formed by the peaks of Curve

B are similar to the chronoamperometric responses for PbO_2 deposition at

a RDE in a conventional cell (25). The increase of peak height in Figure

6B with the first 25 injections clearly demonstrates the catalytic effect

of PbO_2 deposit from the proceeding injection on the deposition current

in the induction period. A similar phenomenon was observed by

consecutive cyclic potential scans (25). It is concluded that the rate

of PbO_2 deposition is faster on PbO_2 than on Au.

While it takes about 10-30 minutes to prepare a PbO_2 coated RDE in a

conventional cell (30-32), it takes less than 3 minutes in the flow-

through system because of the smaller electrode area. The oxide films in the flow-through cell can be removed easily by electrochemical stripping or chemical flush without dismounting the cell.

Flow-injection analysis with amperometric detection   The activities of the oxide electrodes in the FI-EC system can be tested immediately following the preparation because of the convenience in medium switching. The oxidation current for some sulfur-compounds and Mn^{2+} at PbO_2 electrode are shown in Figure 7B as compared to those at bare Au electrode (Figure 7A). Clearly, the peak heights at the PbO_2 are much higher than those at the Au, indicating the electrocatalysis of PbO_2 to some O-t reactions (29,30).

Shown in Figure 7C are the results when 10 mM Pb^{2+} is present in the 10 mM sample solutions. The peak heights in Figure 7C are larger than the sum of those in Figure 7B and the average value of maximum peak heights for 10 mM Pb^{2+} in Figure 6B. This is concluded to be due to the enhanced catalytic activity as a result of the co-existing Pb^{2+}. The reproducibility of the peak heights also was improved by the co-existing Pb^{2+}. As shown in Figure 7, the peak heights for TPCA decreased with injection number on both the Au and PbO_2 electrodes, but were relatively constant if Pb^{2+} was present in the solution.

An alternative way to use the in-situ deposited PbO_2 in the FI-EC system is to add a small amount of Pb^{2+}, e.g., 1 mM, in the eluent instead of the sample solution. A technique similar to pulsed amperometric detection (PAD) (29) was used to avoid the over-accumulation of PbO_2 on the Au. With a two-step potential waveform (1.6 V for 250

msec and 0.7 V for 200 msec), the electrode was subjected to alternate deposition and stripping, while the current was sampled during the deposition at 1.6 V. The results proved that the existence of Pb^{2+} in the eluent also increased the current for oxidation of many substances. The peak heights increased with the increased concentration of $HSCH_2CH_2SO_3^-$ from 0.4 to 2.0 mM.

Spectrophotometry   The electrochemical methods have their limitations in studying electrocatalytic reactions at the in-situ deposited electrodes. For instance, when Δi was compared with i_A, a assumption was made that the co-existing analyte and its oxidation did not affect the i_L component of the i_{L+A}, which might not always be true. Therefore, a separate method is needed to monitor the rate of either PbO_2 formation or analyte oxidation. Since MnO_4^- has well-characterized and strong absorbance (A) of visible light (λ_{max} - 525 nm), a spectrophotometer can be used to monitor the rate of MnO_4^- generation and the final MnO_4^- concentration of the electrolysis process. The absorbance (A) can be measured either vs. wavelength (λ) or vs. time (t). A closed-cycle flow-through system was set up, consisting of an electrolytic cell and a spectrophotometric cell connected by a pump. The delaying time between the two cells was about 1 min, which is small enough compared with the time scale used for electrolysis.

In Figure 8A are the A-t curves recorded at λ - 525 nm (ε - 2200 cm/M) for five electrode/solution combinations. Curve e shows that no MnO_4^- is produced at PbO_2-coated Pt electrode at 1.7 V in the electrolytic solution containing only Mn^{2+}. Some absorption was observed

following the electrolysis of Mn^{2+} at bare Pt (see Curve d); however, the color of the resultant solution appeared to be different from that of MnO_4^-. The increase of absorbance with time in this case lasted for less than 0.5 min, indicating rapid cessation of the electrode reaction, probably due to surface fouling. The meaning of these results will be discussed in a later section. When Pb^{2+} was present, the absorbance increased linearly and rapidly with time (Curve a and b). Disconnection of electrode potential stopped the growth of absorbance, indicating the stop of the MnO_4^- production. The higher the Pb^{2+} concentration, the larger was the slope of the A-t curve, i.e., the faster is the MnO_4^- generation. This is in accordance with previous chronoamperometric results (see Figure 2). Curve b in Figure 8A represents the generation of MnO_4^- in the presence of both Pb^{2+} and Bi^{3+}, as is discussed later.

Curve a in Figure 8B is the spectrum (A-λ) for MnO_4^- prepared by dissolution of $KMnO_4$, which is consistent with the literature data (41). Curve b is the spectrum for the product solution after electrolysis of 10 mM Mn^{2+} at an in-situ deposited PbO_2 electrode. From the resemblance of Curves a and b, it is concluded that the oxidation product for Mn^{2+} is indeed MnO_4^-. Curve d in Figure 8B is the spectrum for the product solution for Curve d in Figure 8A. Thus, the oxidation product at the bare Pt electrode without co-existing Pb^{2+} is not totally MnO_4^-. It is suspected that $MnO_2(s)$ together with some Mn^{3+} and a very small amount of MnO_4^- are produced in this case. Brown MnO_2 precipitate was observed at the electrode and on the inner wall of the electrolysis cell.

In-situ modification of PbO_2 with Bi^{3+}

In-situ modification of PbO_2 with Bi^{3+} can be done in three ways, as discussed in the following sections. Comparison of the resultant Bi-modified PbO_2 electrodes derived from these three methods is expected to give great insight into the mechanism of electrocatalysis at the Bi-modified PbO_2.

Electrocatalysis with Bi^{3+} and Pb^{2+} co-existing in the solution

Bismuth-doped PbO_2 can be deposited in-situ from a sample solution containing Pb^{2+} and Bi^{3+}. The catalytic activity of such an electrode at a GC substrate was demonstrated by the cyclic voltammograms in Figure 9 obtained from a solution of 10 mM Mn^{2+}, 10 mM Pb^{2+}, and 9 mM Bi^{3+}. Compared with those in Figure 4, an even higher current was observed for oxidation of Mn^{2+} to MnO_4^- when 9 mM Bi^{3+} was added in addition to 10 mM Pb^{2+}. Since the co-existing Bi^{3+} does not contribute directly to the total current (42), this increased current is concluded to be due to the further increased catalytic activity for Mn^{2+} oxidation as a result of the Bi^{3+}. Again, the catalytic current arose before the deposition current, which proves the catalytic activity of the initial Bi-doped PbO_2 nuclei. Voltammograms similar to those in Figure 9 also were obtained at Au and Pt electrodes for oxidation of TPCA.

The generation of MnO_4^- from a solution containing 10 mM Mn^{2+} and a small amount of Pb^{2+} and Bi^{3+} also was shown by the A-t response (Curve c) in Figure 8A and the absorbance curve (c) in Figure 8B. It was noticed that A increased with time for about 2 min and then stopped. Thus, fouling of the electrode is concluded still to occur at very low

concentration of co-existing Pb^{2+} and Bi^{3+}.

Electrocatalysis at Bi-doped PbO_2 with Bi^{3+} co-existing in the solution   The oxidation of Mn^{2+} at the Bi-doped PbO_2 electrode was studied with chronoamperometry, as shown in Figure 10. A large current for $Mn^{2+} \rightarrow MnO_4^-$ was observed immediately after the application of potential at a $Bi-PbO_2$ RDE without the presence of Pb^{2+} or Bi^{3+} (Curve a). This observation demonstrates the enhancement in catalytic activity by incorporation of Bi(III) into the PbO_2 matrix and is consistent with the previous results (31-32). However, this large current was not stable for longer than 3 min, after which the current fell gradually to zero. The transition time for the total loss of the electrode activity intended to increase slightly with the increased Bi/Pb ratio in the mixed oxide determined by the Bi^{3+} and Pb^{2+} concentration ratio in the deposition solution. Hence, it is concluded that the lifetime of Bi-doped PbO_2 electrodes for the electrolytic generation of MnO_4^- in acidic media is not long enough for practical applications. However, the addition of Bi^{3+} to the solution greatly enhanced the stability of the current (Curve b and c). The lifetime of the electrode increased with increased Bi^{3+} concentration. In effect, when the amount of Bi^{3+} was high enough, the ultimate lifetime of the electrode was determined by the lifetime of MnO_4^- in the acidic solution. Decomposition of MnO_4^- occurs in acidic media to MnO_2 (41) that can precipitate at the electrode surface and foul the electrode. This phenomenon will be discussed further in the next section.

Also shown in Figure 10 is the oxidation of DMSO at the $Bi-PbO_2$

electrode (Curve d). It is apparent that the oxidation current is very stable even without the Bi^{3+} in the solution. Electrolysis in a DMSO solution at a pre-deposited $Bi-PbO_2$ electrode did not result in electrode fouling during a 3-hr test period. It is, thus, concluded that the sole oxidation product of DMSO, dimethyl sulfone ($DMSO_2$) (25), does not foul the electrode.

Deactivation mechanism of $Bi-PbO_2$ for Mn^{2+} oxidation   At first sight, the activity loss seemed to be related to the gradual dissolution of bismuth ions from the $Bi-PbO_2$, as a trace amount of Bi^{3+} was detected with differential pulse polarography in a Mn^{2+} solution after electrolysis at a $Bi-PbO_2$ electrode (36). However, this argument cannot explain the stable activity of the same electrode for DMSO.

During the electrolysis in the Mn^{2+} solution, the color of the $Bi-PbO_2$ film changed from gray/black (depending on the thickness) to brown, and some brown MnO_2 particles precipitated in the solution. These results suggested that the deposition of an electroinactive layer on the electrode might be the cause for the activity loss. This thinking is supported by further experiments. Firstly, a brown film with an anodic current was observed at Pt, Au, PbO_2, and $Bi-PbO_2$ electrodes after anodization at 1.4 - 1.7 V in a Mn^{2+} solution. The existence of Mn in the brown film was shown by the EDS Curves a and b in Figure 11. The chemical formula for this film is concluded to be MnO_2. The observed anodic current decreased rapidly with time (or cycle number) which indicates that the deposition of this MnO_2 film prevents the further oxidation of Mn^{2+}. Secondly, once the reactivity of the $Bi-PbO_2$

electrode was lost, it could not be resumed by adding Bi^{3+} to the solution. The fouled Bi-PbO_2 electrodes also showed no reactivity for the oxidation of DMSO. When a Au electrode covered by a MnO_2 film was used as the substrate on which to deposit PbO_2 in a Pb^{2+} solution, the induction period was much longer than that at a freshly polished Au RDE. Therefore, this MnO_2 film also greatly decreases the rate of PbO_2 nucleation and deposition. Thirdly, it was observed that the brown MnO_2 film was dissolved in H_2O_2 solution faster than the PbO_2. Hence, it was possible to remove the MnO_2 film from the electrode surface without removing the inner Bi-PbO_2 layer by fast rinsing the electrode with a H_2O_2 solution. The reactivity of a fouled MnO_2-covered Bi-PbO_2 electrode was found to be resumed after this treatment, as determined by the oxidation of DMSO.

It is, therefore, concluded that the activity loss of the Bi-doped PbO_2 electrode for electrolysis of Mn^{2+} is due to the formation of an inert MnO_2 film. This MnO_2 film can be developed by either direct oxidation of Mn^{2+} or chemical decomposition of MnO_4^-.

The above conclusion also explains the catalytic activities of the in-situ deposited PbO_2 electrode. The continuous renewal of the PbO_2 surface by the in-situ deposition prevents the precipitation of MnO_2. However, it is the catalytic effect of the intermediates formed at the in-situ deposited PbO_2 that makes the oxidation of Mn^{2+} to MnO_4^- possible, without which mixed MnO_2 and PbO_2 would be produced. This later point is reasonable because similar catalytic activity of the in-situ deposited PbO_2 was observed also for the oxidation of TPCA. For

TPCA, fouling of the PbO_2 electrode by the oxidation product is unlikely, so the function of surface-renewal is less important.

Electrocatalysis at PbO_2 with Bi^{3+} co-existing in the solution

Strong catalytic activity for oxidation of Mn^{2+}, TPCA, and DMSO was observed at a pure PbO_2 electrode with Bi^{3+} added to the solution. The result for Mn^{2+} is shown in Figure 12. With $[Bi^{3+}]/[Mn^{2+}] = 1/250$, a well-defined voltammetric plateau appeared at 1.5 - 1.6 V, which was not obtained without the co-existing Bi^{3+}. This i-E plateau is similar to that obtained at the Bi-PbO_2 electrode (42). Bismuth was detected at the PbO_2 surface by EDS following the anodization in a Bi^{3+}-containing solution, which might be the key to understand the catalytic activity for this PbO_2 electrode. Much more detailed studies on this subject for oxidation of DMSO and many other substances will be presented in Chapters IV-A and B.

Morphology of the anodized PbO_2 Shown in Figure 13 are the SEM micrographs of the normal PbO_2 film (A) and the PbO_2 films treated anodically in the blank electrolyte (B), and electrolyte containing Bi^{3+} (C) and Mn^{2+} (D). Compared with A, the oxide surfaces in B and C were condensed after the anodization treatment. The similarity between B and C indicates that the difference in catalytic activity between these two electrodes is not due to the morphology change. Pretreatment in Mn^{2+}-containing solution resulted in a totally different morphology (D), which is concluded to be due to the deposition of MnO_2. No difference in morphology was observed between the Bi-PbO_2 electrodes prepared from pre-

deposition and in-situ deposition.

<u>Spectrophotometry</u>   The electrochemistry-spectrophotometry system described earlier also was used to monitor the rate of MnO_4^- production at a PbO_2 electrode with Bi^{3+} present in the solution. The results are shown in Figure 14. When the Bi^{3+} concentration was < 0.02 μM (Curve c), the absorbance first increased slowly with time for ca. 0.5 min and then became constant. The latter indicates that the reaction was stopped and the electrode was fouled. When more Bi^{3+} was present, the increase of A lasted much longer (Curves a and b). The slope ($\Delta A/\Delta t$) of Curve a and b in Figure 14 is much greater than that of Curve a and b in Figure 8A, indicating faster rate of MnO_4^- generation, i.e., stronger catalytic activity at the Bi-modified PbO_2 than at the in-situ deposited PbO_2. These results are consistent with the electrochemical experiments. Calculation from the maximum absorbance after long-term electrolysis indicates that, under certain conditions, the current efficiency for generation of MnO_4^- from Mn^{2+} in acidic media is close to 100%. Similar efficiency is expected also for oxidation of TPCA and DMSO.

<u>References</u>

1. Tenygl, J. In "Electrochemical Detectors: Fundamental Aspects and Analytical Applications"; Ryan, T. H., Ed.; Plenum Press: New York, 1984.

2. Chang, H.; Johnson, D. C. <u>Trend Anal. Chem.</u> 1987, 6 (4), IIX.

3. Lain, M. J.; Pletcher, D. <u>Electrochim. Acta</u> 1987, 32, 99, 109.

4. Cook, R. L.; MacDuff, R. C.; Sammells, A. F. <u>J. Electrochem. Soc.</u> 1987, 134, 2375; 1988, 135, 1320.

5. Swenson, K. E.; Zemach, D.; Nanjundiah, C.; Kariv-Miller, E. J. Org. Chem. 1983, 48, 1777.

6. Kariv-Miller, E.; Nanjundiah, C.; Eaton, J.; Swenson, K. E. J. Electroanal Chem. 1984, 167, 141.

7. Kariv-Milller, E.; Andruzzi, R. J. Electroanal. Chem. 1985, 187, 175.

9. Fleischmann, M.; Korinek, M.; Pletcher, D. J. Electroanal. Chem. 1971, 31, 39.

10. Roberttson, P. M. J. Electroanal. Chem. 1980, 111, 97.

11. Vertes, G.; Horanyi, G. J. Electroanal. Chem. 1974, 52, 47.

12. Amjad, M.; Pletcher, D.; Smith, C. J. Electrochem. Soc. 1977, 124, 203.

13. Robertson, P. M.; Berg, P.; Reimann, H.; Schleich, K.; Seiler, P. J. Electrochem. Soc. 1983, 130, 591.

14. Schafer, H. J. Top. Curr. Chem., Electrochemistry, Steckhan, E., Ed.; Springer-Verlag: Berlin, 1987; Volume 1.

15. Hampson, N. A.; Lee, J. B.; Morley, J. R.; Scanlon, B. Can. J. Chem. 1969, 47, 3729.

16. Hampson, N. A.; Lee, J. B.; Morley, J. R.; MacDonald, K. I.; Bcanlon, B. Tetrahedron 1970, 26, 1109.

17. Hampson, N. A.; Lee, J. B.; MacDonald, K. J.; Shaw, M. J. J. Chem. Soc. B 1970, 1766.

18. Pletcher, D.; Fleischmann, M.; Korinek, K. J. Electroanal. Chem. 1971, 33, 478.

19. Hui, B. S.; Huber, C. O. Anal. Chem. 1986, 58, 2745.

20. Yuan, C. J.; Huber, C. O. Anal. Chem. 1985, 57, 180.

21. Kafil, J. B.; Huber, C. O. Anal. Chim. Acta 1985, 175, 275.

22. Hui, B. S.; Huber, C. O. Anal. Chim. Acta 1982, 134, 221.

23. Fritz, H. P.; Wabner, D. German Patent 3003781, Jan. 14, 1980.

24. Covitz, F. H.; U. S. Patent 350931, Apr. 28, 1970.

25. Chang, H.; Johnson, D. C. J. Electrochem. Soc. 1989, 136, 17; Chapter II-A, this Dissertation.

26. Chang, H.; Johnson, D. C. J. Electrochem. Soc. 1989, 136, 23; Chapter II-B, this Dissertation.

27. Tang, A. P.-C. Ph.D. Dissertation, Iowa State University, Ames, Iowa, 1989.

28. Austin, D. S.; Polta, J. A.; Polta, T. Z.; Tang, A. P.-C.; Cabelka, T. P.; Johnson, D. C. J. Electroanal. Chem. 1984, 168, 227.

29. Johnson, D. C.; Polta, J. A.; Polta, T. Z.; Newburger, G. G.; Johnson, J.; Tang, A. P.-C.; Yeo, I.-H.; Baur, J. J. Chem. Soc., Faraday Trans. 1 1986, 82, 1081.

30. Tang, A. P.-C.; Johnson, D. C. Anal. Chem. Acta, in press.

31. Yeo, I.-H.; Johnson, D. C. J. Electrochem. Soc. 1987, 134, 1973.

32. Yeo, I.-H. Ph.D. Dissertation, Iowa State University, Ames, Iowa, 1987.

33. Chang, H.; LaCource, W.; Johnson, D. C. not published.

34. Johnson, D. C.; Weber, S. G.; Bond, A. M.; Wightman, R. M.; Shoup, R. E.; Krull, I. S. Anal. Chim. Acta 1986, 1980, 187.

35. "Flow Analysis III"; Proceedings for An Internaltional Conference in Flow Analysis, Birmingham, U. K.; 1985.

36. Ruzicka, J. Anal. Chem. 1983, 55, 1040A.

37. Hampson, N. A.; McNeil, A. J. S. Electrochemistry 1984, 9, 1.

38. Newman, J.; Tiedemann, W. In "Advances in Electrochemistry and Electrochemical Engineering"; Gerischer, H.; Tobias, C. W., Eds.; Wiley: New York, 1977; Volume 11.

39. Newman, J.; Tiedeman, W. AIChE J. 1975, 21, 25.

40. Wang, J.; Dewald, H. D. J. Electrochem. Soc. 1983, 130, 1814.

41. Stewart, R. In "Oxidation in Organic Chemistry"; Wiberg, K. B., Ed.; Academic Press: New York, 1965; Part A, Chapter I, p. 1.

42. Chang, H.; Johnson, D. C. In preparation; Chapter III-B, this Dissertation.
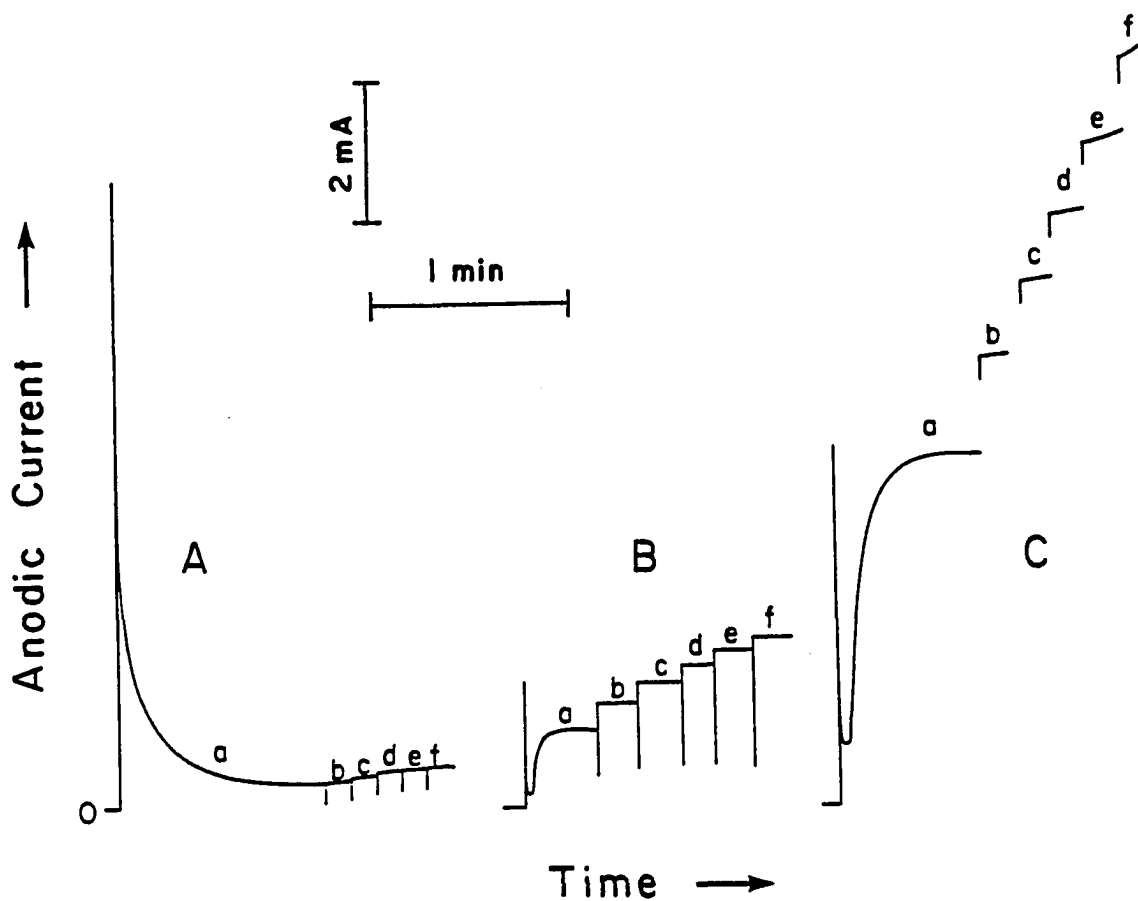
Figure 1. Chronoamperograms for oxidation of Mn^{2+}

Conditions: 1.0 M $HClO_4$, E - 1.70 V,

$w^{1/2}$ (rev $min^{-1})^{1/2}$: (a) 400, (b) 900, (c) 1600,
(d) 2500, (e) 3600

Curves: (A) 10 mM Mn^{2+} on PbO_2/Au, (B) 10 mM Pb^{2+}
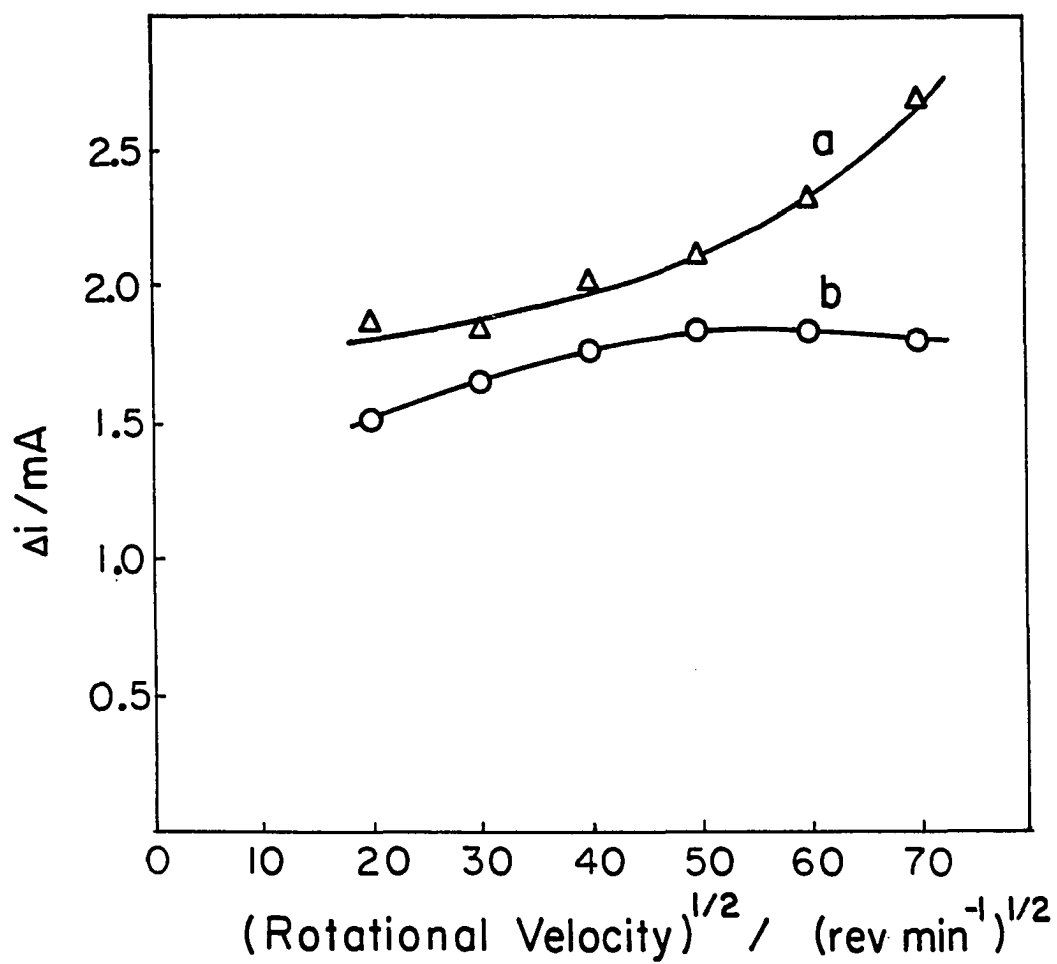on Au, and (C) 10 mM Mn^{2+} and 10 mM Pb^{2+} on Au

Figure 2. Plots of Δi vs. $w^{1/2}$ for Mn^{2+} oxidation at different Pb^{2+} concentrations

Conditions: 10 mM Mn^{2+}, 1.0 M $HClO_4$, E = 1.70 V

Pb^{2+} concentration: (a) 10 mM and (b) 1 mM
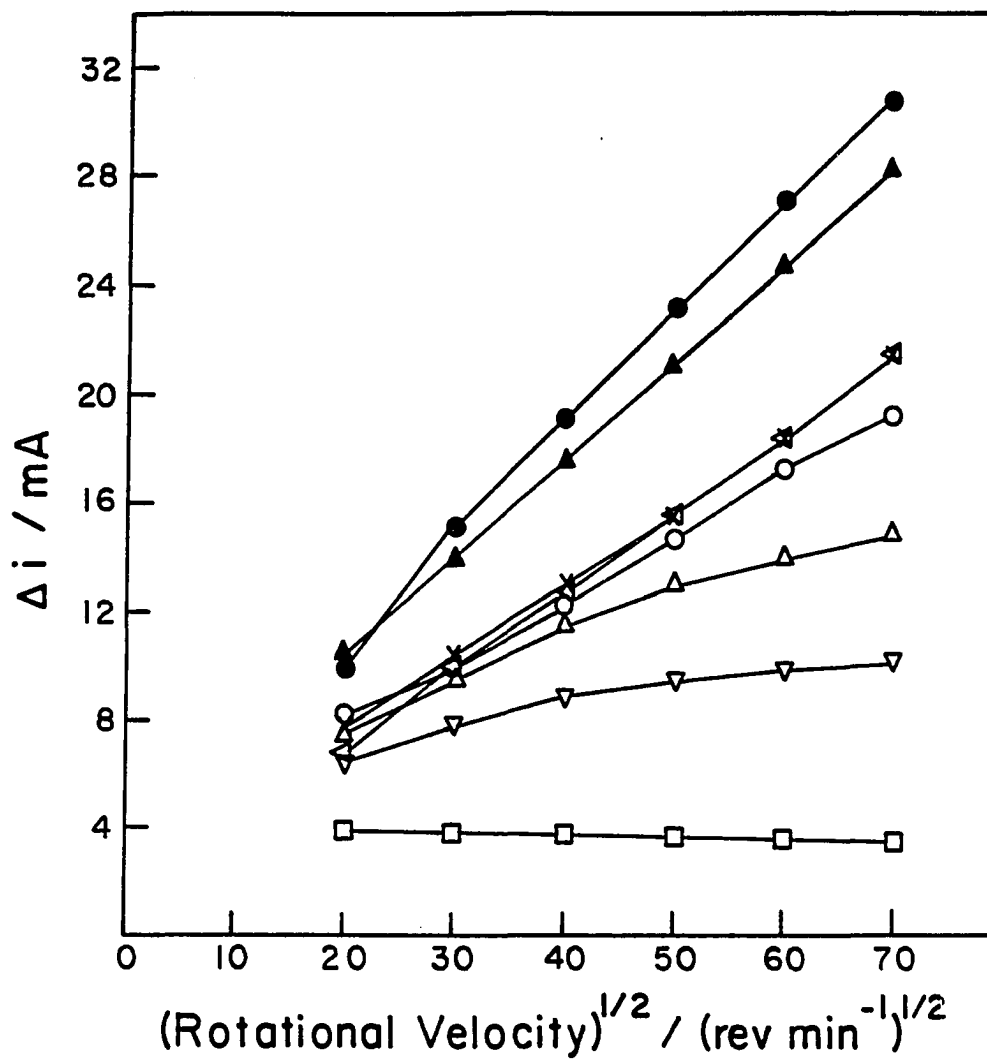
Figure 3. Plots of Δi vs. $w^{1/2}$

Conditions: 10 mM analyte and 10 mM Pb^{2+}
in 1.0 M $HClO_4$, E - 1.70 V

Curves: (●) thiourea, (▲) SCN⁻, (◁) hydroquinone,
(✗) TPCA, (○) EDTA, (△) $HSCH_2CH_2SO_3^-$,
(▼) L-cysteine, (□) L-cystine
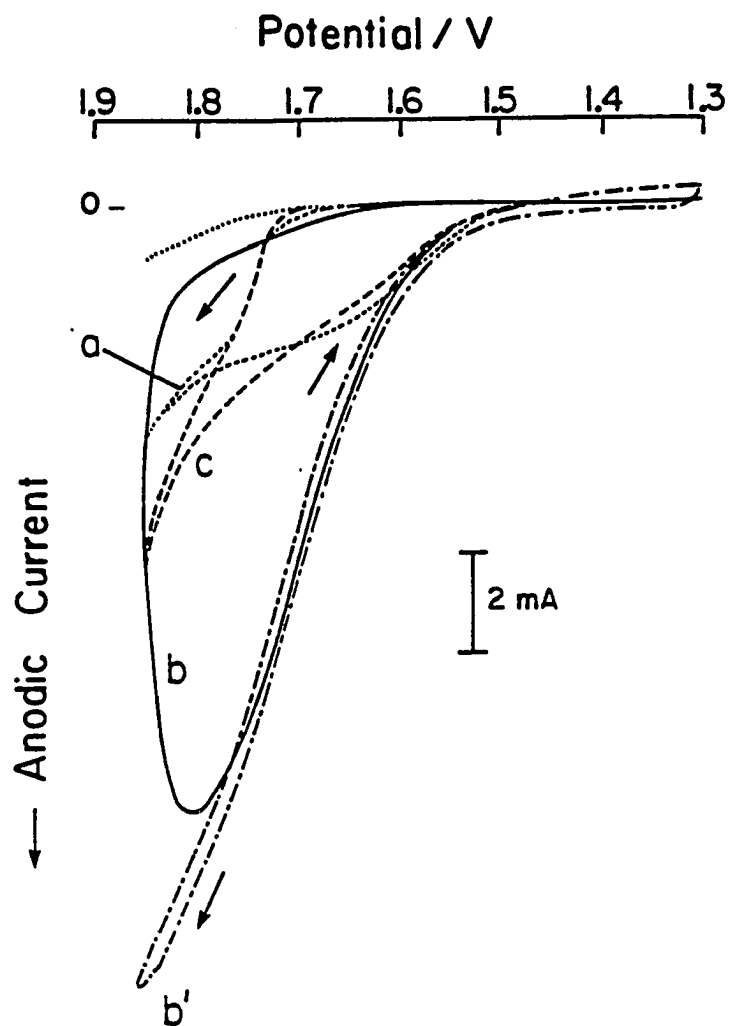
Figure 4. Cyclic voltammograms at in-situ electrodeposited PbO$_2$

Conditions: 400 rev min^{-1}, 20 mV s^{-1},
10 mM analyte in 1.0 M HClO$_4$

Curves: (......) residual,
(-----) Pb^{2+} only, (a),
(———) Pb^{2+} and TPCA, 1st scan, (b),
(———) Pb^{2+} and TPCA, 2nd scan, (b'),
(———) Pb^{2+} and DMSO, (c)
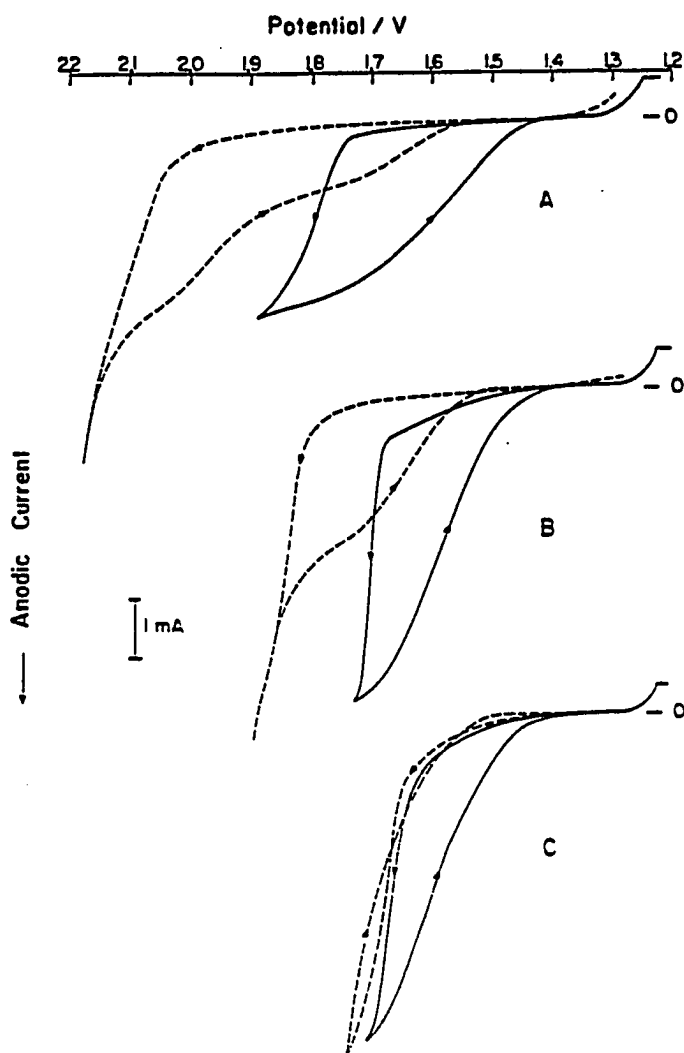
Figure 5. Cyclic voltammograms at in-situ electrodeposited PbO$_2$

Conditions: as given in Figure 4

Solutions: (----) 10 mM Pb^{2+} only,
(——) 10 mM Pb^{2+} and 10 mM Mn^{2+}.

Electrodes: (A) GC, (B) Au, (C) Pt
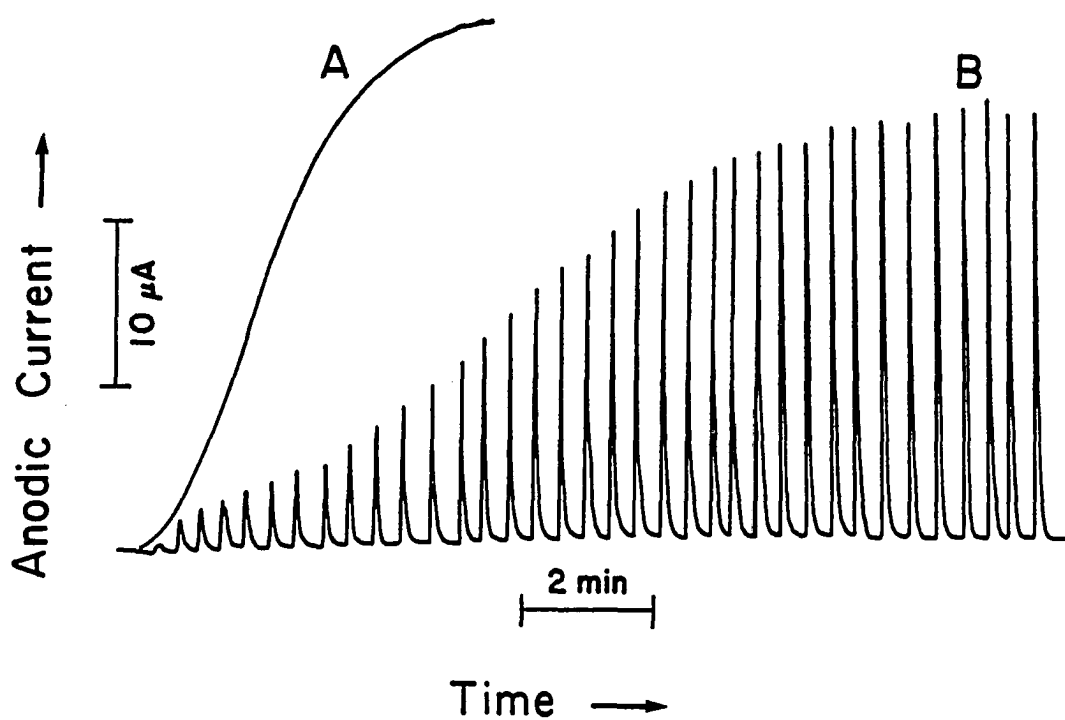
Figure 6. Preparation of PbO$_2$ coating on Au electrode in a
flow-through systems

Conditions: 1.6 V electrode potential, 1.0 M HClO$_4$
carrier stream, 10 mM Pb^{2+} sample solution

Curves: (A) continuous flow of Pb^{2+} at 3 ml min^{-1};
(B) consecutive injections at 9.6 ml min^{-1}
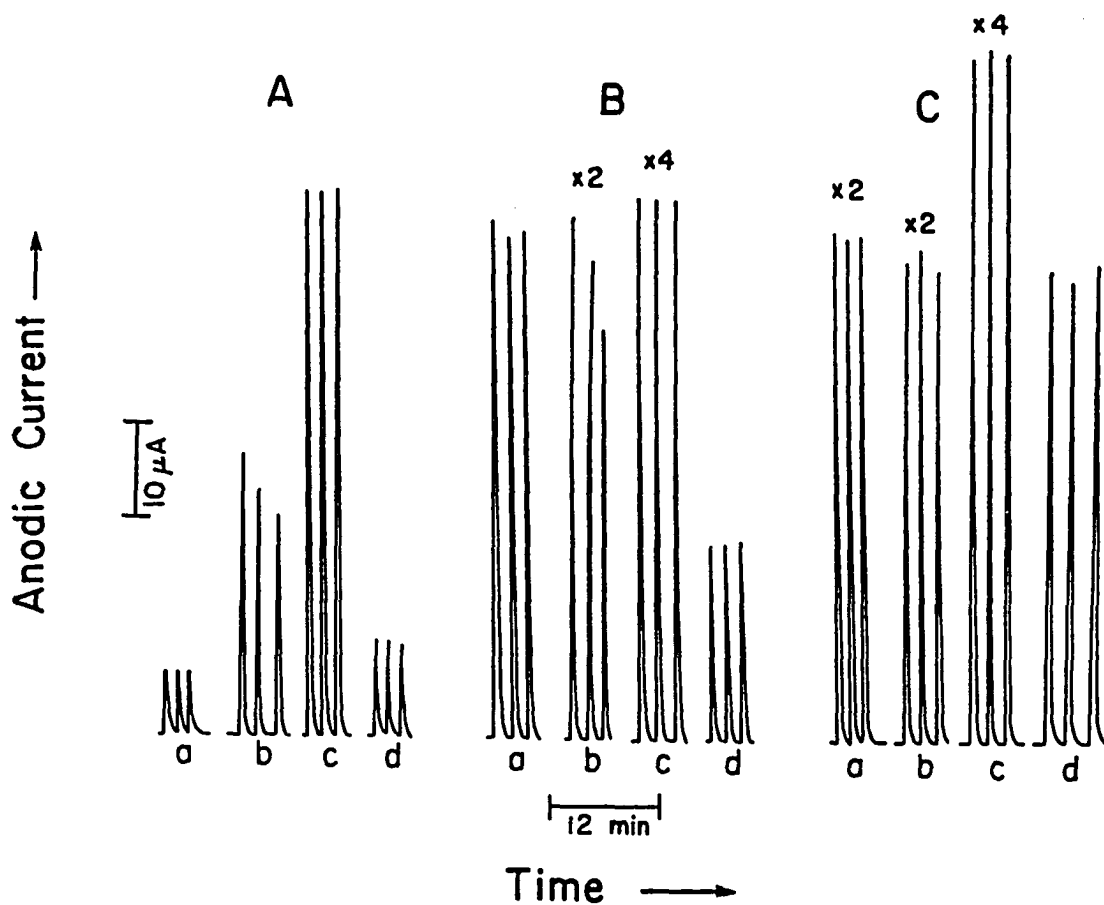
Figure 7. Flow-injection amperometric detection peaks

Conditions: E - 1.6 V, carrier stream: 1.0 M $HClO_4$, flow rate: 9.6 ml min^{-1}, 10 mM analyte

Electrodes: (A) Au, (B) PbO_2 precoated on Au, (C) PbO_2 electrodeposited in situ, with 1 mM Pb^{2+} in the sample solution

Compounds: (a) $HSCH_2CH_2SO_3Na$, (b) 2-thiophene acetic acid, (c) NaSCN, and (d) Mn^{2+}
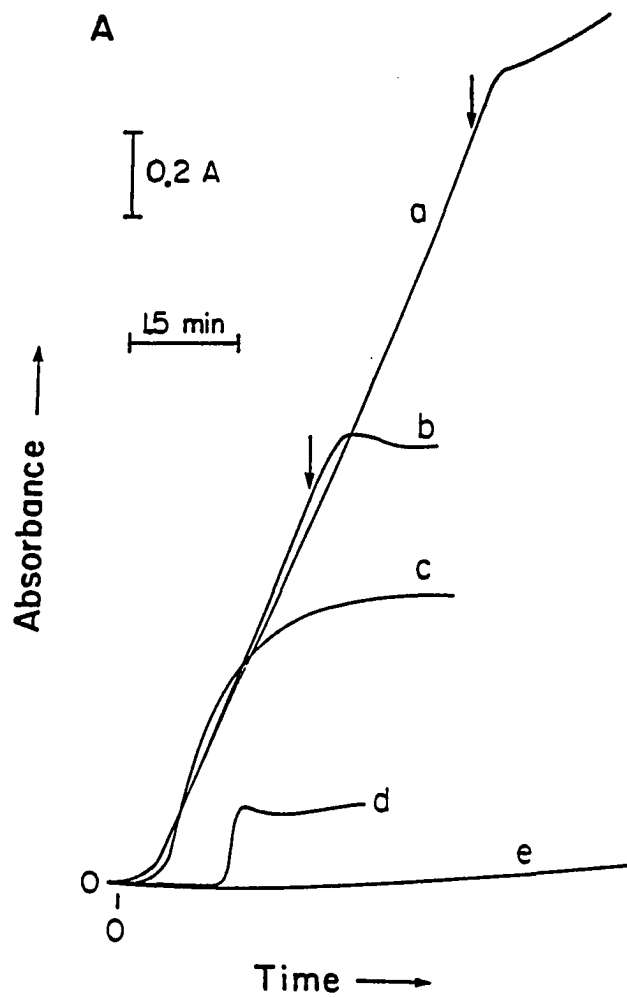
The xn numbers indicate the increase of current scale

Figure 8A. Absorbance vs. time at $\lambda = 525$ nm

Conditions: E = 1.70 V. The potentiostat was
disconnected at the arrows for a and b

Curves: (a) 10 mM Mn^{2+} and 10 mM Pb^{2+} at PbO_2,
(b) the same as (a),
(c) 10 mM Mn^{2+}, 10 μM Pb^{2+}
and 1 μM Bi^{3+} at PbO_2,
(d) 10 mM Mn^{2+} at Pt,
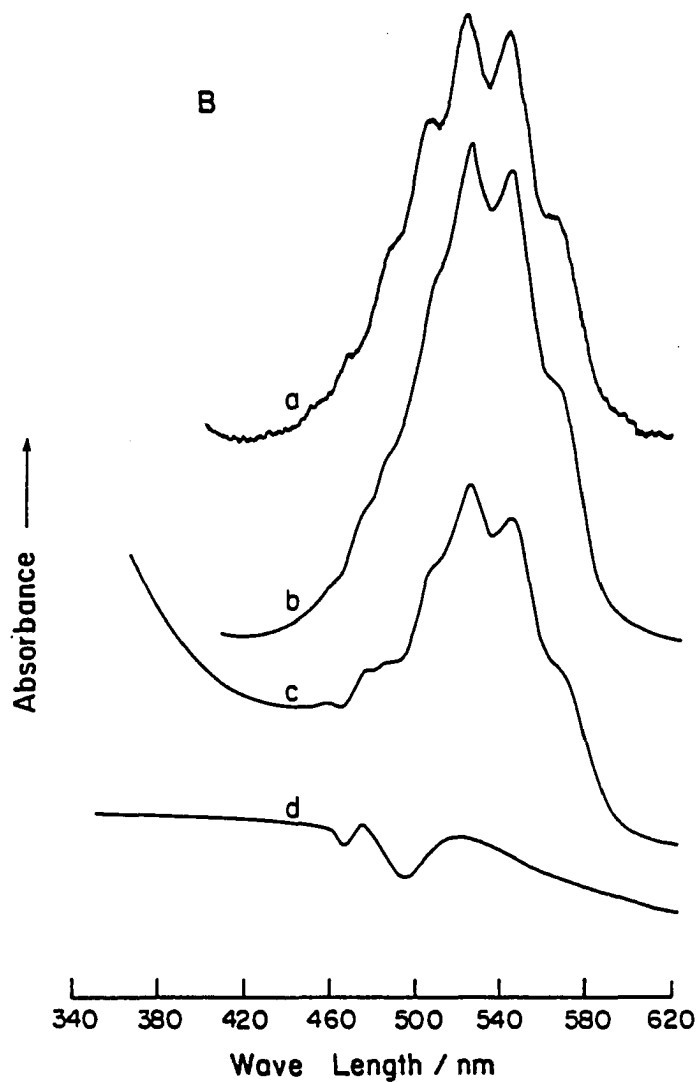(e) 10 mM Mn^{2+} at PbO_2

Figure 8B. Spectroscopy for Mn^{2+} oxidation products

Curves: (a) $KMnO_4$ in 1.0 M $HClO_4$,
(b) electrogenerated MnO_4^- from A(a),
(c) electrogenerated MnO_4^- from A(c),
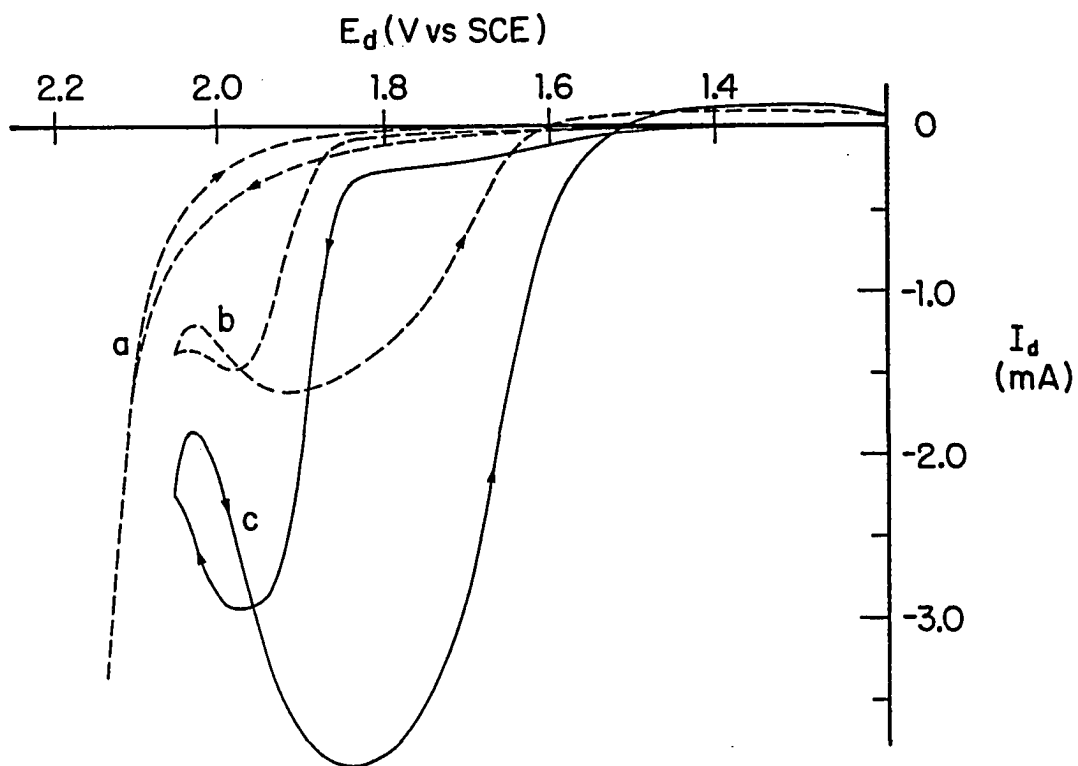(d) product solution from A(d)

Figure 9. Cyclic voltammograms at in-situ electrodeposited Bi-PbO$_2$

Conditions: 400 rev min^{-1}, 20 mV s^{-1}, glassy carbon RDE

Curves: (a) residue, (b) 10 mM Pb^{2+} and 9 mM Bi^{3+},
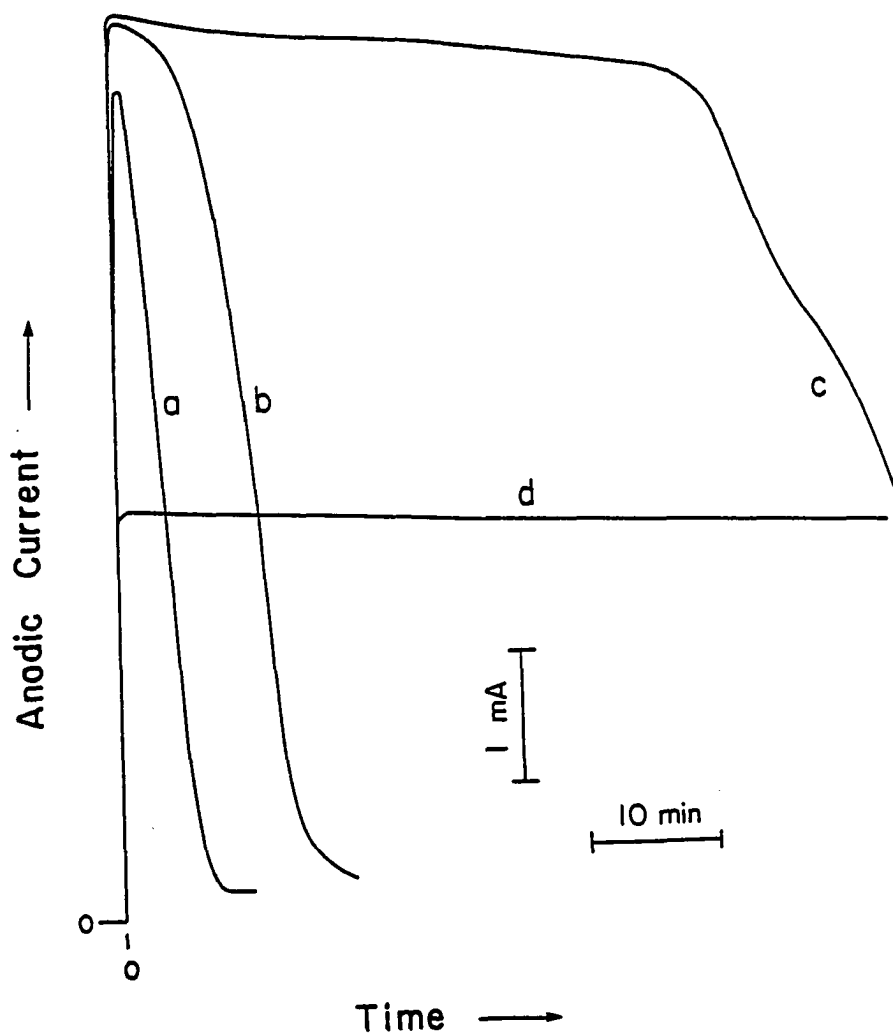(c) the same as (b), plus 10 mM Mn^{2+}

Figure 10. Chronoamperograms for oxidation of 10 mM Mn^{2+} and DMSO
at Bi-PbO_2

Conditions: E $-$ 1.70 V, 400 rev min^{-1}

Deposition conditions: 1 mM Bi^{3+} and 10 mM Pb^{2+}

Solutions: (a) 10 mM Mn^{2+},
(b) 10 mM Mn^{2+} and 40 μM Bi^{3+},
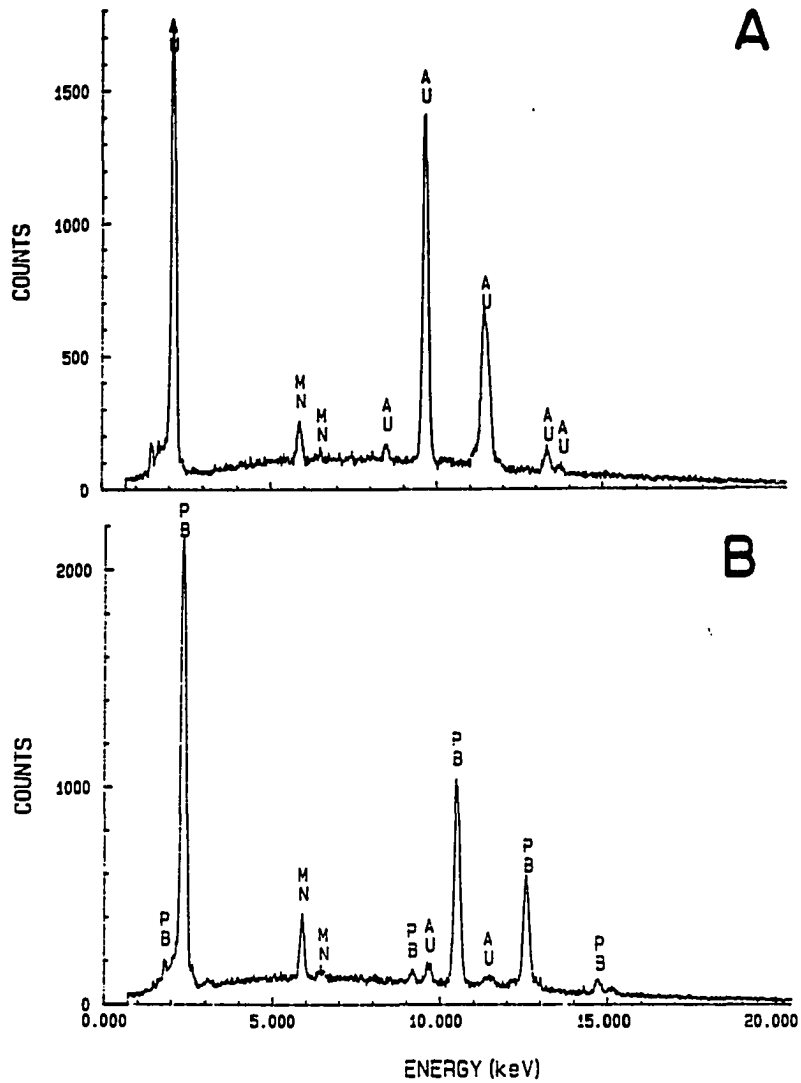(c) 10 mM Mn^{2+} and 60 μM Bi^{3+},
(d) 10 mM DMSO

Figure 11. EDS of different electrodes.

Conditions: Life time for EDS detection — 100 sec

Curves: (A) Au after anodizing in 10 mM Mn^{2+},
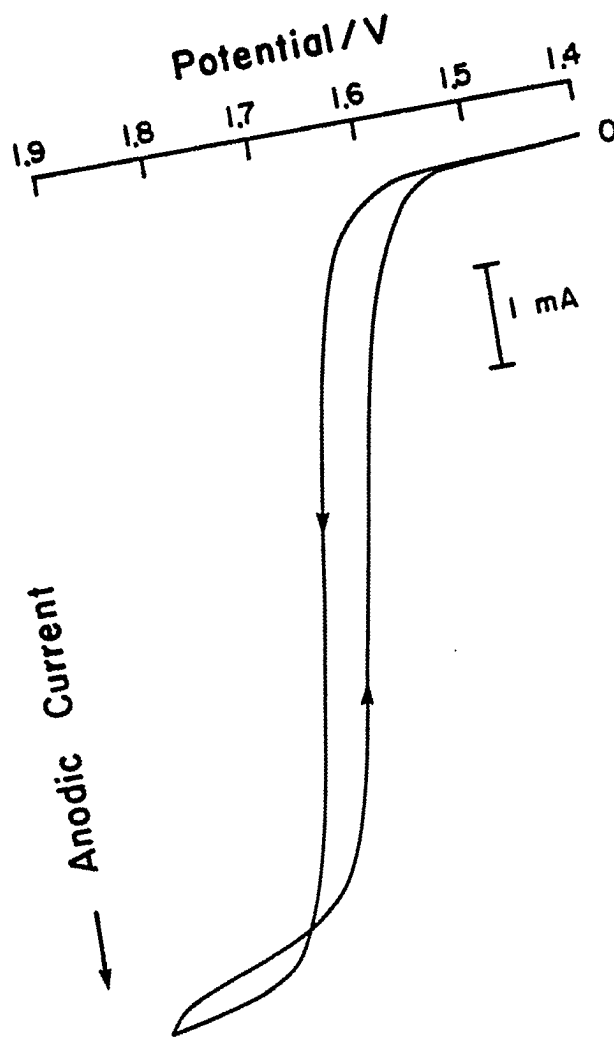(B) PbO_2 after anodizing in 10 mM Mn^{2+},

Figure 12. Cyclic voltammograms at PbO_2 with Bi^{3+} co-existing in the solution

Conditions: 10 mM Mn^{2+} and 40 μM Bi^{3+}; others as given in Figure 9
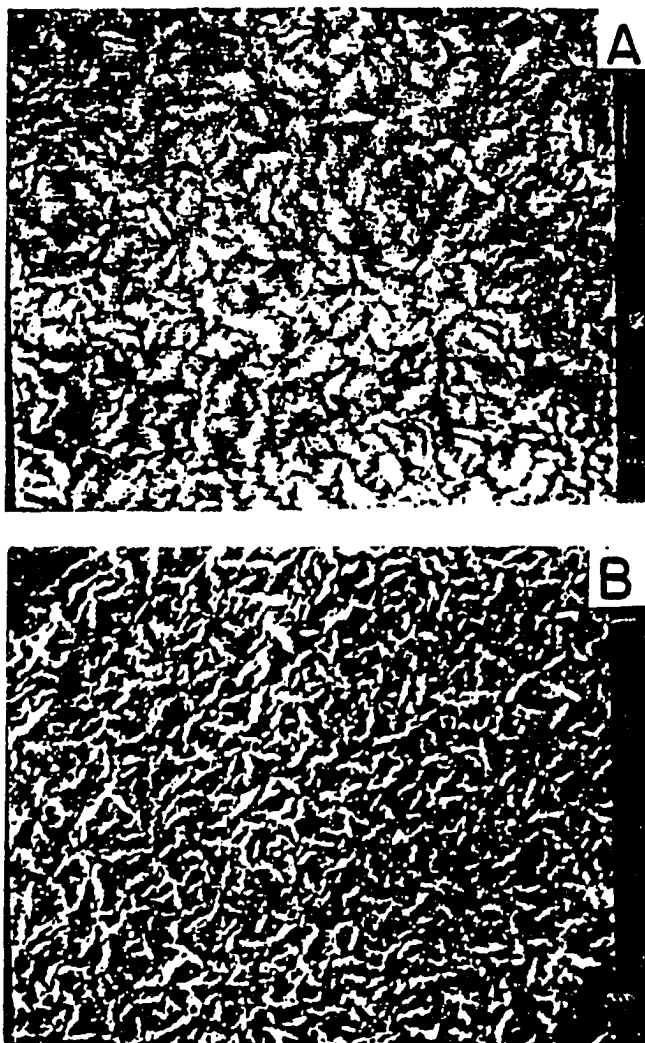
Figure 13A&B.   Effect of anodization pretreatment on the morphology of
                PbO_2

                SEM conditions: 25 keV beam energy, X10000

                Pretreatment conditions: E — 1.7 V for 10 min

                Pictures: (A) PbO_2 before anodization,
                            (B) pretreated in 1.0 M $HClO_4$ blank,
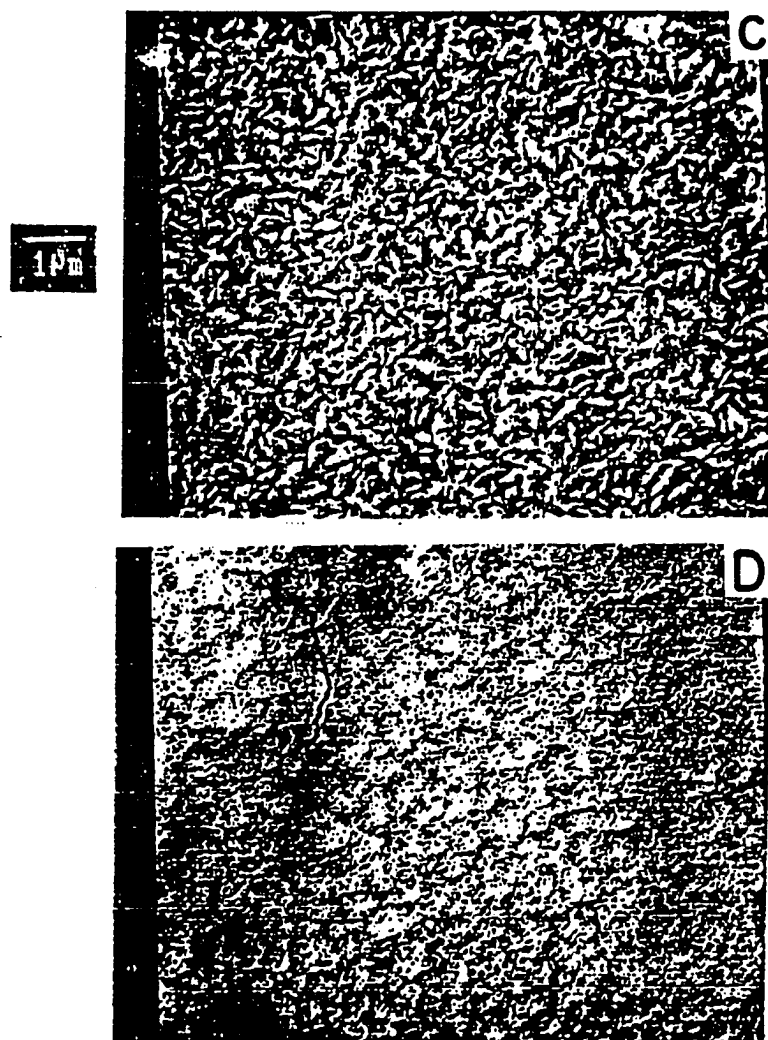
Figure 13C&D. Effect of anodization pretreatment on the morphology of
PbO_2

    Conditions: as given in Figure 13A&B

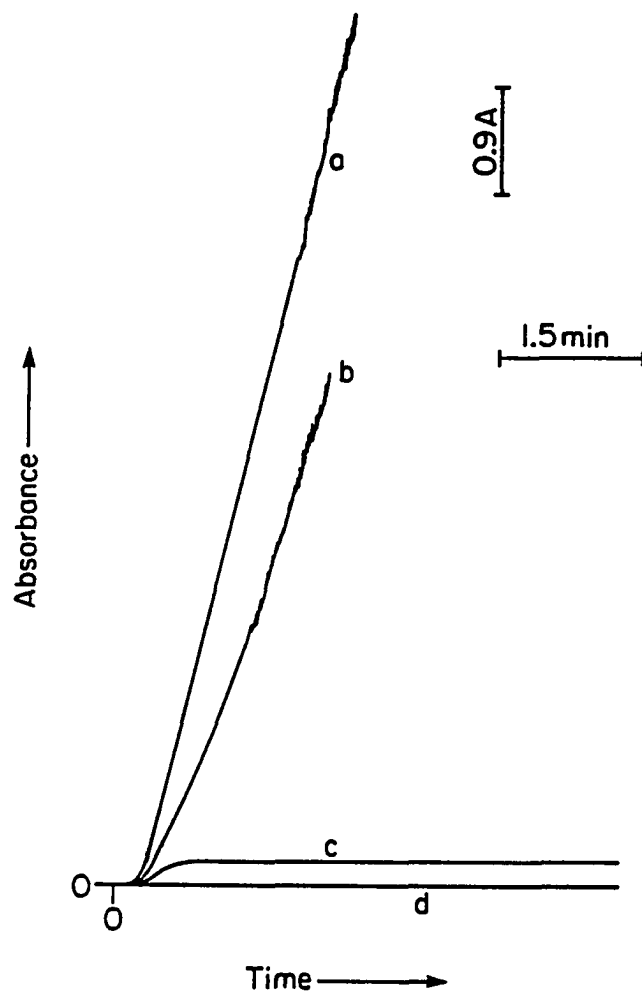   Pictures: (C) 10 mM Bi^{3+} solution,
          (D) 10 mM Mn^{2+} solution

Figure 14. Absorbance vs. time in the flow-through system
at λ — 525 nm

Conditions: E — 1.70 V, at PbO$_2$-coated Pt gauze
electrode, 10 mM Mn^{2+}

Bi^{3+} concentration (μM): (a) 0.3, (b) 0.03,
(c) 0.016, (d) 0

B.   Electrodeposition and Characterization of Bismuth-Doped Lead Dioxide

as Chemically Modified Electrode with

Bismuth as the Immobilized Oxygen-Transfer Mediator[1]

"In our laboratory at the University of Kansas it was my
fond hope to develop electrodes that would not undergo
surface oxidation. We never really succeeded, but,
instead, found a very useful modification of carbon-the
so-called carbon paste electrode."

-R. N. Adams,
cited from Ref. 1

---

[1]To be submitted to J. Electrochem. Soc.

Abstract

The kinetics and mechanisms of the nucleation and growth of Bi-doped PbO_2 (Bi-PbO_2) at rotated disc electrodes in 1.0 M $HClO_4$ were studied by voltammetry and chronoamperometry as a function of the concentration ratio $[Bi^{3+}]/[Pb^{2+}]$, rotational velocity, and electrode material. The formation of Bi-PbO_2 occurs by adsorption and/or inclusion of Bi^{3+} as an impurity at the surface of PbO_2. The nucleation and growth rates of the oxide decrease with increased Bi^{3+} concentration, due to an apparent inhibition effect of Bi at the PbO_2 surface. However, the electrochemical stability of the resultant oxide increases with increased bismuth content. Partial oxidation of Bi^{3+} to Bi(V) occurs during the anodic deposition process.

The Bi-PbO_2 films with their electrocatalytic activities were characterized by electrochemical and spectroscopic methods and concluded to be special cases of the broader category of chemically modified electrodes. Voltammetric waves for the oxidation of Mn^{2+} to MnO_4^- and $(CH_3)_2SO$ to $(CH_3)_2SO_2$ were obtained at the Bi-PbO_2 electrode, but not at conventional electrodes. A mechanism for the electrocatalysis was proposed with oxygen-transfer mediation, in which PbO_2 serves as a supporting matrix to immobilize the catalytic Bi ions at the electrode surface which function as oxygen-transfer mediators by promoting the localized production of hydroxyl radicals.

Introduction

Anodic applications of metal oxide electrodes and metal oxide film-covered electrodes are inevitable in aqueous solutions because surface oxides are formed during anodization of all metals including Pt and Au. The fond hope to develop electrodes that would not undergo surface oxidation never really has succeeded (1). However, this effort has resulted in the development of electrochemistry at metal oxide electrodes (2), and the realization that surface metal oxides sometimes can be beneficial and desirable, due to their unique participation in many electrode processes, e.g., electrocatalysis (2,3).

In recent decades, the development of chemically modified electrodes (CME) has been one of the most intensive research fields within electrochemistry (4). This has resulted in useful techniques for electrode modification and new theories to explain mediated electrochemical reactions. Most of the work on CMEs has been related to organic polymers and polyelectrolytes as coating materials. A minor branch of CME research has been devoted to inorganic coatings. The successful examples are inorganic polymers, e.g., Prussian blue (5), polymeric metal oxides, e.g., the Ni-metal-cyano complex (6), OsO_4 and RuO_2 incorporated with $Ru(CN)_6^{4-}$ (7), other catalyst-incorporated matrices, e.g., zeolite and clay (8), and simple metal oxides, e.g., RuO_2 and TiO_2 (2-3,9). These inorganic film-coated electrodes generally are more tolerant to high temperature, more resistant to strong acids and bases, and have higher mechanical strength and more stable reactivity than the organic CMEs, all of which lead the inorganic electrodes to be

more successful in both electrochemical reactors and electroanalytical devices.

Recently, catalytic metal oxide electrodes for anodic oxygen-transfer (O-t) reactions have been the subject of research in this laboratory (10). A successful model is based on the incorporation of a small amount of Bi(III) into a PbO_2 matrix through electrochemical co-deposition (10b-e). Such Bi-doped PbO_2 films (Bi-PbO_2) showed strong reactivity for anodic oxidation of Mn^{2+}, phenol, and 2-thiophene acetic acid in acidic media (10c,d), all of which involve oxygen transfer.
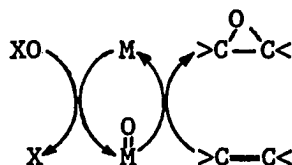
Electrodeposited PbO_2 anodes have been widely used in many commercial and laboratory synthetic processes (11). Efforts have existed, especially in the industrial sector, to improve the behavior of pure PbO_2 anodes by enhancing their dimensional stability and electrochemical reactivity through addition of various other elements to the plating bath by a trial-and-error method (11). Rhees and Halker (12) discovered that Bi-containing PbO_2 anodes have higher current efficiencies than pure PbO_2 for electrosynthesis of chlorate, perchlorate, bromate, iodate, and periodate, all of which are O-t reactions. There are at least two other patents (13) in which the addition of Bi^{3+} to the plating bath is claimed to produce better anodes for electrosynthesis. However, no further work has been published concerning the mechanism for the selective catalytic effect of incorporated Bi^{3+} on the anodic O-t reactions. Initial attempts were made in our laboratory to understand how the Bi-PbO_2 electrodes work (10d,e) by determining their crystal structure and preferred orientation

in correlation with O_2 evolution (10d,e), yet the mechanism and the function of bismuth in the electrocatalysis still are not clear. Therefore, for both practical and theoretical purposes, the mechanism of electrocatalysis at Bi-PbO$_2$ electrodes deserves more intensive investigation.

In the present study, Bi-PbO$_2$ electrodes are considered to be catalyst-incorporated metal oxide electrodes which are chemically modified specifically to promote faster anodic O-t reactions. It is believed that the electrocatalytic benefits from surface oxide will be even greater if simple oxides are chemically and purposely modified. In addition, the kinetics and mechanisms for deposition of Bi-PbO$_2$ also are studied since no research in this respect has been reported before.
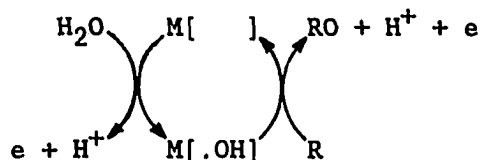
Theory of oxygen-transfer mediation

It is well-known that slow electron-transfer (e-t) reactions can be catalyzed by e-t mediators. Most e-t mediators are transition metal ions which are immobilized and can exist in two oxidation states. These mediated electrochemical e-t reactions have been the subject of intensive studies (4). Similar concepts can be applied to O-transfer (14). Among well-known mediated O-transfer reactions is the oxidation of a variety of substances by dioxygen. Since O_2 is not in an appropriate energetic state, the oxidation is usually slow. Therefore, mediators are important to activate the dioxygen and, thereby, catalyze the reaction. Another typical example of mediated O-transfer is the epoxide deoxygenation reaction mediated by metal ions in high oxidation state or by complexes in a homogeneous solution, as presented below (14d)

$$
\begin{array}{c}
XO \diagdown \quad \diagup M \diagdown \quad \diagup >C \overset{\overset{O}{\diagup\diagdown}}{-} C< \\
\diagup\diagdown \quad \diagdown \underset{M}{\overset{O}{\|}} \diagup \quad \diagdown >C\!-\!C< \\
X \diagup \quad \quad \quad
\end{array}
\qquad [1]
$$

in which XO is the oxygen atom donor or oxygen atom-transfer reagent,
e.g., amine N-oxides, iodosoarenes, peracids and hypochlorite; and M is
the mediator, e.g., Cr(V), Mn(V), Fe(V), Ru(V), or their complexes. This
mechanism, generally called "oxidation-reduction mechanism", also has
been used to explain the catalytic effects of metal oxides in many
gaseous O-t processes, e.g., oxidation of carbon monooxide to carbon
dioxide and methane to methanol (15,16). The mediated O-t reactions have
great importance in biological systems, too. Typical examples are the O-
t reactions catalyzed by oxygen-transfer enzymes (17).

Electrochemical O-t reactions also can be mediated, in which the
oxygen donor is usually water. Examples are the I^--mediated oxidation
of SO_2 to SO_4^{2-} (18) and Cr^{3+}-mediated oxidation of toxic compounds (19).
In these cases, the mediator is in the solution contacting the electrode
surface. Heterogeneous, mediated O-transfer occurs with the mediator
immobilized at the electrode surface. Some known examples of such
mediated O-t reactions are the oxidation of As(III) and carbohydrates at
noble metal electrodes (3,10a,b), and the electrodeposition of PbO_2
(20a), as summarized below

$$
\begin{array}{c}
H_2O \diagdown \quad \diagup M[\quad] \diagdown \quad \diagup RO + H^+ + e \\
\diagup\diagdown \quad \diagdown \diagup \\
e + H^+ \diagup \quad M[.OH] \diagup \quad \diagdown R
\end{array}
\qquad [2]
$$

in which M is the electrode surface which also serves as the mediator for O-transfer by generating the hydroxyl radical (.OH).

The strategy to modify PbO_2 electrodes for selective electrocatalysis of O-t reactions has been described in Chapter I-A. In this chapter, Bi in the $Bi-PbO_2$ is identified as an O-t mediator that is incorporated into the PbO_2 matrix by co-deposition. A parallel study with Bi^{3+}-adsorbed PbO_2 electrode is presented in Chapters IV-A and B.

Experimental

The apparatus for electrochemical experiments and the chemicals were described earlier (20a).

Scanning electron micrographs (SEM), X-ray energy dispersive spectroscopy (EDS), and elemental mappings were taken with a model JSM-840A (JEOL) electron microscope.

A model AEIS 200B (Kratos) X-ray photoelectron spectrometer (XPS) was used with an Al X-ray source and a model 1180 (Nicolet) data acquisition system.

Bismuth(III)/lead(II) concentration ratio in the deposition solution is represented by $[Bi^{3+}]/[Pb^{2+}]$, as $[Pb^{2+}] = 10$ mM.

Results and discussion

<u>Cyclic voltammetric deposition and stripping of Bi-PbO_2</u>   It was observed that the voltammetric response for deposition and stripping of $Bi-PbO_2$ changed with variation of the Bi^{3+}/Pb^{2+} concentration ratio (4c). However, no detailed study was made to explain these changes. Shown in Figure 1A are the cyclic voltammograms (first scan) at a freshly polished

Au RDE as a function of the $[Bi^{3+}]/[Pb^{2+}]$. As the $[Bi^{3+}]$ was increased at a constant $[Pb^{2+}]$, the minimum potential for a noticeable rate of Bi-PbO_2 deposition was shifted to more positive values. Thus, it is concluded that it is more difficult to nucleate the mixed oxide with higher $[Bi^{3+}]$. There are two possible explanations. First, adsorption of Bi^{3+} on the PbO_2 surface (20c,d) might inhibit or block the further deposition of PbO_2. Second, the Bi^{3+} ion in the solution might react with the deposition intermediates, e.g., OH_{ads} and $Pb(OH)_2^{2+}$, which slows down the nucleation process. The anodic i-E wave in the negative scan also shifted to more positive values with increased $[Bi^{3+}]/[Pb^{2+}]$, which means that the rate of further deposition of Bi-PbO_2 on a Au electrode partially covered by Bi-PbO_2 changes with variation of $[Bi^{3+}]/[Pb^{2+}]$.

The cathodic stripping peak of the oxide in Figure 1A shifted to less positive values with increased $[Bi^{3+}]$. It will be proved later that the Bi concentration in the resultant oxide film increases with increased $[Bi^{3+}]$ in the deposition solution. Therefore, it is concluded that the electrochemical stability and the voltammetric potential window at the mixed oxide film increases with increased Bi concentration. The following experiment was done to determine whether the increased stability is of a kinetic or thermodynamic nature. For $[Bi^{3+}]/[Pb^{2+}]$ = 0.7, the negative potential scan was stopped at 1.15 V, a value between the observed stripping peak potentials for pure PbO_2 and Bi-PbO_2. The Bi-PbO_2 film remained on the Au surface after ca. 30 min, so it is concluded that the increased stability for Bi-PbO_2 is of a thermodynamic rather than kinetic origin. The increased stability of Bi-PbO_2 also was

evidenced by the observation that Bi-PbO_2 dissolved in H_2O_2 solution more slowly than pure PbO_2 did.

Causes for the increased stability of Bi-PbO_2 The increased stability of Bi-PbO_2 can be ascribed partially to the decreased alkalinity of the mixed oxide as compared to the pure PbO_2. The stoichiometry for PbO_2 stripping is as follows

$$PbO_2 + 4H^+ + 2e - Pb^{2+} + 2H_2O \qquad [3]$$
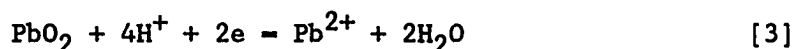
Since protons are consumed, the stripping peak potential for PbO_2 shifts to less positive values as the solution pH is increased (20a). If the solution pH is constant and the alkalinity of the oxide, i.e., its reactivity toward H^+ is increased, the stripping peak potential also should be decreased. It is generally agreed that bismuth oxide is less basic than lead oxide (21a). The alkalinity of the mixed oxide should increase with increased Bi concentration, as observed for other mixed oxides (21b). Therefore, Bi-PbO_2 with higher Bi/Pb atomic ratio is reduced at less positive potential.

The change in cathodic stripping peak for the oxide differed for increasing pH and higher Bi concentration. First of all, the ratio of the stripping peak area to the deposition wave area in Figure 1A decreased with increased $[Bi^{3+}]/[Pb^{2+}]$ as shown in Figure 1B, whereas this ratio was about unity for pure PbO_2 and did not change with increasing solution pH (20a). From this result, it is concluded that Bi-PbO_2 is only partially reducible and the reducible portion decreases with increasing Bi concentration. Secondly, the shape of the stripping peak

in Figure 1A changed with increasing Bi/Pb concentration ratio, whereas

it did not change with increasing solution pH (20a). At $0 <$

$[Bi^{3+}]/[Pb^{2+}] \leq 0.3$, the stripping i-E curves had two peaks, which

indicates that there might exist two phases in the mixed oxide. At

$[Bi^{3+}]/[Pb^{2+}] \geq 0.5$, a single, broad stripping peak appeared, which

indicates a decreased reversibility of the stripping reaction.

A second explanation for the increased stability of Bi-PbO$_2$ came

from the studies in literature on the redox stability of mixed oxides

(22). It is generally agreed that the redox stability of one oxide

increases with increasing amount of a second and inert oxide being

incorporated with (22). As for Bi-PbO$_2$, Bi$_3$O$_2$ can be considered as an

inert matrix for PbO$_2$, which is not stripped electrochemically.

Therefore, the electrochemical stability of Bi-PbO$_2$ increases with

increased Bi concentration.

Constant-potential deposition of Bi-PbO$_2$ Constant-potential

chronoamperometry also was used to study the deposition of Bi-doped PbO$_2$,

as shown in Figure 2. The change of the i-t curves with electrode

material for Bi-PbO$_2$ deposition is similar to that observed for PbO$_2$

(20a). The induction time (t_0) increased in the order of electrode

substrate material: Pt < Au < GC, which indicates an interrelationship

between oxide deposition and oxygen evolution (20a).

Shown in Figure 3 are the dependencies of t_0, t_1, and S (for

definitions, see Ref. 20a) on $[Bi^{3+}]/[Pb^{2+}]$ at a Au RDE. The values of

t_0 and t_1 increased, and S decreased sharply with increased

$[Bi^{3+}]/[Pb^{2+}]$, indicating decreased rates of nucleation and growth. This

conclusion is the same as that based on voltammetric data. When Bi^{3+} was added to a Pb^{2+} solution during the process of depositing PbO_2, the deposition was stopped immediately. A long induction period was needed to restart the deposition. The steady-state current (i_{ss}) first increased and then decreased with increased $[Bi^{3+}/[Pb^{2+}]$ as shown in Figure 4. This is even more obvious at higher rotational velocity (w). This type of relationship indicates the existence of two contradictory contributions of Bi^{3+} to the rate of PbO_2 deposition. The i_{ss} value first increases with increased $[Bi^{3+}]$ due to partial oxidation of Bi^{3+}. However, when $[Bi^{3+}]$ is further increased, the blocking of PbO_2 deposition by adsorbed bismuth ions becomes the dominant factor, so the rate of deposition decreases with further increase in $[Bi^{3+}]$. The i_{ss} value hardly changed with variation of w at high $[Bi^{3+}]/[Pb^{2+}]$ values, which suggests that the deposition shifts from mass-transport control to kinetic control as $[Bi^{3+}]$ is increased.

The following conditions were determined to be optimal for deposition of $Bi-PbO_2$. Solution: 10 mM Pb^{2+} and 1 mM Bi^{3+} in 1.0 M $HClO_4$; potential/time: 1.9 V for 10-20 sec followed by a decrease to 1.8 V for ca. 20 min. For increased $[Bi^{3+}]$, the deposition potential values are increased accordingly.

Morphology and Bi distribution on $Bi-PbO_2$ It was shown by SEM that the crystalline size of $Bi-PbO_2$ was greater than that of pure PbO_2 (10c). More work in this respect was done with a larger variety of Bi/Pb concentration ratios. The results showed that the surface roughness of the electrodeposited mixed oxide was more a function of deposition

conditions than a function of the Bi/Pb concentration ratio. Therefore, changes in morphology following the incorporation of bismuth into PbO_2 are concluded not to result in enhancement in the electrocatalytic activity.

The Bi/Pb atomic ratio in Bi-PbO_2 was measured semi-quantitatively as a function of $[Bi^{3+}]/[Pb^{2+}]$ by both EDS and XPS, as shown in Figures 5. The Bi/Pb atomic ratios measured by these two techniques are representive of different depth in the mixed oxide because these techniques have largely different depth sensitivity.

The Bi/Pb atomic ratio within a depth of ca. 0.5 m was obtained by EDS (Curve b). As expected, the Bi/Pb atomic ratio in the mixed oxide increased with increased $[Bi^{3+}]/[Pb^{2+}]$. At low Bi/Pb concentration ratios, the slope of the plot is close to one, but the curve bends to the ordinate at higher $[Bi^{3+}]/[Pb^{2+}]$ values. It is concluded that at high Bi/Pb concentration ratios, the Bi/Pb atomic ratio in the oxide becomes smaller than that in the solution.

The elemental composition of the Bi-PbO_2 at 20 - 200 atomic layer of the oxide surface was determined by XPS as shown by Curve a in Figure 5. Clearly, the Bi/Pb atomic ratio at the surface increased with increased $[Bi^{3+}]/[Pb^{2+}]$ more linearly than that in the bulk of the oxide as determined by EDS. Therefore, it is concluded that a depth gradient exists in the Bi/Pb atomic ratio in the Bi-PbO_2.

The elemental distribution on the same region of a Bi-PbO_2 sample was imaged by EDS as shown in Figure 6A&B for Bi and Pb, respectively. Fewer spots appeared for Bi than for Pb, which represents the Bi/Pb

atomic ratio in the oxide. It is also concluded from Figure 6B that Bi
is distributed evenly across the surface of the Bi-PbO2.

Catalytic activity of Bi-PbO$_2$ electrodes   The catalytic activity
of the Bi-PbO$_2$ electrode has been characterized using chronoamperometry
(10c,d). Voltammetric studies of this system can yield more information.
In Figures 7 and 8 are the voltammetric responses at Bi-PbO$_2$ for
oxidation of Mn^{2+} to MnO_4^- and dimethyl sulfoxide (DMSO) to dimethyl
sulfone (DMSO$_2$), respectively. Since MnO_2 from the partial oxidation of
Mn^{2+} can foul the Bi-PbO$_2$ electrode (20b), the cyclic voltammograms in
Figure 8 were for the first few cycles.

Both reactions were too slow to occur at pure PbO$_2$ and at Pt, Au,
and C electrodes. However, both reactions were nearly under mass-
transport control at the Bi-PbO$_2$ electrode, as shown by the dependence of
the i-E waves on w in Figures 7 and 8. These two reactions are different
in many respects. For example, DMSO reactant is organic and Mn^{2+} is
inorganic; DMSO is a neutral molecule and Mn^{2+} is a metal cation; DMSO ->
DMSO$_2$ is a 5-electron/4-oxygen transfer and Mn^{2+} -> MnO_4^- is a 2-
electron/1-oxygen transfer; most important of all, the standard
potentials for the two reactions are far apart at 0.0 and 1.45 V vs. SCE,
respectively (23). Despite these differences, their values of half-wave
potential ($E_{1/2}$) are virtually the same (ca. 1.65 V) at Bi-PbO$_2$, which is
a strong indication of mediated electrocatalysis with a common rate-
controlling step.

The catalytic activity of Bi-PbO$_2$ is strongly dependent on the Bi/Pb
atomic ratio in the oxide. As shown in Figure 9, the i-E curve shifted

to less positive values as Bi/Pb ratio increased. At Bi/Pb atomic ratio < 0.3, the i-E curve had a wave shape which increased with increased Bi/Pb atomic ratio. The plateau shaped i-E curves were obtained only at Bi/Pb atomic ratios $\geq$ 0.5. These results are consistent with that the measured kinetic current at the $Bi-PbO_2$ increased with increased Bi/Pb atomic ratio under constant-potential conditions (10c).

Partial oxidation of Bi^{3+} to Bi(V)   The height of the anodic plateau in Figure 1A increased slightly but not as a linear function of $[Bi^{3+}]$. Since the plateau is under mass-transport control, it is concluded that the additional current is due to the oxidation of some Bi^{3+} to Bi(V). Thus, the average oxidation state of Bi in the $Bi-PbO_2$ is somewhere between +3 and +5, which might be a function of depth in the mixed oxide. It is known that Bi^{5+} is unstable in aqueous solution. Direct oxidation of Bi^{3+} was not observed at Pt, Au, GC, PbO_2, or $Bi-PbO_2$ electrodes (20c,d). However, partial oxidation of Bi^{3+} is possible during in-situ deposition of PbO_2 (20b) as a result of the catalytic effect of PbO_2 deposition intermediates and the stabilizing effect of the PbO_2 matrix on Bi^{5+}. The stabilizing effect is based on a similar concept derived from studies on selective oxidation of catalysts in which stabilization of metal cations in high oxidation states is essential (15,16,24).

The existence of Bi(V) on the surface of $Bi-PbO_2$ was proved also by the observation of a very small amount of MnO_4^- generated under open-circuit conditions at the surface of $Bi-PbO_2$ contacting a Mn^{2+} solution. This phenomenon was not observed with pure PbO_2 or Bi^{3+}-adsorbed PbO_2.

The only explanation for this chemical reaction is that Mn^{2+} can be oxidized directly by the highly oxidizing Bi(V) at the surface of Bi-PbO_2. This reaction stopped abruptly, however, probably due to the rapid comsumption of Bi(V). The rate of oxygen evolution at the Bi-PbO_2 was observed to be slightly higher than that at the Bi^{3+}-adsorbed PbO_2, which might be caused by the existence of Bi(V) at the surface of Bi-PbO_2, but not at the Bi^{3+}-adsorbed PbO_2.

Residual voltammetric response at Bi-PbO_2 in aqueous solution

Shown in Figure 10 are the residual i-E curves of different electrodes in 1.0 M $HClO_4$. It is apparent that the residual current for bare Au, Pt, and smooth PbO_2 (Curve a) is virtually zero. The smooth PbO_2 electrode was deposited following optimized conditions (20a) and had a low surface roughness. The latter is concluded to be responsible for the low residual current. Lead dioxide film electrodes with high surface roughness were prepared by increasing the acidity and lowering the Pb^{2+} concentration in the deposition solution. The resultant PbO_2 films had larger residual currents, as shown by Curve b in Figure 10, which increased linearly with increased scan rate but did not change with increased w. This residual current also changed with variation of the preparation conditions which affect the surface roughness. Similar residual i-E was reported for organic polymer-covered electrodes (25), which were ascribed to charging current that is related to the surface porosity.

A high residual current was observed at Bi-PbO_2, as shown by Curve c in Figure 10. The height of the current in both positive and negative

scans increased linearly with increased scan rate, but did not change

with increased w. The current also increased with increased Bi/Pb atomic

ratio in the oxide and the thickness of the film. It is concluded that

this large residual current is a capacitive current in nature, due to the

increased surface roughness of the Bi-PbO_2 compared to that of pure PbO_2.

The latter is related to the decreased rate of oxide deposition in the

presence of Bi^{3+}. This conclusion is supported further by a study of the

oxides with FTIR with photoacoustic detector. Although no distinquished

fine IR structure was observed for pure and Bi-doped PbO_2 except in the

400 - 600 cm^{-1} range, the baseline for Bi-PbO_2 is much higher than that

for PbO_2, especially in the high wave number range (1600 - 4000 cm^{-1}).

This is explained by the stronger absorbance of Bi-PbO_2 as a result of

the higher surface roughness than that of PbO_2. This result is also

consistent with that obtained with diffuse reflectance detector.

Deposition of Bi-PbO_2 with low surface roughness, and so low

residual current can be achieved with careful selection of the deposition

conditions. For instances, a pulsed potential waveform with a high

initial potential value and a lower acidity are in phavor of decreasing

the roughness.

Residual voltammetric response at Bi-PbO_2 in acetonitrile   Cyclic

voltammograms at Bi-PbO_2 electrode also were obtained in non-aqueous

solution with a much wider potential range than in the aqueous solution.

The i-E curves in acetonitrile with 0.1 M tetra-n-butylammonia

perchlorate (TBAP) as the supporting electrolyte are shown in Figure 11.

Additional current in both positive and negative scans was observed at

the $Bi\text{-}PbO_2$, as compared to that at the pure PbO_2. Two peaks (I and II at 1.15 and 1.5 V, respectively) appeared at the Bi-doped PbO_2 in the negative scan, while there was only one at the PbO_2 (1.15 V). One anodic wave (III) appeared in the negative scan for both electrodes. Both curves increased with increased scan rate, but did not change with increased w. The dependence of the i-E curves at $Bi\text{-}PbO_2$ on scan rate is shown in Figure 12. The cathodic Peak I increased with increased scan rate faster than Peak II. The i-E curves also changed with variation of the range of potential scan, especially the anodic limit. As shown in Figure 13A, another anodic peak in the positive scan appeared at ca. 1.28 V (Peak IV) if the scan was limited to 0.4 - 1.35 V. The height of Peak IV decreased with increased scan number, especially when the anodic potential exceeded 1.35 V. As shown by Curve b in Figure 13A, Peak IV disappeared even in the second scan, and was resumed after the electrode potential had been stopped at a lower potential, e.g., 0.4 V. The height of Peak IV also increased with increased scan rate as shown in Figure 13B. The peak potential of Peak IV shifted to more positive value with increased scan rate. No such current was observed at the pure PbO_2 deposited on the same Au RDE as shown in Figure 13C. Therefore, Peak IV is not related to the surface oxide of gold substrate. It is concluded that Peak I and IV correspond to the conversion of Bi(V) $\rightarrow$ Bi(III) and Bi(III) $\rightarrow$ Bi(V), respectively.

Mechanism of electrocatalysis at $Bi\text{-}PbO_2$ Despite the possible existence of the Bi(III)/Bi(V) redox couple in $Bi\text{-}PbO_2$, it has been shown with Bi^{3+}-adsorbed PbO_2 that the electrocatalysis at the Bi-modified PbO_2

does not occur by redox catalysis or e-t mediation (20c,d). Instead, it occurs via O-t mediation as shown by Equation 2. In this mechanism, PbO_2 serves as an inert substrate with high O_2-evolution overpotential and the immobilized Bi ions with low O_2-evolution overpotential serve as the O-t mediator. Here, the assumption has been made that the bismuth sites have stronger affinity for the OH radicals than the lead sites, which are not changed by the oxidation state of the Bi. This assumption is based on a similar one suggested for electrocatalysis of O-t reactions at ad-atom-modified metal electrodes (26) and at binary Pt alloys (27). It is also true that only the Bi ions on the surface of $Bi-PbO_2$ can function as catalytic sites. Based on this mechanism, the electrocatalytic activitiy of $Bi-PbO_2$ is dependent on the surface concentration of Bi ion, i.e., surface density of the catalytic sites. Therefore, the i-E curves observed in Figure 9 are as expected for "partially blocked" or "microarray" electrodes (28).

Oxygen evolution at PbO_2 and $Bi-PbO_2$ electrodes   The generation of OH radicals was proposed within the mechanism of mediated anodic O-transfer. Since OH radicals are also intermediate products for O_2 evolution (27), it was expected that incorporation of Bi ions into PbO_2 matrix would slightly decrease the O_2 overpotential. It was demonstrated (10d) that the rate of O_2 evolution at $Bi-PbO_2$ was faster than that at pure PbO_2 at the same electrode potential and increased with increased Bi content in the mixed oxide from 0 to 0.5. No explanation was given in (10d). Here, it is concluded that these results are further evidence in direct support of the O-t mediation as Equation 2.

An attempt was made to detect the electrogenerated OH radicals at $Bi-PbO_2$ with a rotating ring-disc electrode (RRDE). It failed, however, probably because the RRDE technique is not sensitive enough to detect the small amount of OH radicals that decompose too fast once they leave the electrode surface by convective-diffusional transport.

Conclusions

Despite the clear evidence for the existence of a small amount of Bi(V) and the possible interconversion between Bi(III) and Bi(V) in the Bi-doped PbO_2, we conclude that the electrocatalytic reactions at the Bi-doped PbO_2 do not take place by redox catalysis or e-t mediation, but rather by an O-t mediation. Both Bi(III) and Bi(V) at the electrode surface can function as the O-t mediator by promoting the generation of OH radical. Some similarities exist between the O-t and e-t mediations, e.g., the independence and dependence of $E_{1/2}$ values on the identity of analytes and catalyst concentration, respectively.

The existence of Bi^{3+} in the Pb^{2+} solution decreases the rate of PbO_2 deposition and the existence of Bi in the PbO_2 decreases the rate of PbO_2 dissolution. Therefore, the Bi ions decrease the overall reversibility of the PbO_2-Pb^{2+} couple. Bismuth(III) ions can be adsorbed onto a PbO_2 surface and incorporated into a PbO_2 matrix as impurities along with the electrocrystallization of PbO_2. Thus, the Bi-doped PbO_2 is neither a binary oxide compound nor a solid solution of two oxides. As a result, the $Bi-PbO_2$ has the same rutile crystal structure as the pure PbO_2, as studied in (10c). The existence of adsorbed Bi^{3+} at the surface of PbO_2 makes the further crystallization of PbO_2 difficult.

References

1. Adams, R. N. "Electrochemistry at Solid Electrodes"; M. Dekker: New York, 1969.

2. (a) Makrides, A. C. J. Electrochem. Soc. 1966, 113, 1159. (b) Conway, B. E.; Marincic, N.; Gilroy, D.; Rudd, E. J. Electrochem. Soc. 1966, 113, 1144. (c) "The Anodic Behaviour of Metals and Semiconductors Series: Oxides and Oxide Films"; Vijh, A. K., Ed.; M. Dekker: New York, 1972-1977; Volumes 1-5. (d) Trasatti, S. "Electrodes of Conductive Metallic Oxides"; Elsevier: Amsterdam, 1980. (e) Trasatti, S. Materials. Chem. Phys. 1987, 16, 157. (f) Trasatti, S. J. Electroanal. Chem. 1980, 111, 125. (g) Schmickler, W.; Schultze, J. W. In "Modern Aspects of Electrochemistry"; Bockris, J. O'M; Conway, B. E.; White, R. E., Eds.; Plenum: New York, 1985; No. 17. (h) Burke, L. D.; Lyons, M. E. G. In "Modern Aspects of Electrochemistry"; White, R. E.; Bockris, J. O'M.; Conway, B. E., Eds.; Plenum: New York, 1986; No. 18. (i) O'Sullivan, E. J. M.; Calvo, E. J. In "Comprehensive Chemical Kinetics"; Compton, R. G., Ed.; Elsevier: Amsterdam, 1987; Volume 27, p. 247.

3. (a) Johnson, D. C. J. Electrochem. Soc. 1972, 119, 331. (b) Austin, D. S.; Johnson, D. C.; Hines, T. G.; Berti, E. T. Anal. Chem. 1983, 55, 2222. (c) Cabelka, T. D.; Austin, D. S.; Johnson, D. C. J. Electrochem. Soc. 1984, 131, 1596; 1985, 132, 359.

4. (a) Sneil, K. D.; Keenan, A. G. Chem. Soc. Rev. 1979, 8, 259. (b) Murray, R. W. Acc. Chem. Soc. 1980, 13, 135. (c) Albery, W. J.; Hillman, A. R. Ann. Reports Progress Chem. C. Phys. Chem. 1981, 78, 377.

5. (a) Neff, V. D. J. Electrochem. Soc. 1978, 125, 886. (b) Ellis, D.; Eckhoff, M.; Neff, V. D. J. Phys. Chem. 1981, 85, 1225. (c) Itaya, K.; Shibayama, K.; Akahoshi, H.; Toshima, S. J. Appl. Phys. 1982, 53, 804. (d) Itaya, K.; Ataka, T.; Toshima, S. J. Am. Chem. Soc. 1982, 104, 4767.

6. (a) Borcarsly, A. B.; Sinha, S. J. Electroanal. Chem. 1982, 137, 157; 1982, 140, 167. (b) Sinha, S.; Humphrey, B. D.; Borcarsly, A. B. Inorg. Chem. 1984, 23, 203.

7. (a) Fox, J. A.; Kulesza, P. J. Anal. Chem. 1984, 56, 1021. (b) Fox, J. A.; Kulkarni, K. Talanta, 1986, 33, 911. (c) Fox, J. A.; Das, B. K. Anal. Chem. 1985, 57, 2739. (d) Fox, J. A.; Das, D. B. J. Electroanal. Chem. 1987, 233, 87. (e) Kulesza, P. J. J. Electroanal. Chem. 1987, 220, 295.

8. (a) Murray, C. G.; Nowak, R. G.; Rolison, D. R. J. Electroanal. Chem. 1984, 164, 205. (b) Ghosh, P. K.; Bard, A. J. J. Am. Chem. Soc. 1983, 105, 5691. (c) Ghosh, P. K.; Mau, A. W.-H.; Bard, A. J. J. Electroanal. Chem. 1984, 169, 315. (d) Liu, H. Y.; Anson, F. C. J. Electroanal. Chem. 1985, 184, 411.

9. (a) Janssen, L. J. J.; Starmans, L. M. C.; Visser, J. G.; Barendtecht, E. Electrochim. Acta 1977, 22, 1093. (b) Burke, L. D.; O'Neill, J. F. J. Electroanal. Chem. 1979, 101, 341. (d) Burke, L. D.; Murphy, O. J. J. Electroanal. Chem. 1979, 101, 351. (e) Novak, D. M.; Tilak, B. V.; Conway, B. E. In "Modern Aspects of Electrochemistry"; Bockris, J. O'M.; Conway, B. E.; White, R. E., Eds.; Plenum Press: New York, 1982; No. 14.

10. (a) Austin, D. S.; Polta, J. A.; Polta, T. Z.; Tang, A. P.-C.; Cabelka, T. P.; Johnson, D. C. J. Electroanal. Chem. 1984, 168, 227. (b) Johnson, D. C.; Polta, J. A.; Polta, T. Z; Neuburger, G. G.; Johnson, J.; Tang, A. P.-C.; Yeo, I.-H.; Baur, J. J. Chem. Soc., Faraday Trans. 1 1986, 82, 1081. (c) Yeo, I.-H.; Johnson, D. C. J. Electrochem. Soc. 1987, 134, 1973. (d) Yeo, I.-H.; Ph.D. Thesis, Iowa State University, Ames, 1987. (e) Yeo, I.-H.; Kim, S.; Jacobson, R.; Johnson, D. C. J. Electrochem. Soc. Submitted. (f) Tang. A. P.-C.; Johnson, D. C. Anal. Chim. Acta, in press.

11. (a) "The Electrochemistry of Lead"; Kuhn, A. T., Ed.; Academic Press: London, 1979. (b) Nagy, Z. "Electrochemical Synthesis of Inorganic Compounds: A Bibliography"; Plenum: New York, 1985.

12. (a) Rhees, R. C.; Halker, B. B. U. S. Pat. 4,038,170, July 26, 1977. (b) Rhees, R. C.; Halker, B. B. U. S. Pat. 4,101,390, July 18, 1978.

13. (a) Thangappan, R. Indian Pat. 156,545, Aug. 31, 1985; Chem. Abstr. 1986, 105, 142124. (b) Radoi, I.; Vartires, I.; Bocea, G.; Bandi, A; Rodeanu, T.; Mihelis, A.; Vass, C.; Hainavcsie, C.; Cosma, A. Romania Pat. 88,596, March 31, 1986; Chem. Abstr., 1987, 106, 40457.

14. (a) Sheldon, R. A.; Kochi, J. K. "Metal-Catalyzed Oxidations of Organic Compounds"; Academic Press: New York, 1981. (b) Holm, R. H. Chem. Rev. 1987, 87, 1401. (c) Berg, J. M.; Holm, R. H. Acc. Chem. Rev. 1986, 19, 363. (d) Moloy, K. G. Inorg. Chem. 198, 27, 677. (e) Sheldon, R. Bull. Soc. Chim. Belg. 1985, 94, 9. (f) Meyer, T. J. J. Electrochem. Soc. 1984, 131, 221C. (g) Parravano, G. Catal. Rev. 1971, 4, 53. (h) Sachtler, W. M. H. Catal. Rev. 1971, 4, 27. (i) Sharma, C. S.; Ramachandran. P. A.; Hughes, R. J. Appl. Chem. Biotechnol. 1976, 26, 231. (j) Petro, N.; El-Shobaky, G; Misak, N. Z.; Mikhail, R. Sh. Surf. Tech. 1975, 5, 315. (k) Haggins, J. C&EN, 1987; June 8, p. 20; June 22, p. 22; Sept. 14, p. 19.

15. (a) Buttrey, D. J.; Jefferson, D. A.; Thomas, J. M. Mat. Res. Bull. 1986, 21, 739. (b) Theobald, F.; Laarif, A.; Hewat, A. W. Mat. Res. Bull. 1985, 20, 653. (c) Schneemeyer, L. F.; Spengler, S. E.; DiSalvo, F. J.; Waszczak, J. V. Mat. Res. Bull. 1984, 19, 525.

16. (a) ter Maat, J. H. H.; van Dijk, M. P.; Roelofs, G.; Bosch, H.; Van de Velde, G. M. M.; Gellings, P. J.; Burggraaf, A. J. Mat. Res. Bull. 1984, 19, 1271. (b) Beyerletin, R. A.; Jacobson, A. J.; Yacullo, L. N Mat. Res. Bull. 1985, 20, 877. (c) Oka, H.; Harano, Y.; Imoto, T. J. Appl. Chem. Biotechnol. 1976, 26, 274.

17. (a) "Molecular Mechanisms of Oxygen Activation"; Hayaishi, O., Ed.; Academic Press: New York, 1974. (b) Latham, J.; Walsh, C. Ann. N. Y. Acad. Sci. 1986, 471, 207.

18. Cho, B. W.; Yun, K. S.; Chung, I. J. J. Electrochem. Soc. 1987, 134, 1664.

19. (a) Matveeva, E. S.; Shepelin, V. A.; Kasatkin, E. V. Elektrokhimiya 1984, 20, 316. (b) Matveeva, E. S.; Kasatkin, E. V. Elektrokhimiya 1984, 20, 586.

20. (a) Chang, H.; Johnson, D. C. J. Electrochem. Soc. 1989, 136, 17, 23; Chapters II-A and B, This Dissertation. (b) Chang, H.; Johnson, D. C., in preparation; Chapter III-A, this Dissertation. (c) Chang, H.; Johnson, D. C. In preparation; Chapter IV-A, this Dissertation. (d) Chang, H.; Johnson, D. C., in preparation; Chapter IV-B, this Dissertation.

21. (a) Smith, D. W. J. Chem. Ed. 1987, 64, 480. (b) Tanabe, K. "Solid Acids and Bases: their catalytic properties"; Academic: New York, 1970.

22. Seiyama, T. In "Surface and New-Surface Chemistry of Oxide Materials"; Nowotny, J.; Dufour, L. C., Eds.; Elsevier: Amsterdam, 1988; Chapter 4, p. 189.

23. "Standard Potentials in Aqueous Solutions"; Bard, A. J.; Parson, R.; Jordan, J., Eds.; M. Dekker, New York, 1985; (a) p. 220. (b) p. 186.

24. (a) Grasselli, R. K.; Burrington, J. D.; Brazdil, J. F. Faraday Soc. Discuss. 1982, 72, 203. (b) Bielanski, A.; Haber, J. Catal. Rev. Sci. Eng. 1979, 19, 1.

25. (a) Bull, R. A.; Fan, F.-R. F.; Bard, A. J. J. Electrochem. Soc. 1982, 129, 1009. (b) Bull, R. A.; Fan, F.-R. F.; Bard, A. J. J. Electrochem. Soc. 1984, 131, 687.

26. (a) Motoo, S.; Watanabe, M. J. Electroanal. Chem. 1979, 98, 203; 1976, 69, 429. (b) Watanabe, M. J. Electroanal. Chem. 1975, 60, 275. (c) Beden, B. Kadirgan, F.; Lamy, C.; Leger, J. M.; J. Electroanal. Chem. 1982, 142, 171. (d) Kadirgan, F.; Beden, B.; Lamy, C. J. Electroanal. Chem. 1983, 143, 135.

27. (a) Koch, D. F. A.; Rand, D. A. J.; Woods, R. J. Electroanal. Chem. 1976, 70, 73. (b) McNicol, D. B.; Short, R. T. J. Electroanal. Chem. 1977, 81, 249. (c) Kadirgan, F.; Beden, B.; Leger, J. M.; Lamy, C. J. Electroanal. Chem. 1981, 125, 89. (d) Beden, B.; Kadirgan, F.; Kahyaoglu, A.; Lamy, C. J. Electroanal. Chem. 1982, 135, 329. (e) Beden, B.; Lamy, C.; Leger, L. M. Electrochim. Acta 1979, 24, 1157.

28. (a) Caprani, A.; Deslouis, C.; Robin, S.; Tribollet, B. J. Electroanal. Chem. 1987, 238, 67. (b) Levart, E. J. Electroanal. Chem. 1985, 187, 247. (c) Amatore, C.; Saveant, J. M.; Tessier, D. J. Electroanal. Chem. 1983, 147, 39. (d) Contamin, O.; Levart, E. J. Electroanal. Chem. 1982, 136, 259. (e) Gueshi, T.; Tokuda, K.; Matsuda, H. J. Electroanal. Chem. 1979, 101, 29; 1978, 89, 247. (f) Tokuda, K.; Gueshi, T.; Matsuda, H. J. Electroanal. Chem. 1979, 102, 41.
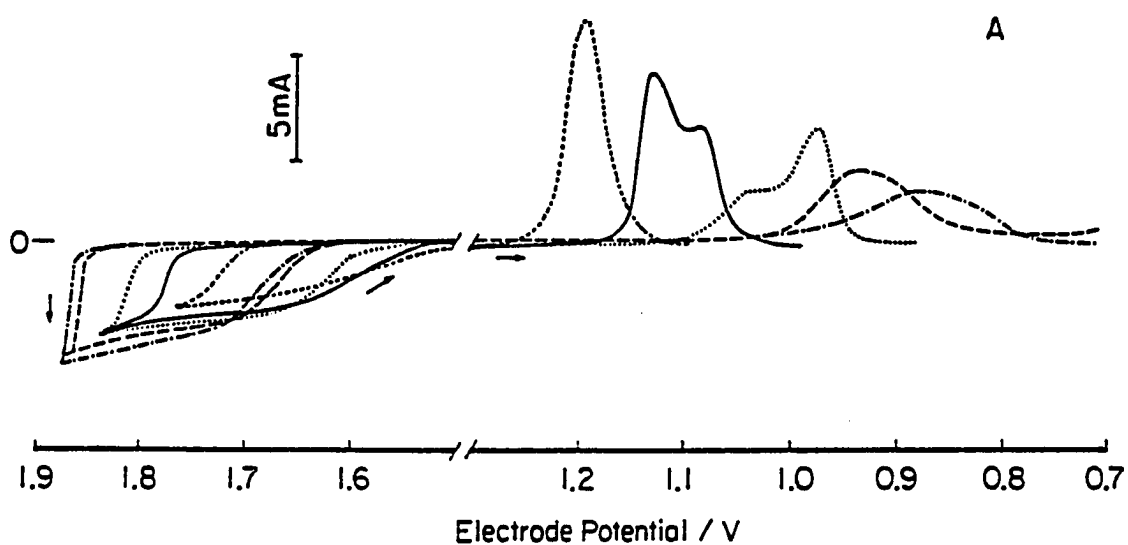
Figure 1A. Cyclic voltammograms at Au RDE in Bi^{3+} and Pb^{2+} mixture solutions

Conditions: 400 rev min^{-1}, 20 mV s^{-1}, 1.0 M $HClO_4$, 10 mM Pb^{2+}

$[Bi^{3+}]/[Pb^{2+}]$: (------) 0,
(————) 0.1,
(··········) 0.3,
(— — —) 0.5,
(—·—·—) 0.7
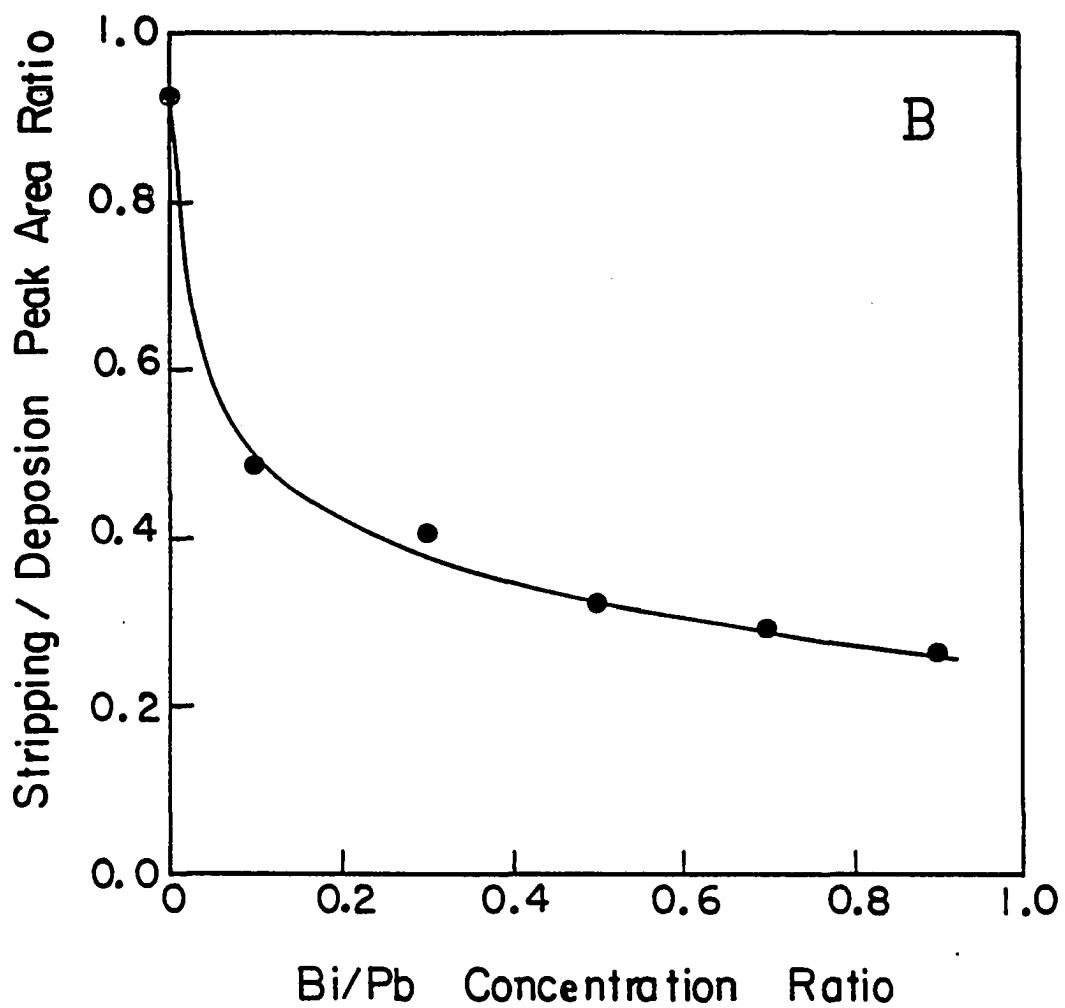
Figure 1B. Plot of stripping/deposition peak area ratio in Figure 1A vs. Bi/Pb concentration ratio
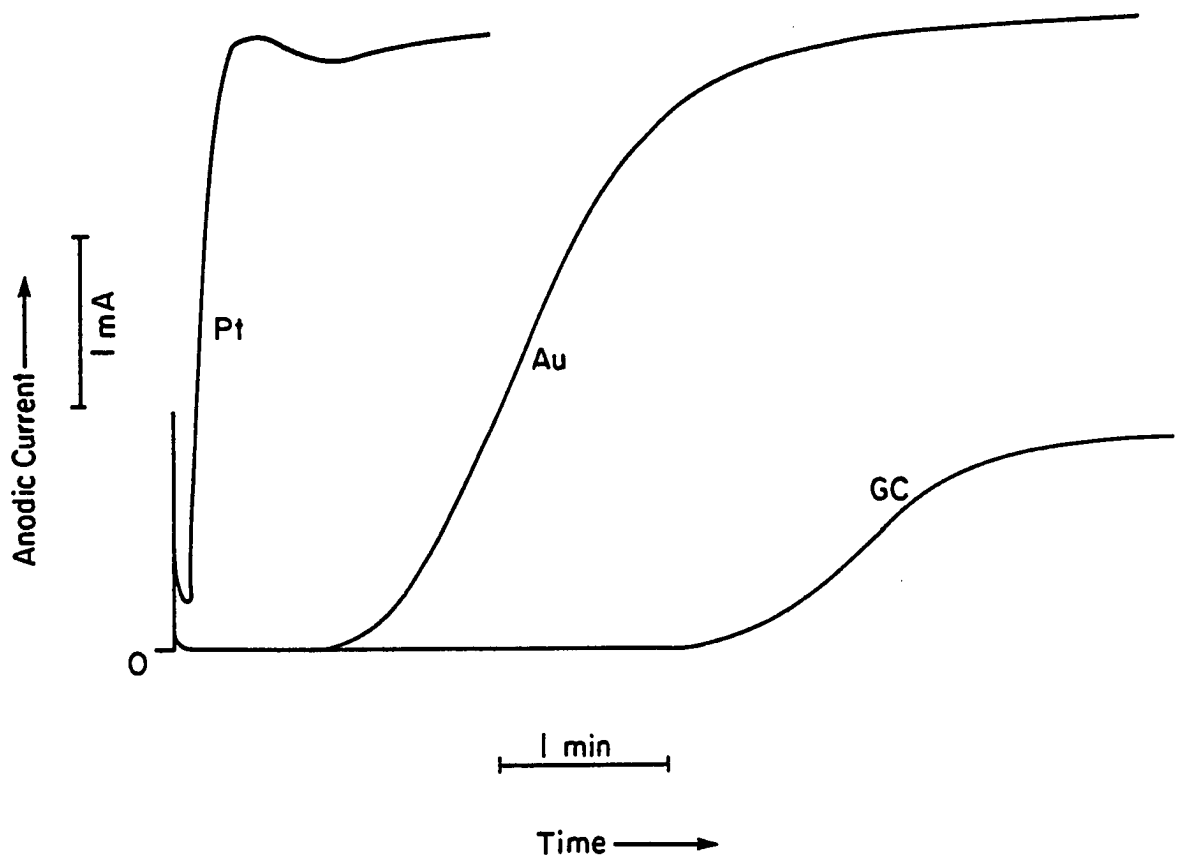
Figure 2. Chronoamperograms for Bi-PbO$_2$ deposition

Conditions: E = 1.70 V, 5 mM Bi^{3+}, 10 mM Pb^{2+}, 400 rev min^{-1}

Electrodes: (a) Pt, (b) Au, and (c) GC
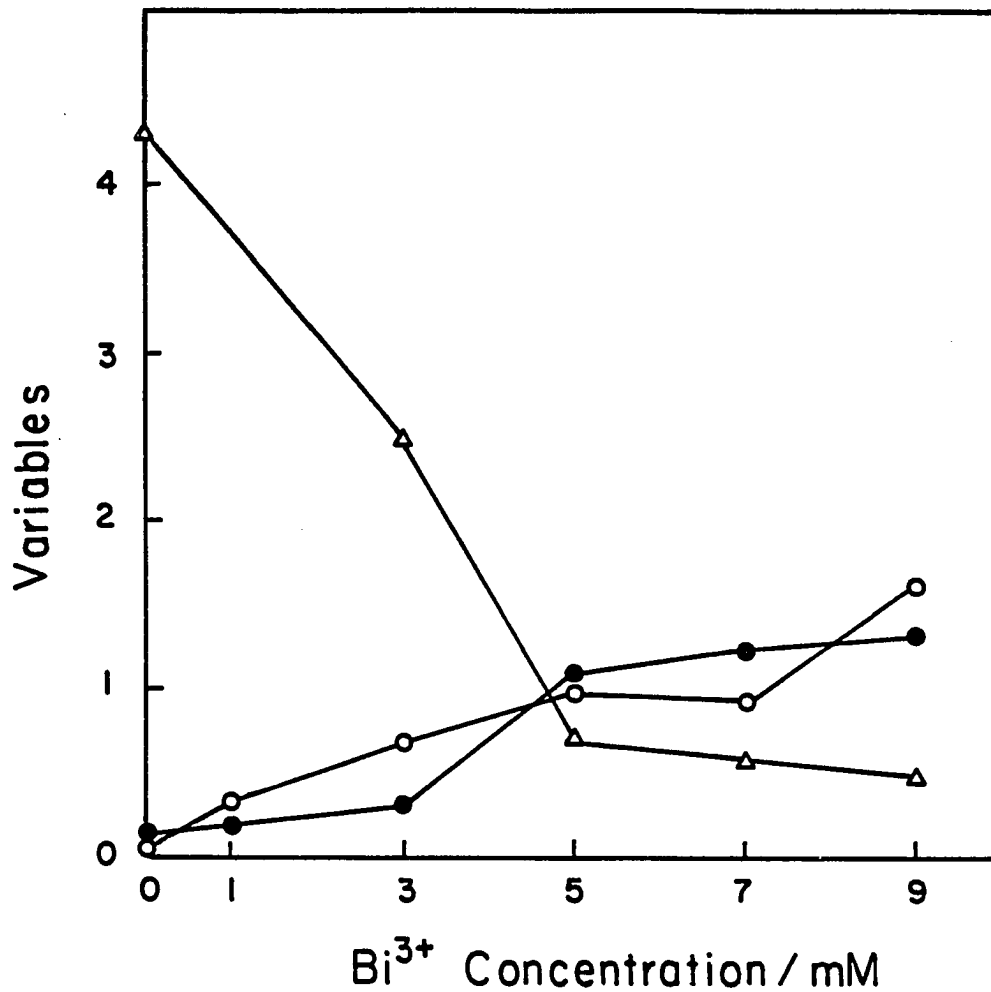
Figure 3. Plots of t_o, t_1, and S vs. $[Bi^{3+}]/[Pb^{2+}]$

Conditions: 400 rev min^{-1}, E - 1.70 V

Variables: (O) t_o/min, (●) t_1/min, and (△) S/5 mA/min
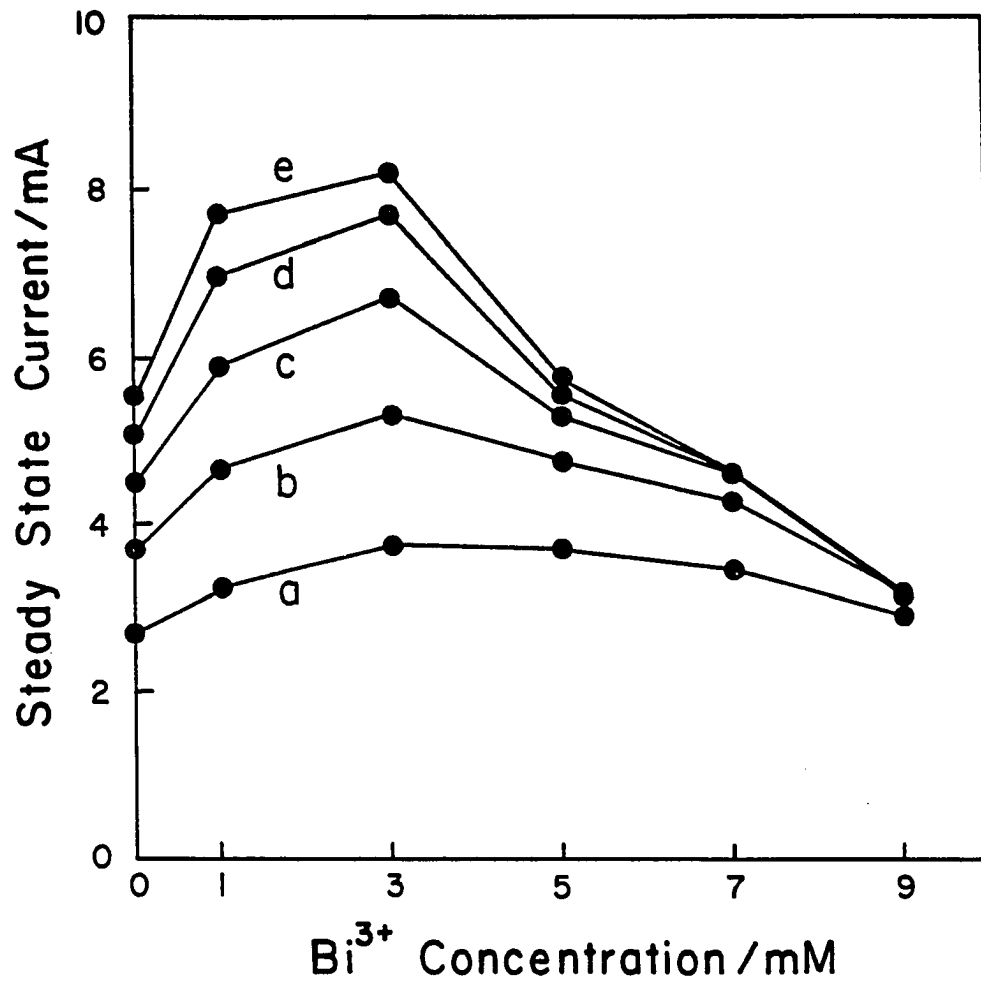
Figure 4. Plots of i_{ss} vs. $[Bi^{3+}]/[Pb^{2+}]$

Conditions: $E = 1.70$ V

w (rev min^{-1}): (a) 400, (b) 900, (c) 1600, (d) 2500, (e) 3600
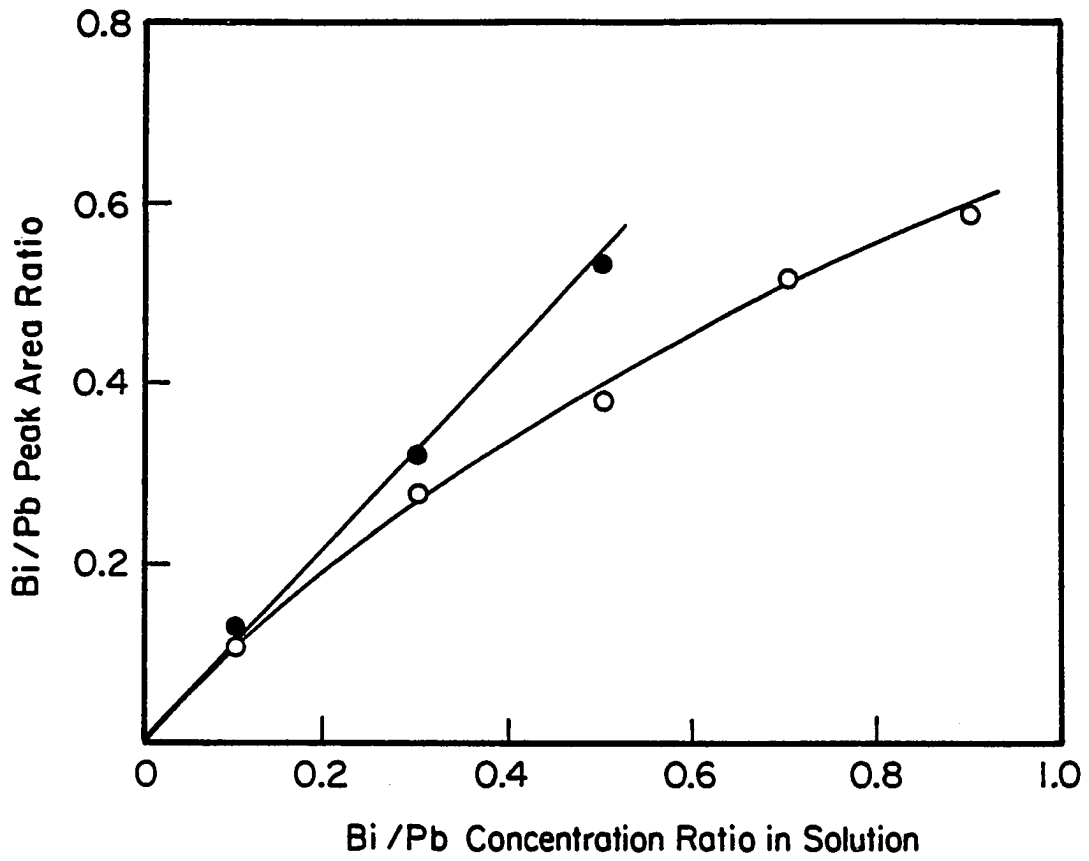
Figure 5. Plot of Bi/Pb peak area ratio for Bi-PbO_2 vs. Bi/Pb
concentration ratio in the deposition solution

Curves: (●) XPS data, (O) EDS data
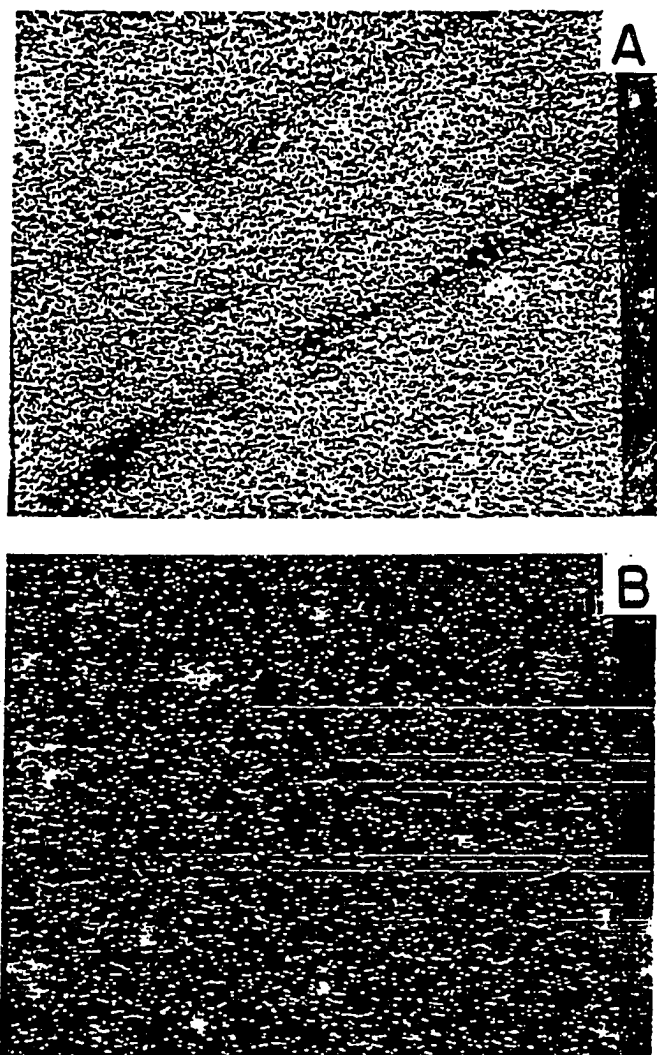
Figure 6. Elemental maps for Pb and Bi on Bi-PbO_2 surface

Deposition conditions: $[Bi^{3+}]/[Pb^{2+}]$ — 0.1

Pictures: (A) Pb, (B) Bi

SEM conditions: 25 keV beam energy, X2000
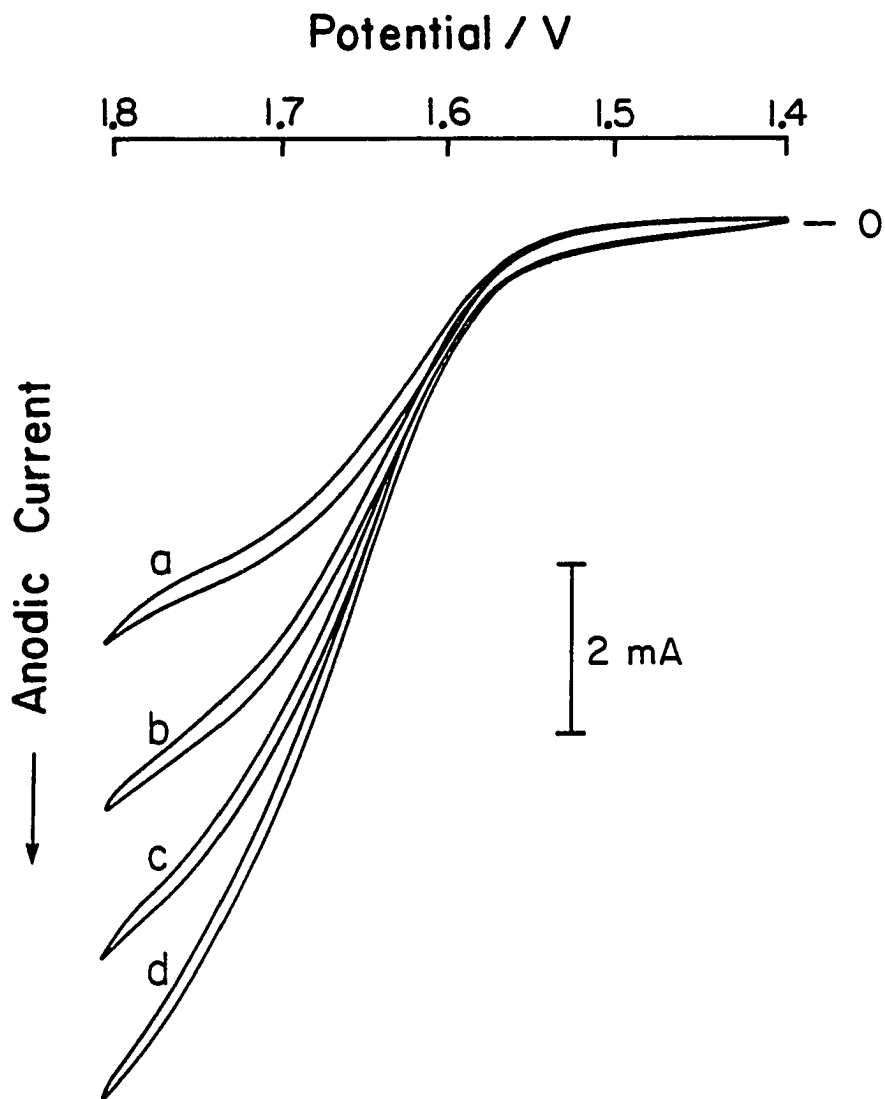
Figure 7. Voltammetric response of 10 mM DMSO oxidation at
Bi-PbO$_2$ electrode

Conditions: 20 mV s^{-1}; 1.0 M HClO$_4$; electrode deposited
from [Bi^{3+}]/[Pb^{2+}] = 0.5 solution

w (rev min^{-1}): (a) 400, (b) 900, (c) 1600, and (d) 2500

POTENTIAL / V
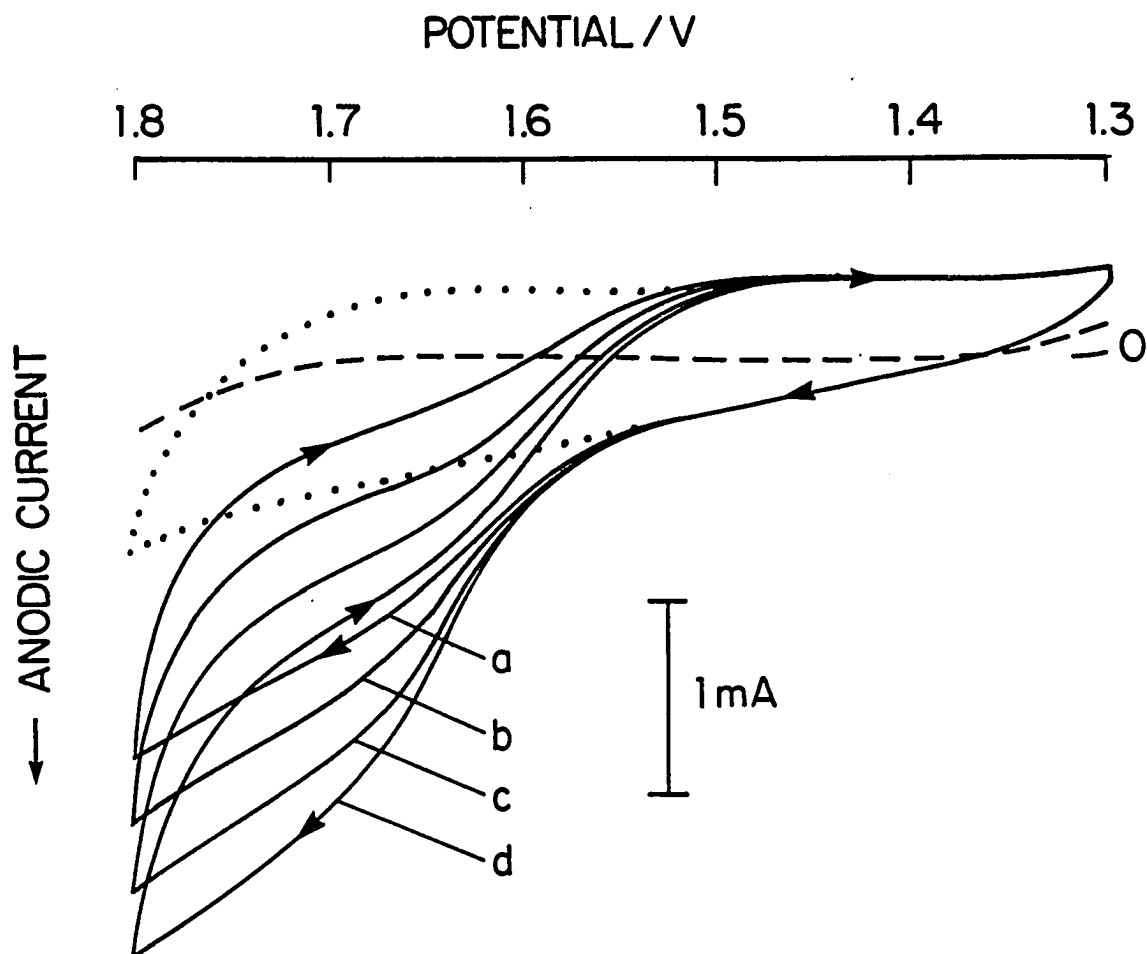
Figure 8. Voltammetric response of 10 mM Mn^{2+} oxidation at
Bi-PbO_2 electrode

Solution: 1.0 M $HClO_4$; (...) blank

Electrode: (---) PbO_2/Au; others: Bi-PbO_2 deposited from
[Bi^{3+}]/[Pb^{2+}] = 0.9 solution;

Other conditions are as given in Figure 7

w (rev min^{-1}): (a) 400, (b) 900, (c) 1600, and (d) 2500

Inset: plot of i at 1.7 V vs. $w^{1/2}$

Potential / V
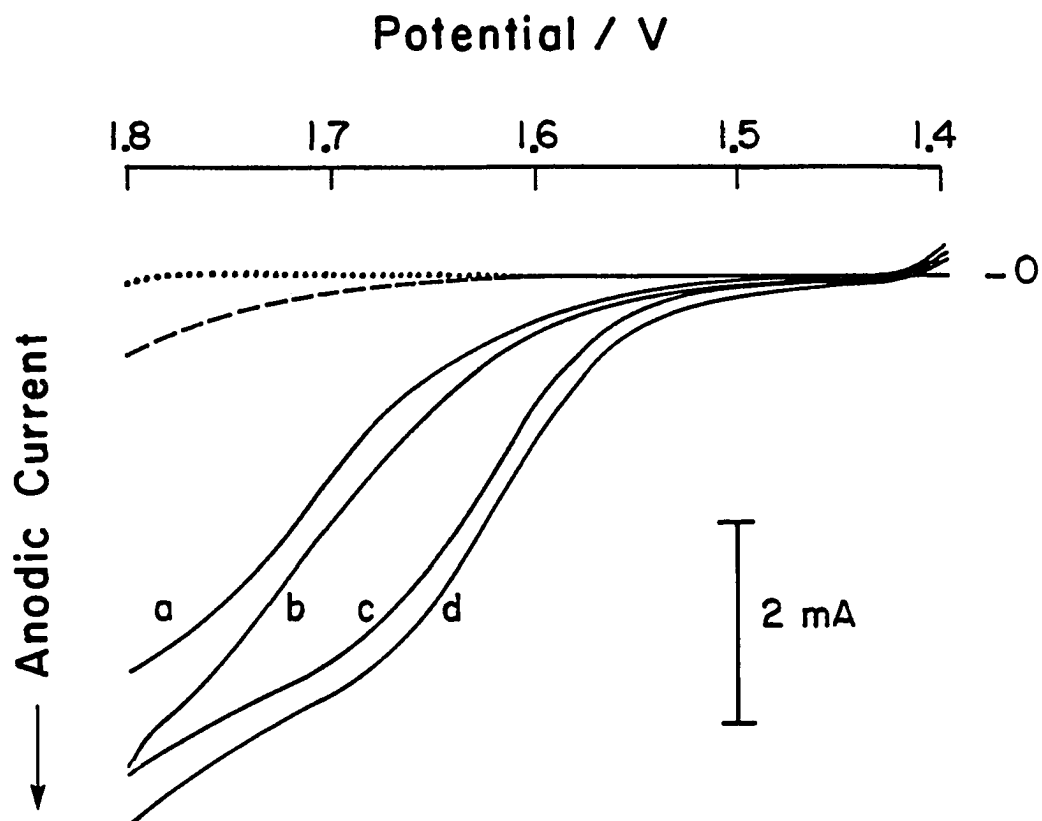
Figure 9. Effect of Bi/Pb atomic ratio in the Bi-PbO$_2$ on the
voltammetric response of 10 mM DMSO

Conditions: 20 mV s^{-1}, 400 rev min^{-1}; 1.0 M HClO$_4$

Electrodes: (——) Bi-PbO$_2$, (....) Au, (— — —) PbO$_2$

[Bi^{3+}]/[Pb^{2+}]: (a) 0.1, (b) 0.3, (c) 0.5, (d) 0.9

Only positive scan is shown
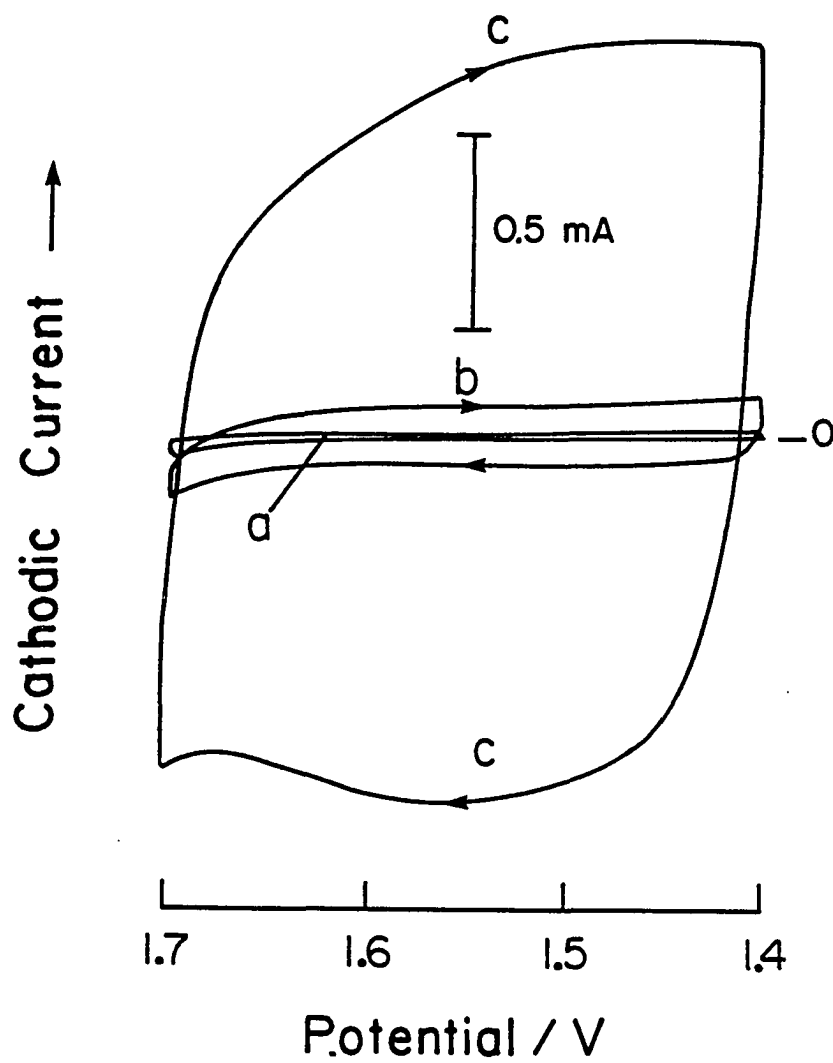
Figure 10. Cyclic voltammograms at $Bi\text{-}PbO_2$ in 1.0 M $HClO_4$

Conditions: 40 mV s^{-1}, 400 rev min^{-1}

Electrode: (a) Au, Pt or smooth PbO_2,
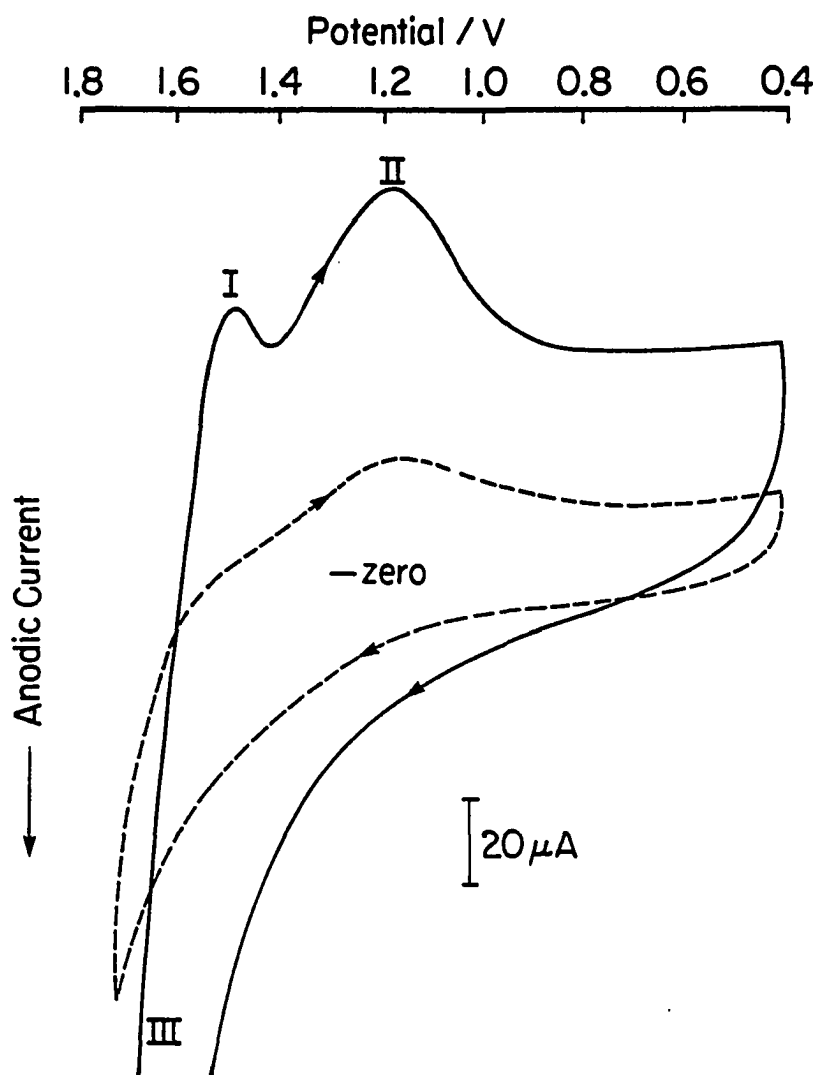(b) rough PbO_2,
(c) $Bi\text{-}PbO_2$

Figure 11. Cyclic voltammograms in acetonitrile

Conditions: 0.1 M TBAP; 200 mV s^{-1}, 0 rev min^{-1}

Electrodes: (——) Bi-PbO$_2$, from [Bi^{3+}]/[Pb^{2+}] = 0.1
solution
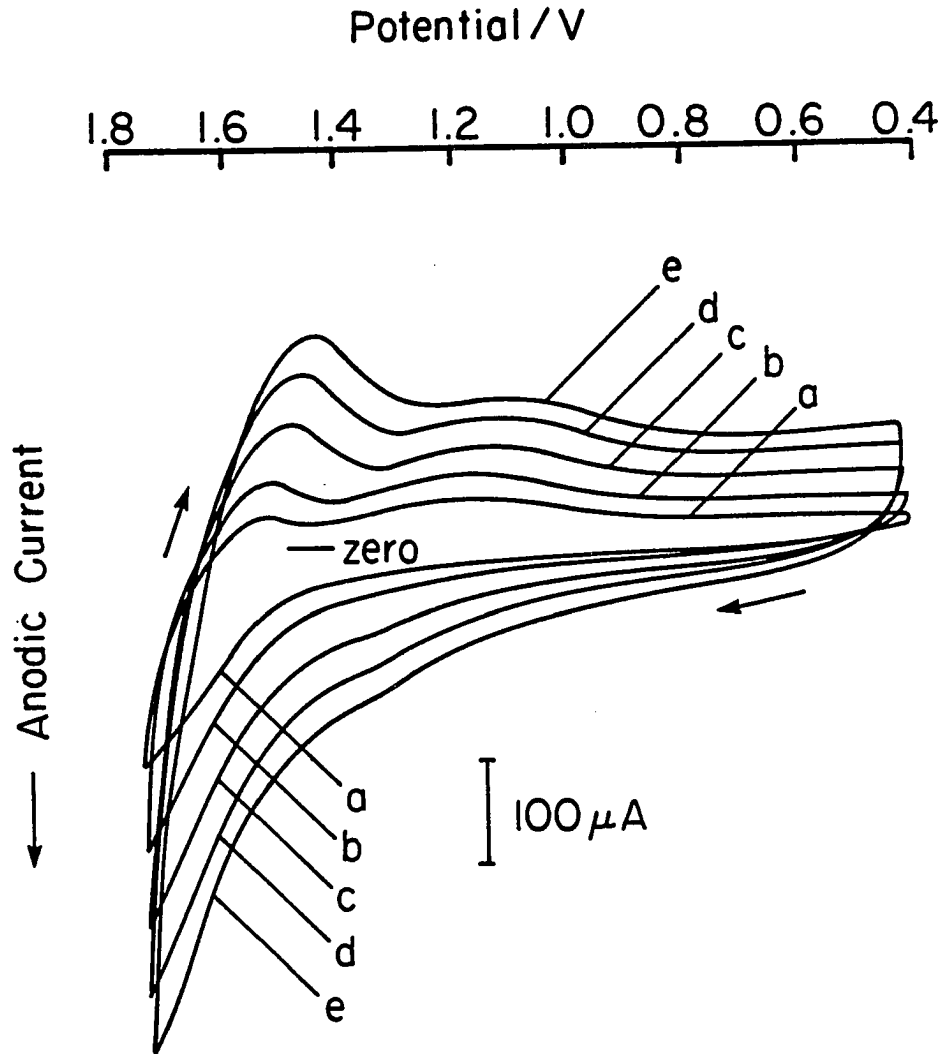(----) pure PbO$_2$

Potential / V

Figure 12. Effect of scan rate on the i-E curves at Bi-PbO$_2$ in acetonitrile

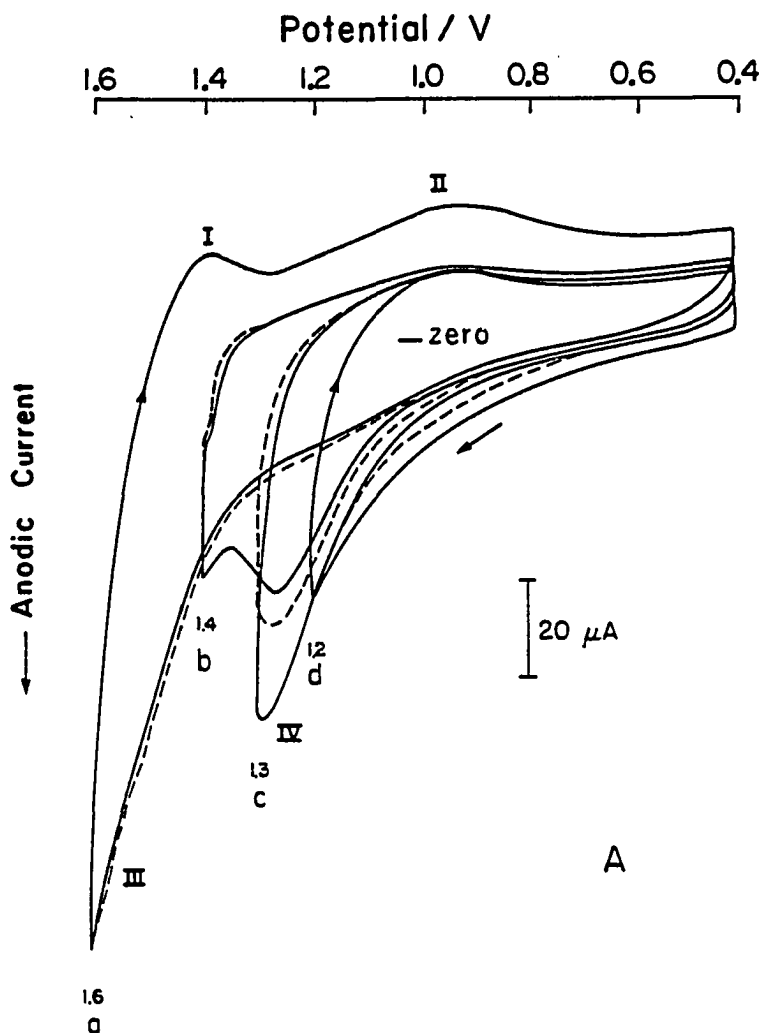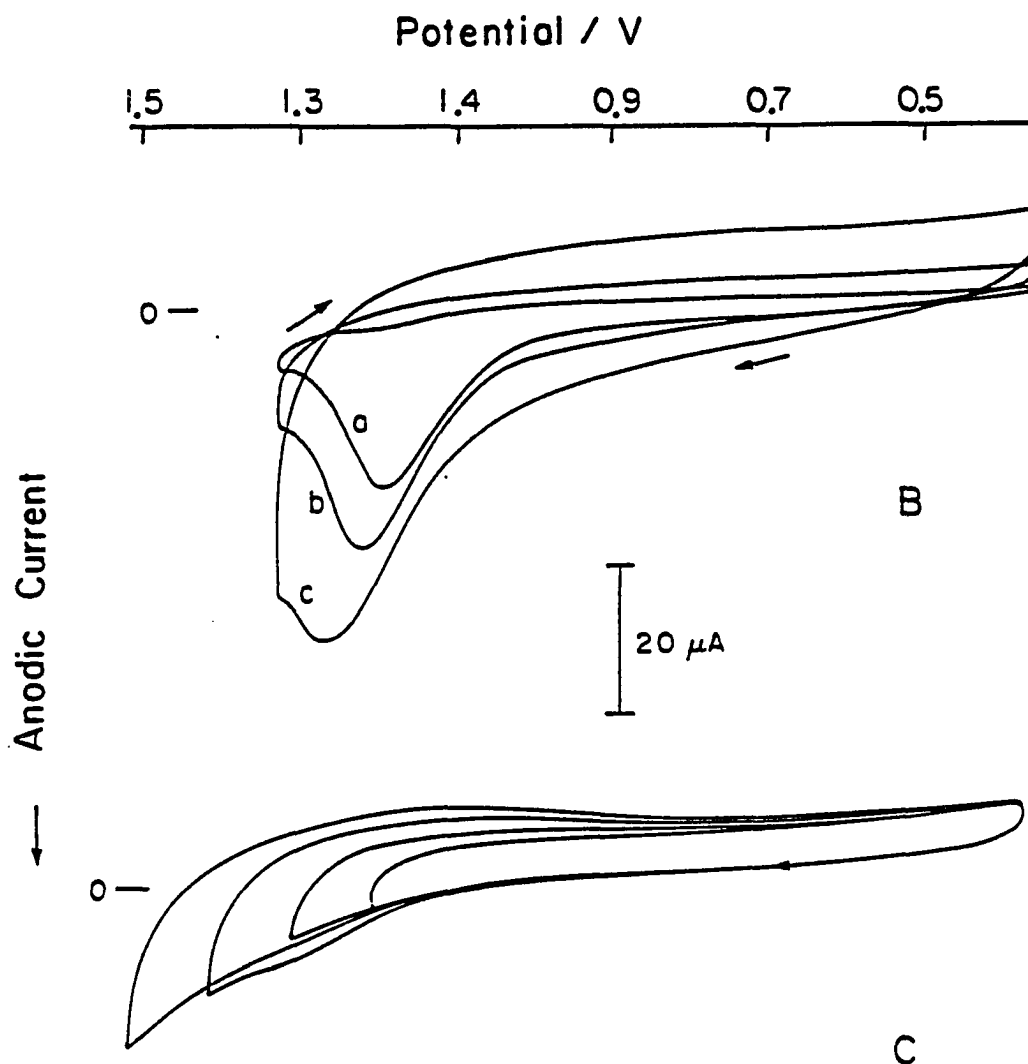Scan rate (mV s^{-1}): (a) 100, (b) 200, (c) 400, (d) 600, (e) 800

Figure 13A. Cyclic voltammograms at Bi-PbO$_2$ in acetonitrile at different anodic potential limits

Conditions: 80 mV s^{-1}, 0 rev min^{-1}; Bi-PbO$_2$ deposited from [Bi^{3+}]/[Pb^{2+}] = 0.1 solution

Solid line: first scan; Dashed line: second scan

Positive potential limit (V): (a) 1.6, (b) 1.4, (c) 1.3, (d) 1.2

Potential / V

Figures 13B,C. Cyclic voltammograms in acetonitrile

Electrodes: (B) Bi-PbO$_2$

Effect of scan rate (mV s^{-1}):
(a) 5, (b) 20, (c) 80

(C) PbO$_2$

Conditions: as given in Figure 13A.

IV. MODIFICATION OF LEAD DIOXIDE ELECTRODES BY ELECTROADSORPTION

A. Electrocatalytic Oxidation of Dimethyl Sulfoxide at Lead Dioxide Electrode Modified with Bismuth(III) by Electroadsorption[1]

"It is a capital mistake to theorize before one has data. Insensibly one begins to twist facts to suit theories, instead of theories to suit facts."

-Sir Arthur Conan Doyle,
"A Study in Acarlet"

"It is also a good rule not to put too much confidence in experimental results until they have been confirmed by theory."

-Sir Arthur Eddington

[1]To be submitted to J. Electrochem. Soc.

Abstract

Anodic oxidation of dimethyl sulfoxide (DMSO) in 1.0 M $HClO_4$ does not occur at any conventional anode materials, but proceeds readily at PbO_2 electrode with a small amount of Bi^{3+} added to the solution as catalyst. This phenomenon was studied as a model of electrocatalytic oxygen-transfer reactions. Voltammetric and chronoamperometric data were obtained as a function of rotational velocity, DMSO and Bi^{3+} concentrations, potential scan rate, electrode potential, solution pH, properties of the PbO_2 film (structure, thickness, and porosity) and the substrate material. A well-defined i-E plateau was observed even for a $DMSO/Bi^{3+}$ concentration ratio — 750. The height of this plateau increased linearly with increased DMSO concentration and the square root of rotational velocity. It is concluded that this catalytic reaction resulted from the surface modification of the PbO_2 electrode by electroadsorption of Bi^{3+}. The Bi^{3+}-adsorbed PbO_2 electrode showed better catalytic activity than the Bi-doped PbO_2 electrode prepared by co-deposition. The initial rate of DMSO oxidation at a constant applied potential was proportional to the surface coverage by adsorbed Bi^{3+} for low fractional coverages. However, the oxidation rate decreased for high coverages, i.e., $[Bi^{3+}] > 0.01$ mM. These results are consistent with the mechanism of electrocatalytic O-transfer in which the surface-immobilized Bi^{3+} functions as a spatially separated O-transfer mediator. The oxidation product of DMSO was identified with GC/MS as dimethyl sulfone $(DMSO_2)$.

Introduction

Incorporation of ionic catalysts into metal oxide matrices has been the subject of intensive research in our laboratory in recent years (1,2). The goal is to selectively promote the rate of anodic oxygen-transfer (O-t) reactions by immobilization of O-t mediators (2a) onto an inert support, e.g., PbO_2. A successful early example was the incorporation (doping) of Bi^{3+} into PbO_2 by electrochemical co-deposition, which has resulted in a fundamental study of the electrochemistry and applications of Bi-doped PbO_2 (Bi-PbO_2) electrodes.

One of the most interesting discoveries is that a pure PbO_2 electrode can have catalytic activity for O-transfer, similar to that observed for Bi-PbO_2, if a small amount of Bi^{3+} is added to the solution containing the reactant (2b). Such a PbO_2 electrode modified in-situ with Bi^{3+} has higher stability than the Bi-PbO_2 for oxidation of Mn^{2+} to MnO_4^-, by preventing the fouling of the oxide through continuous renewal of the surface catalytic sites. A more detailed study is described in the present report on the kinetics and mechanisms of electrocatalysis at a pure PbO_2 film electrode with Bi^{3+} co-existing in the solution.

The oxidation of DMSO was chosen as a model reaction in the present study, because of the assumption that the reaction stoichiometry is relatively simple (1 oxygen and 2 electron) and the product $DMSO_2$ does not deactivate the electrode surface.

$$(CH_3)_2SO + H_2O \longrightarrow (CH_3)_2SO_2 + 2H^+ + 2e$$
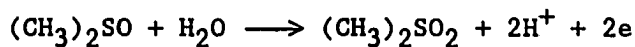
It is generally agreed that DMSO is anodically inert on most electrodes

due to a very high value of overpotential, despite the low value for the standard potential (0.0 V vs SCE) (3). Hence, the electrochemical oxidation of DMSO has not been studied in detail because of a lack of catalytic electrodes. There are a few papers in which electrochemical oxidation of pre-adsorbed DMSO on Pt were described (4), aiming at the possible effects of DMSO adsorption on other anodic processes when DMSO is used as a solvent. Since only adsorbed DMSO can be oxidized, the extent of oxidation is very limited. In contrary, the chemical oxidation of DMSO proceeds easily with a variety of oxidants (5-8), whose kinetics and mechanisms are summarized in the next section. Therefore, it is very desirable if a catalytic electrode can be found at which the oxidation of DMSO can proceed readily.

Kinetics and mechanism of chemical oxidation of DMSO

The oxidation of DMSO has been studied as a typical radical reaction with O-transfer and as a model for oxidation of simple organic sulfur compounds (5-8). The mechanisms of DMSO oxidation are dependent on solution pH. In acidic media, the mechanisms also depend on the oxidant used: e.g., peroxyanions (5), halide and halide ions (6), and metal cations (7). In alkaline media, the mechanism seems independent of the oxidants (8). The four basic mechanisms are presented below.
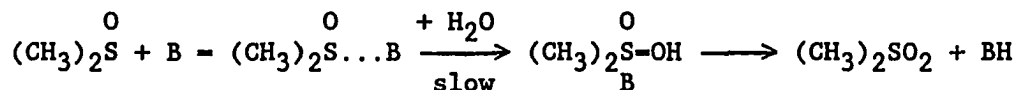
In acidic media

Scheme 1   The direct oxygen-transfer from a peroxyanion (5).

$$(CH_3)_2S + \,^-OOR \xrightarrow{\text{slow}} [(CH_3)_2S...O-O-R] \longrightarrow (CH_3)_2SO_2 + \,^-OR$$
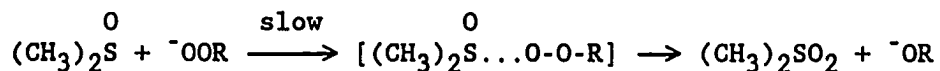
in which R — alkyl, acyl, H_2SO_3, H_3PO_4, etc.

This reaction uses the high oxidizing power of various organic and inorganic peroxyanions. In most cases, the reaction is first order in DMSO and ROO^-.

Scheme 2   The nucleophilic attack of the S-atom followed by oxygen and proton transfer from H_2O (6).

$$(CH_3)_2\overset{O}{S} + B - (CH_3)_2\overset{O}{S}...B \xrightarrow[\text{slow}]{+ H_2O} (CH_3)_2\overset{O}{\underset{B}{S}}-OH \longrightarrow (CH_3)_2SO_2 + BH$$

in which B — Br_2, Br^-, OBr^-, Cl^-, N-bromophthalimide, N-bromobenzenesulfonamide, etc. In this case, the reaction is first order in both DMSO and B, but zeroth order in DMSO if B is a large molecule. The dissociation of the complex is the rate-determining step and it must occur before the attack of the S-atom by water. The $(CH_3)_2S(O)^+$ radical was detected by electron spin resonance spectroscopy (5a).

Scheme 3   Direct oxidation by metal cations followed by oxygen transfer from H_2O (7).

$$(CH_3)_2S-O + M^h \longrightarrow (CH_3)_2\overset{+}{S}-O + M^l \xrightarrow{+ H_2O} (CH_3)_2SO_2 + 2H^+$$
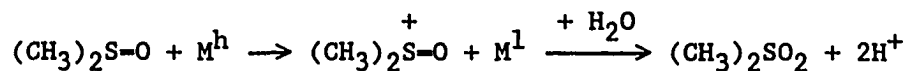
in which M — Mn^{3+}, Ce^{4+}, Cr^{5+} and Pb^{4+}. The superscripts (h and l) specify the high and low oxidation state of the metal ions. For this mechanism, the reaction is first order in DMSO and M^h.

In alkaline media

Scheme 4   Catalytic oxidation (8).

In alkaline solutions, the direct oxidation of DMSO is slow and a catalyst must be used.

$$(CH_3)_2S + cat\text{-}M^h \rightarrow (CH_3)_2\overset{O}{S}...cat\text{-}M^h \xrightarrow{+ H_2O} (CH_3)_2SO_2 + cat\text{-}M$$
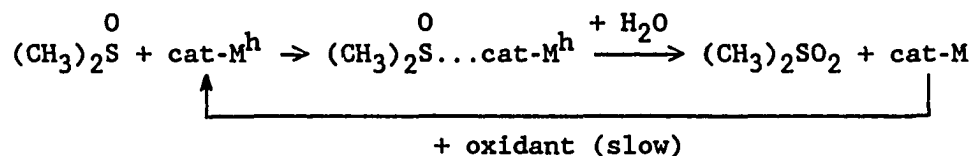
+ oxidant (slow)

Typical oxidants are O_2, BrO^{3-}, IO^{3-}, IO^{4-}, H_2O_2, and $S_2O_8^{2-}$. Typical catalysts (cat-M) are Ru(III), Os(VIII), WO_4^{2-}, Ag(I), and Cu(I). It can be seen in this mechanism that the oxidant is not used to oxidize DMSO directly, but to oxidize the catalyst M^1. Therefore, the reaction is first order in the oxidant and catalyst, but zeroth order in DMSO.

Experimental

Experimental apparatus and chemicals have been described earlier (2), except otherwise stated below.

The PbO_2 films were deposited on a Au rotated disc electrode (RDE) following the optimal conditions described in (2c). Lead(II) and bismuth(III) solutions were prepared from their nitrate salts. A microsyringe was used to add Bi^{3+} stock solution to the electrolysis solution of constant volume to vary the Bi^{3+} concentration. A model 400 GC/MS system (Finnigan) was used with a 13-m DB1 capillary column (thickness: 1 μm).

A model SHS-200 flow-injection analysis system (Fiatron, Milwaukee, WI) was used with a 25-μl sample injector. The flow rate was 3 ml min^{-1}.

Results and discussion

Cyclic voltammetry   In Figure 1A are the cyclic voltammograms of 10 mM DMSO at bare and PbO_2-coated Au RDEs with and without Bi^{3+} co-existing in the solution.   It is apparent that no DMSO oxidation occurs at Au whether or not Bi^{3+} is present.   There is no reactivity also at bare Pt and glassy carbon (GC) (data not presented).   The anodic current at PbO_2 was slightly higher than that at Au, indicating a very modest oxidation of DMSO at pure PbO_2 due to the native catalytic effect of pure PbO_2 (1).   Following the addition of 80 μM Bi^{3+}, a well-defined anodic plateau appeared.   The height of this plateau (i_1) increased linearly with increased square root of rotational velocity ($w^{1/2}$), as shown in Figure 1B, and with increased DMSO concentration (C_{DMSO}), as shown in Figures 2A,B.   These results indicate that this current plateau is under the control of mass transport of DMSO.

As is shown in Figures 1B and 2B, the experimental i_1 values are very close to those calculated from Levich equation using number of electron transfer (n) = 2 eq mol^{-1}, diffusion coefficient for DMSO (D) = 1.0×10^{-5} cm^2 s^{-1}, and kinetic viscosity (v) = 1.0×10^{-2} cm^2 s^{-1}.   A small difference exists between the theoretical and experimental values, probably due to error in the estimated values of D and v.   In effect, the experimental curves in Figures 1 and 2 can be used to determine D and v, provided one of them can be measured by another independent method.

An increase in Bi^{3+} concentration (C_{Bi}) up to 0.2 mM did not increase i_1 at the positive scan, as shown by the unfolded voltammograms in Figure 3.   This is concluded to indicate that the co-existing Bi^{3+}

does not undergo oxidation at the electrode but rather functions only as a catalyst. However, each time when Bi^{3+} was added to the DMSO solution, the i-E curve became distorted irregularly to anodic direction, even in the 1.3 - 1.55 V region where no oxidation current for DMSO was observed. This irregular current disappeared within the time scale of one full potential scan (ca. 2 min). Similar phenomena were observed also with chronoamperometry. This irregular current is a strong evidence for the interaction of Bi^{3+} ions with the surface of PbO_2.

Voltammetry at a PbO_2-PbO_2 rotated ring-disc electrode (RRDE) also was used to study the catalytic oxidation of DMSO. This electrode was prepared by depositing PbO_2 onto the ring and disc of a Au-Au RRDE. The ring current (i_r) for DMSO oxidation at constant ring potential $(E_r - 1.7$ V) was monitored as a function of the disc potential (E_d) which was cycled between 0.9 and 1.7 V. The i_r-E_d voltammograms are shown in Figure 4. At $E_r - 1.7$ V, an anodic ring current was observed for oxidation of DMSO in the presence of Bi^{3+}. When E_d was scanned, a shielding effect was observed in i_r at $E_d > 1.5$ V, where anodic oxidation of DMSO occurs at the disc. The shielding effect was greater at higher w values.

Effects of Bi^{3+} concentration and scan rate   In Figures 1 and 2, the i-E curves for the positive and negative scans do not match. Hence, there can be two values of half-wave potential $(E_{1/2})$ for the current plateau, namely, one for positive scan $(E_{1/2,p})$ and one for negative scan $(E_{1/2,n})$. Unfolded voltammograms were used to separate the i-E curves for the positive and negative scans in order to clearly show their

differences. The relative values of $E_{1/2,p}$ and $E_{1/2,n}$ depended on C_{Bi}, as is shown in Figure 3. While $E_{1/2,p}$ was changed only slightly by increased C_{Bi}, $E_{1/2,n}$ was increased greatly. For instances, at $C_{Bi} = 83$ µM in Figure 1A, $E_{1/2,n}$ was slightly smaller than $E_{1/2,p}$. However, at $C_{Bi} = 110$ µM in Figure 2B, $E_{1/2,n}$ was greater than $E_{1/2,p}$. As shown by Figure 3, at certain C_{Bi} value (10 - 20 µM), $E_{1/2,n}$ equaled $E_{1/2,p}$. At $C_{Bi} > 30$ µM, the i-E curve in the negative scan no longer had a plateau shape. Instead, the current dropped rapidly once it reached the plateau value and gave a peak-shaped i-E curve. At even higher C_{Bi} (> 0.5 mM), the current plateau in the forward scan also became a current peak. Also seen from this figure is the achievement of catalytic effect at a Bi/DMSO concentration ratio as small as 1/1000. The relationship between the i-E curves and the rotational velocity also was changed by C_{Bi}. As shown in Figures 5A,B, the current increased not linearly with increased $w^{1/2}$ at $C_{Bi} = 150$ µM, in contrary to the linear relation in Figure 1. It was noticed in the same figure that the $E_{1/2,p}$ shifted to more positive values with increased w at high C_{Bi} value.

The effects of scan rate (Ø) on the i-E curves are depicted in Figure 6. As Ø was decreased, $E_{1/2,f}$ shifted to less positive values, $E_{1/2,p}$ to more positive values, and the slope of the current plateau increased. At 5 mV s^{-1}, a very steep i-E plateau was observed for the positive scan, but the current dropped rapidly upon scan reversal. The height of the current plateau for the positive scan was not changed by a change in Ø within 100 mV s^{-1}, especially for low C_{Bi} values.

The voltammograms for DMSO oxidation were very reproducible. When a

well-defined i-E plateau was obtained, continuous cycling of more than 50 times yielded less than 2% change in i_1. This result means that the preceding potential cycle does not affect the succeeding i-E curve. However, at high C_{Bi} values, the i-E curve tended to drop with cycle number, especially for the negative scan. The current as shown in Figure 6 did not remain constant when the potential scan was stopped in the range of 1.65 - 1.85 V. Rather, it dropped to zero at a rate depending on experimental conditions, especially on C_{Bi}. The current drop was slower for lower C_{Bi}. When a very low value of C_{Bi} was used (e.g., < 10 μM), the current remained constant even if the potential scan was stopped.

<u>Chronoamperometry</u> and <u>mechanism</u> of <u>electrocatalysis</u>   From the voltammetric data, it is difficult to argue whether the bismuth ion functions as a catalyst in the bulk solution, in the diffusion layer, or in a chemically-bonded form at the electrode surface. This question can be answered with chronoamperometry at a constant anodic potential (E) as the reaction rate (i) is monitored with time (t).

The i-t response is shown in Figures 7, 8, 9, and 10, as a function of C_{DMSO}, w, C_{Bi}, and E, respectively. Newly prepared PbO_2 films were used to obtain each curve to avoid any influence from the preceding experiment. It is noticeable immediately that an initial time period elapses before the current grows to a limiting value. This initial period was not observed for pre-deposited Bi-PbO_2 electrodes where Bi(III) is already on the surface of the electrode (1d-f,2b). Thus, it is concluded that Bi^{3+} in the solution first must be adsorbed onto PbO_2 surface to function as catalyst. This conclusion is consistent with the i-t behavior observed.

Presumably, the coverage by adsorbed Bi^{3+} on PbO_2 surface should increase with time until an equilibrium value is reached. Hence, the current for catalytic oxidation of DMSO at the Bi^{3+}-adsorbed PbO_2 (Bi^{3+}/PbO_2) also should increase with time, assuming that the catalytic efficiency of the Bi^{3+}/PbO_2 electrode increases with increasing Bi^{3+} coverage. The i-t curves in Figures 7 - 10 actually represent the adsorption isotherm curves for Bi^{3+} on PbO_2. The transition time (τ), as defined graphically in Figure 7, should be inversely proportional to the rate of Bi^{3+} adsorption on PbO_2. It is thus expected that the τ values would decrease with increasing C_{Bi} and E, but remain independent of C_{DMSO}. The τ value also should be independent of w at low C_{Bi} values, but increase with increased w at high C_{Bi} values. These are exactly the results obtained, as demonstrated in Figures 7 - 10.

Effect of Bi^{3+} surface coverage   The surface coverage by adsorbed Bi^{3+} on PbO_2 changes with the bulk concentration of Bi^{3+}, which plays an important role in the electrocatalysis at the modified PbO_2. Thus, the change of i-t (Figure 9) and i-E (Figure 3) curves with C_{Bi} is further discussed below.

When C_{Bi} was < 2 μM, the current in Figure 9 increased very slowly. At C_{Bi} = 4 - 8 μM, the current reached a limiting value quickly and remained constant. These results are consistent with the kinetic analysis at partially covered electrodes (9). However, if C_{Bi} was > 10 μM, the current reached a peak value and then dropped quickly. It is concluded that an optimal range of Bi^{3+} coverage exists for the Bi^{3+}/PbO_2 electrode to obtain maximum catalytic activity. The same conclusion also

was drawn from the voltammetric data.

The optimal C_{Bi} range was independent of C_{DMSO} and w, but was different for constant-potential and potential-scan experiments. As seen in Figure 9, the maximum current for the i-t curves remained at a steady-state value for C_{Bi} values lower than needed to obtain reproducible i-E curves. For instance, whereas reproducible i-E curves were obtained at C_{Bi} — 83 μM in Figure 1, no steady-state current could be obtained at constant potential for C_{Bi} as low as 16 μM. This result is concluded to be because the accumulation of adsorbed Bi^{3+} at PbO_2 surface is different under constant-potential and potential-scanning conditions. For voltammetric experiments, desorption of adsorbed Bi^{3+} might occur when the potential is scanned to less positive values in the negative scan. Readsorption takes place in the next positive scan. Thus, Bi^{3+} ions are not accumulated continuously over time, so reproducible i-E curves are obtained. The occurrence of potential dependent adsorption and desorption of Bi^{3+} will be proved in the next section. Under constant-potential conditions, no desorption occurs at E > 1.55 V. Hence, the adsorbed Bi^{3+} accumulates continuously with time, which quickly leads to a high value of coverage and, as a result, a decrease in the catalytic current even at relatively low values of C_{Bi}.

The changes observed in i-E curves with variation of C_{Bi} and Ø, as shown in Figures 3 and 6, respectively, also are a reflection of the change of Bi^{3+} surface coverage. The coverage by adsorbed Bi^{3+} is different at potential values along with the scan, which is further a function of C_{Bi} and Ø, so the shape as well as $E_{1/2}$ values for the i-E

curves change with C_{Bi} and $\emptyset$.

As shown in Figure 7, the steady-state current did not increase linearly with increased $w^{1/2}$, which was especially true at high C_{Bi} values. The dependence of the steady-state current on variation of w was studied also by variation of w at the plateau region of the i-t curves. The resultant i-$w^{1/2}$ relation was non-linear, too. A linear relationship between the current and $w^{1/2}$ was observed only within a limited range of C_{Bi} values (4 - 8 μM) which is the same as the range to obtain steady-state currents as shown in Figure 9. Similar results were obtained in voltammetric experiments. It is concluded that the catalytic oxidation of DMSO is under mass-transport control only for an optimal surface coverage by adsorbed Bi^{3+}.

Electrocatalysis at PbO_2 pretreated with Bi^{3+} and effect of electrode potential   The results described above were obtained in such a manner that the adsorption of Bi^{3+} on PbO_2 surface and the resultant catalytic oxidation of DMSO were simultaneous processes. In this section, experiments are described in which these two processes were separated.

An anodic current for 10 mM DMSO without co-existing Bi^{3+} was observed at a PbO_2-film electrode which was previously immersed in a 10 mM Bi^{3+} solution for 10 min followed by rinsing with distilled water and air drying (see Figure 11a). This observation directly proves the adsorption of Bi^{3+} on PbO_2 at open-circuit conditions. It is concluded that some of the adsorbed Bi^{3+} remain at the PbO_2 surface throughout the rinsing and drying processes. However, it is expected that Bi^{3+} adsorbed on PbO_2 in this manner has only limited stability. Thus, the activity of

this Bi^{3+}/PbO_2 electrode is low and does not persist very long, especially at rotated electrodes, as is shown by the decrease of current with cycle number.

Adsorption of Bi^{3+} onto PbO_2 is much more effective under potentiostatic conditions. A voltammogram of 10 mM DMSO is shown in Figure 11b for a PbO_2 electrode pre-anodized in a 10 mM Bi^{3+} solution at E - 1.7 V. An anodic wave for DMSO oxidation was observed, although it was not as well-defined a plateau as those in Figure 1 obtained with the co-existing Bi^{3+}. The i-E curve in Figure 11b was much more reproducible than that in Figure 11a and did not change with repetitive potential cycles over the period of two hours. The activity of Bi^{3+}/PbO_2 electrodes also was tested by constant-potential chronoamperometry and the results are shown in Figure 11c. The anodic current for 10 mM DMSO reached a maximum value immediately following the application of electrode potential, which is different from the response shown in Figures 7 - 10 with the presence of Bi^{3+}. This further reveals the existence of stable, adsorbed Bi^{3+} on the PbO_2 after anodic pretreatment in the Bi^{3+} solution.

The coverage by pre-adsorbed Bi^{3+} at PbO_2 is expected to be a function of adsorption potential (E_{ads}) and time for the adsorption (t_{ads}). The current plateau for Figure 11b increased with increased E_{ads} and t_{ads}. No catalytic current was observed for $E_{ads} < 1.4$ V. After a Bi^{3+}/PbO_2 electrode was potentiostated at 1.3 V in 1.0 M $HClO_4$, the reactivity was partially lost, due to desorption of adsorbed Bi^{3+} at the low potential values.

If the limiting current as shown in Figure 11b or c is plotted against E_{ads}, an i-E_{ads} wave similar to those in Figure 1 is expected. From this one might speculate that the $E_{1/2}$ value observed in Figures 1 and 2 is related to a critical value of electrode potential for Bi^{3+} adsorption. This is, however, shown not to be true since the same $E_{1/2}$ value was observed at electrodes where. Bi^{3+} is present only at the electrode surface and not in the solution.

Flow-injection analysis   The effect of co-existing Bi^{3+} on the catalytic activity of PbO_2 also can be studied continuously and rapidly with a flow-injection system. The oxidation of DMSO at Bi^{3+}/PbO_2 is shown by the amperometric detection peaks in Figure 12, in comparison with that at pure PbO_2 and $Bi-PbO_2$. The amperometric response was very small at Au (Curve a), and modest at pure PbO_2 without co-existing Bi^{3+} (Curve c). However, the response was much increased at the $Bi-PbO_2$ (Curve e) and at pure PbO_2 with Bi^{3+} present in the sample solution (Curve d). The co-existing Bi^{3+} cannot be oxidized (Curve b), so Curve d represents the net oxidation current for DMSO. The increase of peak height in Curve d with the first three injections is similar to the increase of current with time in Figure 7, indicating the increase of Bi^{3+} coverage on PbO_2. The existence of Bi ions at the surface of PbO_2 after injections of the Bi^{3+} solution was demonstrated by Curve f for which no Bi^{3+} was present in the sample solution. The adsorbed Bi ions remained at the PbO_2 surface in a flow stream for a long time. The peak heights for Curve d and f are higher than those for Curve e, due to a higher Bi concentration at the surface of Bi^{3+}/PbO_2 than that of $Bi-PbO_2$.

The difference in peak height between Curve d and f is also due to the difference in Bi surface concentration. The maximum peak height in Figure 12d increased with DMSO concentration (10 - 50 mM) while Bi^{3+} concentration was kept constant, but did not change with flow rate in the range 1.5 - 3 ml/min.

Surface analysis of Bi^{3+}/PbO_2 electrode and comparison with that of $Bi\text{-}PbO_2$ The existence of Bi at a PbO_2 electrode pretreated in a Bi^{3+} solution was demonstrated directly by X-ray photoelectron spectroscopy (XPS), as is shown in Figure 13. The Bi/Pb atomic ratio at the surface of Bi^{3+}/PbO_2, as measured by the peak area ratio (0.25), is much higher than that at $Bi\text{-}PbO_2$ prepared from a $[Bi^{3+}]/[Pb^{2+}]$ - 0.1 solution (0.13) (2a). Since the Bi^{3+}/PbO_2 electrode in Figure 13 was obtained in a solution with high C_{Bi} during a long t_{ads}, the PbO_2 surface probably was saturated with Bi^{3+}. It is speculated that the Bi/Pb peak area ratio in Figure 13 could increase with an increase of initial t_{ads} at low C_{Bi} value.

The same $E_{1/2}$ value was obtained for DMSO oxidation at these two electrodes with the optimal Bi/Pb atomic ratio (for the results at $Bi\text{-}PbO_2$, see Ref. 2a). However, a high value of Bi^{3+} concentration comparable to that of Pb^{2+} was required to obtain a $Bi\text{-}PbO_2$ with optimal Bi/Pb atomic ratio, while a very small value of C_{Bi} was needed for Bi^{3+}/PbO_2. This is because it is difficult to increase the Bi concentration on the surface of the $Bi\text{-}PbO_2$ simply by increasing the Bi^{3+} concentration in the plating bath, since most of the Bi ions are embedded into the PbO_2 matrix during the deposition of $Bi\text{-}PbO_2$, which cannot

function as catalyst. Besides, the bulk properties of the Bi-PbO_2 are changed with increased Bi/Pb ratio, e.g., electronic structure, conductivity, adhesion, and mechanical strength. In contrast, all adsorbed Bi^{3+} ions stay at the surface of Bi^{3+}/PbO_2 where the bulk PbO_2 film remains chemically and physically unchanged.

One unanswered question regarding the mechanisms of electrocatalysis at the Bi-modified PbO_2 electrodes (2c) is whether a change in the oxidation state of bismuth is required to enable the catalysis. As discussed earlier, Bi^{3+} is not oxidized at Au, Pt, GC, or PbO_2. Thus, it is concluded that the oxidation state of Bi adsorbed on PbO_2 remains as +3 that is not necessarily changed during the catalytic process.

Effects of substrate and PbO_2 property   The i-E curves for DMSO oxidation were shifted to more positive potential values when the substrate was changed from Au to GC. This shift corresponds to a higher value of O_2 evolution overpotential at GC than at Au. There might be a difference in O_2 overpotential values between PbO_2/Au and PbO_2/GC electrodes, because of the small thickness of the PbO_2 films. Therefore, the observed i-E curve shift as the substrate was changed is concluded to be caused by a higher value of O_2 evolution at the PbO_2/GC than that at PbO_2/Au. This conclusion is consistent with the relationship between O_2 evolution and oxygen-transfer reaction and the general mechanism for electrocatalytic oxygen-transfer.

With the same Au substrate used, the properties of PbO_2 film can be changed by varying the deposition conditions (2a,c). For instance, while α-PbO_2 is obtained in acidic solution, β-PbO_2 is obtained from alkaline

solution of Pb^{2+}. Identical i-E curves were obtained at α- and β-PbO_2 film electrodes of different thickness and porosity, which further proves the independence of the electrocatalysis on the bulk structure of the PbO_2 film. Even ultra-thin PbO_2 films (<0.5 μm) show the same activity as the thick PbO_2 films (ca. 0.1 mm) (2d).

Mechanisms of Bi^{3+} adsorption on PbO_2 Adsorption on metal oxides
is a well-known phenomenon used in many practial processes, e.g., ion chromatography, catalysis, and waste treatment (10,11). Most of the adsorptions occur by ion exchange through the surface hydroxide species at the oxides which have been demonstrated by infrared spectroscopy (11). With the amphoteric property of the surface hydroxide, both cation and anion can be adsorbed onto metal oxides depending on the isoelectric point of the metal oxide and the solution pH. The most widely used examples of such metal oxides are Al_3O_2, SiO_2, and SnO_2.

Although mechanism other than ion exchange is also possible for Bi^{3+} adsorption on PbO_2, e.g., physical adsorption as counter ions, the high stability of the adsorbed Bi^{3+} on PbO_2 strongly indicates the involvement of specific interaction between Bi^{3+} and the PbO_2 surface. An ion exchange capability is speculated to exist for PbO_2 based on its similarity to SnO_2 and SiO_2. An ion-exchange mechanism is, therefore, proposed for Bi^{3+} adsorption on PbO_2, as illustrated schematically in the following.

$$\begin{array}{c}\text{-O-Pb-O-Pb-O-Pb-O-}\\ |\quad\quad|\quad\quad| \\ \text{OH}\quad\text{OH}\quad\text{OH}\end{array} + 2\ Bi^{3+} \longrightarrow \begin{array}{c}\text{-O-Pb-O-Pb-O-Pb-O-}\\ |\quad\quad|\quad\quad| \\ \text{O}\quad\text{O}\quad\text{O} \\ \backslash\ /\quad\ \ | \\ Bi^{+}\quad Bi^{2+}\end{array} + 3\ H^{+}$$
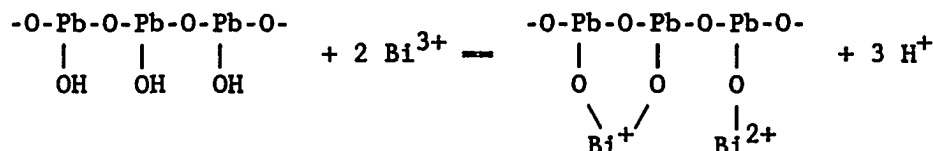
Similar mechanism should hold also for adsorption on PbO_2 of other species, e.g., As(V), Ag^+, and Cl^-, which will be discussed in the following paper. Based on the occurrence of desorption of adsorbed Bi^{3+}, the adsorption is concluded to be quasi-reversible.

Untreated and Bi^{3+}-adsorbed PbO_2 samples were studied by FTIR with both photoacoustic and diffuse reflectance detectors to determine the surface structure changes of the PbO_2 following the adsorption of Bi^{3+}. However, the results showed no difference in the IR spectra.

Oxygen evolution at Bi^{3+}/PbO_2 electrode   The Bi sites at the surface of Bi^{3+}/PbO_2 can act as O-transfer mediator by promoting the localized discharge of water to yield OH radicals (see Chapter I-A). One side effect of this reaction is expected to be the slight decrease in O_2 evolution overpotential at high Bi coverage, because OH is also an intermediate product of O_2 evolution (2c). This was proved by the voltammograms in Figure 14, which were obtained in a blank solution of 1.0 M $HClO_4$ as a function of C_{Bi}. A high scan rate and a very sensitive current scale were used to exaggerate the appearance of small changes in the background current. It is apparent that the i-E peaks for both positive and negative scans increase for higher C_{Bi}. In comparison, the background current at a bare Au electrode under the same conditions did not change with addition of Bi^{3+}. Therefore, the additional current is

concluded to indicate an increased rate of O_2 evolution as a direct consequence of adsorbed Bi^{3+} at high coverages. This additional current is responsible also for the slight increase of the current with increased scan rate, as shown in Figure 6.

The increase in O_2 evolution current is, nevertheless, very small, especially at low C_{Bi} values. This is because the Bi sites at the surface of Bi^{3+}/PbO_2 are spatially separated from each other. The second step for O_2 evolution has been speculated as requiring the joining of two neighboring hydroxyl species (12), which is difficult to achieve at the Bi^{3+}/PbO_2 for low Bi coverage.

An unsuccessful attempt was made to detect the enhanced generation of OH radicals at the disc electrode of a PbO_2 disc-Au ring electrode in the presence of Bi^{3+}. However, it was found that the presence of Bi^{3+} in the solution increased the reduction of dissolved oxygen at Au electrode, which is a cathodic O-t reaction catalyzed by the underpotential deposition of atomic Bi on Au.

Effect of pH and foreign ·substances   The $E_{1/2}$ values for DMSO shifted to more negative values with an increase in solution pH, at ca. -60 mV/pH for pH 1 - 4. This is concluded to be due to the inclusion of two protons in the electrocatalytic reaction. No catalytic activity for co-existing Bi^{3+} was observed at pH > 11, probably due to the hydrolysis of Bi^{3+}.

Also studied were the effects of co-existing dioxygen and many anions on the catalytic oxidation of DMSO. There was no effect from the presence of O_2, NO_3^-, ClO_4^- and HSO_4^-. Since Pb^{2+}, Pb^{4+} and Bi^{3+} ions

can be chelated by EDTA, the effect of co-existing EDTA also was studied in a variety of pH (0 - 7), EDTA concentration, and the way in which EDTA was added (before the first scan or after several cycles, as the PbO_2 was free of Bi^{3+} and had adsorbed Bi^{3+}, respectively). The results show no effect.

Voltammograms were obtained in DMSO solution of a small amount of Bi^{3+} as a function of the concentration of added H_2O. An anodic wave was obtained for oxidation of DMSO with H_2O as the limiting reagent, which might be used to detect water in DMSO. Further research in this aspect is still awaited.

Identification of DMSO oxidation product and reversibility of the catalytic oxidation   A PbO_2-film deposited on a large-area Pt screen electrode was used for exhaustive electrolysis of 0.1 M DMSO. The number of electron transfer was estimated with coulometry as 2. The resultant product solution was extracted with ether and the organic phase was analyzed by a gas chromotograph system with mass spectrometric detector (GC/MS). The resulting GC trace and mass spectrum are shown in Figures 15A and 15B, respectively. Based on the simple product peak and a libary search on the peak, it is apparent that $DMSO_2$ is the only product.

The cyclic voltammetry of DMSO was studied at 0 rev min^{-1} to determine whether there was a cathodic wave on the reverse scan. No cathodic peak was observed, as is shown in Figure 16. Therefore, the electrocatalytic oxidation of DMSO is concluded to be irreversible. The adsorbed Bi^{3+} ion only catalyzes the anodic process of O-transfer but not the reverse cathodic process. This result is consistent with the result

obtained at $Bi-PbO_2$ electrode (1d).

The decrease of current with cycle number in Figure 16 is due to the depletion of DMSO in the diffusion layer and the loss of adsorbed Bi^{3+}, since supply of DMSO and Bi^{3+} is much slower at 0 rev min^{-1} than that at 400 or higher rev min^{-1}.

Intermediate product for anodic oxidation of DMSO   The adsorption of Bi^{3+} is highly possible at other oxide electrodes, e.g., MnO_2, and surface oxide-covered Au and Pt. However, no current for oxidation of DMSO was observed at these electrodes in the presence of Bi^{3+}. Therefore, the lead sites at the surface of Bi-modified PbO_2 might play a unique role in the electrocatalysis.

From the literature review on chemical oxidation of DMSO, it can be seen that all the schemes of mechanism involve intermediate products in which the sulfur atom is activated. The same is believed to be true for electrode oxidation of DMSO. For Scheme 2 - 4, the formation of intermediates are followed by O-transfer from H_2O to DMSO that is the same as the anodic oxidation of DMSO. Thus, an intermediate product similar to that in Schemes 2 and 4 is proposed for electrocatalytic oxidation of DMSO. This intermediate is formed rapidly by an interaction between the S atom in DMSO and the Pb site at the electrode surface, which is followed by an oxidative O-transfer step from a hydroxyl radical formed at a neighboring Bi site. Under certain conditions, the overall reaction is under the control of mass transport of DMSO.

Conclusions

Adsorption is one of the four major methods for chemical modification of electrode surfaces (13). However, the adsorption method used thus far is confined to adsorption of organic species on metal and carbon surfaces. The adsorption of ionic species on metal oxide surfaces through ion exchange has long been recognized and subjected to intensive studies (10), but it has not been used to modify metal oxide electrodes. In this report, we have demonstrated that adsorption of simple inorganic ions from aqueous solution is more effective than the electrochemical co-deposition as a method for modification of PbO_2 surface.

DMSO is a versatile solvent, well-known for its high polarity, essentially aprotic nature, and its high solvating ability (14). The chemical and electrochemical inertness of DMSO is also essential in its applications as solvent in electrochemistry at conventional electrodes (14b,c). Nevertheless, we have shown that DMSO can be oxidized to $DMSO_2$ at nearly 100% current efficiency at the Bi^{3+}/PbO_2 electrode. One potential application of this catalytic reaction is for the electroanalytical determination of DMSO.

There are two possible explanations for the low catalytic activity observed for Bi^{3+}/PbO_2 electrode with high Bi^{3+} coverage. First, the increase in O_2-evolution rate as a result of the higher Bi^{3+} coverage can reduce the rate of O-transfer reaction, because the O_2-evolution process is in competition for the hydroxyl radicals. Second, the surface of Bi^{3+}/PbO_2 may be bi-functional; the Pb sites serve to interact with the S atom in DMSO, while the Bi sites serve to generate hydroxyl radicals. A

too high coverage of adsorbed Bi^{3+} will block the lead sites at the

electrode surface, and, as a result reduce the rate of O-transfer.

References

1. (a) Austin, D. S.; Polta, J. A.; Polta, T. Z.; Tang, A. P.-C.; Cabelka, T. P.; Johnson, D. C. J. Electroanal. Chem. 1984, 168, 227. (b) Johnson, D. C.; Polta, J. A.; Polta, T. Z.; Neuburger, G. G.; Johnson, J.; Tang, A. P.-C.; Yeo, I.-H.; Baur, J. J. Chem. Soc., Faraday Trans. 1 1986, 82, 1081. (c) Tang, A. P.-C.; Johnson, D. C. Anal. Chim. Acta in press. (d) Yeo, I.-H.; Johnson, D. C.; J. Electrochem. Soc. 1987, 134, 1973. (e) Yeo, I.-H. Ph.D. Dissertation, Iowa State University, Ames, Iowa, 1987. (f) Yeo, I.-H.; Kim, S.; Jacobson, R. Johnson, D. C. J. Electrochem. Soc. in press.

2. (a) Chang, H.; Johnson, D. C., in preparation; Chapter III-B, this Dissertation. (b) Chang, H.; Johnson, D. C., in preparation; Chapter III-A, this Dissertation. (c) Chang, H.; Johnson, D. C. J. Electrochem. Soc. 1989, 136, 22; Chapter II-B, this Dissertation. (d) Chang, H.; Johnson, D. C., in preparation; Chapters IV-A&B, this Dissertation.

3. "Standard Potentials in Aqueous Solution"; Bard, A. J.; Parsons, R.; Jordan, J., Eds.; M. Dekker: New York, 1985.

4. (a) Franklin, T. C.; Kagawa, H. Electrochim. Acta 1972, 17, 1223. (b) Sobknowski, J.; Szklarczyk, M. Electrochim. Acta 1980, 25, 383. (c) Alekseeva, E. Yu.; Safonov, V. A.; Petrii, O. A. Elektrokhimiya, 1982, 18, 1452; Chem. Abstr. 1983, 98, 42843. (d) Baruzzi, A. M.; Iwasita, T.; Giordano, M. C. An. Assoc. Quim. Argent. 1982, 70, 669; Chem. Abstr. 1982, 97, 62922. (e) Lane, R. F.; Hubbard, A. T. J. Phys. Chem. 1977, 81, 734.

5. (a) Davies, M. J.; Gilbert, B. C.; Norman, R. O. C. J. Chem. Soc., Perkin Trans. 2 1984, 503. (b) Viswamurthy, R.; Maruthamuthu, P. Oxid. Commun. 1981, 2, 37. (c) Pandurengan, T.; Maruthamuthu, P. Bull. Chem. Soc. Jpn. 1981, 54, 3551. (d) Ogata, Y.; Tanaka, K. Can. J. Chem. 1981, 59, 718. (e) Mahapatro, S. N; Panda, R.; Panigraphy, G. P. Indian J. Chem. A 1980, 19A, 905. (f) Panigraphy, G. P.; Panda, R. Int. J. Chem. Kinet. 1980, 12, 491. (g) Curci, R.; DiFuria, F.; Modena, G. J. Chem. Soc., Perkin Trans. 2 1978, 603. (h) Maruthamuthu, P.; Santappa, M. Indian J. Chem. A 1978, 16A, 43. (i) Ogata, Y.; Suyama, S. J. Chem. Soc., Perkin Trans. 2 1973, 755. (j) Bhavani, N.; Lily, K. Acta Cienc. India, Sect. Chem. 1984, 10, 90.

6. (a) Mahadevappa, D. S.; Ananda, S.; Murthy, A. S. A.; Rangappa, K. S. Tetrahedron 1984, 40, 1673. (b) Radhakrishnamurti, P. S.; Sahu, N. C. Indian J. Chem. A 1981, 20A, 269. (c) Mahadevappa, D. S.; Jadhav M. B.; Naidu, H. M. K. React. Kinet. Catal. Lett. 1980, 14, 15. (d) Mahadevappa, D. S.; Jadhav, M. B.; Naidu, H. M. K. Int. J. Chem. Kinet. 1979, 11, 261. (e) Pandey, S. M.; Sharma, J.; Prakash, O.; Mushran, S. P. Indian J. Chem. A 1981, 20A, 1011. (f) Radhakrishnamurty, P. S.; Padhi, S. C. Curr. Sci. 1977, 46, 517. (g) Rangaswamy, H.; Yathirajan, H. S. Curr. Sci. 1981, 50, 757. (h) Cox, G.; Gibson, A. J. Chem. Soc., Perkin Trans. 2 1973, 1355.

7. (a) Murti, P. S. R.; Tripathy, K. S. Indian J. Chem. A 1985, 24A, 217. (b) Rao, K. N.; Sethuram, B.; Rao, T. N. Oxid. Commun. 1984, 7, 199. (b) Murti, P. S. R.; Padi, S. C. J. Indian Chem. Soc. 1977, 54, 1097. (c) Pratihari, H. K.; Roy, A. K.; Nayak, P. L. J. Indian Chem. Soc. 1976, 53, 4. (d) Devi, N. G.; Mahadevan, V. J. Chem. Soc. D 1970, (13), 797.

8. (a) Radhakrishnamurty, P. S.; Sahu, N. S. Kinet. Katal. 1981, 22, 627. (b) Radhakrishnamurty, P. S.; Padhi, S. C. Indian J. Chem. A 1979, 17A, 57. (c) De Oliveira, L. A.; Toma, H. E.; Giesbrecht, E. Inorg. Nacl. Chem. Lett. 1976, 12, 195. (d) Gampp, H.; Haspra, D.; Spieler, W.; Zuberbuehler, A. D. Helv. Chim. Acta 1984, 67, 1019. (e) Sawaki, Y.; Ogata, Y. J. Am. Chem. Soc. 1981, 103, 5947. (f) Mashkina, A. V.; Varnakova, G. V.; Zagryatskaya, L. M.; Suleimanova, Z. A.; Masagutov, R. M; Sharipov, A. Kh.; Yakovleva, V. N.; Vlasova, L. V.; Kirik, N. P. Kinet. Katal. 1981, 22, 607.

9. (a) Caprani, A.; Deslouis, C.; Robin, S.; Tribollet, B.; J. Electroanal. Chem. 1987, 238, 67. (b) Levart, E. J. Electroanal. Chem. 1985, 187, 247. (c) Amatore, C.; Saveant, J. M.; Tessier, D. J. Electroanal. Chem. 1983, 147, 39. (d) Contamin, O.; Levart, E. J. Electroanal. Chem. 1982, 136, 259. (e) Gueshi, T.; Tokuda, K.; Matsuda, H. J. Electroanal. Chem. 1979, 101, 29; 1978, 89, 247. (f) Tokuda, K.; Gueshi, T.; Matsuda, H. J. Electroanal. Chem. 1979, 102, 41. (g) Filinovsk, V. Yu. Electrochim. Acta 1979, 25, 309.

10. (a) Kokarev, G. A.; Kolesnikov, V. A.; Fioshin, M. Ya. Elektrokhimiya 1983, 19, 481. (b) Andreev, V. N.; Heckner, K. H.; Glass, M.; Kazarinov, V. E. Elektrokhimiya 1983, 19, 1558. (c) Kazarinov V. E.; Andreev, V. N. Elektrokhimiya 1977, 13, 685. (d) Mark, P.; Chang, S.-C. In "Oxides and Oxide Films"; Diggle, J. W.; Vijh, A. K., Eds.; Marcel Dekker: New York, 1987; Volume 3. (e) Tadros, Th. F.; Lyklema, J. J. Electroanal. Chem. 1969, 22, 1. (f) Schmitt, G. L.; Pietrzyk, D. J. Anal. Chem. 1985, 57, 2247.

11. (a) Hair, M. L. "Infrared Spectroscopy in Surface Chemistry"; M. Dekker: New York, 1967. (b) Ruvarac, A. In "Inorganic Ion Exchange Materials"; Clearfield, A., Ed.; CRC Press: Boca Raton, 1982; Chapter 5, p. 141. (c) Abe, M. In "Inorganic Ion Exchange

Materials"; Clearfield, A., Ed.; CRC Press: Boca Raton, 1982; Chapter 6, p. 161.

12. (a) Tarasevich, M. R.; Sadkowski, A.; Yeager, E. In "Comprehensive Treatise of Electrochemistry"; Conway, B. E.; Bockris, J. O'M.; Yeager, E.; Khan, S. U. M; White, R. E., Eds.; Plenum Press: New York, 1983; Volume 7, p. 301. (b) O'Sullivan, B. J. M.; Calvo, E. J. In "Comprehensive Chemical Kinetics"; Compton, R. G., Ed.; Elsevier: Amsterdam, 1987; Volume 27, p. 247.

13. (a) Sneil, K. D.; Keenan, A. G. Chem. Soc. Rev. 1979, 8, 259. (b) Murray, R. W. Acc. Chem. Soc. 1980, 13, 135. (c) Albery, W. J.; Hillman, A. R. Ann. Reports Progress Chem. C., Phys. Chem. 1981, 78, 377.

14. (a) "Demethyl Sulfoxide Technical Bulletin"; Crown Zellerbach, Chemical Products Division, Vancouver (Orchards), WA 98662. (b) Butler, J. N. J. Electroanal. Chem. 1967, 14, 89. (c) Fry, A. J.; Britton, W. E. In "Laboratory Techniques in Electroanalytical Chemistry"; Kissinger, P. T.; Heinamen, W. R., Eds.; M. Dekker: New York, 1984.
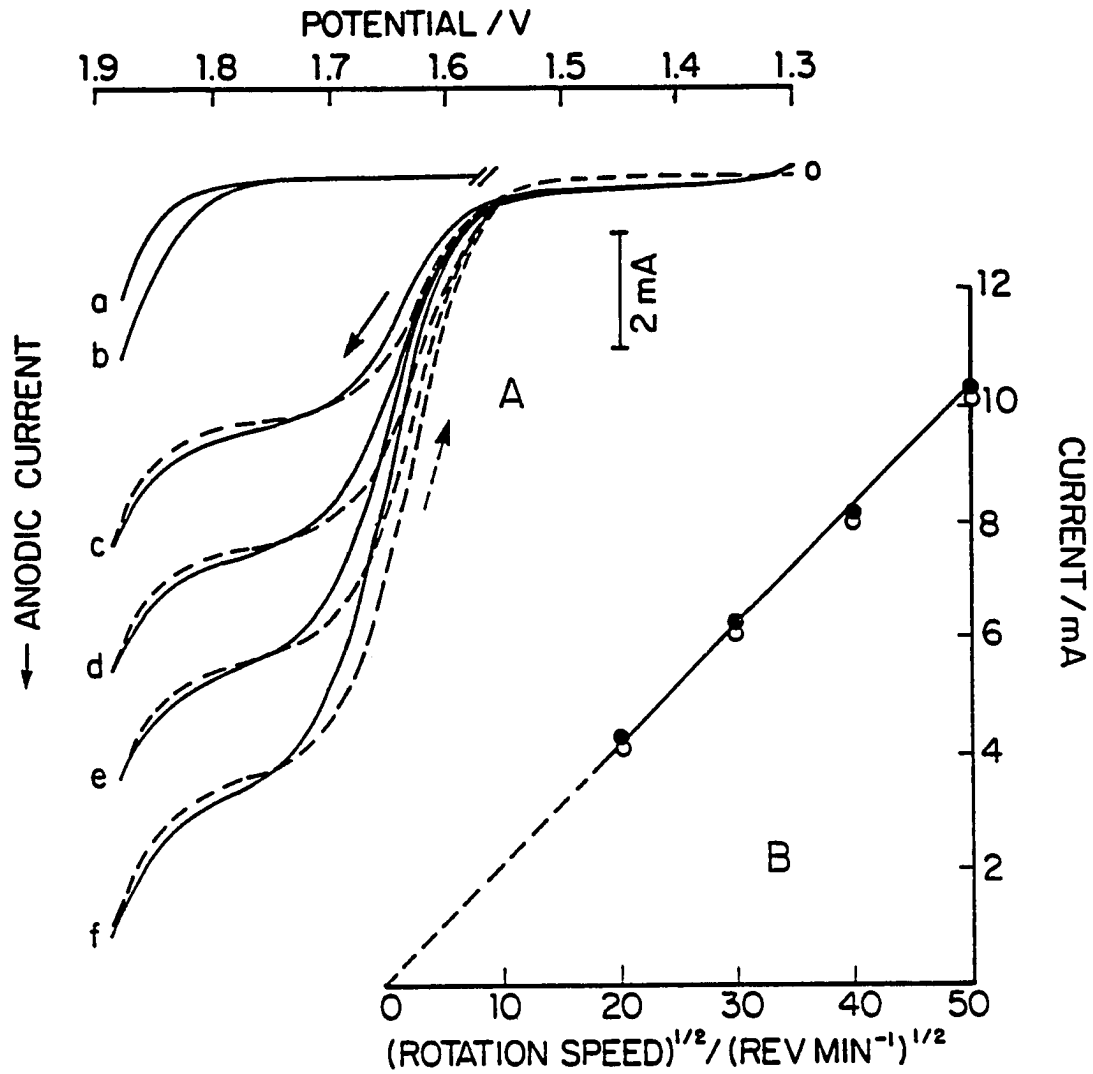
Figure 1. Voltammograms of 10 mM DMSO at bare and PbO_2-coated Au RDE

(A) Effect of w (rev min^{-1}): (a-c) 400, (d) 900, (e) 1600, (f) 2500

Conditions: 1.0 M $HClO_4$; 20 mV s^{-1}; C_{Bi}/electrode:
(a) 83 μM at Au, (b) 0 μM at PbO_2,
(c-f) 83 μM at PbO_2;
Solid: forward scan; dashed: backward scan

(B) Plot of i_1 in (A) vs. $w^{1/2}$

(●) Experimental values; (O) theoretical values
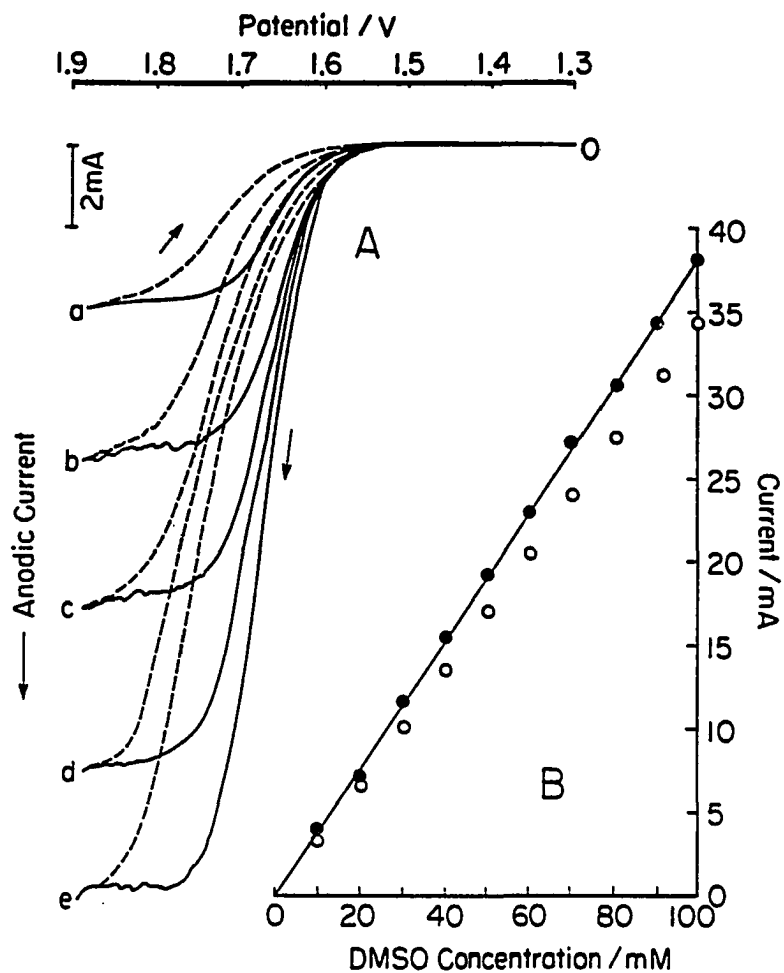
Figure 2. Voltammograms of DMSO at PbO_2 Coated Au RDE

(A) Effect of C_{DMSO} (mM): (a) 10, (b) 20, (c) 30, (d) 50, (e) 60, (f) 70

Conditions: 20 mV s^{-1}, 10 μM Bi^{3+}, 400 rev min^{-1}. Solid: positve scan; Dashed: negative scan

(B) Plot of i_1 in (A) vs. C_{DMSO}.

(●) Experimental values; (O) theoretical values
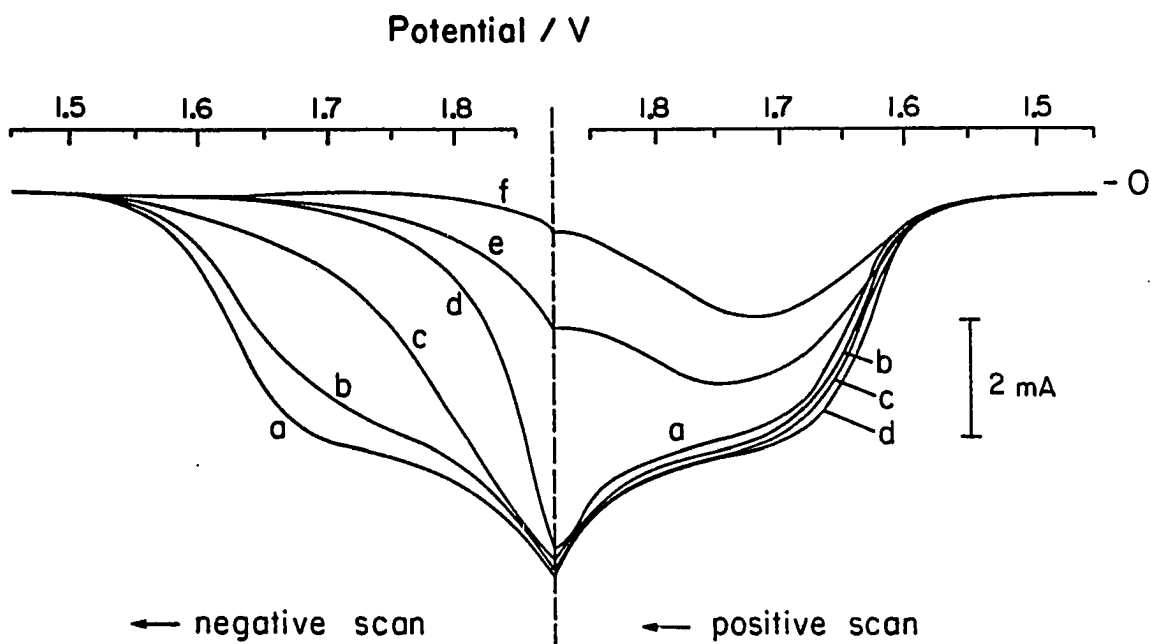
Figure 3. Effects of C_{Bi} on the cyclic voltammograms of 10 mM
DMSO at PbO_2-coated Au RDE

Conditions: 20 mV s^{-1}, 400 rev min^{-1}

C_{Bi} (μM): (a) 10, (b) 20, (c) 30, (d) 40, (e) 100, (f) 200
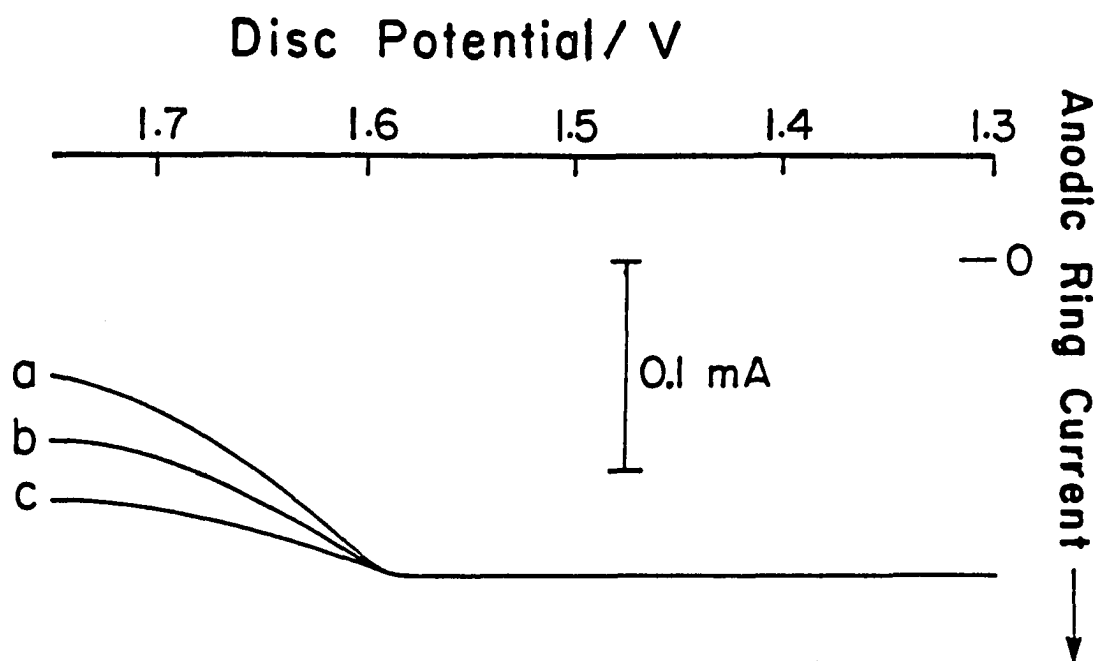
Figure 4. Ring-disc voltammograms (i_r-E_d) of 10 mM DMSO at
a PbO_2-PbO_2 RRDE

Conditions: E_r - 1.7 V; E_d: scanned at 20 mV s^{-1}

w (rev min^{-1}): (a) 400, (b) 900, (c) 1600, (d) 2500
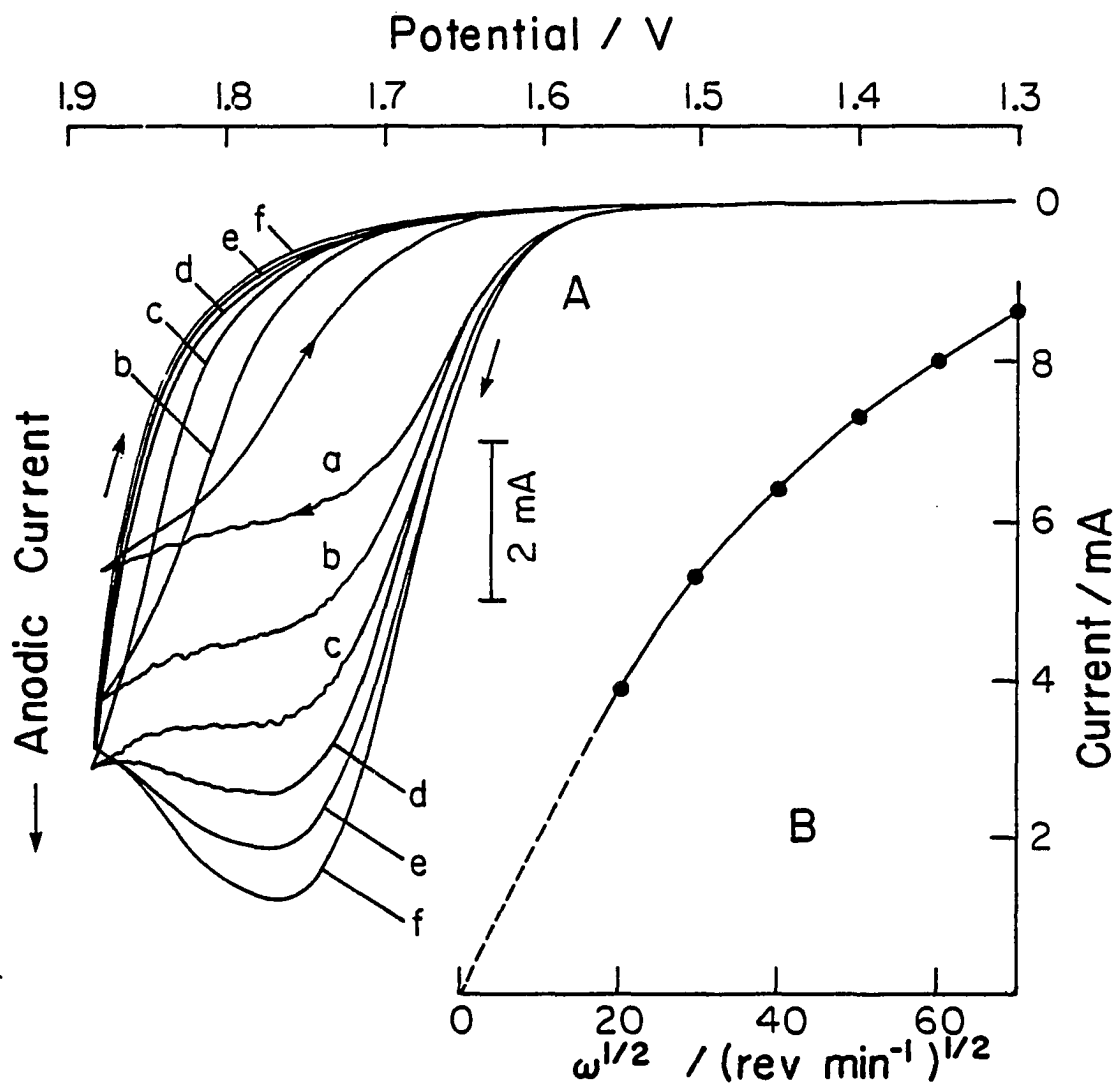
Figure 5. Voltammograms of 10 mM DMSO at PbO_2/Au RDE at high C_{Bi} level

    (A) Effect of w (rev min^{-1}):   (a) 400, (b) 900, (c) 2500,
                                        (d) 3600, (e) 4900, (f) 6400

        Conditions: 20 mV s^{-1}, C_{Bi} = 150 μM

    (B) Plot of peak current in (A) vs. $w^{1/2}$

Potential / V
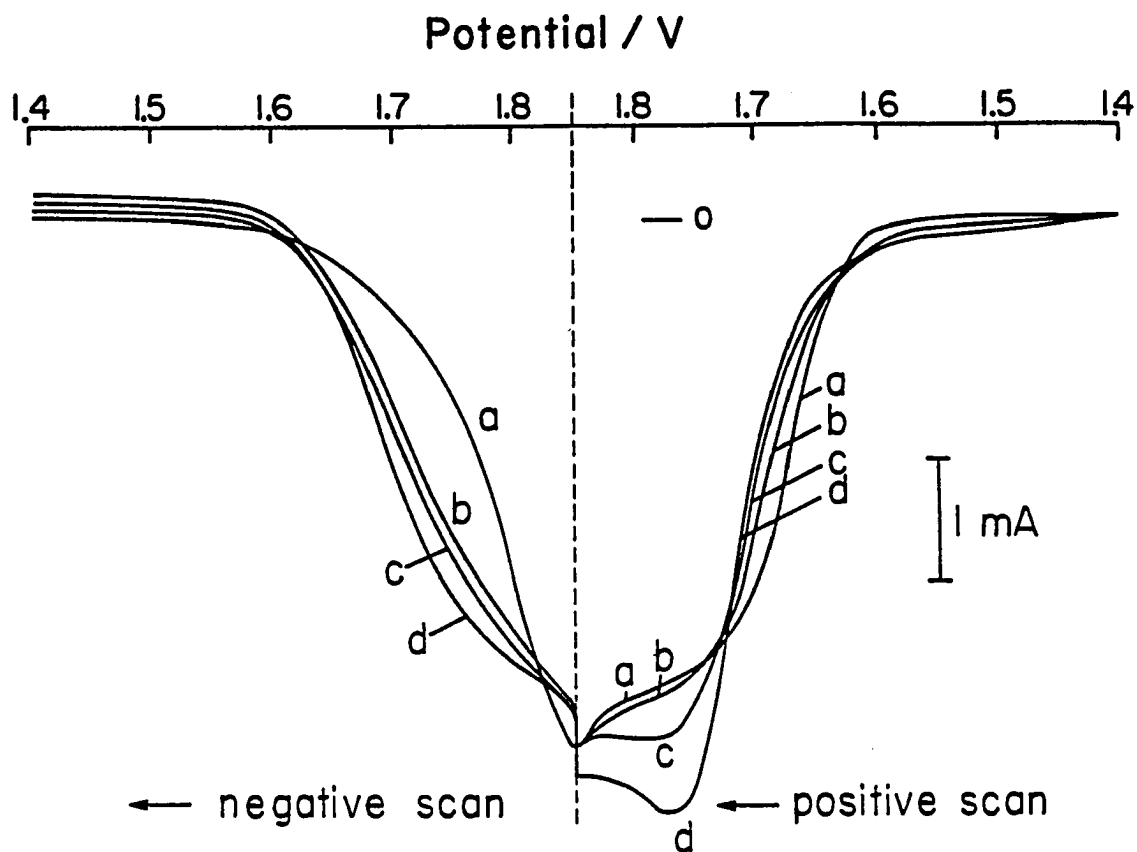
Figure 6. Effects of scan rate on the cyclic voltammograms of
10 mM DMSO at PbO_2 coated Au RDE

Conditions: w = 400 rev min^{-1}, C_{Bi} = 40 μM

$\emptyset$ (mV s^{-1}): (a) 5, (b) 100, (c) 200, (d) 300
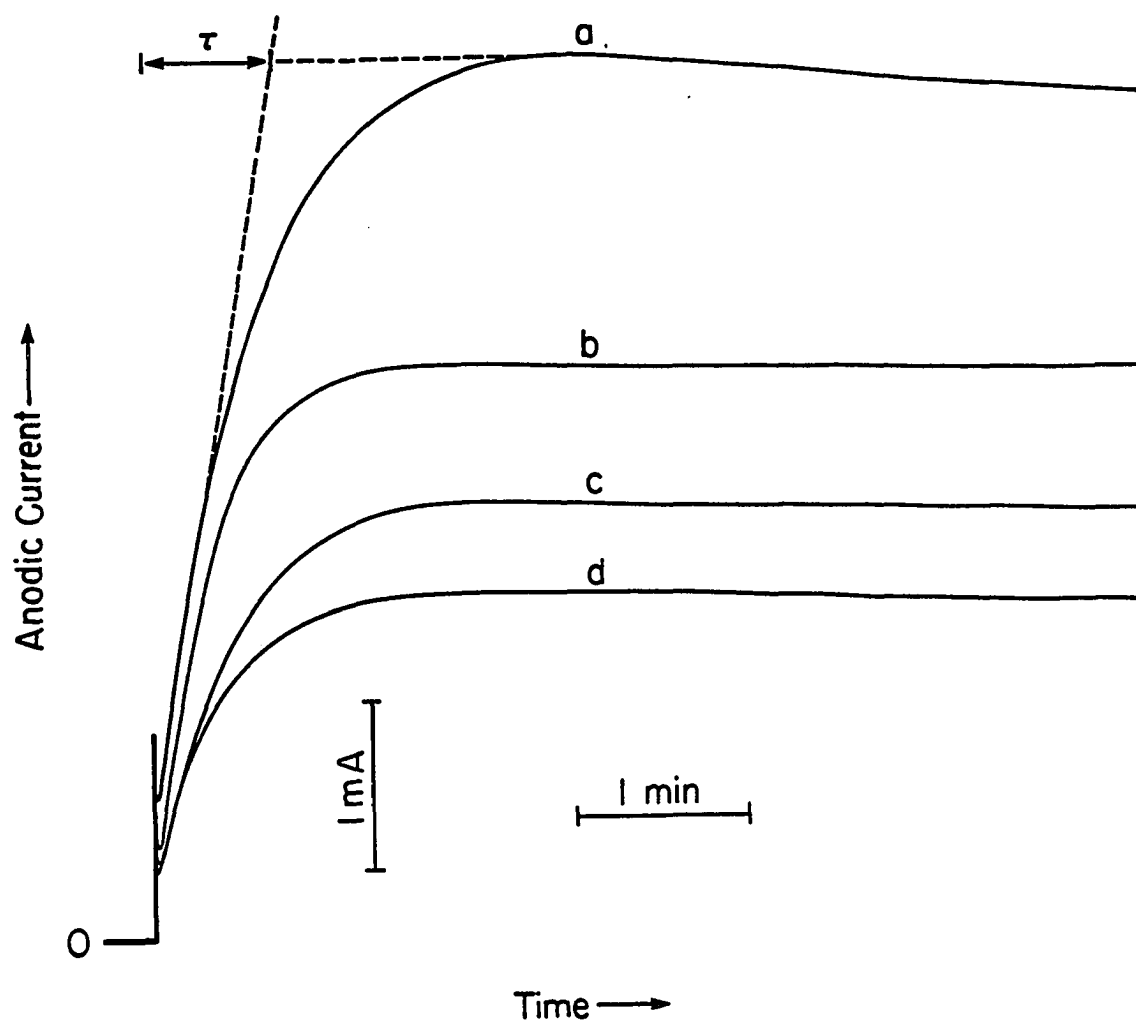
Figure 7.   Effects of DMSO concentration on the chronoamperograms
of DMSO at PbO_2-coated Au RDE with co-existing Bi^{3+}

Conditions: E - 1.7 V, w - 400 rev min^{-1}, C_{Bi} - 0.1 mM

C_{DMSO} (mM):   (a) 30, (b) 20, (c) 10, (d) 5
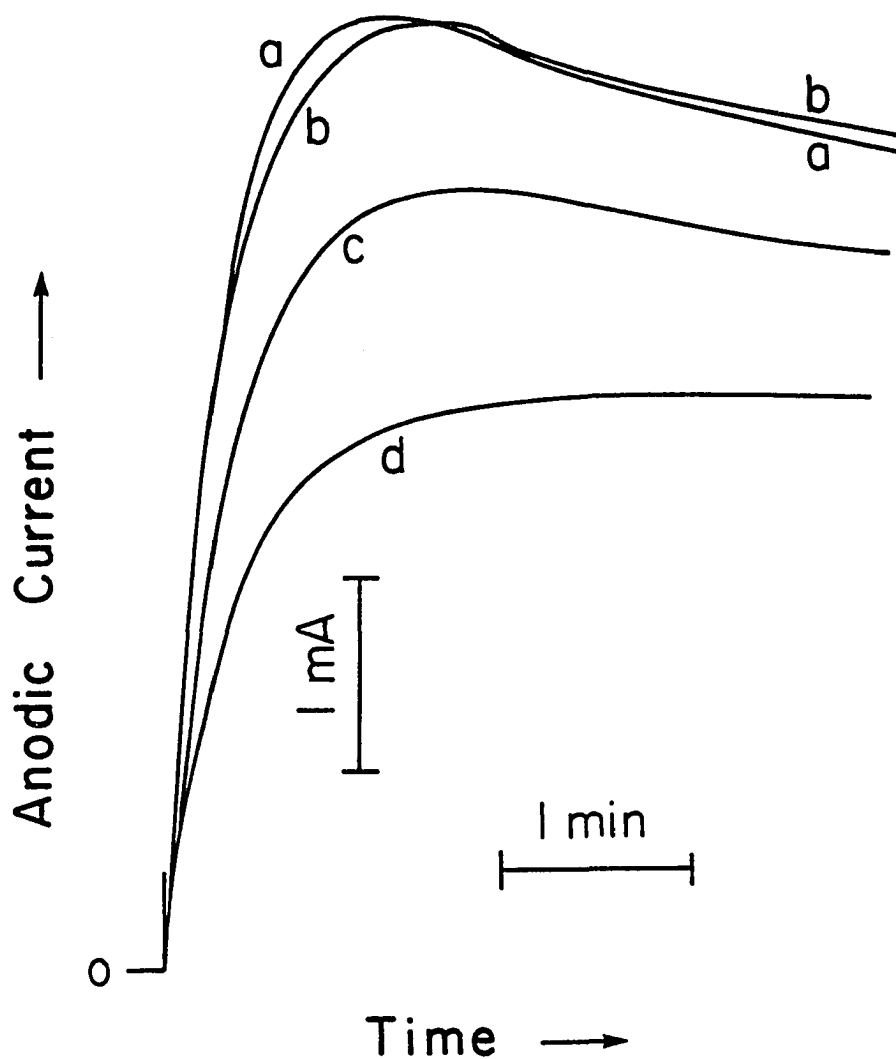
Figure 8. Effects of rotational velocity on the chronoamperograms
of 10 mM DMSO at PbO_2-coated Au RDE with co-existing Bi^{3+}

Conditions: E — 1.7 V, C_{Bi} — 10 μM

w (rev min^{-1}): (a) 2500, (b) 1600, (c) 900, (d) 400
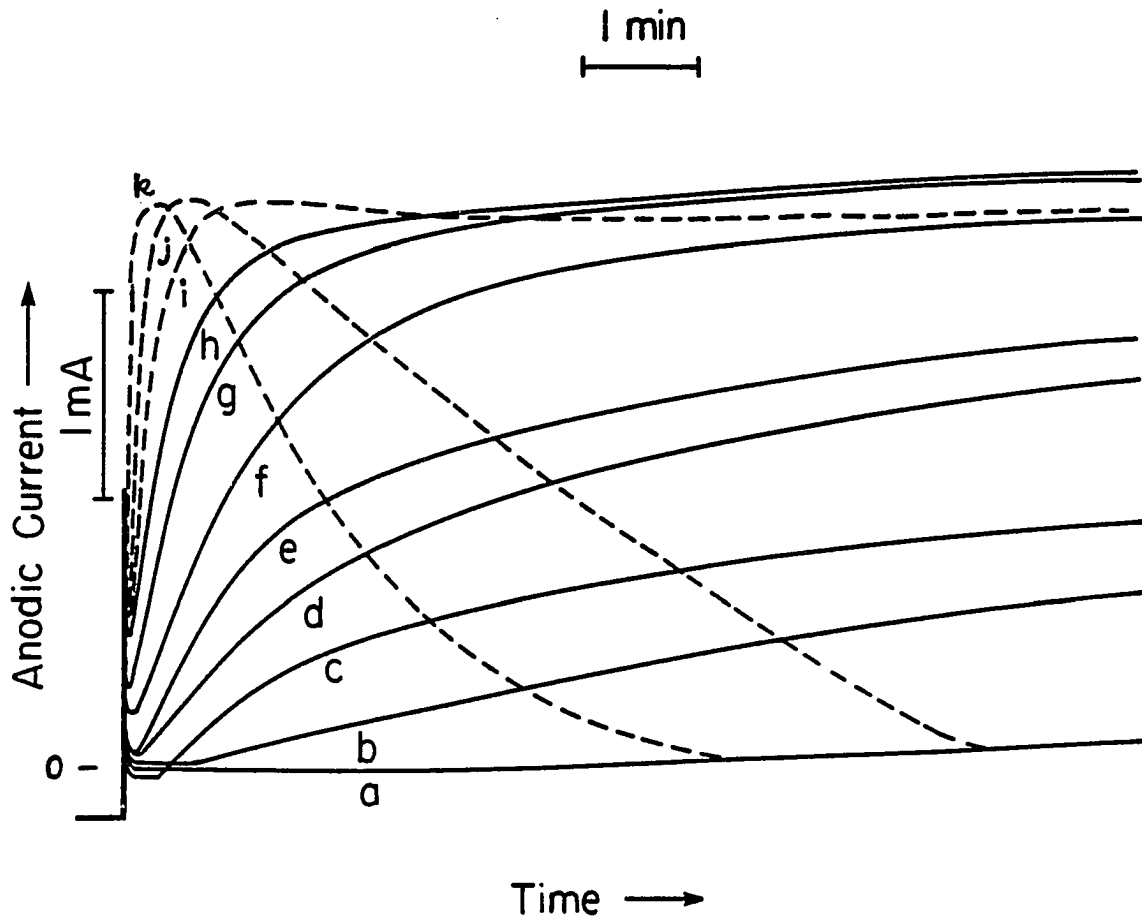
Figure 9. Effects of C_{Bi} on the chronoamperograms of 10 mM
DMSO at PbO_2 coated Au RDE

Conditions: $E = 1.7$ V, $w = 400$ rev min^{-1}

C_{Bi} (M): (a) 0, (b) 0.2, (c) 0.3, (d) 0.5, (e) 0.75,
(f) 2, (g) 4, (h) 6, (i) 8, (j) 16, (k) 32
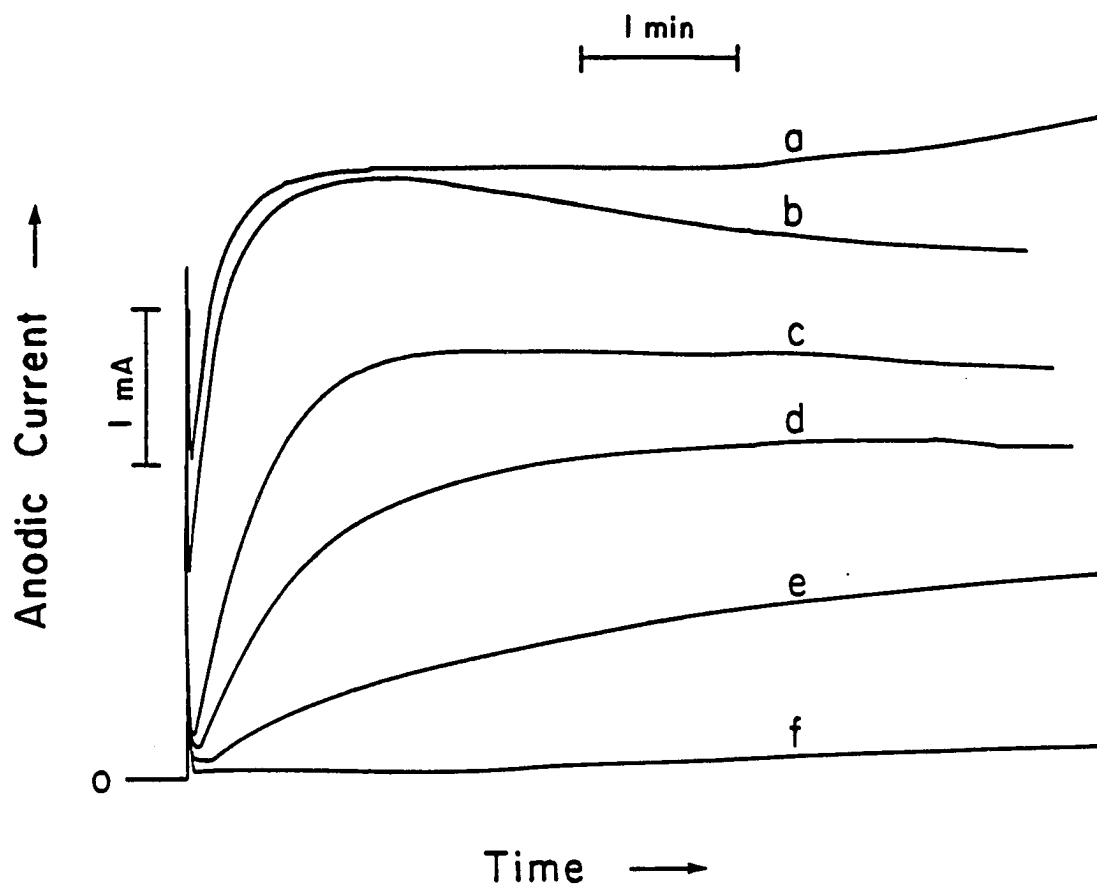
Figure 10. Effects of potential on the chronoamperograms of 10
mM DMSO at PbO_2-coated Au RDE with co-existing Bi^{3+}

Conditions: 400 rev min^{-1}, 0.1 mM Bi^{3+}

E (V): (a) 1.85, (b) 1.80, (c) 1.70, (d) 1.68,
(e) 1.63, (f) 1.60
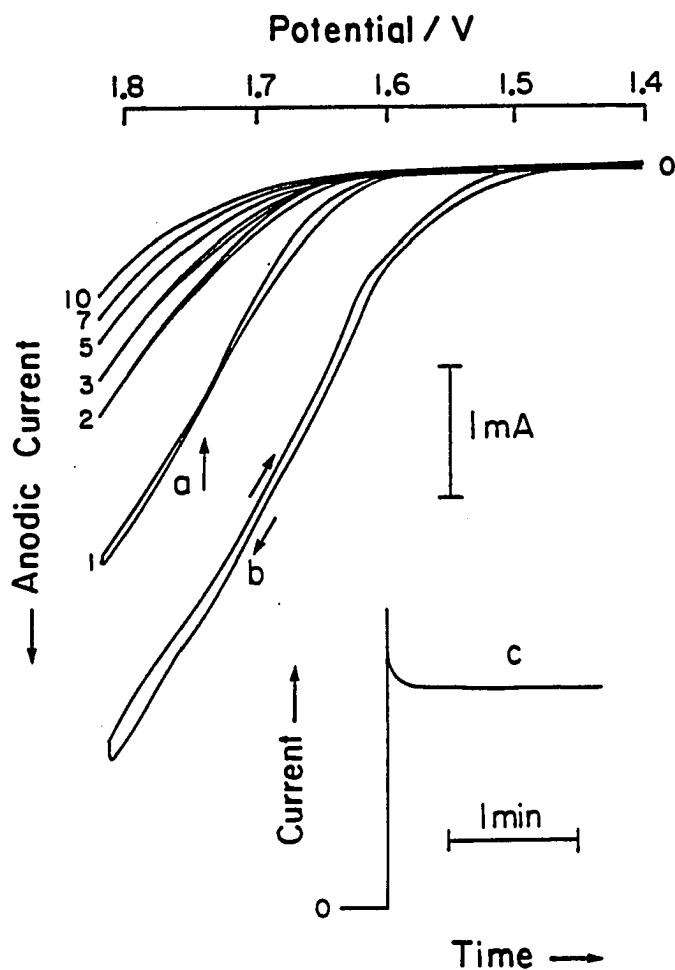
Figure 11. Effect of PbO_2 pretreatment in 10 mM Bi^{3+} solution on the oxidation of 10 mM DMSO in 1.0 M $HClO_4$

(a) Cyclic voltammograms at PbO_2-coated Au RDE pre-immersed in 10 mM Bi^{3+} solution for 10 min at open circuit. 20 mV/s, 400 rev min^{-1}

(b) Cyclic voltammograms at PbO_2 film electrode pretreated at E_{ads} = 1.7 V for 10 min in 10 mM Bi^{3+}. Other conditions as given in (a)

(c) i-t curve at the same electrode as in (b) at E = 1.7 V. 400 rev min^{-1}
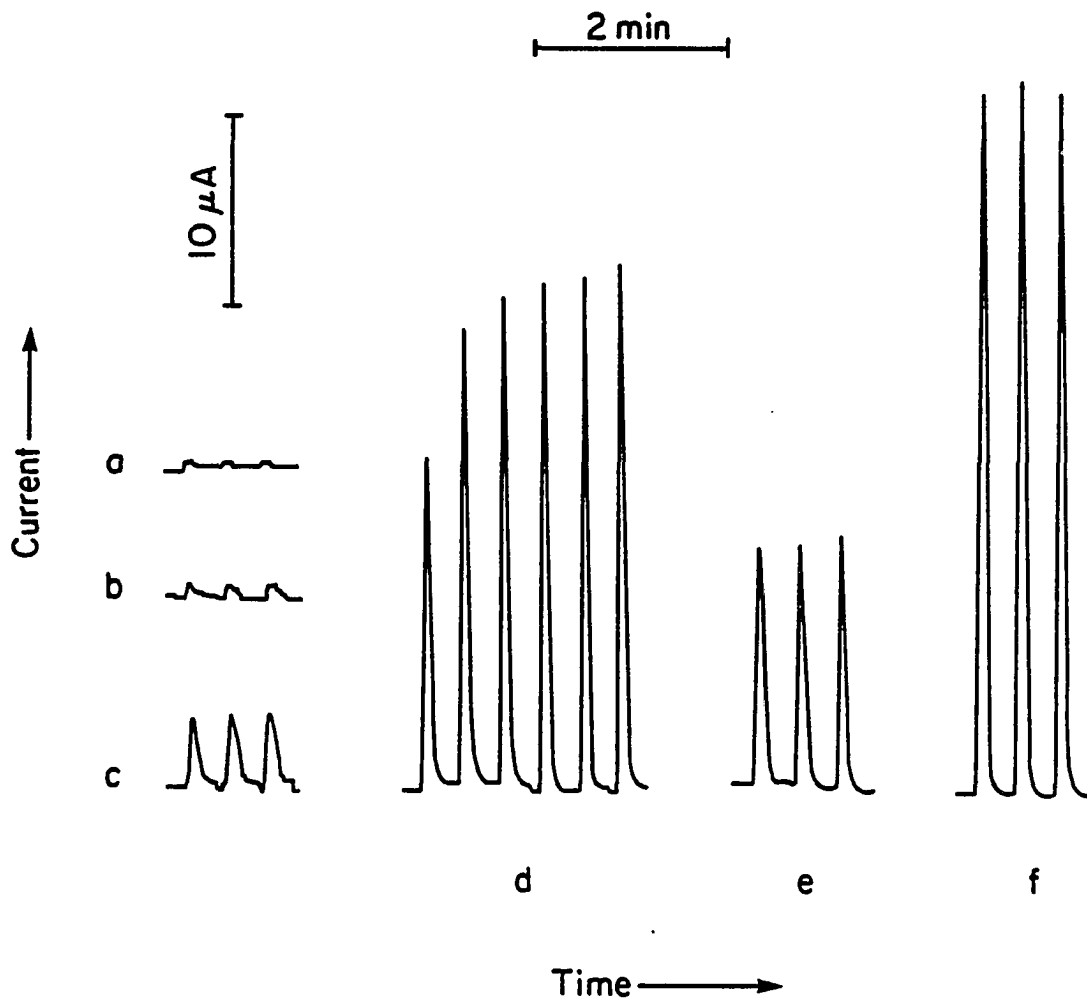
Figure 12. Flow-injection amperometric detection peaks for
oxidation of DMSO

Conditions: 1.7 V electrode potential, 1.0 M $HClO_4$ carrier
stream at 3 ml min^{-1}

Curves: (a) 10 mM DMSO and 0.1 mM Bi^{3+}, at Au,
(b) 1 mM Bi^{3+}, at PbO_2,
(c) 10 mM DMSO, at PbO_2,
(d) 10 mM DMSO and 0.1 mM Bi^{3+}, at PbO_2,
(e) 10 mM DMSO, at Bi-PbO_2 prepared from 10 mM
Pb^{2+} and 1 mM Bi^{3+} mixture,
(f) 10 mM DMSO, at Bi^{3+}/PbO_2 as in b
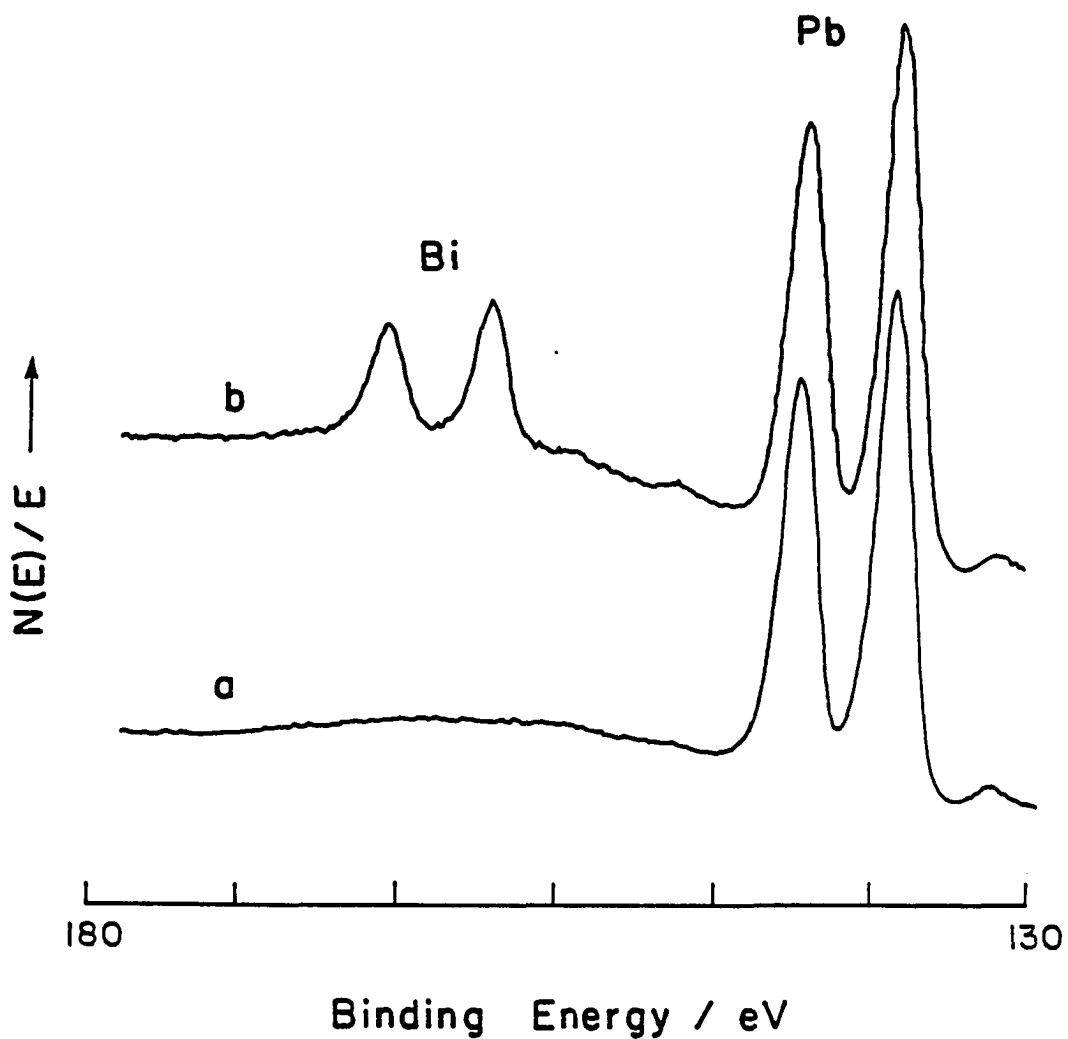
Figure 13.   X-ray photoelectron spectroscopy of pure PbO_2 (a) and
Bi^{3+}/PbO_2 (b)

Conditions for (b):   pretreated in 10 mM Bi^{3+} at 1.6 V
for 10 min; Au peak from the
substrate at 84.0 eV was used as the
standard
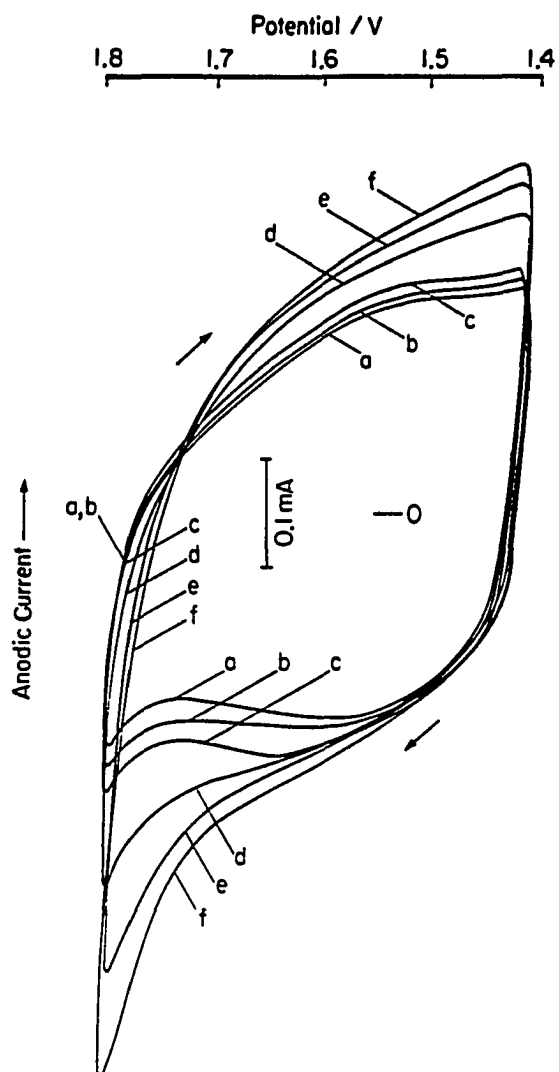
Figure 14.   Cyclic voltammograms at PbO_2 film electrode in 1.0 M
$HClO_4$ blank solution with different amount of Bi^{3+}

Conditions: 300 mV s^{-1}, 400 rev min^{-1}

C_{Bi} (µM):   (a) 55, (b) 73, (c) 91,
(d) 273, (e) 455, (f) 636
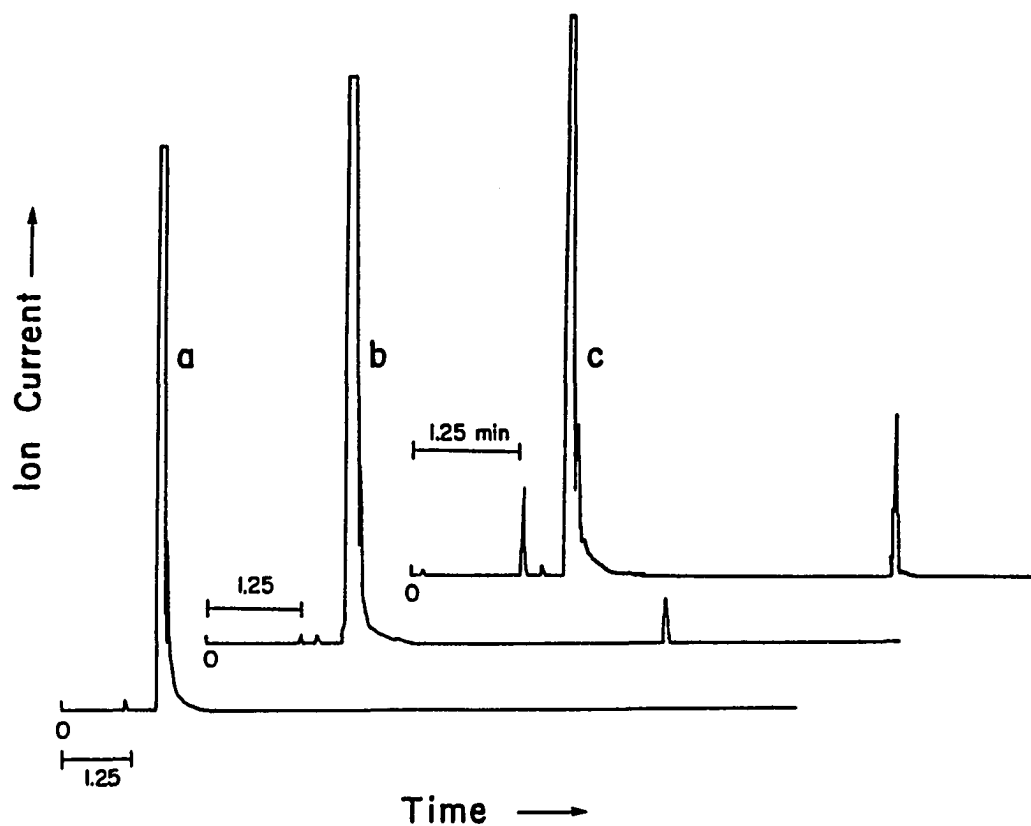
Figure 15A. GC/MS trace

Curves: (a) ether blank,
(b) electrolysis sample extracted in ether,
(c) standard $DMSO_2$ in acetone

MASS SPECTRUM
07/08/88 16:55:00 + 5:58
SAMPLE: #2
CONDS.: 60(2)-300/20

DATA: FINN12462 #478
CALI: C169 #33

BASE M/Z: 79
BIC: 67200.
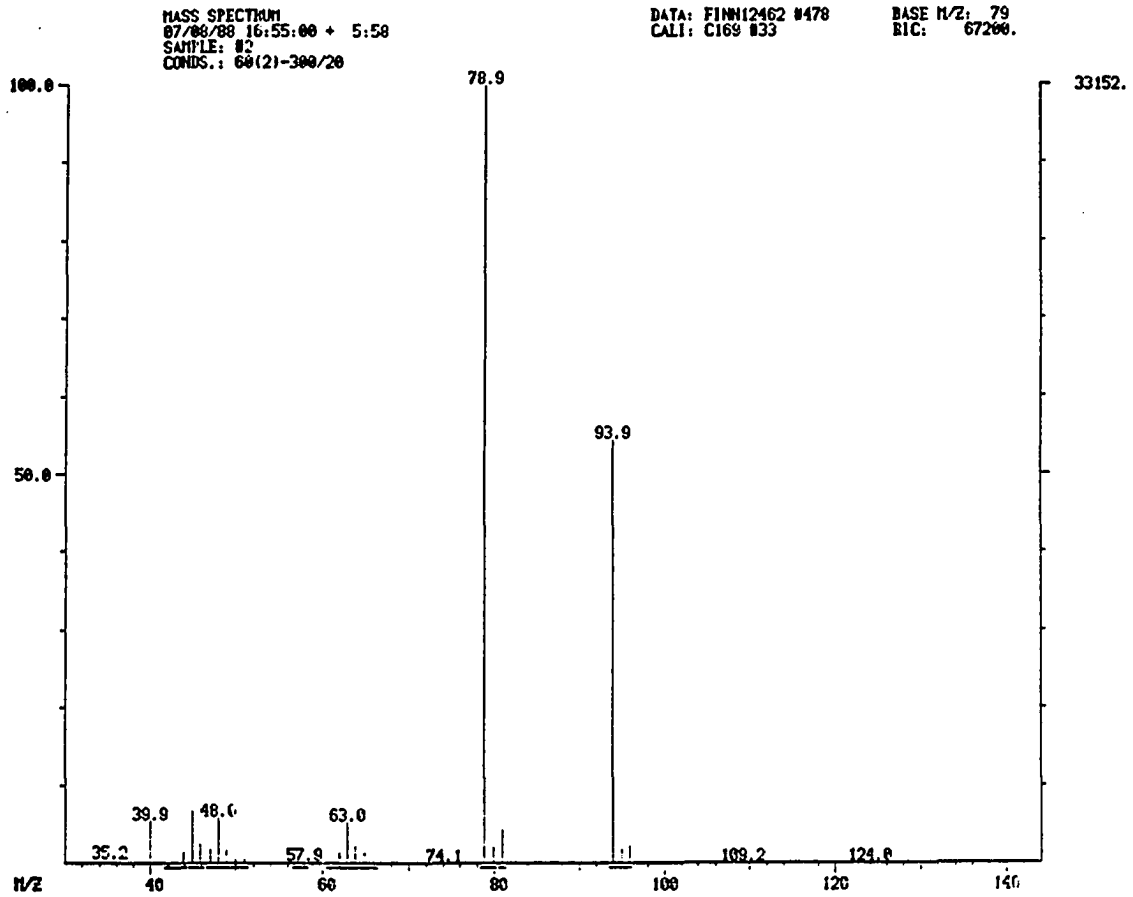
Figure 15B.   Mass spectrum for the second peak in Curve b in Figure 15A

Potential / V
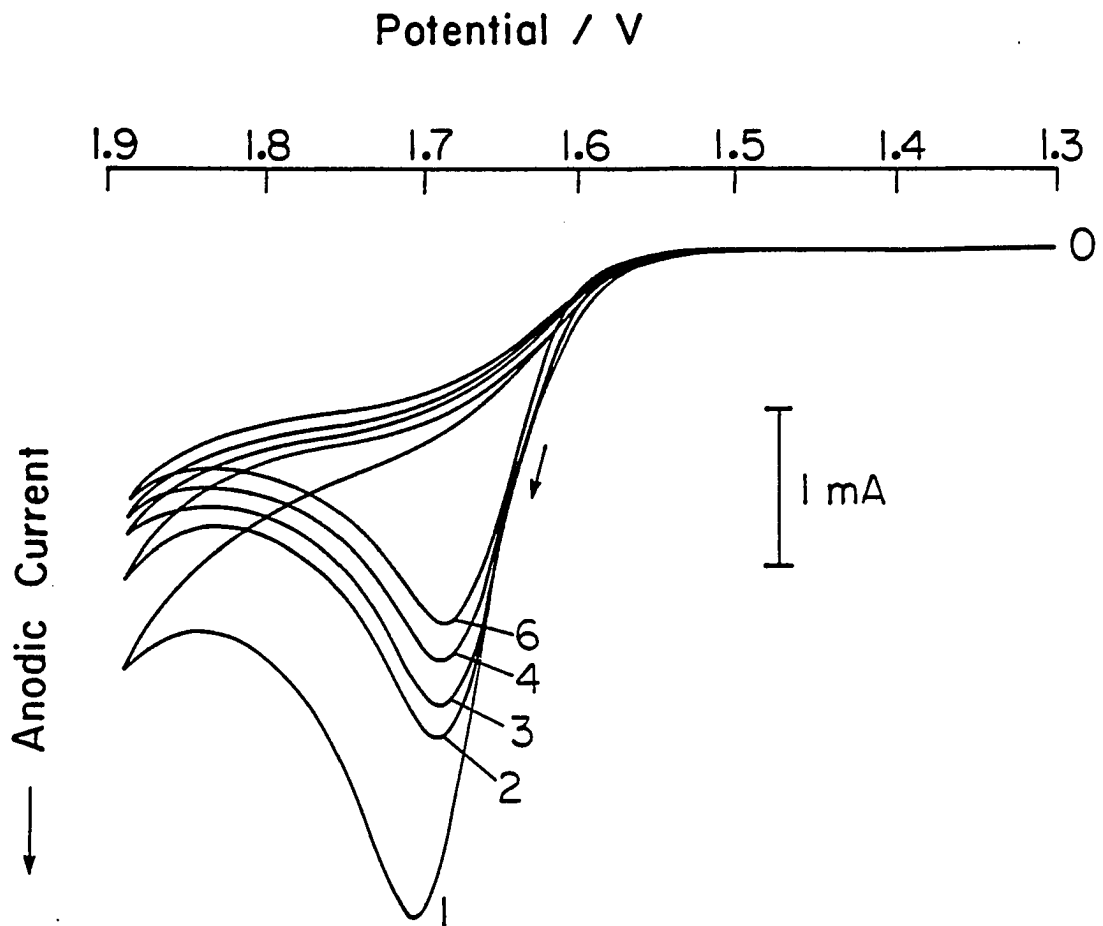
Figure 16. Cyclic voltammograms of 10 mM DMSO at $w = 0$ at PbO_2-
coated Au RDE with co-existing Bi^{3+}

Conditions: 20 mV s^{-1}, $C_{Bi} = 0.1$ mM

B. Modification of Lead Dioxide Electrodes by Electroadsorption of

Ionic Catalysts: Effects of Analyte and Catalyst Identities[1]

"Any time you think you have influence, try ordering around someone else's dog."

-The Cockle Bur

"Question authority, but raise your hand first."

-Bob Thaves

----

[1]To be submitted to J. Electrochem. Soc.

Abstract

Many oxygen-transfer reactions are catalyzed and proceed readily at Bi^{3+}-adsorbed PbO_2 electrodes, in addition to the oxidation of dimethyl sulfoxide (DMSO) which has been described in the previous chapter. These include: oxidations of tetramethyl sulfoxide to tetramethyl sulfone, 2-thiophene carboxylic acid to an unknown product, chloride to hypochlorite, manganese(II) to manganese(VII), chromium(III) to chromium(VI), and benzene to benzoquinone. The same value of voltammetric half-wave potential ($E_{1/2}$) was observed for all reactions in spite of their widely different standard potential values.

The adsorption method for modification of PbO_2 surface is fast and efficient for the purpose of screening new catalysts. High catalytic activity for oxidation of DMSO was found at As(V)-adsorbed PbO_2, with a $E_{1/2}$ value similar to that obtained at Bi^{3+}-adsorbed PbO_2. Moderate catalytic activity also was found for PbO_2 modified by Cl^- and Ag^+ in a potential region similar to that for PbO_2 modified by Bi^{3+} and As(V).

It is concluded that the $E_{1/2}$ value represents a common rate-determining step for all anodic oxygen-transfer reactions. The $E_{1/2}$ value is independent of the identities of the analyte and catalyst, but dependent on the coverage of catalyst on the electrode surface.

Introduction

There are several questions which remain unanswered from the preceding paper (1) which described the electrocatalytic oxidation of dimethyl sulfoxide (DMSO) at PbO_2 electrodes chemically modified by adsorbed Bi^{3+}. For example, what is the meaning of the voltammetric

half-wave potential $(E_{1/2})$? Can a Bi^{3+}-adsorbed PbO_2 electrode

(Bi^{3+}/PbO_2) be used to catalyze any other oxygen-transfer (O-t)

reactions? Is there any other species that can be adsorbed onto PbO_2

electrodes which can function as O-t catalysts? How will the $E_{1/2}$ value

change with variation of the identities of analyte and catalyst? These

questions will be answered in the present report.

Experimental

Apparatus, chemicals, and procedures were described earlier (1),

except as noted below.

The As(III) and As(V) solutions were prepared from As_2O_3 and As_2O_5,

respectively. The oxides were dissolved in concentrated NaOH solutions

followed by acidification with $HClO_4$ to pH = ca. 0. Actually, the As

species exist at this pH value as H_3AsO_3 and H_3AsO_4, respectively, since

their pK_1 values are 9.23 and 2.25 (2). However, for simplicity, they

are represented by As(III) and As(V) in this paper.

Results and discussion

Oxidation of tetramethyl sulfoxide and 2-thiophene carboxylic acid

The structure as well as many other properties of tetramethyl sulfoxide

(TMSO) are very similar to that of DMSO, e.g., solubility in aqueous

solution and high oxidation overpotential. The oxidation of TMSO at a

PbO_2 electrode in the presence of Bi^{3+} was studied by voltammetry, as

shown in Figure 1. A well-defined i-E plateau appeared only if a small

amount of Bi^{3+} was present. The plateau current for both DMSO and TMSO

increased linearly with increased square root of rotational velocity

$(w^{1/2})$, indicating mass-transport control. The dependencies of the i-E curves for TMSO on variation of scan rate, and TMSO and Bi^{3+} concentrations are similar to those observed for DMSO (1). Similar i-t curves for the two compounds also were obtained by chronoamperometry at constant potential. Thus, it is concluded that the catalytic effects of Bi^{3+} for anodic oxidation of TMSO are due to the adsorption of Bi^{3+} onto PbO_2 surface, as was concluded in the previous study of the oxidation of DMSO.

Another sulfur compound tested was 2-thiophene carboxylic acid (TPCA) which is water soluble and exists as a neutral molecule in highly acidic media. Oxidation of TPCA did not occur at pure PbO_2, but proceeded readily at Bi^{3+}/PbO_2, as shown in Figure 2. The voltammetric curve is similar to those obtained for DMSO and TMSO, despite the obvious differences in their molecular structure. The number of electrons transferred was estimated as 8 - 10 eq mol^{-1} based on the height of the i-E plateau, assuming a complete mass-transport control. Therefore, a ring-opening reaction is probable. The oxidation product had a brown-yellow color and was soluble in both water and ether.

<u>Oxidation of chloride and chromium(III)</u> An anodic wave for chloride anion was observed at PbO_2 in the presence of Bi^{3+}, as shown in Figure 3. The i-E response for the positive scan became slightly peak-like at high w values, but the i-E curve in the negative scan always remained as a plateau. Since no gas bubble was observed at the electrode surface, it is unlikely that the oxidation product is chlorine. The estimated number of electron-transfer was ca. 2 eq mol^{-1} and the

corresponding oxidation product is concluded to be ClO⁻.

Besides the reaction Mn(II) -> Mn(VII), as described in Chapter III-A, another important oxidation reaction of a metal ion is Cr(III) -> Cr(VII), which was studied at Bi^{3+}/PbO_2 electrode. The voltammograms at Au, PbO_2, and Bi-adsorbed PbO_2 electrodes for 10 mM Cr(III) are shown in Figure 4a, b, and c, respectively. The oxidation potential measured at a constant current clearly shifted to less positive value by about 25 mV moving from the Au to PbO_2 electrodes. However, a further shift of 125 mV and a nearly plateau-shaped i-E curve were observed when Bi^{3+} was added. This anodic wave for catalytic oxidation of Cr^{3+} to CrO_4^{2-} (Curve c) was observed only at elevated temperatures, which is consistent with the results from other work with unmodified PbO_2 electrodes (3). The large decrease in overpotential for oxidation of Cr^{3+} in the presence of Bi^{3+} is of great importance in practical applications of this reaction.

Oxidation of benzene   The oxidation behavior of benzene at Bi^{3+}/PbO_2 is quite different from that of others, as shown in Figure 5. The solution consisted of 45% 1 M $HClO_4$, 45% methanol, and 10% acetonitrile to enhance the solubility of benzene. The i-E curve for benzene was shifted about 150 mV less positive after the addition of a small amount of Bi^{3+}. This indicates that adsorbed Bi^{3+} indeed also catalyzes the oxidation of benzene. However, no current plateau was obtained and the current did not change with variation in w (Figure 5c). The absence of a limiting current plateau is probably due to the extremely high value of standard potential (E°) for oxidation of benzene. Studies by other researchers indicated that oxidation of benzene to
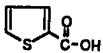
benzoquinone occurred only in the potential region of O_2 evolution (4).

Comparison of half-wave potential   A half-wave potential value ($E_{1/2}$) can be measured accurately for the catalytic oxidation reactions at Bi^{3+}/PbO_2 (5,6). This $E_{1/2}$ value is considered to be characteristic of the mechanism of electrocatalysis at the modified PbO_2 electrode.

Listed in Table 1 are the $E_{1/2}$ values in the positive scan ($E_{1/2,p}$) for oxidation of the above substances, DMSO (1), and Mn(II) (6) at the Bi^{3+}/PbO_2 electrode. Since $E_{1/2,p}$ changes with variation of Bi^{3+} concentration (1), the least positive value for every substance was measured as Bi^{3+} concentration was changed. These substances varied from inorganic to organic, and from anions to neutral molecules and to cations. Also listed in Table 1 are the E° values for the corresponding oxidation reactions (7). These E° values vary over a large range from -0.1 V to 1.45 V. Despite all these differences, virtually an identical value of $E_{1/2,p}$ was obtained, indicating a single mechanism of O-transfer. The very small differences among the $E_{1/2,p}$ values may be the result of different experimental conditions, especially C_{Bi} and temperature. The shape of the i-E curves for these substances is also similar to one another. Based on these results, it is concluded that the catalytic activity of Bi-modified PbO_2 for anodic O-t reactions is independent of the identity of analytes.

It should be pointed out that the standard potential values for these substances are all accessible at normal solid electrodes. However, no distinct oxidation wave for these substances was observed at PbO_2 before the addition of Bi^{3+}, or at Au, Pt, and GC, with co-existing Bi^{3+}.

Table 1. Comparison of $E_{1/2,p}$ values for oxidation of different substances at Bi^{3+}-adsorbed PbO_2

reactant[a]	product	E° (V vs. SCE)	$E_{1/2,p}$ (V)
$(CH_3)_2SO$	$(CH_3)_2SO_2$	-0.004[b]	1.68[c]
$(CH_2)_4SO$	$(CH_2)_4SO_2$	-0.1[d]	1.68
	unknown	1.0[d]	1.71
Mn^{2+}	MnO_4^-	1.268[b]	1.65[e]
Cr^{3+}	CrO_4^-	1.138[b]	1.69
Cl^-	ClO^-	1.450[b]	1.68
		1.6[d]	-

[a] For conditions, see Figures 1 - 5.

[b] From Ref. 7.

[c] From Ref. 1.

[d] Estimated value.

[e] From Ref. 6.

Screening of new catalysts   The conventional electrochemical co-deposition method to produce modified PbO_2 is very time-consuming and tedious for selection of new catalysts out of large numbers of candidates (8). It is expected that the adsorption method of PbO_2 modification can be faster and more efficient for this purpose. By continuous recording of cyclic voltammograms in a 10 mM DMSO solution at PbO_2 while small amounts of varied candidate species are added, the catalytic effects of the added species can be monitored by changes in the i-E curve. This technique of catalyst screening is very effective because the electrode modification and activity testing are conducted in a single step. This technique also can be combined with a flow-injection system with benefits of continuous operation and small volume.

Out of more than 30 different species tested with this adsorption method, catalytic activity enhancement was observed for As(III), As(V), Cl^-, and Ag^+, which are discussed in the following sections.

Effect of As(III)   Following the addition of As(III), a distinct voltammetric wave appeared for oxidation of DMSO at PbO_2, as shown in Figure 6. This wave increased and shifted to less positive potential values as the concentration of As(III) was increased, until a well-defined i-E plateau emerged. The height of this plateau increased linearly with increased $w^{1/2}$, as shown in Figure 7, and DMSO concentration, but did not change with variation in scan rate. These results are similar to those obtained at Bi^{3+}/PbO_2. Thus, it is concluded that arsenic ion also can be adsorbed onto PbO_2 electrode surface and function as a catalyst for anodic O-t reactions.

A difference exists in the redox property of Bi^{3+} and As(III). Arsenic(III) can be oxidized to As(V) at oxide-covered solid electrodes (9), while Bi^{3+} cannot be oxidized to Bi^{5+}, partially because the E^o value for As(V)/As(III) (0.32 V vs. SCE) is much smaller than that for Bi^{5+}/Bi^{3+} (ca. 1.8 V). A reproducible limiting voltammetric plateau for oxidation of As(III) was observed at pure PbO_2 at E > 1.3 V. If the concentration of As(III) is comparable to that of DMSO, the anodic DMSO wave is superimposed on the As(III) wave, as a current offset was observed as shown in Figure 8. The amplitude of the current offset increased linearly with increased As(III) concentration, but the net height of the plateau for DMSO remained unchanged. It is noticeable that the limiting i-E plateau is stable even at an As(III)/DMSO concentration ratio as high as 0.3, which was not observed for Bi^{3+}/PbO_2 electrode. Hence, the effect of coverage observed at Bi^{3+}/PbO_2 does not exist at the As-adsorbed PbO_2, probably due to a difference in adsorption behavior of arsenic and bismuth ions on PbO_2. It is expected that Bi ions are adsorbed more easily on PbO_2 than As ions by the ion-exchange mechanism (1), because of the similarity between Bi^{3+} and Pb^{4+} and the difference between As(III) (or As(V), as discussed later) and Pb^{4+}.

There appear to be two explanations for the steady oxidation of As(III) at PbO_2, which was not observed at Pt or Au. First, it is related to the power of PbO_2 to stoichiometrically oxize As(III). It was observed that for [As(III)] > 1 mM, the PbO_2 film was dissolved in the As(III) solution under open-circuit conditions. Secondly, the As-adsorbed PbO_2 can catalyze the further oxidation of As(III) which is also

an O-transfer reaction.   Asorption of As ions does not occur at Pt or Au.

Effect of As(V)   Since As(III) is oxidized easily to As(V) in the same potential region for oxidation of DMSO, it is interesting to know whether the adsorbed arsenic species exist in +3 or +5 oxidation state. This puzzle was solved by addition of As(V) instead of As(III). As a result, a voltammetric plateau for oxidation of DMSO also was obtained as shown in Figure 9. The shape and $E_{1/2}$ value of the plateau are very similar to those obtained with As(III). The i-E curves also changed with variation of w, $\emptyset$, [DMSO], and [As(V)] similarly with those for As(III). Thus, it is concluded that As(V) can function as an O-transfer mediator. Since As(III) is not stable at the surface of PbO_2 with a high positive potential, it is also concluded that As(III) is oxidized to As(V) before being adsorbed. However, it is not clear what is the form of the adsorbed As(V). From comparison between Figures 9A and 6, it is obvious that a higher As(V) concentration is required to achieve the same level of catalytic effect than As(III) concentration. This is probably because As(V) is adsorbed more easily following the oxidation from As(III) than directly from As(V) in the solution, due to the interactions of As ions with the oxide surface, especially oxygen species during the oxidation.

Mechanism of electrocatalytic O-transfer   Since As(V) cannot be further oxidized, the results above also prove that a catalyst at the modified PbO_2 electrodes for O-t reactions does not have to undergo a change in oxidation state during the process of catalysis. This further proves that the mechanism of electrocatalysis at these electrodes is via

oxygen-transfer mediation instead of the more commonly known electron-transfer mediation, as is illustrated in (1,4). In the O-t mediation mechanism, $E_{1/2}$ represents the potential at which the promoted discharge of water takes place. Therefore, $E_{1/2}$ is independent of the identities of the analyte under certain catalyst coverages.

<u>Effect of arsenic doping</u>   Arsenic also can be incorporated electrochemically into PbO_2 by adding As(III) to the Pb^{2+} deposition solution. However, the deposition of As-doped PbO_2 is much more difficult than that of Bi-doped PbO_2, since As(III) can react rapidly with PbO_2. Thus, As(III) was added to the solution only after a thin film of PbO_2 had been deposited. Otherwise, the presence of As(III) made the nucleation period become indefinite. It is speculated that the average oxidation state of As in the As-doped PbO_2 is close to +5.

The catalytic effect of As-doped PbO_2 on DMSO oxidation is shown in Figure 10. An anodic i-E wave was observed, which increased with increased DMSO concentration. The i-E curves are not plateau-shaped and are very similar to those obtained for As-adsorbed PbO_2 with very low As(III) concentration (see Figure 6). This kind of similarity in the i-E curves also was observed between Bi-doped PbO_2 and Bi-adsorbed PbO_2 (4), which is concluded to be due to a lower surface concentration of the catalyst at the catalyst-doped PbO_2 than at the catalyst-adsorbed PbO_2.

<u>Effect of and Cl⁻ and Ag⁺</u>   The addition of a small amount of Cl⁻ also increased the anodic current for DMSO oxidation at PbO_2, as is shown in Figure 11. This additional anodic current is concluded not to be the

result of the direct oxidation of Cl⁻, based on two reasons. First, the direct oxidation of Cl⁻ in highly acidic media is very slow at non-catalytic electrodes like pure PbO_2, as demonstrated by the low current obtained at PbO_2 electrode for [Cl⁻] much higher than used in Figure 11. Second, the concentration of Cl⁻ is much lower than that of DMSO. It is impossible for Cl⁻ to show this level of anodic current at such a low concentration.

After being washed and air-dried, the PbO_2 electrode used to produce the data in Figure 11 still exhibited catalytic activity in a new DMSO solution free of Cl⁻. Thus, it is concluded that Cl⁻ can be adsorbed onto the PbO_2 surface and the adsorbed chlorine species remains in the -1 oxidation state. The resultant Cl⁻-adsorbed PbO_2 is catalytically active for anodic O-transfer. However, the shape of the i-E curve in Figure 11 is different from those obtained at Bi^{3+}-adsorbed and As(V)-adsorbed PbO_2 electrodes. No limiting current plateau appeared in the case of Cl⁻ as was the case of Bi^{3+} and As(III). Hence, Cl⁻ is not as effective an O-transfer catalyst.

Two plating solutions were used to deposit PbO_2 electrodes for comparison: 10 mM $Pb(NO_3)_2$ in 1.0 M $HClO_4$ with [Cl⁻] < 1 μM; and 10 mM $PbCl_2$ in 1.0 M $HClO_4$. Voltammograms of 10 mM DMSO at these two PbO_2 electrodes are shown in Figure 12. Clearly, the PbO_2 electrode deposited from Cl⁻-containing solution has some catalytic activity similar to that observed for Cl⁻-adsorbed PbO_2. Thus, it is concluded that Cl⁻ also can be incorporated into PbO_2 matrix by electrochemical co-deposition.

The catalytic effect of Ag^+ is very similar to that of Cl⁻, as

tested by both the co-deposition and adsorption methods. No i-E plateau was observed for DMSO, however, indicating only modest catalytic activity. However, the oxygen evolution background was increased much more rapidly with increased $[Ag^+]$ than with $[Bi^{3+}]$, $[As(III)]$, and $[Cl^-]$.

Electrodeposition of Cl-doped PbO_2 In parallel to the studies on the Bi-doped PbO_2 (5), the kinetics and mechanism of electrodeposition of Cl-doped PbO_2 on Au was studied, as is described below.

Shown in Figure 13 are the i-t curves for deposition of PbO_2 on a Au RDE from solutions of varied $[Cl^-]$ and constant $[Pb^{2+}]$. It is apparent that the i-t curve is not changed much for $[Cl^-] \leq 0.01$ μM. However, with increased $[Cl^-]$, the induction time increased and the steady-state current decreased. Hence, the existence of Cl^- in the plating bath decreases the rate of PbO_2 nucleation and growth, which is similar to the effect of Bi^{3+} on the electrodeposition of PbO_2 (5). The increase of induction time with increased $[Cl^-]$ is concluded to be due to the rapid dissolution of Au during anodization in Cl^--containing solution, as was observed in this study and in literature (10). The higher is $[Cl^-]$, the faster is the dissolution rate; so the longer is the induction period for PbO_2 deposition on the top of Au. The decrease of steady-state current with increased $[Cl^-]$ is concluded to be due to the complication in the crystallization process by the adsorbed Cl^- at the PbO_2 surface. The incorporation of Cl^- into PbO_2 matrix occurs via adsorption and inclusion of Cl^- as impurities on the surface of PbO_2, based on the conclusion for Bi-doped PbO_2 (5). Since Cl^- did not contribute directly to the anodic process, it is concluded that the chlorine species incorporated into PbO_2

matrix remains at -1 oxidation state.

Conclusions

We have clearly shown that the $E_{1/2}$ values obtained for numerous catalyzed O-transfer reactions are independent of the identity of the reactants at the Bi^{3+}-adsorbed PbO_2 electrode. Therefore, a single mechanism of electrocatalysis for O-transfer reaction is concluded to exist at the Bi-modified PbO_2 electrode.

It is also obvious that the $E_{1/2}$ values for oxidation of DMSO are virtually the same at the Bi^{3+}-adsorbed PbO_2 and As(V)-adsorbed PbO_2. Based on this result, it is concluded that the mechanism of electrocatalysis at the modified PbO_2 electrodes is independent of the identity of catalyst. This result sharply differs from the electron-transfer mediation and is a strong evidence for O-transfer mediation. However, in comparison with PbO_2 modified by Bi^{3+} and As(V), different voltammetric behavior for oxidation of DMSO was observed at the PbO_2 electrodes modified by Cl^- and Ag^+. This difference is concluded to be caused by the different adsorption or ion exchange affinity of Cl^- and Ag^+ to PbO_2 as compared to that of Bi^{3+} and As(V), but not due to a different mechanism of electrocatalysis. This explanation is reasonable because despite the absence of i-E plateau, the anodic waves for DMSO at PbO_2 modified by Cl^- and Ag^+ are located in the same potential region as those obtained at Bi-doped PbO_2 and As-doped PbO_2, and those obtained at Bi^{3+}-adsorbed PbO_2 and As(V)-adsorbed PbO_2 with low catalyst concentrations. This potential region is also close to that for anodic oxygen evolution at PbO_2. None of these O-transfer catalysts has been

identified before as electron-transfer mediator that are usually transition metal ions. In effect, these species do not meet the requirements for e-transfer mediation, so they can only serve as O-transfer mediators.

References

1. Chang, H.; Johnson, D. C., preceding paper; Chapter IV-A, this Dissertation.

2. "CRC Handbook of Chemistry and Physics"; Weast, R. C.; Astle, M. J.; Beyer, W. H., Eds.; CRC Press: Boca Raton, 1985; 68th ed., p. D163.

3. (a) Kuhn, A. T.; Clarke, R. J. Appl. Chem. Biotechnol. 1976, 26, 407. (b) Pletcher, D.; Tait, S. J. D. J. Appl. Electrochem. 1981, 11, 493. (c) Tarasevich, M. R.; Sadkowski, A.; Yeager, E. In "Comprehensive Treatise of Electrochemistry"; Conway, B. E.; Bockris, J. O'M.; Yeager, E.; Khan, S. U. M.; White, R. E., Eds.; Plenum: New York, 1983; Volume 7.

4. Sunderland, J. G. The Electricity Council Research Center Report, No. M1065, 1977.

5. Chang, H.; Johnson, D. C., in preparation; Chapter III-B, this Dissertation.

6. Chang, H.; Johnson, D. C., in preparation; Chapter III-A, this Dissertation.

7. "Standard Potentials in Aqueous Solution"; Bard, A. J.; Parsons, R.; Jordan, J., Eds.; M. Dekker: New York, 1985.

8. (a) Yeo, I.-H.; Johnson, D. C. J. Electrochem. Soc. 1987, 134, 1973. (b) Yeo, I.-H. Ph.D. Dissertation, Iowa State University, Ames, Iowa, 1987. (c) Yeo, I.-H.; Kim, S.; Jacobson, R.; Johnson, D. C. J. Electrochem. Soc. in press.

9. (a) Cabelka, T. K. Ph.D. Dissertation, Iowa State University, Ames, Iowa, 1983. (b) Cabelka, T. K.; Austin, D. S.; Johnson, D. C. J. Electrochem. Soc. 1984, 131, 1595; 1985, 132, 359.

10. (a) Diard, J. P.; Saint-Amen, B. Le G. et E. Electrochim. Acta 1983, 28, 1211. (b) Lovrecek, B.; Moslavac, K.; Matic, D. Electrochim. Acta 1981, 26, 1087. (c) Podesta, J. J.; Piatti, R. C. V.; Arvia, A. J. Electrochim. Acta 1979, 24, 633. (d) Radeka, R.; Moslavac, K.; Lovrecek, B. J. Electroanal. Chem. 1977, 84, 351. (e) Nicol, M.

J. National Institute for Metallurgy, Report, No. 1844, No. 1846, Randburg, South Africa, 1976. (f) Schalch, E.; Nicol, M. J.; Balestra, P. E. L.; Stapleton, W. M. National Institute for Metallurgy, Report, No. 1979, 1978. (g) Frankenthal, R. P.; Thompson, D. E. J. Electrochem. Soc. 1976, 123, 799. (h) Gallego, J. H.; Castellano, C. E.; Calandra, A. J.; Arvia, A. J. J. Electroanal. Chem. 1975, 66, 207. (i) Cadle, S. H.; Bruckenstein, S. J. Electroanal. Chem. 1973, 48, 325. (j) Moslavac, K.; Lovrecek, B.; Radeka, R. Electrochim. Acta, 1972, 17, 415.

Potetial / V
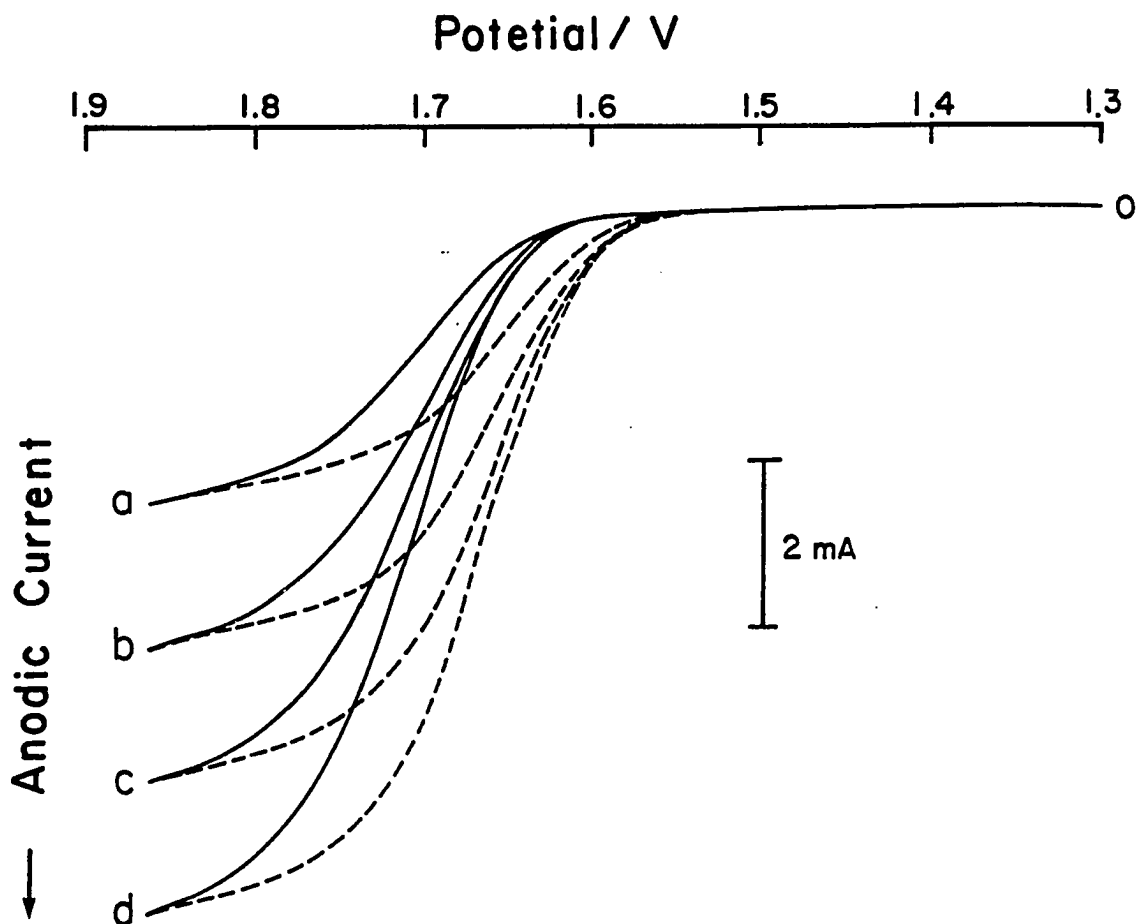
Figure 1. Cyclic voltammograms of 10 mM TMSO at PbO_2 coated Au RDE
in the presence of Bi^{3+}

Conditions: C_{Bi} = 10 μM, 1.0 M $HClO_4$, 20 mV s^{-1};
room temperature

w (rev min^{-1}): (a) 400, (b) 900, (c) 1600, (d) 2500

Solid line: positive scan; dashed line: negative scan
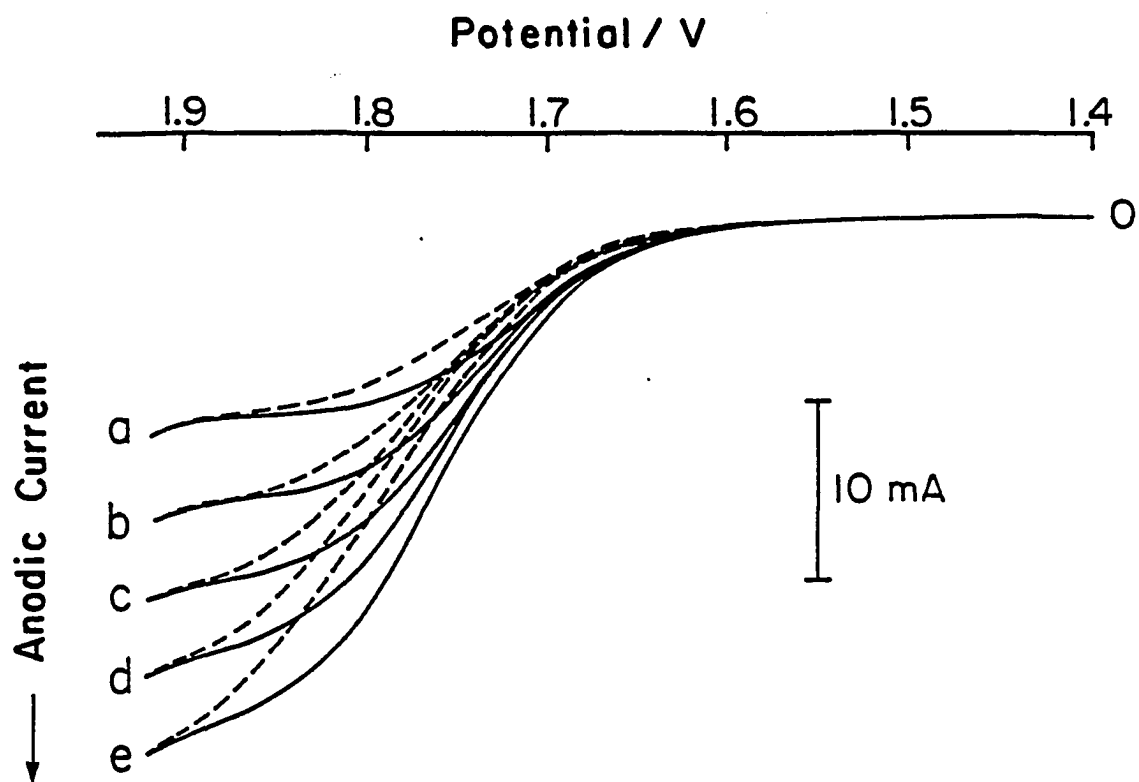
Figure 2. Voltammograms of 10 mM 2-thiophene carboxylic acid

Conditions: as given in Figure 1

w (rev min^{-1}): (a) 400, (b) 900, (c) 1600,
(d) 2500, (e) 3600

Potential / V
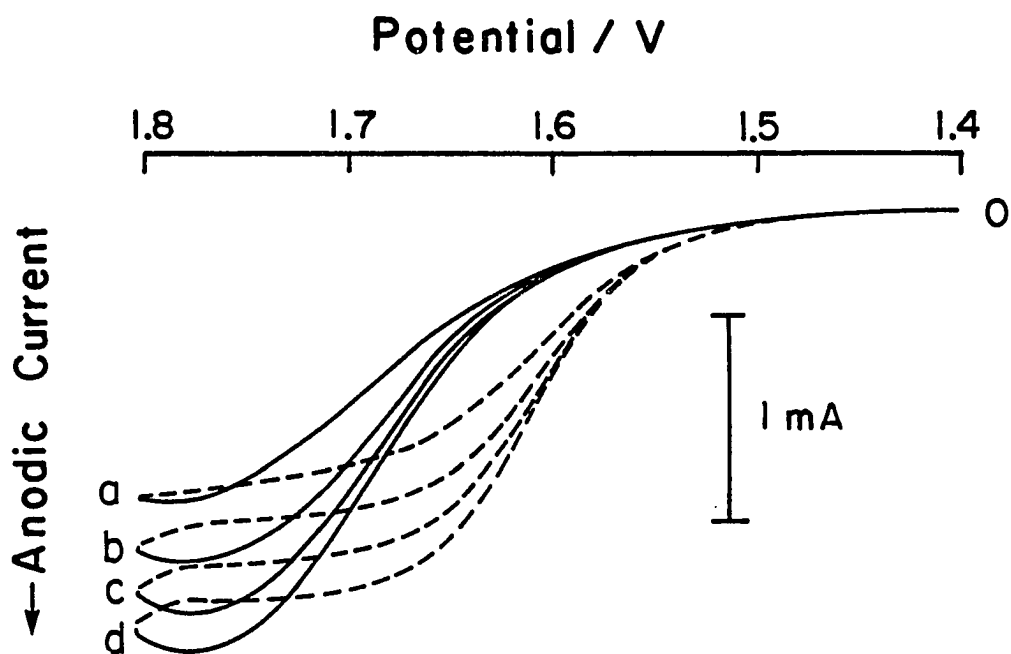
Figure 3. Voltammograms of 10 mM Cl$^-$

Conditions: 280 µM Bi^{3+}, others as given in Figure 1
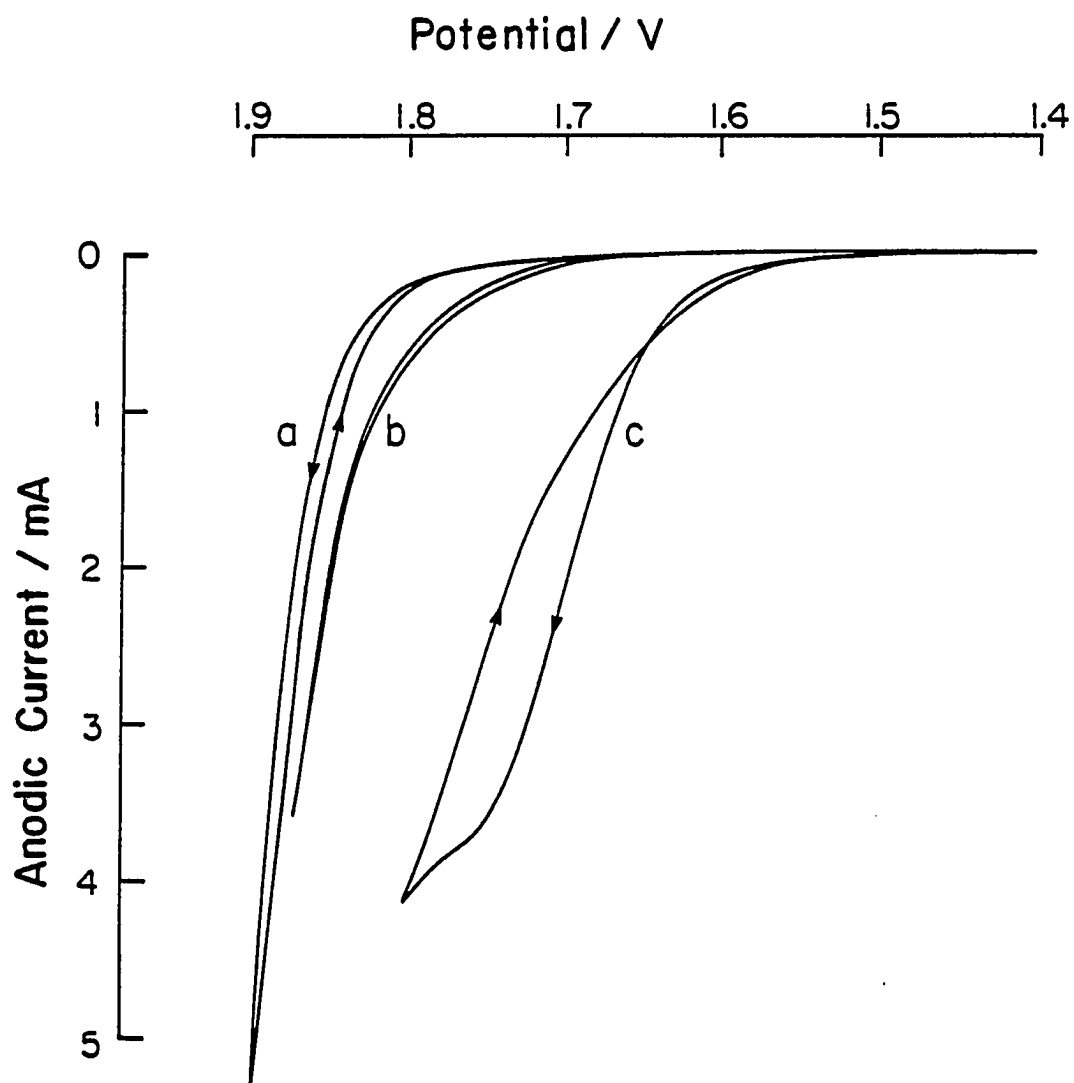
Figure 4. Voltammograms of 10 mM Cr^{3+}

Conditions: 65°, others as given in Figure 1

Curves: (a) 0.1 mM Bi^{3+} at Au,
(b) 0 mM Bi^{3+} at PbO_2,
(c) 0.1 mM Bi^{3+} at PbO_2
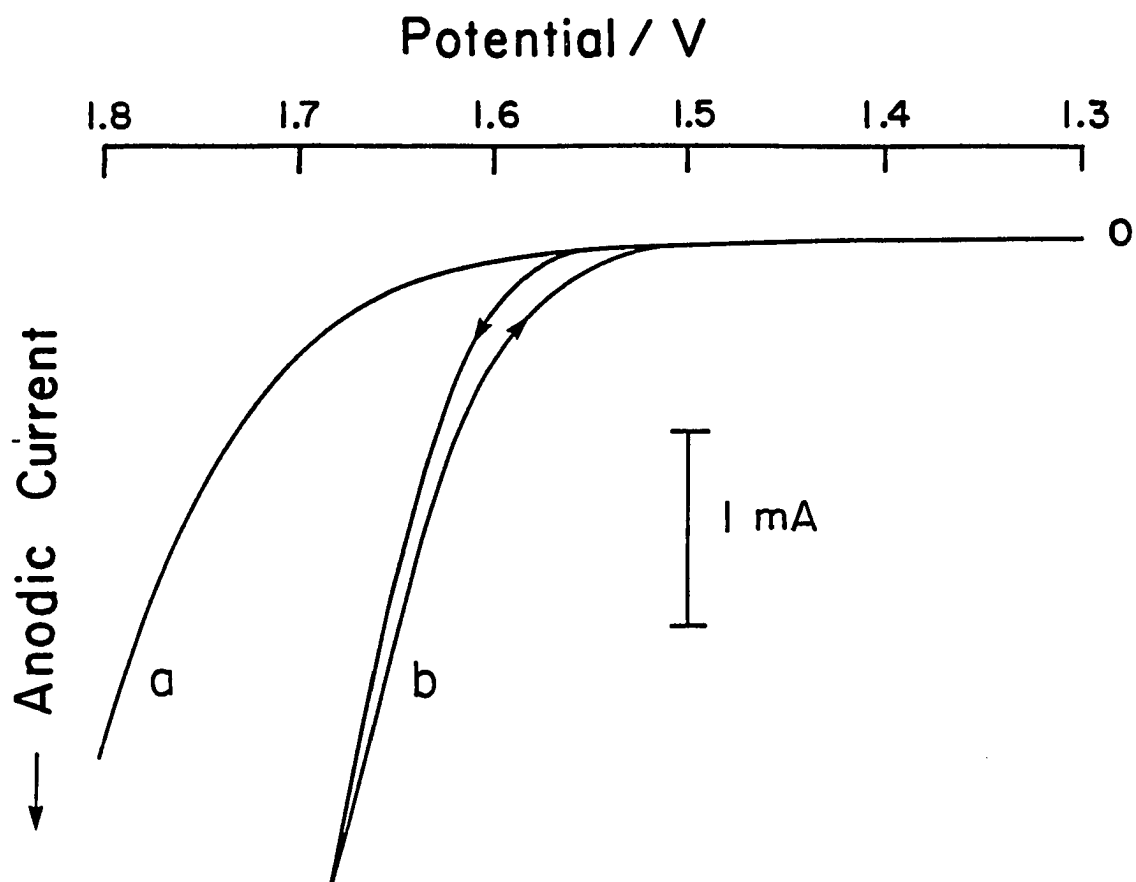
Figure 5. Voltammograms of benzene

Solution: ca. 1% benzene, 45% 1.0 M $HClO_4$, 45% CH_3OH, and 9% acetonitrile

C_{Bi} (μM): (a) 0; (b) 10

Other conditions: as given in Figure 1

Potential / V
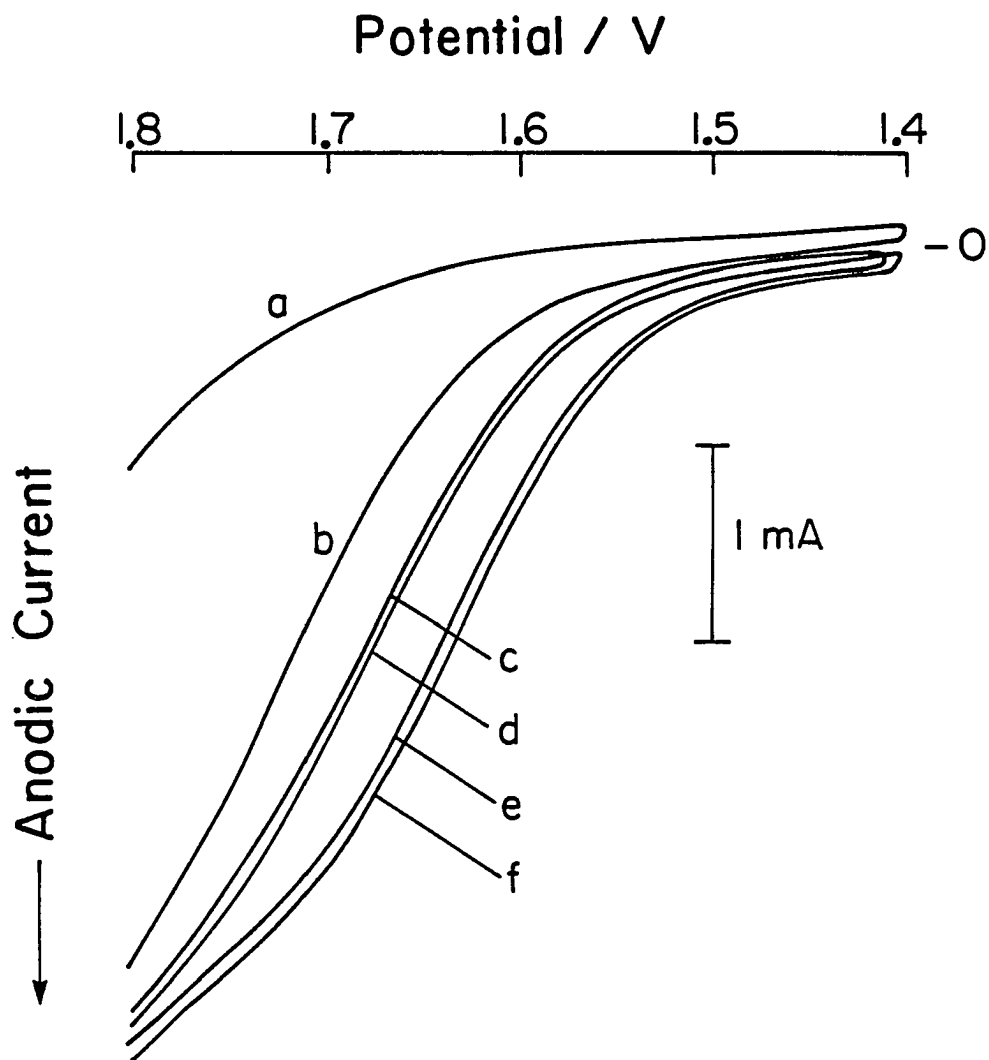
Figure 6. Voltammograms of 10 mM DMSO at PbO_2 in the presence
of As(III)

[As(III)] (µM):   (a) 0, (b) 36, (c) 72, (d) 108, (e) 218,
(f) 327

Conditions: 1.0 M $HClO_4$, 20 mV/s, 400 rev min^{-1}

Only the positive scan is shown. The i-E curve in the
negative scan had the same pattern as the positive scan,
but had slightly smaller values of current
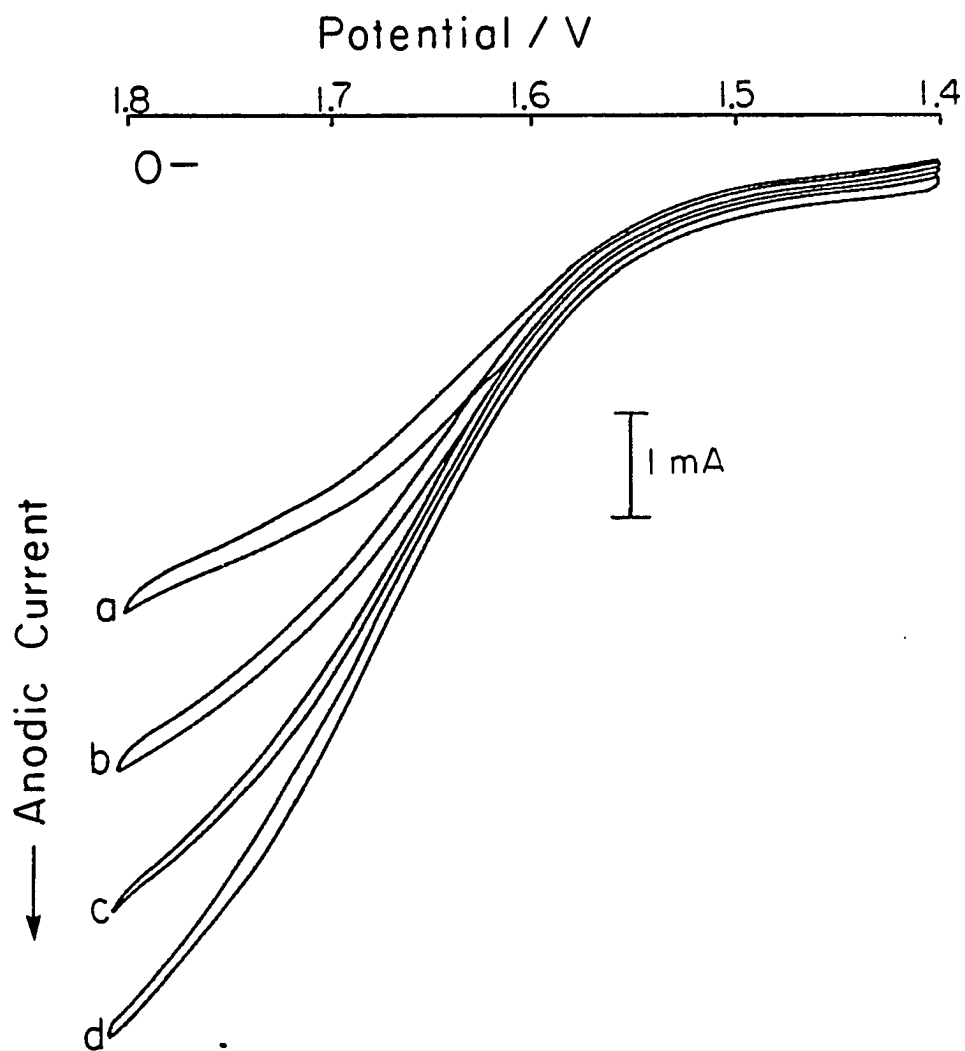
Figure 7. Voltammograms of 10 mM DMSO at As-adsorbed PbO_2

Effects of w (rev min^{-1}): (a) 400, (b) 900, (c) 1600,
(d) 2500

Conditions: 0.33 mM As(III), others as given in Figure 6
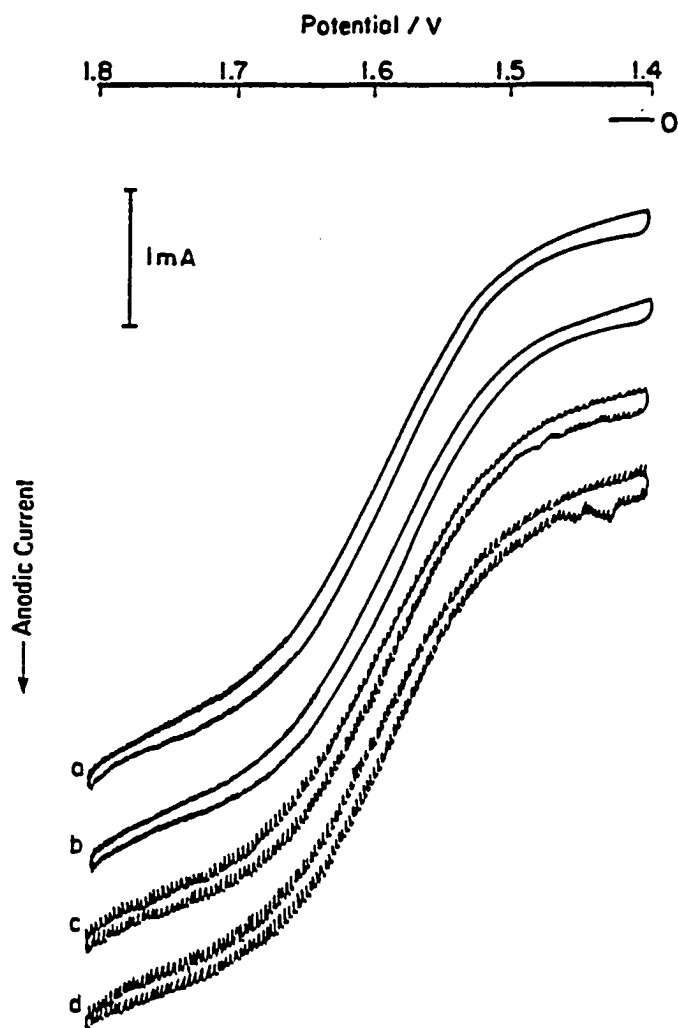
Figure 8. Voltammograms of 10 mM DMSO at As-adsorbed PbO_2

[As(III)] (mM): (a) 2.0, (b) 3.8, (c) 5.6, (d) 7.5
Conditions: as given in Figure 6
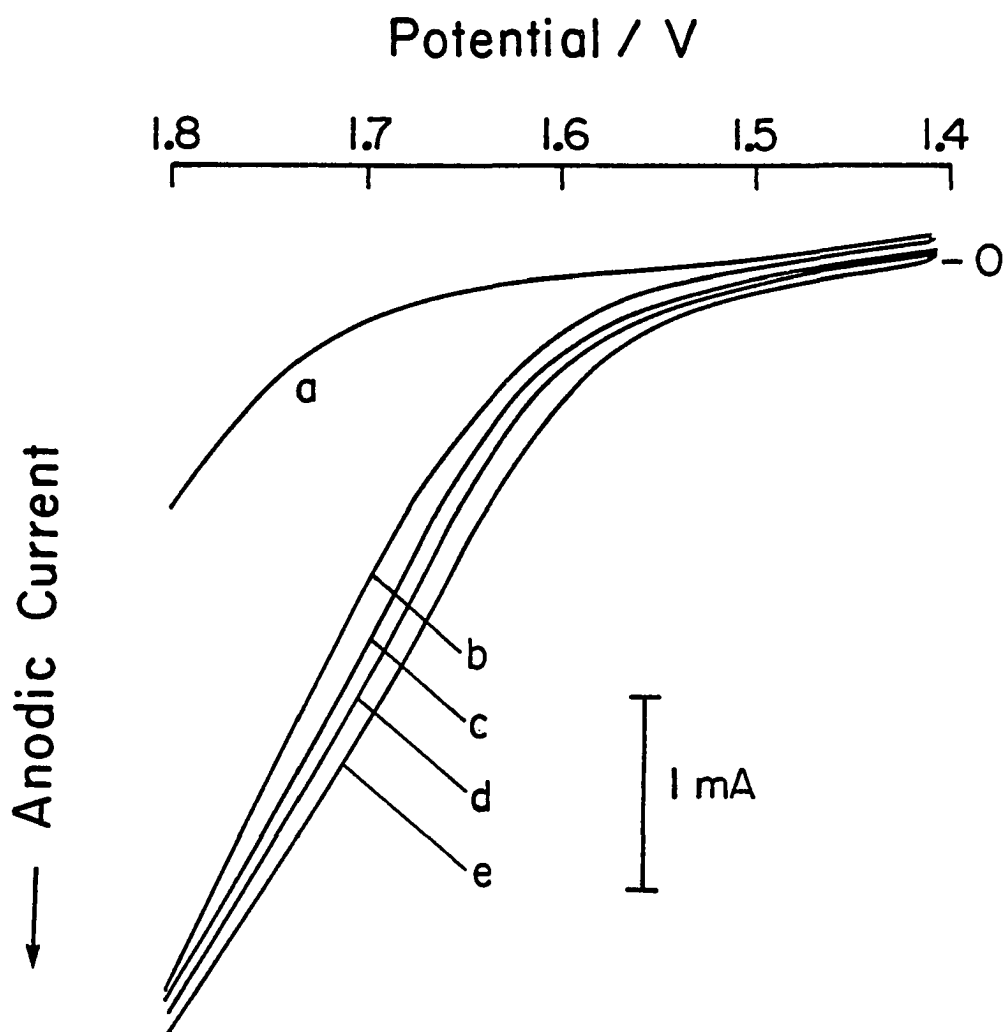
Figure 9A.   Voltammograms of 10 mM DMSO at PbO_2 in the presence of As(V)

Effect of [As(V)] (mM):   (a) 0, (b) 0.54, (c) 1.8,
(d) 3.6, (e) 10

Conditions: 20 mV s^{-1}, 400 rev min^{-1}, 1.0 M $HClO_4$
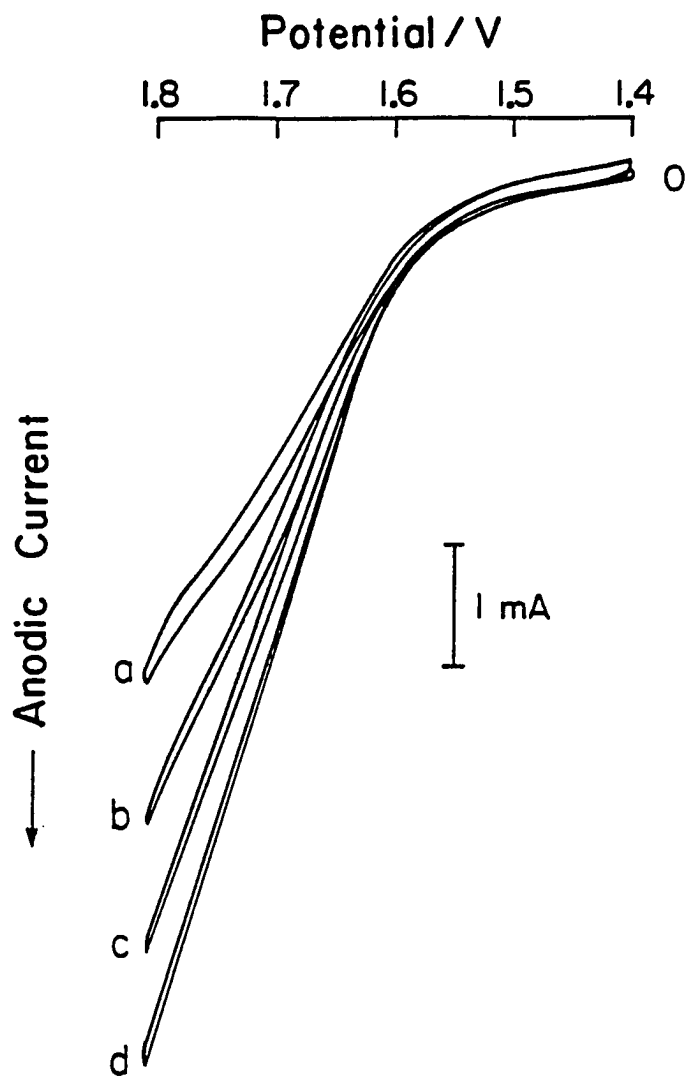
Figure 9B. Voltammograms of 10 mM DMSO at PbO_2 in the presence of As(V)

Effect of w (rev min^{-1}): (a) 400, (b) 900, (c) 1600, (d) 2500

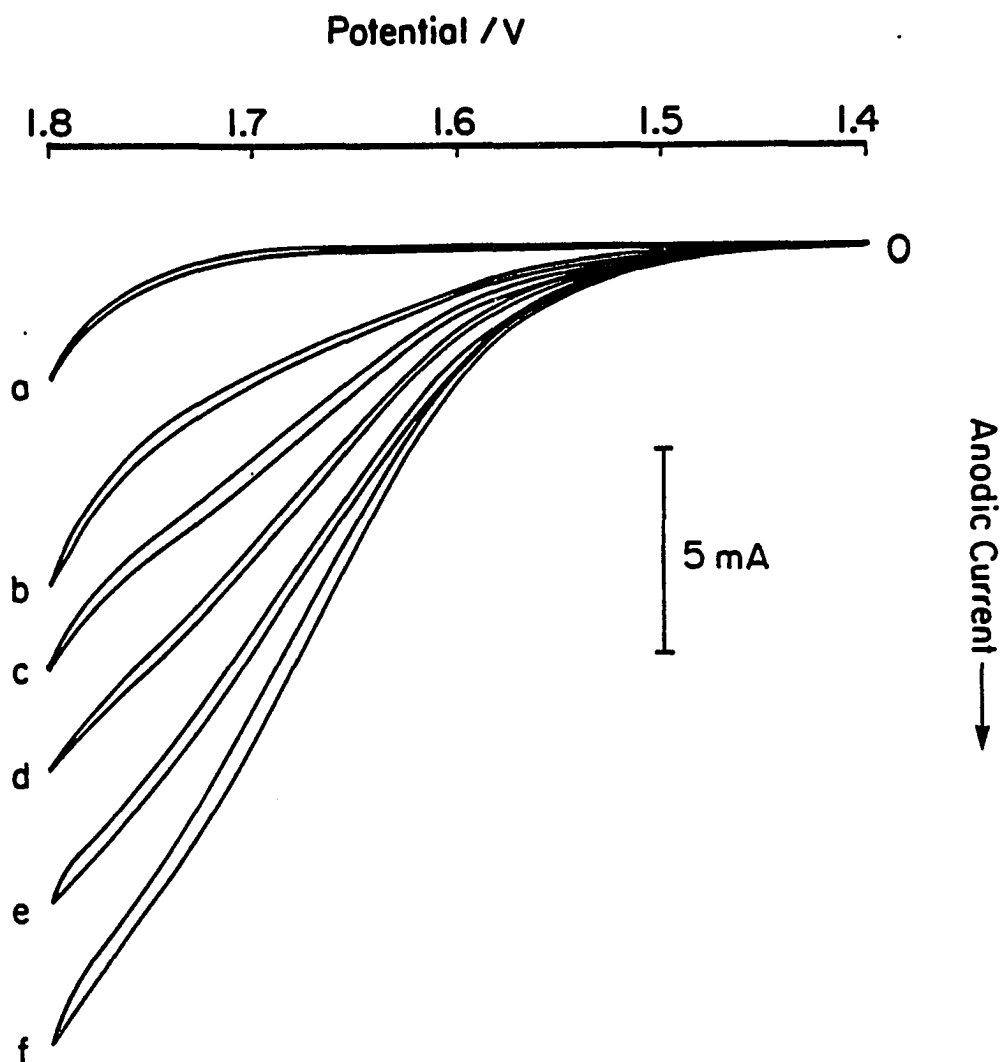Conditions: 10 mM As(V); others as given in Figure 9A

Potential / V

Figure 10. Voltammetric responses at As-doped PbO$_2$

Electrode preparation: deposition from 20 mM Pb^{2+} and 0.1 M HClO$_4$ first; then add 0.1 mM As(III)

Condtions: 20 mV s^{-1}, 400 rev min^{-1}

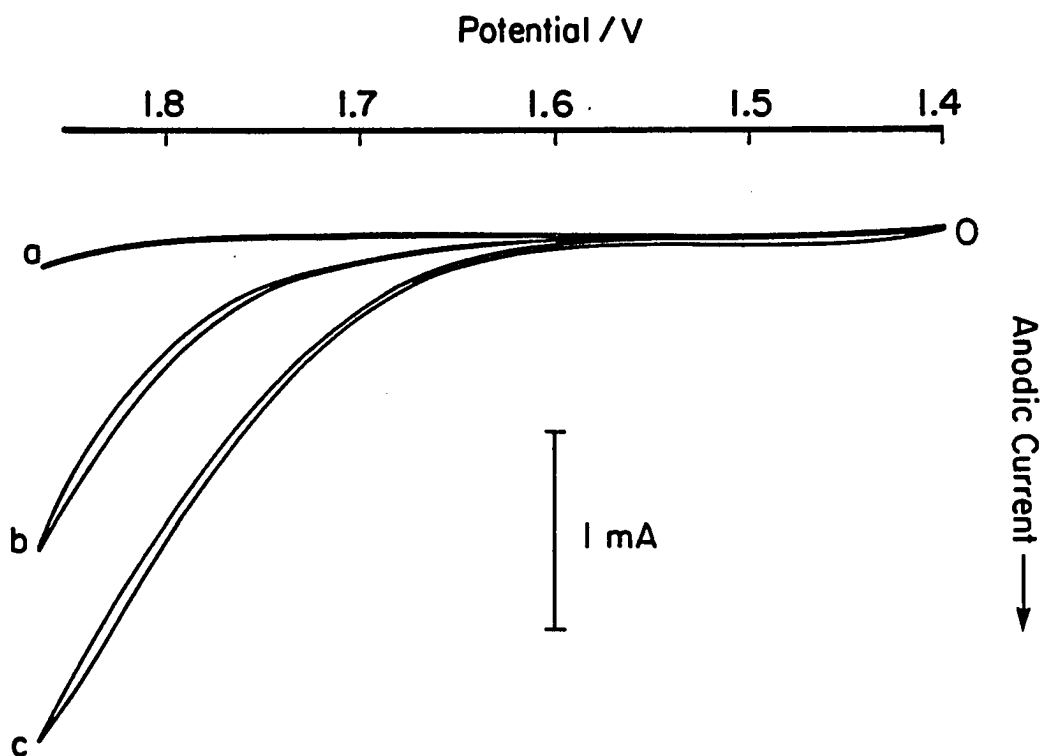DMSO concentration (mM): (a) 0, (b) 10, (c) 20, (d) 30, (e) 40, (f) 50

Potential / V

Figure 11. Voltammograms of 10 mM DMSO in 1.0 M HClO₄

        Electrode: (a) Au, (b) PbO₂, (c) PbO₂ with 0.1 mM Cl⁻

        Conditions: 20 mv s⁻¹, 400 rev min⁻¹
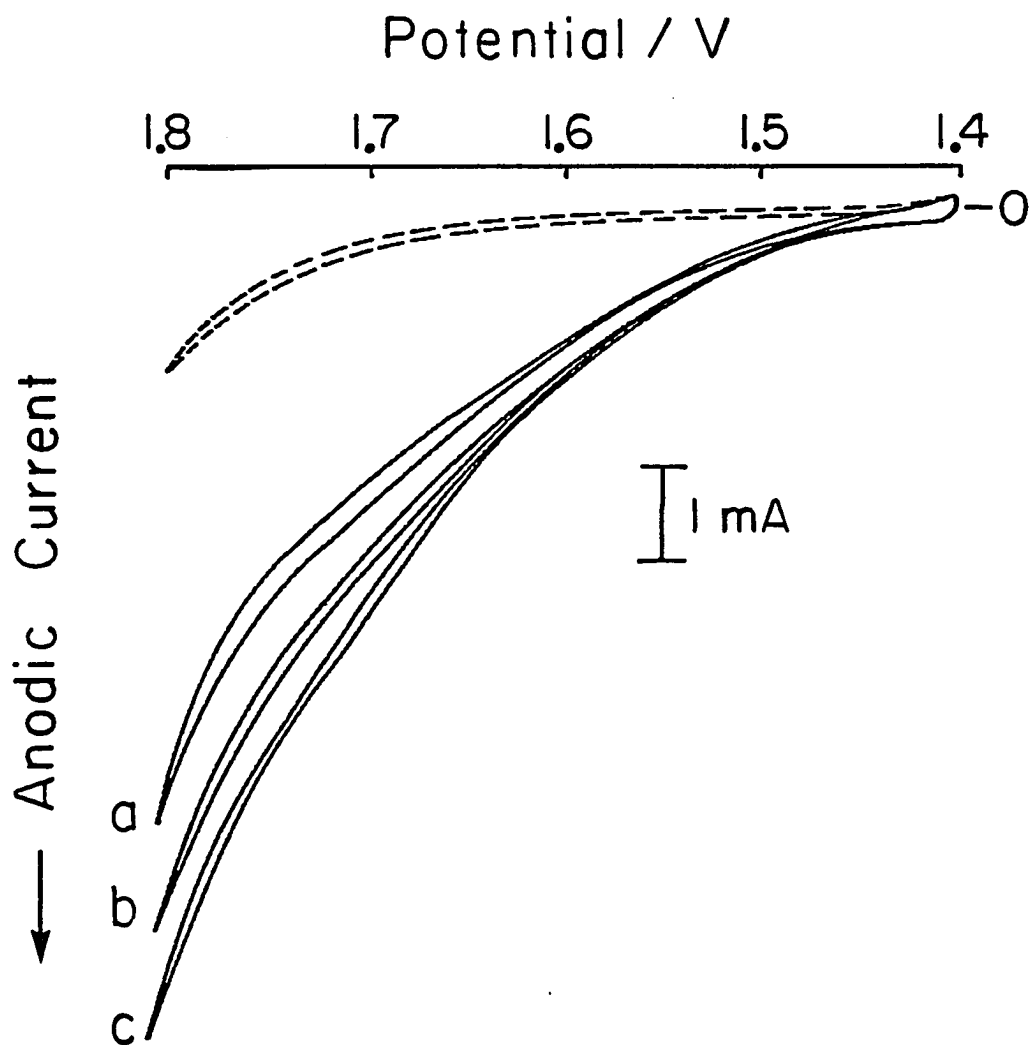
Figure 12. Voltammograms at Cl⁻-doped PbO_2 in 10 mM DMSO and 1.0 M $HClO_4$

Electrode deposition condition:
(— — —) 20 mM $Pb(NO_3)_2$, 0.1 M $HClO_4$,
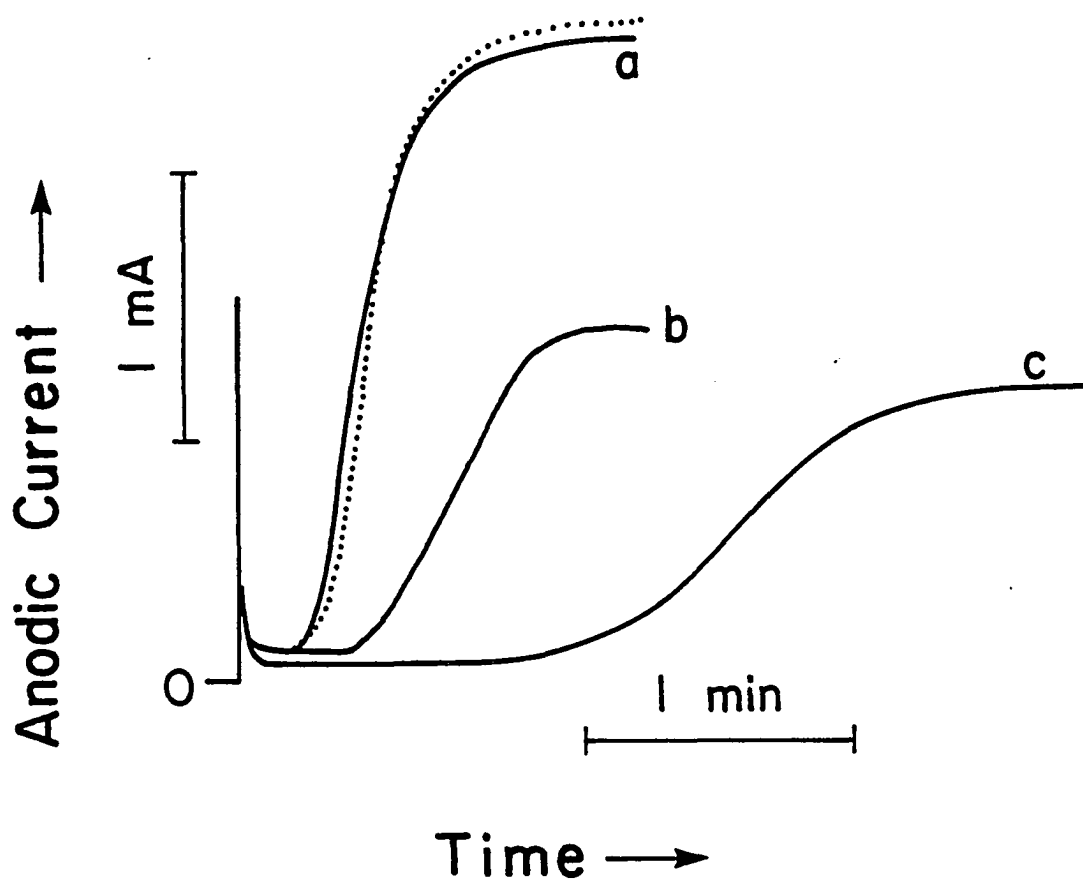(———) 20 mM $PbCl_2$, 0.1 M $HClO_4$

w (rev min⁻¹): (a) 400, (b) 900, and (c) 1600

Figure 13. Effect of co-existing Cl⁻ on constant-potential deposition of PbO_2 at Au RDE.

Solution: 10 mM $Pb(NO_3)_2$ and 1.0 M $HClO_4$

Conditions: 1.70 V, 400 rev min⁻¹,

Cl⁻ concentration (mM):
solid lines: (a) 0.01, (b) 0.21, (c) 0.41
dotted line: 0

V. FORMATION AND CHARACTERIZATION OF ULTRA-THIN FILMS OF PURE AND MODIFIED LEAD DIOXIDE ON SOLID ELECTRODES

A. Formation of Ultra-Thin Films of Lead Dioxide on Solid Electrodes by Consecutive Electrochemical Deposition and Stripping[1]

"Learning is an ornament in prosperity, a refuge in adversity."

-Aristotle

"The fewer the facts, the stronger the opinion."

-Arnold H. Glasow

---

[1]To be submitted to J. Electrochem. Soc.

Abstract

An ultra-thin (0.01 - 0.5 μm) film of lead oxide (PbO) remains on the surfaces of Au, Pt, Ti, and GC substrates after an electrodeposited lead dioxide (PbO_2) film (10 - 50 μm) is stripped electrochemically from these surfaces in acidic media. This PbO film is converted to an ultra-thin PbO_2 film by anodic recharging in a blank solution of electrolyte. As shown by electron microscopy, both ultra-thin films have microcracked surface structure that was not observed at the original PbO_2 films. Results from X-ray diffraction studies suggest that the PbO film has the same rutile crystal structure as the original, bulk beta-PbO_2. The ultra-thin PbO_2 films have similar anodic behavior as the normal, thicker PbO_2 films, as indicated by the voltammetric stripping of PbO_2 and the catalytic oxidation of DMSO at PbO_2 in the presence of Bi^{3+}.

The mechanism for the formation of the ultra-thin films also was studied. It is concluded that the films are formed by a reduction of the internal layers of thick PbO_2 films to undissolved PbO rather than Pb^{2+} due to the deficiency of H^+ at the substrate-oxide interface. This reaction takes place in the solid state and the resultant ultra-thin film is stabilized by interaction with the substrate. This mechanism is supported by the results of many experiments, including a study of the dependencies of the ultra-thin-film formation upon solution pH, thickness of the original PbO_2 film, and voltammetric stripping.

Introduction

Recently, it was discovered in our laboratory that a small amount of a Pb(II)-containing species could remain on the surface of a Au electrode

after cyclic electrodeposition and stripping of PbO_2 in an acidic solution of Pb^{2+} (1). The adsorbed Pb(II) species formed after one deposition/stripping cycle can serve as nuclei for the deposition of PbO_2 in the next cycle. Hence, both the deposition and stripping currents increase with cycle number (1).

The above phenomena are studied further in the present paper. It is expected that a stable, ultra-thin film of PbO_2 can be formed by anodic recharging of the Au electrode covered by the adsorbed Pb(II) species, which gives a new method to modify solid-electrode surface with metal oxides. Conditions to produce these ultra-thin PbO_2 films on varied solid electrodes are described. Many electrochemical and spectroscopic methods are used to characterize the electrode behavior, morphology, and structure of the resultant ultra-thin films, which are compared to those of the normal, thicker PbO_2 films.

Experimental

The apparatus and reagents used in this study were described earlier (1), except as noted below.

The titanium rotated disc electrode (RDE) (31.2 mm^2) was constructed from a Ti rod (Titanium Metals Corporation of America, Henderson, Nevada) mounted on a stainless steel shaft. The side wall of the electrode was sealed with PTFE hydrophobic tape. Lead dioxide was deposited on Ti after polishing the Ti surface consecutively with sand paper and 0.05-um Alumina to remove the non-conductive titanium surface oxide layer.

A model D500 X-ray diffraction (XRD) machine (Siemens, West Germany) was used.

Results and discussion

Formation of a Pb-containing film by the stripping of a PbO_2 film on Au   More evidence was obtained herein for the existence of an adsorbed Pb(II) species (probably PbO) on Au electrode surface after the cathodic dissolution of an electrodeposited PbO_2 film.

First, it was expected that the PbO film could be converted to a PbO_2 film by anodically recharging the PbO-covered Au electrode in a blank solution of the acid electrolyte. This expectation was varified by the current-time (i-t) curves obtained following a potential step to 1.7 V vs. SCE, as shown in Figure 1. Zero rotational velocity (w) was used to decrease the possible dissolution of lead species during the recharging (2). Clearly, a larger anodic current was observed at the PbO-covered Au in comparison with a freshly polished Au. This anodic signal is concluded to correspond to the conversion of Pb(II) to Pb(IV) at the Au surface. It will be proved later that this Pb(IV) species (probably PbO_2) also remains on the Au surface.

Second, the formation of PbO_2 from PbO also was demonstrated by the consecutive voltammograms shown in Figure 2. To increase the formation rate of the PbO film, a higher Pb^{2+} concentration and a lower acidity (0.1 M) were used for the data in this Figure than for that in Figure 8 of (1). The positive scan limit in Figure 2 was adjusted to keep the charge for PbO_2 deposition relatively constant in each scan. Both the anodic deposition and the cathodic stripping currents increased with cycle number from 1 to 3. The potential at which the initial deposition current appeared shifted toward negative values with increasing cycle

number. A prewave or shoulder in the anodic current region was observed to be developed from the 3rd scan at a potential (1.45 V) less positive than that for PbO_2 deposition at the PbO_2-covered Au electrode (1.5 V). This prewave is concluded to result in part from the oxidation of a strongly adsorbed Pb(II) species formed in the previous cycle (3). If the anodic limit potential was kept at ca. 1.65 V as in the 1st cycle, an anodic limiting plateau appeared, instead of the current peak. However, the shape of the i-E curves in the negative scans was not changed by changing in the anodic limit potential. The prewave disappeared in the negative scan and the i-E curves in the negative scans were virtually independent of the cycle number. Therefore, it is concluded that the oxidation product corresponding to the prewave is the same as that in the 1st and 2nd scans, i.e., PbO_2. The increase of the prewave indicates an increase in the amount of the adsorbed species and an increase in the nucleation rate of PbO_2 depositio with scan number.

Thickness and morphology of the film   The thickness of the adsorbed PbO or PbO_2 films was measured with SEM. The result was 0.01 - 0.5 μm, depending on the conditions of preparation, but not affected by the anodic recharging. Therefore, the PbO and PbO_2 films will be called "ultra-thin films." If the ultra-thin PbO and PbO_2 films were thick enough (> ca. 0.1 μm), they could be be seen by the naked eye. The ultra-thin film on Au electrodes looked slightly more reddish than the freshly polished Au substrate. The color of the film changed with the thickness and became slightly darker after anodic recharging. However, if the film was too thin (< ca. 0.1 μm), the surface was hardly

distinquishable with naked eye from a freshly polished Au.

The morphology of the ultra-thin films was observed also with SEM, as shown in Figure 3 in comparison to a normal PbO_2 film. A portion of the Au RDE was covered with Parafilm and the oxide film was deposited only on the uncovered side of the disc electrode. Figure 3A clearly shows that a film remains on the Au substrate after the stripping of PbO_2. The surface of this film had a microcracked structure which is totally different from that of the normal PbO_2 film as shown in Figure 3C. The cracks had an average width of about 0.5 μm. The shapes of the cracks differed from spot to spot and from sample to sample. In Figure 3B is another SEM picture from a different region of the same sample as given in Figure 3A. The microcracked structure is very similar to that of thermally prepared RuO_2/Ti, known as a "dimensionally stable anode (DSA)" and used extensively for chlorine production (4). The microcracks of the films were not due to dehydration during storage of the samples, because the normal PbO_2 film, also stored in the air, did not show any crack (see Figure 3C).

The morphology of the ultra-thin PbO was not changed by recharging. Hence, no recrystallization or phase-change takes place during recharging.

The surfaces of the normal PbO_2 films and the ultra-thin films shown in Figure 3 are much smoother than those shown in the literature (5). This is because the PbO_2 films used in this study were prepared under the optimal conditions determined in Chapter 2 for obtaining smooth and reflective surfaces. Figure 3C depicts how smooth the PbO_2 surface is at

the microscopic level. The resultant ultra-thin films have similar surface smoothness.

The ultra-thin PbO_2 films can be deposited also onto other substrates, e.g., Pt, GC, and Ti. The morphology of a ultra-thin PbO film on Ti is shown in Figure 4. Again, microcracks were observed. The surface of the film (Figure 4A) was not as flat as those in Figures 3A,B, but, it was in the same pattern as the original PbO_2 film on Ti (Figure 4B) that had a high roughness due to a high roughness of the Ti substrate.

Factors affecting the formation of the ultra-thin films   The thickness of the ultra-thin PbO films changed with the conditions of PbO_2 deposition and stripping. Studies in this respect can yield much information about the mechanism for the formation of the ultra-thin films.

It was observed that the amount of adsorbed PbO on Au depended on the solution pH for stripping and the thickness of the original PbO_2 film. The higher the pH, the easier was the formation of the ultra-thin PbO film. Generally, the thicker the original PbO_2 film, the thicker was the ultra-thin film. For very high acidity when generating ultra-thin PbO_2 film, the adsorbed PbO species was hardly observable by the naked eye.

The formation of PbO film also depended on the solution pH for PbO_2 deposition and the influence is the same as that of solution pH during stripping. The formation of PbO varied slightly with the rate of potential decrease for stripping. The slower the potential decrease from

1.7 to 0.3 V, the less PbO was formed and vice versa. However, if the scan rate was too high, e.g., a potential step from 1.7 V to 0.3 V, the entire PbO_2 film rapidly came off the Au surface, so no stable PbO film was formed.

It is concluded that any factor that increases the rate of PbO_2 deposition or decreases the rate of PbO_2 stripping favors the formation of ultra-thin PbO films. In addition, the ultra-thin PbO_2 film prepared by multiple potential cycles was not very adhesive to the substrate and could be easily wiped off. Thus, the following optimal conditions were obtained to deposit ultra-thin PbO films on Au: deposition of PbO_2 at 1.6 V (1.7 V for the first 10 sec) in 0.1 M $HClO_2$ containing 20 mM Pb^{2+} for 70 - 90 sec; followed by gradual potential decrease (ca. 0.2 V/s) to 0.6 V for stripping. The formation of PbO film was not affected by the existence of Pb^{2+} in the stripping solution, so the stripping step could be done in the same solution as deposition. Similar conditions, except for the values of deposition and stripping potentials, also hold for production of ultra-thin PbO films on other electrode materials.

Crystal structure and elemental determination of the ultra-thin film
Shown in Figure 5A are the XRD results for the Au substrate and three normal PbO_2 films of similar thickness. The diffraction patters for the normal PbO_2 films varied with the conditions of electrodeposition. The peaks were the widest for the PbO_2 sample prepared under the optimal conditions for a smooth and reflective deposit (Curve a). It is concluded that this PbO_2 sample has a smaller average crystalline size, due to an enhanced rate of deposition. As the rate of deposition was

increased from sample a to c, the sharpness of the diffraction peaks was increased. Clearly, the relative peak ratios also varied for the three pure PbO_2 samples, yet their catalytic activity did not change. Therefore, the preferred surface orientation of the crystal structure is not the key factor in the electrocatalysis of anodic O-transfer reactions.

In the region $2\theta = 20 - 40°$, the diffraction pattern for PbO_2 is totally different from that for the Au substrate, so this region can be used to compare the XRD results for the ultra-thin PbO film and the normal, thicker PbO_2 film, as shown in Figure 5B. Despite the observed noise, it is clear that the PbO layer has the same crystal structure as the normal PbO_2 film.

The existence of both lead and oxygen in the ultra-thin film was demonstrated with X-ray photoelectron spectroscopy and the film is concluded to be PbO.

Mechanism for the formation of the ultra-thin film   Based on the above results, the mechanism described below is proposed for the formation of the ultra-thin PbO film.

The cathodic stripping of PbO_2 can be written as

$$PbO_2(s) + 4H^+ + 2e \rightarrow Pb^{2+} + 2H_2O \qquad [1]$$
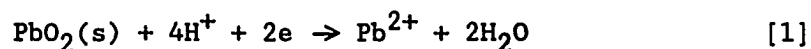
Since four protons are consumed for each formulae of PbO_2, the stripping normally occurs only at the oxide-solution interface and the stripping rate is dependent on the mass-transport of H^+ from solution to the electrode surface. This is consistent with our observation that the

stripping of a thick PbO_2 film proceeded layer-by-layer. As the PbO_2 film gradually becomes thinner during constant-potential stripping, the apparent color of the film changed in the following order: black → gray → brown → red → yellow → green, which is just the opposite to that observed during PbO_2 deposition. Thus, it is concluded that Equation 1 does not occur at the internal layers of the PbO_2 film before exposing to H^+ or H_2O. However, when the electrode potential is scanned to a value at which the internal PbO_2 layer is no longer thermodynamically stable, the following reduction reactions can occur at the substrate-oxide interface:

$$PbO_2(s) + 2H^+ + 2e \rightarrow PbO(s) + H_2O$$

or

$$PbO_2(s) + H_2O + 2e \rightarrow PbO(s) + 2OH^- \qquad [2]$$
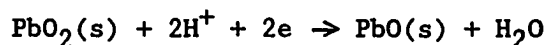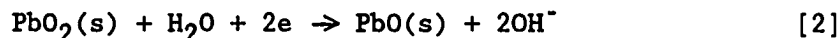
which produces a PbO layer stabilized by and attached to the substrate. The H^+ or H_2O used in this reaction exists inside the oxide film as trapped during the deposition of PbO_2. Since the process [2] can be regarded as an electrochemical reaction in the solid state, the crystal structure of the resultant PbO film is the same as that of the orginal PbO_2 film.

This mechanism explains the dependencies of the formation of ultra-thin films on the experimental conditions. Naturally, the thicker the original PbO_2 film and the lower the solution acidity, i.e., the slower the Reaction 1, the greater is the chance for Reaction 2 to occur and the greater is the amount of the resultant adsorbed PbO. Since the PbO_2 film

deposited from solutions with higher H^+ concentration has higher H^+ content inside the oxide, the chance for Reaction 2 to occur is smaller for PbO_2 films from higher acidity than for those from lower acidity. The microcracks at the ultra-thin films are formed by contraction of the internal PbO_2 layer during the reduction in the solid phase under dehydrated conditions.

The mechanism also is supported by the following observation: When a piece of gold sheet was used as the substrate, the PbO_2-covered Au sheet covered with a thin layer of solution was subjected first to a reductive potential for PbO_2 stripping with most portion of the sheet lifted above the solution before the entire sheet was immersed in the solution. It was easier to form the ultra-thin PbO film at the portion of the Au sheet that had been lifted in the air than the portion that had not been. It is concluded that this pretreatment procedure forces the reduction of PbO_2 as Equation 2 at the Au-PbO_2 interface under difficiency of H^+.

Cathodic stripping voltammetry of PbO_2 The above mechanism was proved further by the stripping voltammograms in Figures 6A,B as a function of PbO_2 thickness and solution pH. When the PbO_2 film was thin, a single stripping peak appeared as Peak I in Figure 6A. As the thickness of the PbO_2 increased, the stripping peak became more broadened. Peak I became a plateau and a second peak (II) appeared when the PbO_2 was even thicker. Peak I did not change with variation of rotational velocity as much as Peak II, indicating that the initial rate of PbO_2 stripping is a surface controlled process and independent of the mass-transport of H^+. However, for a thick layer of PbO_2, the stripping

rate eventually became controlled by the mass-transport of H^+ due to the depletion of H^+ by reduction of the outer PbO_2 layers. Observable PbO species were formed only if the deposition time was equal or greater than 40 sec (Curve d) which corresponds to a transition point in the i-E curves in Figure 6A. It is believed that this transition represents the reduction of the internal PbO_2 layer as Reaction [2].

As shown in Figure 6B, the stripping peak shifted to less positive and broadened as the solution pH was increased and the thickness of the film was kept constant. As a result, it was easier to form the adsorbed PbO film with increased pH.

It is noticed in Figure 6A that the stripping peak (III) for Au surface oxide is suppressed by the stripping peak of PbO_2, as the peak potential of III shifted to the negative values with an increased thickness of PbO_2. It is concluded from this observation that the reductions of Au surface oxide and PbO_2 are independent of each other. Further experiments show that ultra-thin PbO films can be formed at stripping potential values equal, larger, or smaller than the value of reduction potential for Au surface oxide. Therefore, the reduction of Au surface oxide is not involved in the formation of the ultra-thin PbO film.

Chemical properties of the ultra-thin film   The ultra-thin PbO film does not dissolve in acidic solution, while the chemical PbO does as follows:

$$PbO(s) + 2H^+ \rightarrow Pb^{2+} + H_2O \qquad\qquad [3]$$
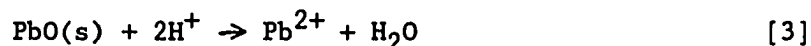
Both PbO and PbO_2 ultra-thin films can be removed from the Au surface by electrochemical H_2 evolution and by chemical stripping in a 1:1 mixture of hydrogen peroxide and acetic acid. The same is true for the normal, thicker PbO_2 deposits.

Voltammetric reduction of the ultra-thin PbO_2 film   The ultra-thin PbO_2 film formed after recharging a PbO film-covered Au electrode was characterized by linear sweep voltammetry in a blank solution of 1.0 M $HClO_4$, as shown in Figure 7. A scan rate (80 mV s^{-1}) higher than that for Figure 2 was used to increase the height of the stripping peak. A distinct stripping peak (a) was observed prior to the that for surface Au oxide (b). The peak potential of Peak a (1.24 V) is the same as that observed for stripping of normal PbO_2 film (1). Hence, Peak a is concluded to correspond to the reduction of ultra-thin PbO_2 film. It also is concluded that the ultra-thin PbO_2 has the same reduction property as the normal PbO_2 film.

Following the first scan, consecutive cyclic voltammograms were recorded in the same solution as shown also in Figure 7. The i-E curve in the positive scan did not have any anodic wave between 0.7 - 1.0 V, so it is concluded that no metallic Pb is produced via underpotential deposition during the negative scan. Some anodic current appeared in the 1.5 - 1.7 V range, corresponding to the conversion (recharging) of PbO to PbO_2. However, the height of the anodic current in Figure 7 is much lower than those in Figure 2. The stripping Peak a decreased with cycle number dramatically. After ten cycles, the i-E curve becomes virtually the same as the i-E residue at Au. It is concluded that some PbO_2 are

dissolved in each negative scan and the whole ultra-thin film is lost after several cycles of recharging and stripping. The loss is concluded to be partially caused by the dissolution of Au substrate in the surface oxide formation/stripping process (2,6).

Electrode behavior of the ultra-thin PbO$_2$ film   It has been shown that dimethyl sulfoxide (DMSO) is readily oxidized at a PbO$_2$ electrode with Bi^{3+} co-existing in the solution, due to the adsorption of Bi^{3+} onto the PbO$_2$ surface (7). Using this experimental procedure, the properties of the ultra-thin PbO$_2$ film were compared to those of the normal PbO$_2$ film. As shown by the voltammograms in Figure 8A, a well-defined i-E plateau appeared at an ultra-thin PbO$_2$ film-covered Au electrode with a small amount of Bi^{3+} co-existing in the solution. The shape of the i-E curve and the value of half-wave potential are very similar to those obtained at the normal PbO$_2$ film electrodes (7). The height of the current plateau increased with increased $w^{1/2}$, as shown in Figure 8B, but not as linearly as those observed at the normal PbO$_2$ film probably because Au surface is covered only partially by the ultra-thin PbO$_2$ film due to the microcracked surface structure. The current plateau also increased with increased DMSO concentration, but did not change with variation of Bi^{3+} concentration in a large range (0.01 - 1 mM). The voltammograms also had similar dependence on scan rate as those at the normal PbO$_2$ film electrode. Similar chronoamperograms at constant potential also were obtained at these two kinds of PbO$_2$ electrodes. Therefore, it is concluded that the ultra-thin PbO$_2$ film has very similar electrochemical properties as the normal PbO$_2$ film. It is also clear

that the catalytic oxidation of DMSO at the Bi^{3+}-adsorbed PbO_2 electrode is independent of the thickness of the PbO_2 film.

The above results were obtained at a Au substrate. Work also was done at ultra-thin PbO_2 film-covered Pt, Ti, and GC electrodes following the same procedures. Similar i-E curves for oxidation of DMSO were obtained at these substrates, except that the background current shew the characteristics of the substrate, obviously because some portion of the substrate is exposed to the solution through the microcracks.

Stability of the ultra-thin PbO_2 film   The i-E curves in Figure 8A were very reproducible. It also was observed that the current under constant potenial for oxidation of 10 mM DMSO with 0.1 mM Bi^{3+} did not change for more than 2 hours at an ultra-thin PbO_2 film-covered Au RDE, which is similar to what was observed at the normal PbO_2 film-covered electrode. However, the reactivity of the ultra-thin PbO_2 film-covered Au electrode was lost if the electrode had been subjected to a treatment as shown in Figure 5, obviously due to the removal of the ultra-thin PbO_2 film by potential cycles in 1.7 - 1.0 V region. The same was true if the electrode had been treated with 1:1 mixture of acetic acid and hydrogen peroxide.

The chemical and electrochemical properties of the ultra-thin PbO_2 film was maintained after the electrolysis, but, the film became brown, powder-like and could be wiped off easily with tissues, indicating poor adherence to the Au substrate. The adherence of the ultra-thin film to the substrate surface depended on the roughness of the substrate. The rougher the substrate surface, the more adherent was the film.

References

1. Chang, H.; Johnson, D. C. <u>J. Electrochem. Soc.</u> 1989, 136, 17; Chapter II-A, this Dissertation.

2. Chang, H.; Johnson, D. C. <u>J. Electrochem. Soc.</u> 1989, 136, 23; Chapter II-B, this Dissertation.

3. Bard, A. J.; Faulkner, L. R. "Electrochemical Methods-Fundamentals and Applications"; John Wiley & Sons: New York, 1980; p. 525

4. Novak, D. M.; Tilak, B. V.; Conway, B. E. In "Modern Aspects of Electrochemistry"; Bockris, J. O'M.; Conway, B. E.; White, R. E., Eds.; Plenum Press: New York, 1982; No. 14.

5. (a) Yeo, I.-H.; Johnson, D. C. <u>J. Electrochem. Soc.</u> 1987, <u>128</u>, 1973. (b) Yeo, I.-H. <u>Ph.D. Dissertation</u>, Iowa State University, Ames, Iowa, 1987.

6. Cadle, S. H.; Bruckenstein, S. <u>Anal. Chem.</u> 1974, 46, 16.

7. (a) Chang, H.; Johnson, D. C., in preparation; Chapter III-A, this Dissertation. (b) Chang, H.; Johnson, D. C., in preparation; Chapter III-B, this Dissertation.
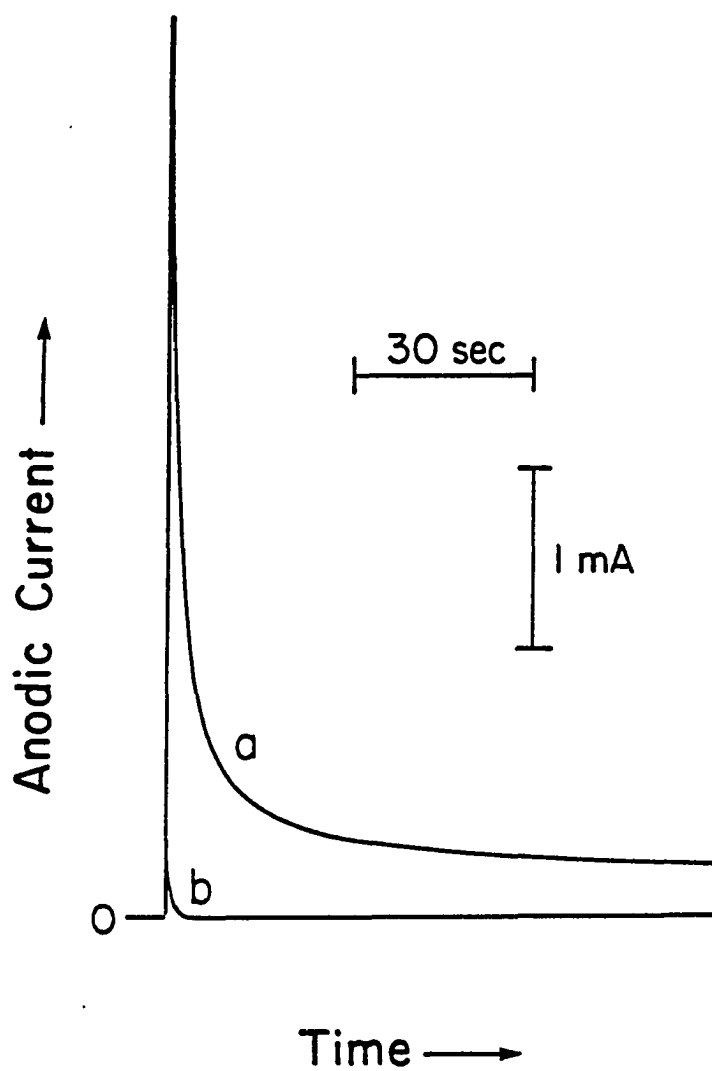
Figure 1. Chronoamperometric response in 1.0 M $HClO_4$

Conditions: E - 1.7 V, 0 rev min^{-1}

Electrode: (a) PbO film covered Au,
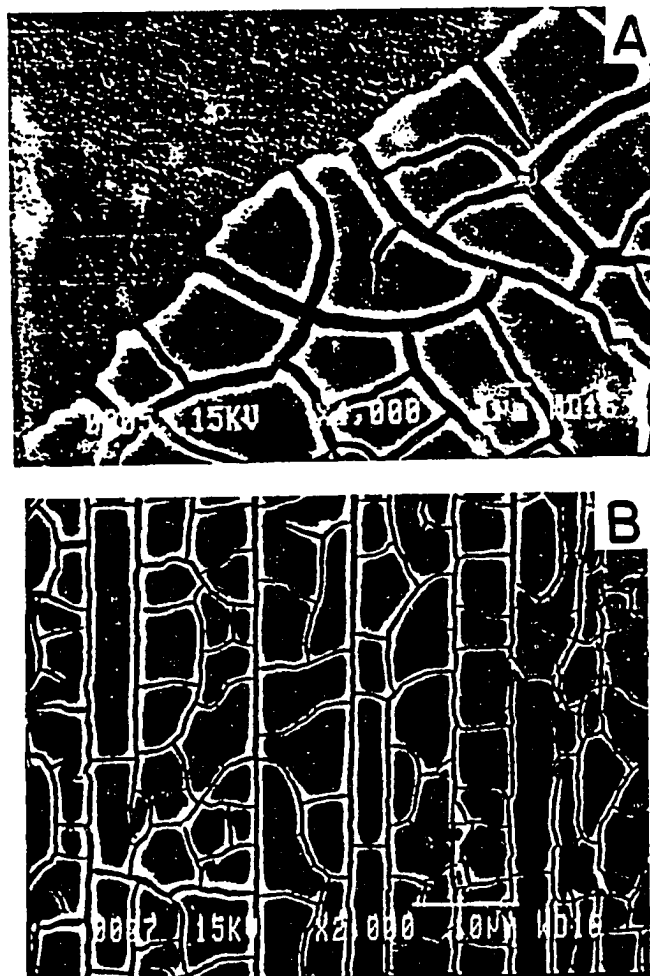(b) freshly polished Au
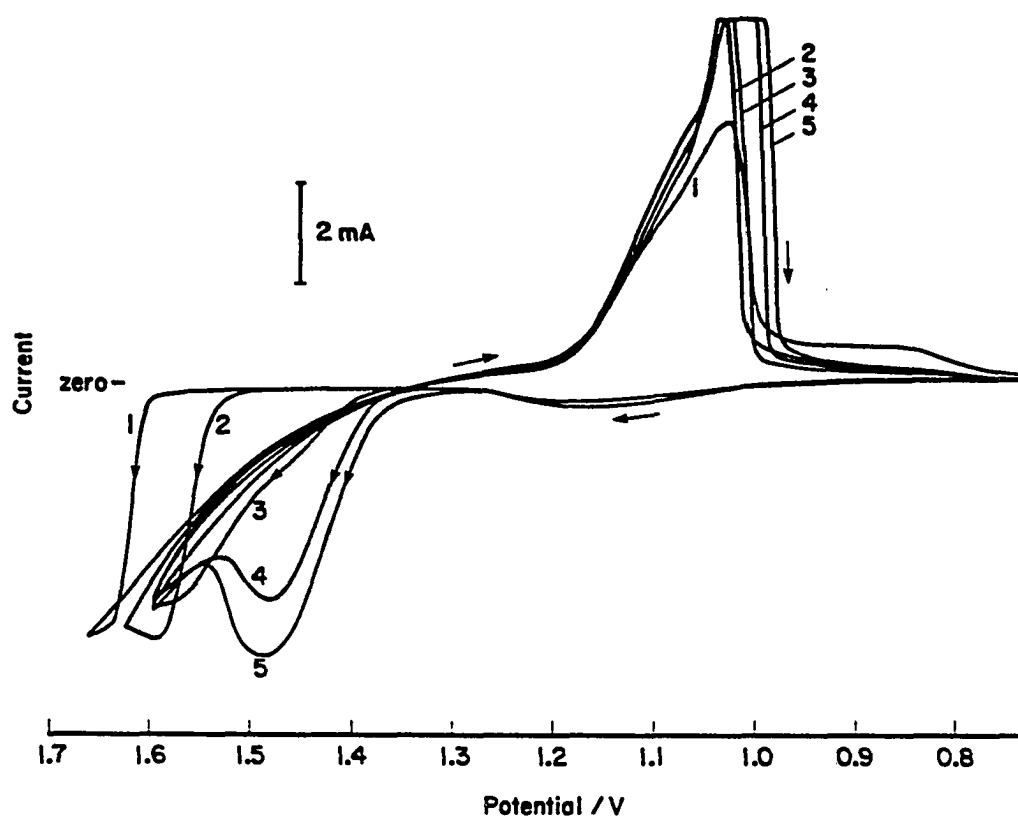
Figure 2. Consecutive i-E curves at freshly polished Au

Solution: 20 mM Pb^{2+}, 0.1 M $HClO_4$

Conditions: 20 mV s^{-1}, 400 rev min^{-1}

Cycle numbers shown; scans originate at 0.7 V

Figures 3A,B. Electron micrographs of PbO_2 films at Au

Solution for electrodeposition: 20 mM Pb^{2+}, 0.1 M $HClO_4$

Pictures: (A) ultra-thin PbO film at half covered Au,
(B) the same as (A) at a different spot
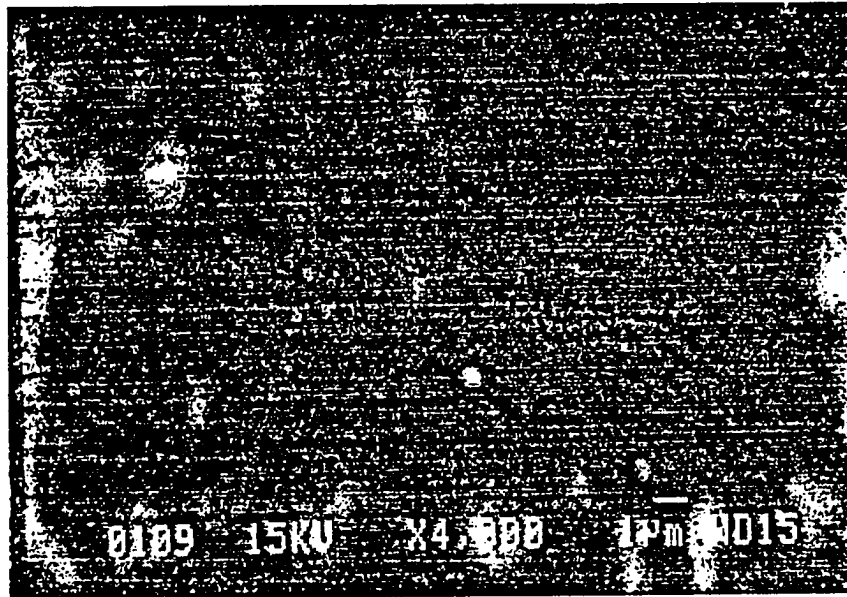
Figure 3C. Electron micrograph of normal PbO_2 film

Deposition conditions: see context
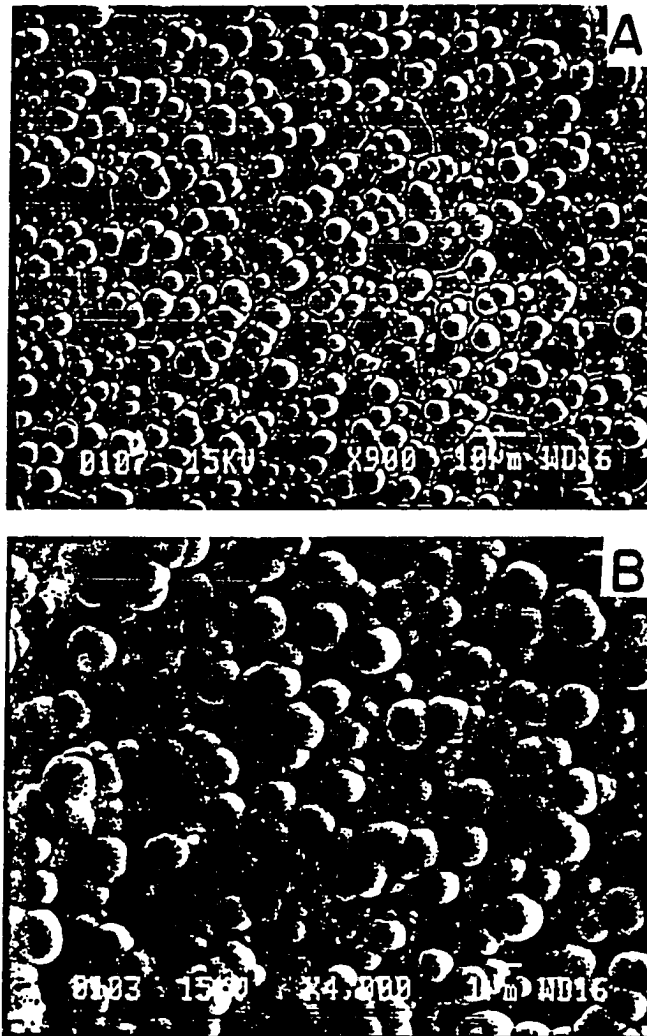
Figure 4.   Electron micrographs of PbO_2 films at Ti

Deposition solution: the same as give in Figure 3

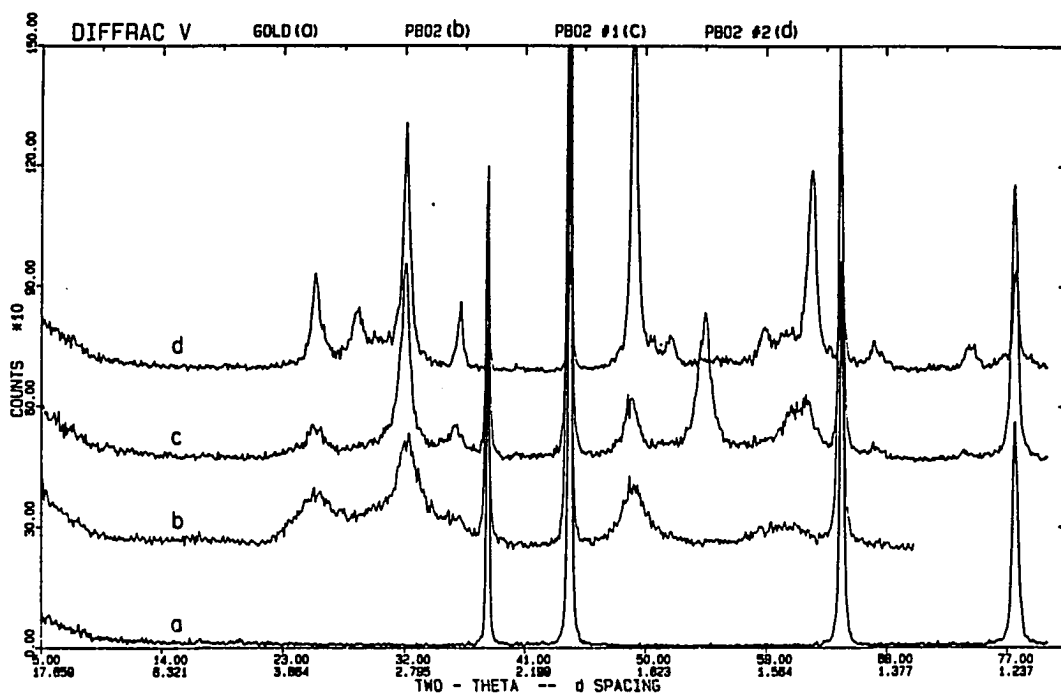Pictures: (A) ultra-thin PbO film
            (B) normal PbO_2 film.

Figure 5A. X-ray diffraction patterns

Curves: (a) Au, (b-d) normal PbO_2 film on Au

Deposition conditions:
    (b) 20 mM Pb^{2+}, 0.1 M $HClO_4$,
        E - 1.6 (10 sec) → 1.55 V (5 min), stirred
    (c) Solution: the same as given in (b), E - 1.5 V
        (10 sec)₂→ 1.4 V (10 min), not stirred
    (d) 10 mM Pb^{2+}, 1.0 M $HClO_4$, e - 1.6 V for 1.5
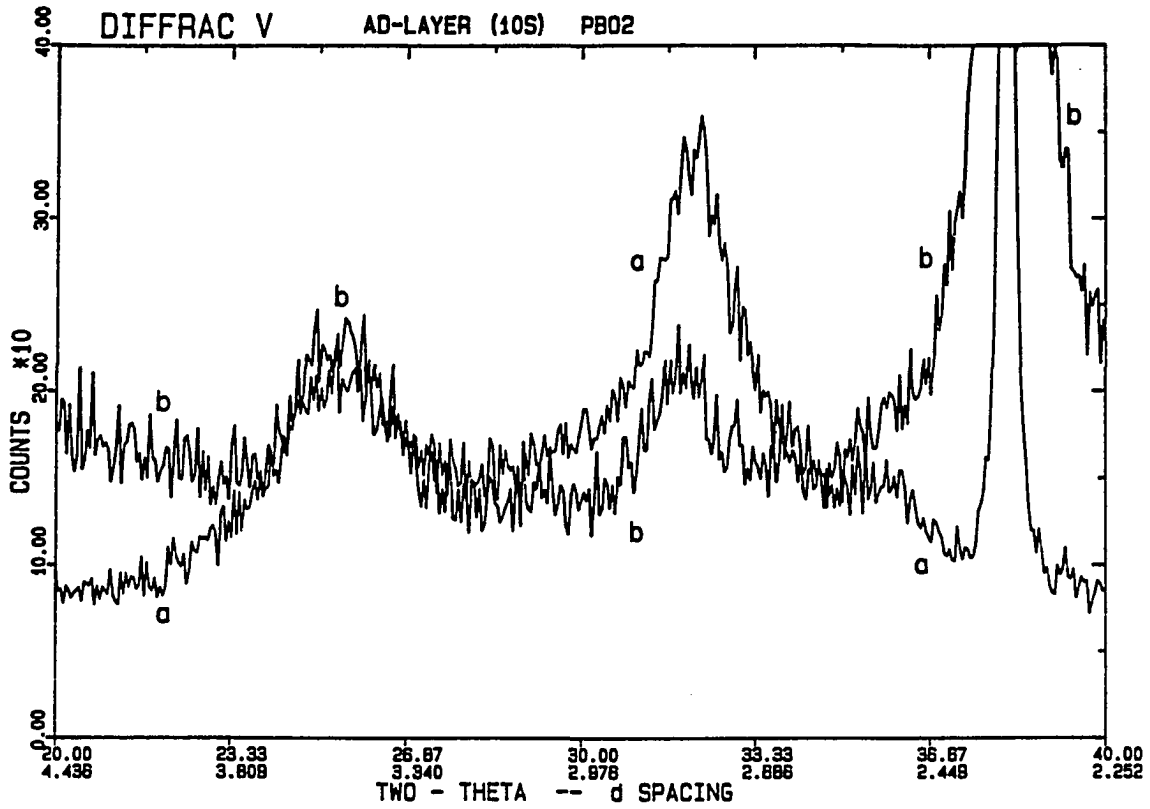   hour, not stirred

Figure 5B. X-ray diffraction patterns

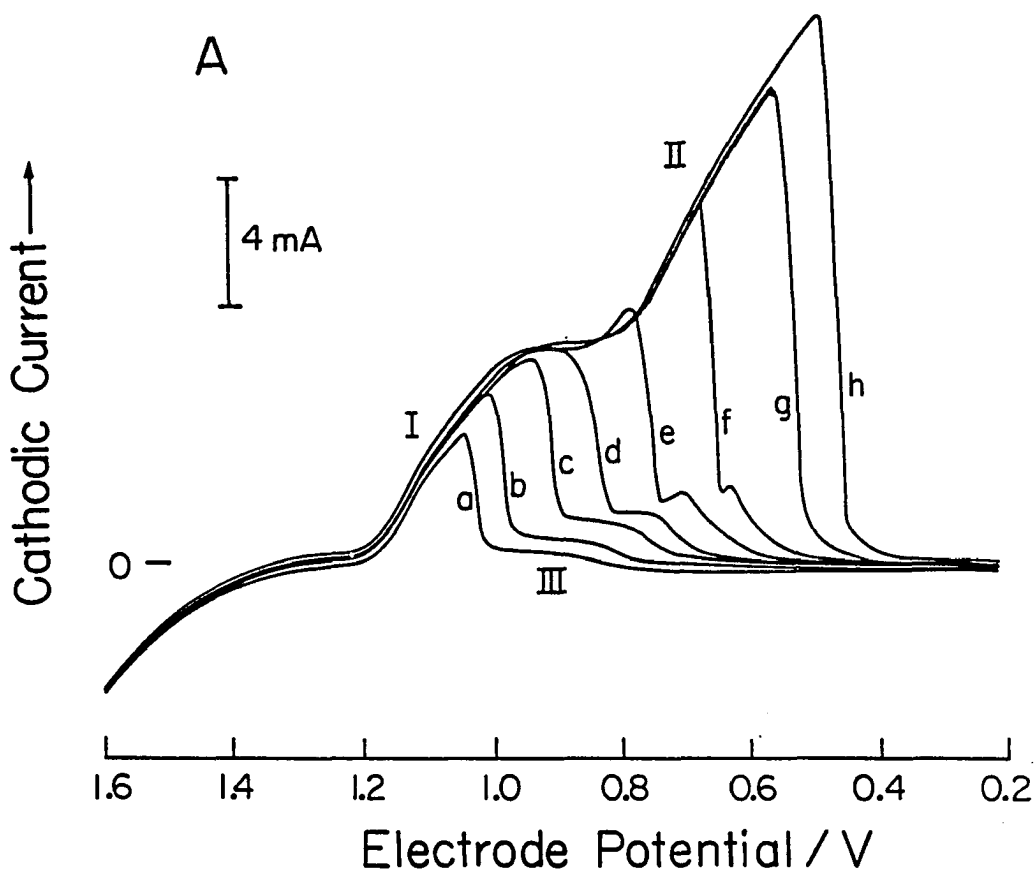Curves: (a) normal PbO_2 film on Au,
         (b) ultra-thin PbO film on Au

Figure 6A. Effect of film thickness on the stripping voltammograms
of PbO_2 on Au RDE

Conditions: 20 mM Pb^{2+}, 0.1 M $HClO_4$, 20 mV s^{-1},
400 rev min^{-1}

Deposition time at 1.6 V (sec): (a) 5, (b) 10, (c) 20,
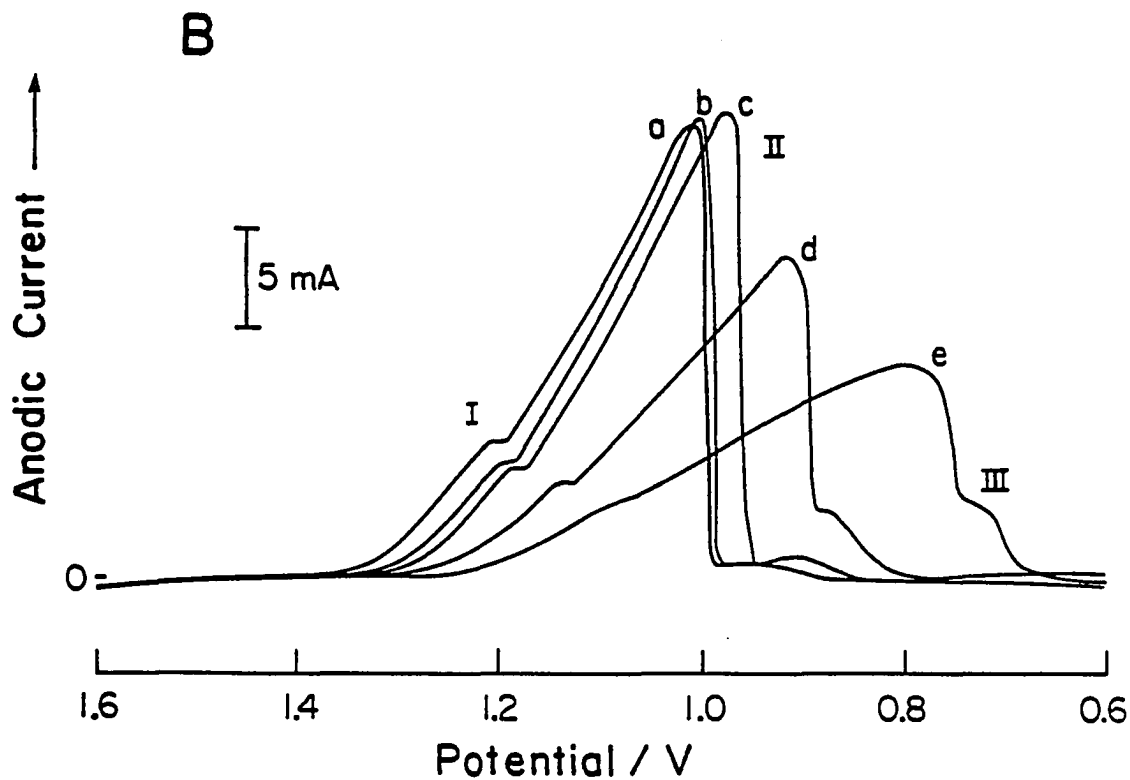(d) 30, (e) 40, (f) 60, (g) 90, (h) 110

Au RDE polished each time

Figure 6B. Effect of solution pH on the stripping voltammograms of PbO_2 on Au

Deposition conditions: 1.6 V, 20 mM Pb^{2+},
0.1 M $HClO_4$, 400 rev min^{-1}

Stripping conditions: 20 mV s^{-1}, 400 rev min^{-1},
x M $HClO_4$.

x: (a) 1.7, (b) 1.4, (c) 0.8, (d) 0.4
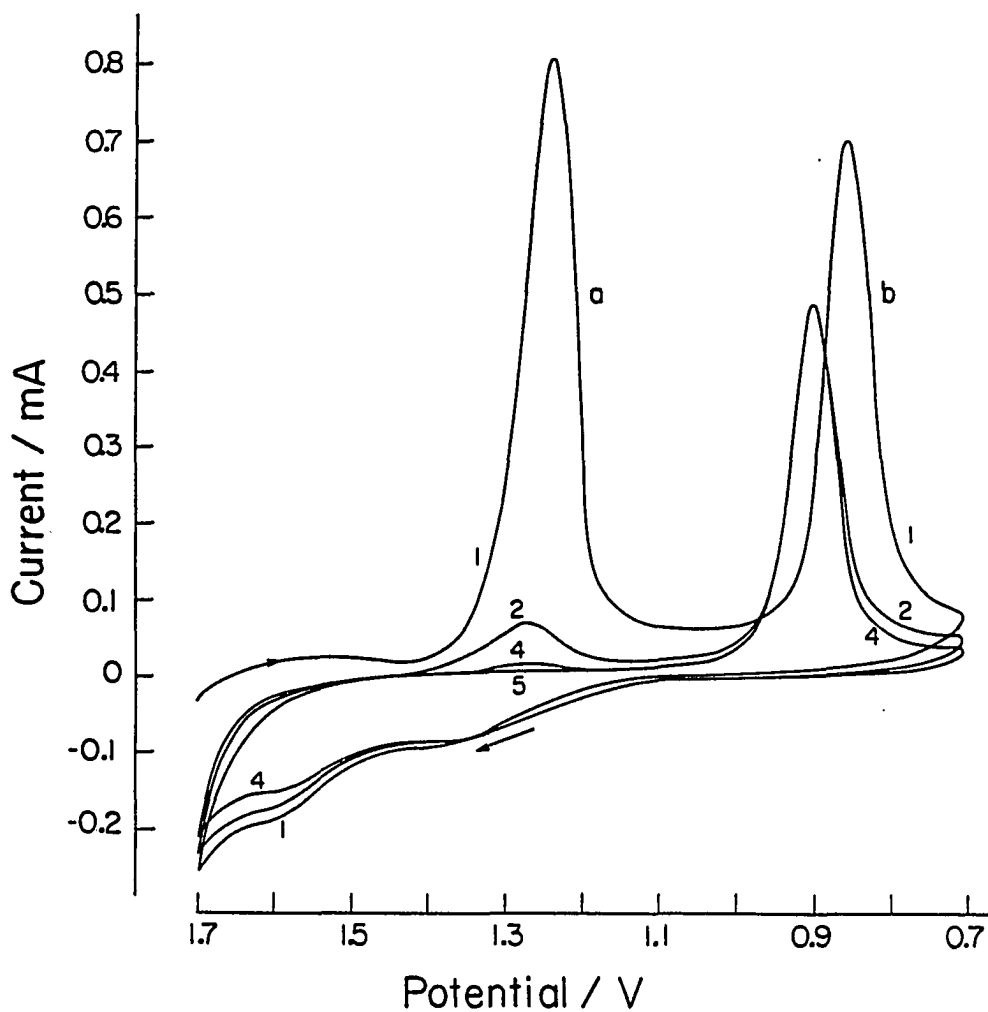
Figure 7. Cyclic voltammograms in 1.0 M $HClO_4$

Conditions: 80 mV s^{-1}, 0 rev min^{-1}

Electrode: ultra-thin PbO film covered Au RDE
            Anodized at 1.7 V for 1.5 min before the
            recording of the voltammograms

Peaks: (a) stripping peak of PbO_2,
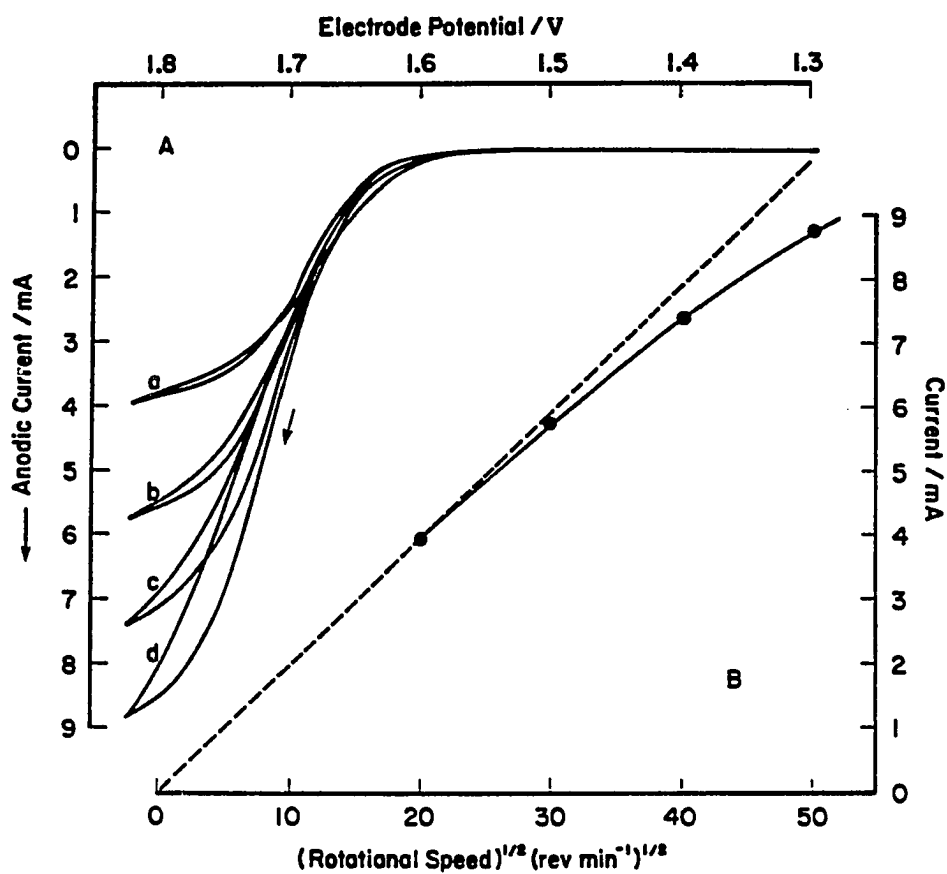   (b) stripping peak of surface Au oxide

Figure 8. Voltammetric responses of 10 mM DMSO at ultra-thin PbO_2 film covered Au RDE

(A) Effect of w (rev min^{-1}): (a) 400, (b) 900, (c) 1600, (d) 2500

Conditions: 0.1 mM Bi^{3+}, 20 mV s^{-1}

(B) Plot of the current at 1.825 V in (A) vs. $w^{1/2}$

B. Modification of Solid-Electrode Surfaces by Ultra-Thin Film

of Bismuth-Doped Lead Dioxide[1]

"The ultimate criterion leading to the commercialization
of an organic electrochemical process is that it
provides the desired product at a lower overall cost
(including costs of disposing properly of environmental
pollutants) than any competitive process. It's that
crass. Novelty, elegance, publishability and
patentability are irrelevant factors."
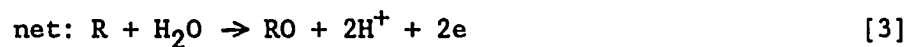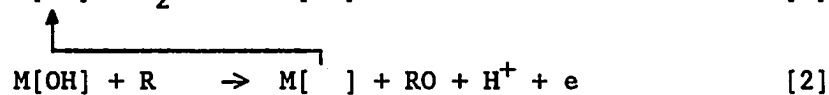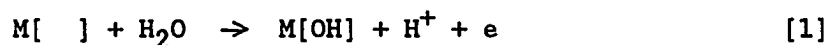
-M. M. Baizer,
Pure Appl. Chem. 1986, 58, 889.

---

[1]To be submitted to J. Electrochem. Soc.

Abstract

An ultra-thin (0.01 - 0.5 μm) film of Bi-doped PbO_2 (Bi-PbO_2) remains at the surfaces of Au, Pt, Ti, and GC electrodes after the cathodic dissolution of a normal, thick Bi-PbO_2 film (10 - 50 μm) followed by anodic recharging. The resultant solid electrodes have higher electrochemical stability and electrocatalytic activity for anodic oxygen-transfer reactions than the normal, thick Bi-PbO_2 film electrodes prepared from the same solution. This is concluded to result because the Bi/Pb atomic ratio at the surface of the ultra-thin film is higher than that of the normal Bi-PbO_2 films, as determined by X-ray photoelectron spectrscopy. The procedures to form the ultra-thin Bi-PbO_2 films represent a new method for chemical mofication of solid-electrode surfaces with metal oxides. The ultra-thin Bi-PbO_2 film was also determined to have a microcracked surface structure as was described in the previous paper for the ultra-thin pure PbO_2 films.

Introduction

Recently, anodic oxygen-transfer (O-t) reactions and their catalysis at metal oxide electrodes have been the subject of study in this laboratory (1-4). It has been shown that a variety of inorganic and organic oxidation reactions involving O-t from H_2O to the oxidation products occur through catalytic participation of surface oxide as illustrated below (1-3):

$$M[\ ] + H_2O \rightarrow M[OH] + H^+ + e \qquad [1]$$

$$M[OH] + R \rightarrow M[\ ] + RO + H^+ + e \qquad [2]$$

$$\text{net: } R + H_2O \rightarrow RO + 2H^+ + 2e \qquad [3]$$

where M is the metal, M[OH] represents the surface hydroxyl or semi-stable surface oxygen, R is the reactant (O-acceptor), and RO is the oxidation product. The efficiency of O-t reactions can be enhanced greatly through selective electrocatalysis at the chemically modified metal oxide electrodes, e.g., Bi-doped PbO_2 (Bi-PbO_2) (2-3).

Conventional Bi-PbO_2 films are prepared by electrochemical co-deposition on Au or Pt substrate from a mixture solution of Pb^{2+} and Bi^{3+}. The resultant Bi-PbO_2 films have a thickness of ca. 10 - 50 μm. It was discovered that ultra-thin films of PbO or PbO_2 were formed on the surfaces of solid electrodes after electrolytic stripping of bulk PbO_2 films (4a,5). It is then interesting to see whether ultra-thin Bi-doped PbO or Bi-doped PbO_2 films can be obtained following the cathodic dissolution of the normal Bi-PbO_2 films. If the answer is "yes," the catalytic reactivity and other properties of the ultra-thin Bi-PbO_2 films are studied in comparison with those of the normal Bi-PbO_2 films and the procedure to produce the ultra-thin Bi-PbO_2 films will become a new method to modify solid-electrode surfaces with modified metal oxides.

Experimental

Apparatus for electrochemical experiments were described in (4a). The X-ray photoelectron spectrometer (XPS) and scanning electron microscope (SEM) were described in (4c).

Bismuth(III)/lead(II) concentration ratio in the solution is represented by $[Bi^{3+}]/[Pb^{2+}]$, as $[Pb^{2+}] = 10$ mM.

Results and discussion

Formation of ultra-thin Bi-PbO film   As shown in Figure 1, the induction time for constant-potential deposition of Bi-PbO_2 at a Au RDE in a solution containing Bi^{3+} and Pb^{2+} decreased with the number of consecutive deposition/stripping cycles. This is concluded to indicate the existence and accumulation of an adsorbed oxide species (probably Bi-containing PbO, indicated here as Bi-PbO) on the Au surface after each deposition/stripping cycle. After the 3rd cycle, the coverage of the adsorbed oxide on Au was sufficiently large so that the induction time became virtually zero (Curve 3 in Figure 1).

A similar conclusion can be obtained from inspection of the consecutive voltammograms in Figure 2. Both the anodic deposition current and the cathodic stripping peak increased with cycle number from 1 to 3, indicating the effect of previous cycle on the i-E curves. An anodic prewave for conversion (recharging) of the adsorbed Bi-PbO to Bi-PbO_2 was observed at ca. 1.6 V for the 3rd and later positive scans. However, the current in these scans at the negative direction followed the same trace as that of the 2nd scan, which gives a reproducible i-E plateau with half-wave potential about 1.65 V. This is because the i-E

curve is no longer sensitive to the previous cycle when the electrode already is covered by a film of the oxide at constant thickness. The increase of the prewave with cycle number from 3 to 4 indicates the accumulation of the adsorbed Bi-PbO species. The anodic potential limit was lowered from 1.8 to 1.7 V for the 4th and 5th scans in order to obtain the stripping peaks for the Bi-PbO$_2$ converted from the adsorbed Bi-PbO. For the 2nd and 3rd scans, the i-E curves clearly had two stripping peaks, as shown in Figure 2. However, only one peak appeared in the 4th and 5th scans whose peak potential is the same as that of the first peak in the 2nd and 3rd scans.

Voltammetry at ultra-thin Bi-PbO$_2$ film electrode   The existence of a Bi-PbO$_2$ film converted from a Bi-PbO film is further proved by the observance of a recharging current when Bi-PbO was subjected to a positive potential in a blank solution of electrolyte and a consequent voltammetric stripping peak. The latter is shown in Figure 3. The anodic recharging current for Bi-PbO (not presented) was smaller than that for PbO (see Figure 1 in the previous paper), probably because the Bi(III) species in the Bi-PbO does not contribute to the anodic process. Two voltammetric stripping peaks appeared in Figure 3. Peak a corresponds to the stripping of Bi-PbO$_2$ converted from Bi-PbO and Peak b corresponds to the stripping of surface gold oxide. The stripping peak potential for Peak a (1.05 V) in Figure 3 is about 200 mV less positive than that for pure PbO$_2$ (1.25 V, see Figure 5 in the previous paper), due to an increased stability of the Bi-doped PbO$_2$. This is consistent with the result obtained at the normal PbO$_2$ and Bi-PbO$_2$ film-covered

electrodes (4c).

Consecutive voltammograms were recorded following the first potential scan, as shown in Figure 3. Peak a disappeared in the 2nd and following cycles. However, Peak b did not retreat to the same level as the stripping peak at the freshly polished Au after ten cycles. This is also true in the anodic region (1.5 - 1.7 V), as Wave c persisted for many cycles. It is concluded that there is always a thin film of lead oxide remaining on the surface after these potential cycles. This conclusion was supported further by results obtained in the testing of catalytic activities of the electrode, as discussed in a later section.

Thickness, morphology, and formation mechanism of the ultra-thin Bi-PbO$_2$ film   The visual appearance of the adsorbed Bi-PbO films on Au was similar to that of the PbO films. The film looked slightly darker after the recharging treatment. The thickness as well as the apparent color of the Bi-PbO films depended on the conditions of preparation, e.g., solution pH and thickness of the original oxide film, in the same way as that of the PbO (5). It was easier to form the adsorbed Bi-PbO films with lower Bi^{3+}/Pb^{2+} concentration ratios. This is probably because the higher the Bi^{3+} concentration, the more difficult is the deposition of Bi-PbO$_2$ and the more stable is the resultant metal oxide (4c).

The thickness and morphology of the Bi-PbO films at Au is visualized by the SEM micrograph in Figure 4. Figure 4A, obtained at a partially covered Au surface, clearly shows a Bi-PbO$_2$ film with a thickness of about 0.5 m. The thickness changed with variation of the deposition conditions, from 0.01 to 0.5 m. Therefore, these films are called

"ultra-thin" Bi-doped PbO and Bi-doped PbO_2 films.

Microcracked surface structure also was observed at the ultra-thin Bi-PbO and Bi-PbO_2 films, which is similar to that of the ultra-thin PbO_2 film except that the number of cracks per unit area is higher for the mixed oxide films. Thus, the surface area of Bi-PbO_2 film is expected to be higher than that of the normal oxide film. The surface roughness at the non-cracked portion of the Bi-PbO films is higher than that observed at the ultra-thin PbO films (5), which corresponds to the higher roughness of the original, normal Bi-PbO_2 film than that of the normal PbO_2 film (4a,5). The morphology of the ultra-thin Bi-PbO_2 films did not change much with $[Bi^{3+}]/[Pb^{2+}]$ in the deposition solution.

Ultra-thin Bi-PbO films also can be formed at Pt, GC, and Ti substrates, which indicates that the formation of the ultra-thin films is not specific to the substrate materials. The SEM micrograph of an ultra-thin Bi-PbO_2 film on Ti is shown in Figure 5A as compared to that of a normal Bi-PbO_2 film on Ti in Figure 5B. Again, microcracks were observed in the ultra-thin film. However, the overall morphology of the ultra-thin film is different from that in Figures 4A,B, but it follows the same pattern as the original normal oxide film on Ti.

It is apparent from the above that ultra-thin pure PbO_2 and Bi-doped PbO_2 films are formed very much in the same way and they have many similar electrochemical properties. Therefore, it is concluded that they are formed by the same mechanism as proposed and studied in Chapter V-A.

Catalytic activities of the ultra-thin Bi-PbO$_2$ film   The cyclic

voltammetric response of dimethyl sulfoxide (DMSO) at ultra-thin Bi-PbO$_2$

film-covered Au RDE is shown in Figures 6 and 7 as a function of

rotational velocity (w) and DMSO concentration, respectively. An anodic

plateau was obtained which was not observed for DMSO at the normal Bi-

PbO$_2$ film-covered Au (4c). Since no Bi^{3+} was added to the solution, the

anodic plateau in Figure 6 proves the existence of bismuth ion in the

ultra-thin films. The height of the current plateau increased linearly

with increased w$^{1/2}$ and DMSO concentration. This is evidence for a

reaction under mass-transport control.

The residual current at the ultra-thin Bi-PbO$_2$ film electrode shown

in Figure 6 is larger than that obtained at the ultra-thin PbO$_2$ film

electrodes (5). The residual current at the ultra-thin Bi-PbO$_2$ film

changed with variation of scan rate as shown in Figure 8, which is

similar to that obtained at the normal Bi-PbO$_2$ film electrode.

Oscillation of the residual current was observed (Figure 9), the

frequency of which depended on the rotational velocity and scan rate. At

non-zero values of rotational velocity, the frequency of oscillation was

inversely proportional to the scan rate. The oscillation is concluded

tentatively to be caused by the motion of electrogenerated dioxygen

bubbles trapped in the cracks at the electrode surface.

Change of the substrate from Au to Pt, Ti, and GC slightly changed

the residual current and the values of half-wave potential (E$_{1/2}$) for

DMSO oxidation. The E$_{1/2}$ values at these electrodes had the following

order: Pt – Ti < Au ≪ GC, which is the same as the order of oxygen

evolution overpotential at the substrate electrodes. Therefore, the substrate has an impact on the reactions at the ultra-thin Bi-PbO_2 film electrode, in contradiction to that at the normal Bi-PbO_2 film electrodes (3b). This is because some portion of the substrate is exposed to the solution through the microcraks.

Considering the expense for large-scale electrolysis, Ti and GC will be the best choices for substrate. It was observed, however, that the electrode potential applied at the Bi-PbO_2 covered GC could not exceed 1.9 V. Otherwise, a blue, non-conductive film developed between the GC and Bi-PbO_2. The Bi-PbO_2 could be removed by treating with 1:1 mixture of acetic acid and hydrogen peroxide; however, the blue interlayer could be removed only by polishing. The formation of this blue film with unknown composition caused electrode reactions to cease.

Stability of the ultra-thin Bi-PbO_2 film   Similar i-E curves to those in Figure 6A were obtained after the ultra-thin Bi-PbO_2 film-covered Au electrode was subjected to consecutive potential cycles as shown in Figure 3. This result clearly indicates the existence of an ultra-thin Bi-PbO_2 film after the consecutive reduction/recharging treatment. This was not the case for the ultra-thin PbO_2 films where were determined to be dissolved completely by repetitive cycles. Therefore, the ultra-thin Bi-PbO_2 film is more stable and adherent than the ultra-thin PbO_2 film, apparently as a direct consequence of the Bi ion in the oxide. That Peak b is located at the same potential as the stripping peak for Au surface oxide in Figure 3 suggests that the increased stability of the ultra-thin Bi-PbO_2 film also might be caused

by an interaction with the substrate. The most beneficial aspect of the increased stability is that a larger voltammetric potential window is available at the ultra-thin $Bi-PbO_2$ electrode than that at the normal $Bi-PbO_2$ electrode. The negative potential limit can be as low as 0.3 V in 1.0 M $HClO_4$.

The stability of the ultra-thin $Bi-PbO_2$ film also was examined at constant-potential conditions. It was observed that the anodic current for oxidation of 10 mM DMSO at 1.6 V and 400 rev min^{-1} did not change with time for more than 3 hours in a large volume cell. The ultra-thin $Bi-PbO_2$ film was determined not to be easily wiped off the substrate as compared to the ultra-thin PbO_2 film. Hence, the ultra-thin $Bi-PbO_2$ film obviously is more resistive to large-term electrolysis and has stronger adherence to the Au substrate. Complete removal of the $Bi-PbO_2$ film was achieved by treating the electrode with 1:1 mixture of acetic acid and hydrogen peroxide.

In conclusion, solid electrodes modified with the ultra-thin $Bi-PbO_2$ films are judged to be excellent candidates as anodes for practical electrolysis.

Catalytic comparison of the ultra-thin $Bi-PbO_2$ film to other Bi-modified PbO_2 electrodes   The catalytic activities of the ultra-thin $Bi-PbO_2$ film electrode was compared to those of the normal $Bi-PbO_2$ prepared from the solution with the same $[Bi^{3+}]/[Pb^{2+}]$ (4c) as well as Bi^{3+}-adsorbed PbO_2 (4d), based on the voltammograms shown in Figure 10. The $E_{1/2}$ value at the ultra-thin $Bi-PbO_2$ film electrode was the least positive, which means that the ultra-thin $Bi-PbO_2$ film has the lowest

overpotential for anodic oxygen-transfer reactions.

The activity of ultra-thin Bi-PbO$_2$ film was also compared to that of normal Bi-PbO$_2$ and Bi^{3+}-adsorbed PbO$_2$ films with a very small thickness prepared by a very short time of deposition. It was seen that the i-E Curves b and c in Figure 10 did not change with the thickness of the Bi-PbO$_2$ or PbO$_2$ film. Hence, the difference between the ultra-thin Bi-PbO$_2$ film and the normal Bi-PbO$_2$ film is not simply a result of differences in thickness.

Elemental analysis of the ultra-thin Bi-PbO$_2$ films with XPS

The Bi/Pb atomic ratio in the surface of the ultra-thin Bi-PbO$_2$ films was determined by measuring the Bi/Pb peak area ratio in the XPS data, as plotted against [Bi^{3+}]/[Pb^{2+}] in Figure 11a. The Bi/Pb atomic ratio in the ultra-thin film increased linearly with increased [Bi^{3+}]/[Pb^{2+}] in the deposition solution, which is consistent with the results for the normal Bi-PbO$_2$ electrodes (Curve b) (4c). Clearly, the Bi/Pb atomic ratio in the ultra-thin film is higher than that in the normal film for the same value of [Bi^{3+}]/[Pb^{2+}]. There are two possible explanations. First, Pb ions in Bi-PbO$_2$ is more easily dissolved than the Bi ions by electrochemical reduction. Therefore, enrichment of Bi occurs at the surface of the ultra-thin film after the outer oxide layer is stripped off. This explanation is supported by that the Lines a and b in Figure 11 are parallel to one another. This explanation is also consistent with the mechanism for the formation of the ultra-thin films proposed previously (5) and the increased stability of Bi-doped over pure PbO$_2$ (4c). The increased Bi/Pb atomic ratio is concluded to be responsible

for the enhanced catalytic activities and stability of the ultra-thin Bi-PbO_2 film. Also shown in Figure 11 is the Bi/Pb atomic ratio for the Bi^{3+}-adsorbed PbO_2. Obviously, the value of Bi/Pb atomic ratio at $[Bi^{3+}]/[Pb^{2+}] = 0.1$ is in the reverse order of $E_{1/2}$ values observed in Figure 10, i.e., the higher the Bi/Pb atomic ratio, the smaller is the $E_{1/2}$ value.

References

1. (a) Johnson, D. C. J. Electrochem. Soc. 1972, 119, 331. (b) Austin, D. S.; Johnson, D. C.; Hines, T. G.; Berti, E. T. Anal. Chem. 1983, 55, 2222. (c) Cabelka, T. D.; Austin, D. S.; Johnson, D. C. J. Electrochem. Soc. 1984, 131, 1596; 1985, 132, 359. (d) Hughes, S.; Meschi, P. L.; Johnson, D. C. Anal. Chim. Acta 1981, 132, 1. (e) Hughes, S.; Johnson, D. C. Anal. Chim. Acta 1981, 132, 11; 1983, 149, 1. (f) Polta, J. A.; Johnson, D. C. J. Liq. Chrom. 1986, 6, 1727.

2. (a) Austin, D. S.; Polta, J. A.; Polta, T. Z.; Tang, A. P.-C.; Cabelka, T. D.; Johnson, D. C. J. Electroanal. Chem. 1984, 168, 227. (b) Johnson, D. C.; Polta, J. A.; Polta, T. Z.; Neuburger, G. G.; Johnson, J.; Tang, A. P.-C.; Yeo, I.-H.; Baur, J. J. Chem. Soc., Faraday Trans. 1 1986, 82, 1081.

3. (a) Yeo, I.-H.; Johnson, D. C. J. Electrochem. Soc. 1987, 128, 1973. (b) Yeo, I.-H.; Ph.D. Dissertation, Iowa State University, Ames, Iowa, 1987. (c) Yeo, I.-H.; Kim, S.; Jacobson, R.; Johnson, D. C. J. Electrochem. Soc. in press.

4. (a) Chang, H.; Johnson, D. C. J. Electrochem. Soc. 1989, 136, 17; Chapter II-A, this Dissertation. (b) Chang, H.; Johnson, D. C. J. Electrochem. Soc. 1989, 136, 23; Chapter II-B, this Dissertation. (c) Chang, H.; Johnson, D. C., in preparation; Chapter III-B, this Dissertation. (d) Chang, H.; Johnson, D. C., in preparation; Chapter III-A, this Dissertation. (e) Chang, H.; Johnson, D. C., in preparation; Chapter IV-A, this Dissertation.

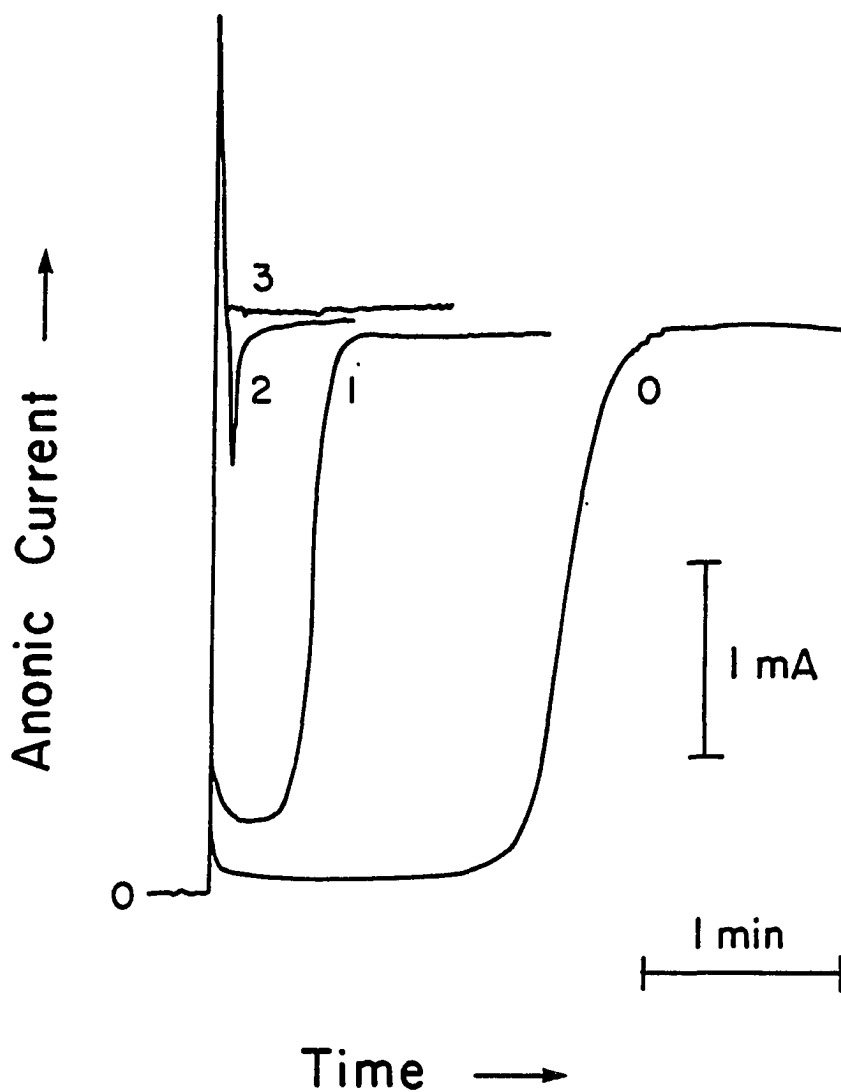5. Chang, H.; Johnson, D. C., preceding paper; Chapter V-A, this Dissertation.

Figure 1. Chronoamperometric response for deposition of Bi-PbO$_2$ at Au

Solution: 10 mM Pb^{2+}, 1 mM Bi^{3+}, 1.0 M HClO$_4$

Conditions: deposition potential — 1.7 V,
stripping potential — 0.5 V,
w — 400 rev min^{-1}
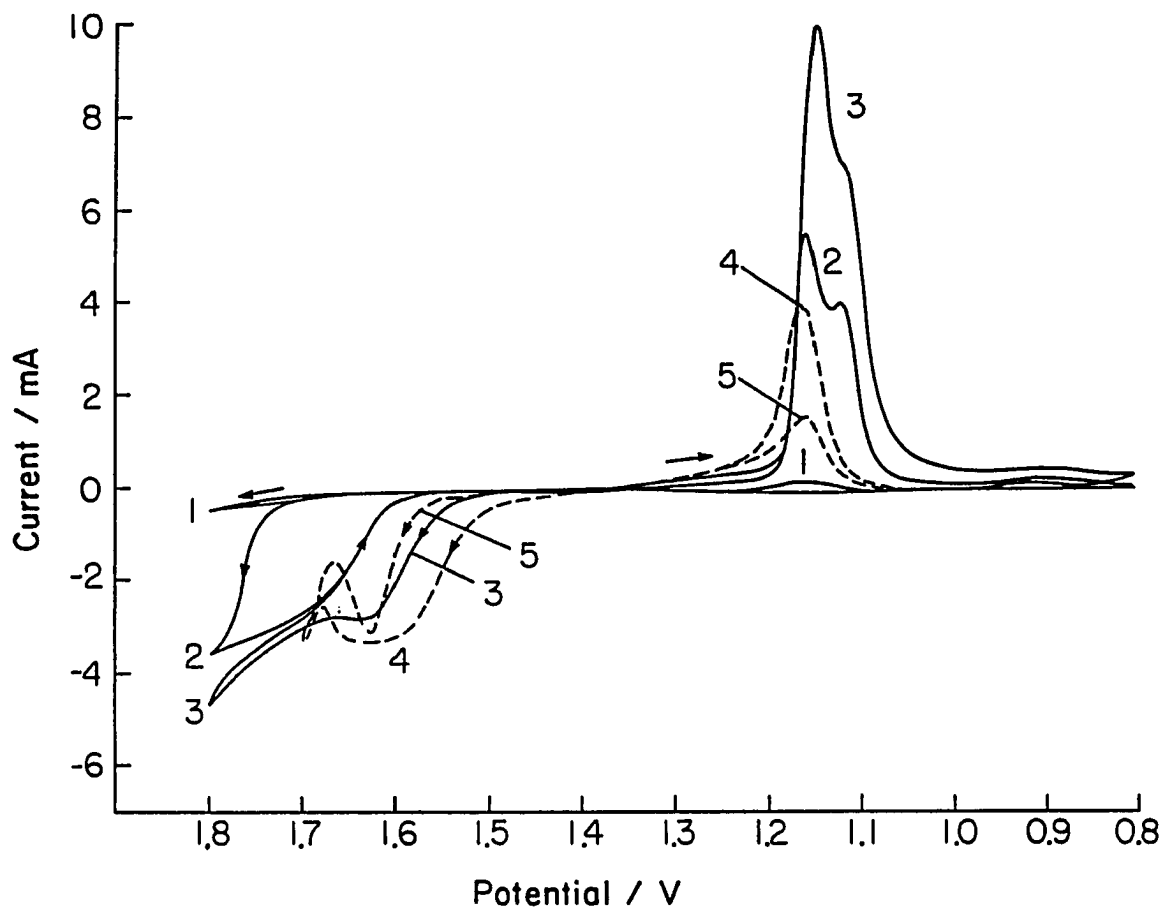
Number of deposition/stripping pretreatment shown

Figure 2. Consecutive cyclic voltammogram at freshly polished Au

Solution: the same as given in Figure 1

Conditions: 20 mV s^{-1}, w - 400 rev min^{-1}
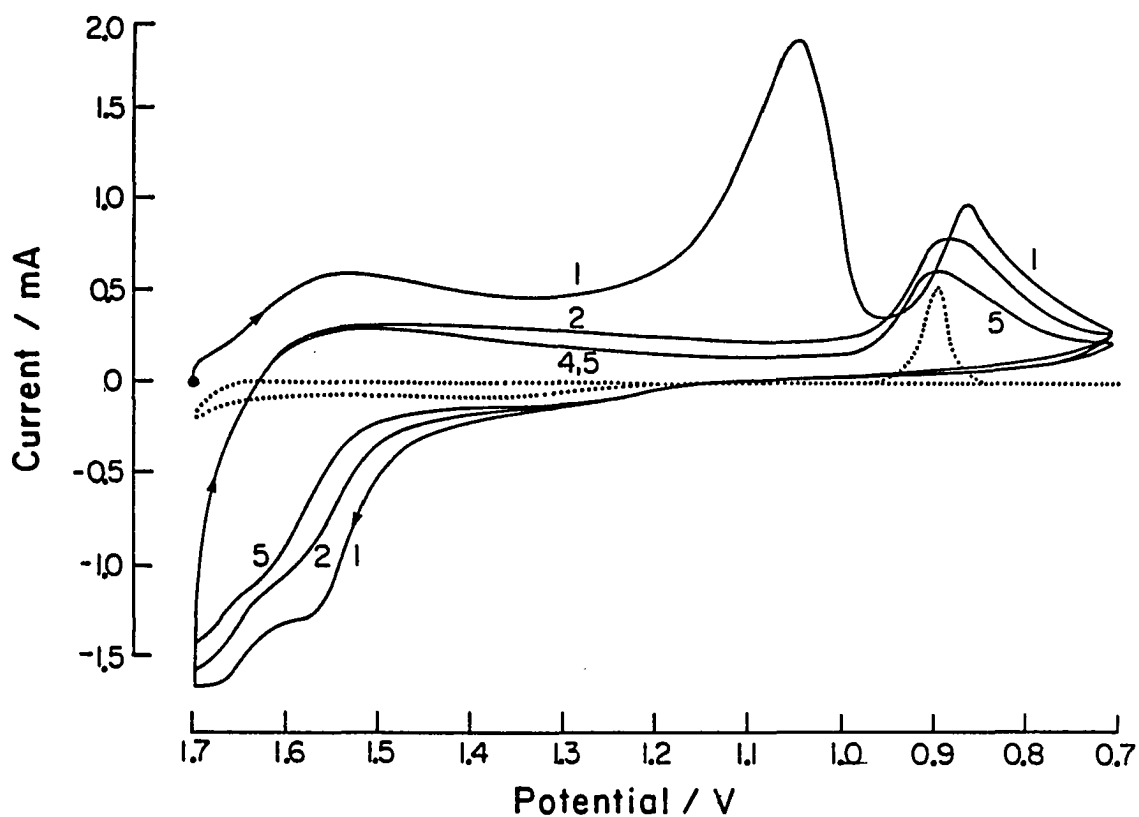
Anodic limit potential: (——) 1.8 V; (— —) 1.7 V

Figure 3. Consecutive stripping voltammograms at a Au RDE covered by
an ultra-thin film of Bi-PbO$_2$ in 1.0 M HClO$_4$

Conditions: 80 mV s^{-1}, 0 rev min^{-1}; the electrode was
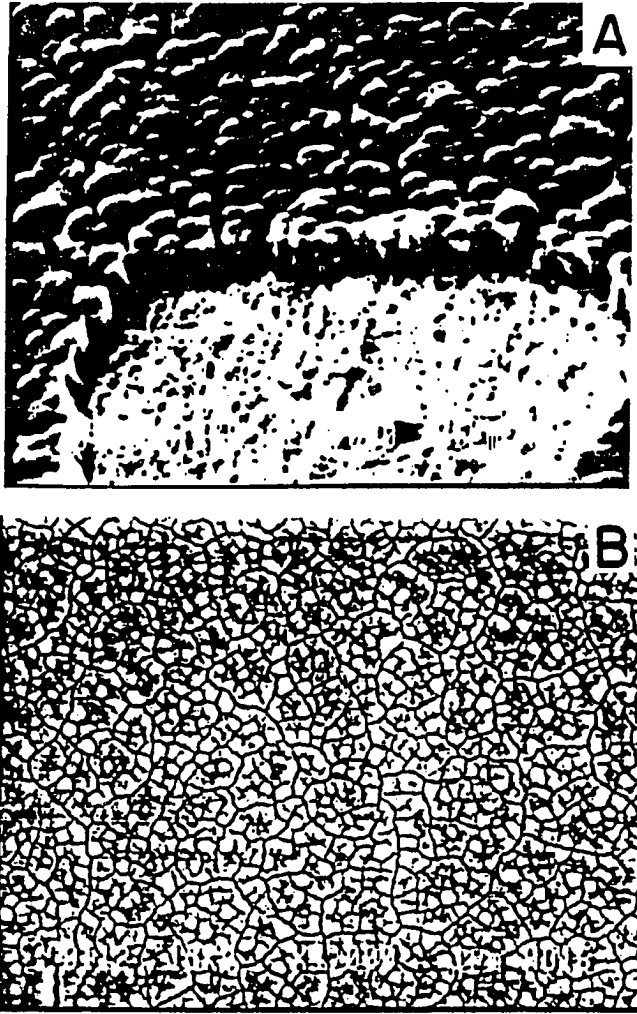anodized at 1.7 V for 1 min before the scan

(.....) response at Au

Figure 4A&B.   Electron micrograph of ultra-thin Bi-PbO film on Au

(A) ultra-thin Bi-PbO film, sampled tilted for 51°,
(B) ultra-thin Bi-PbO film, not tilted

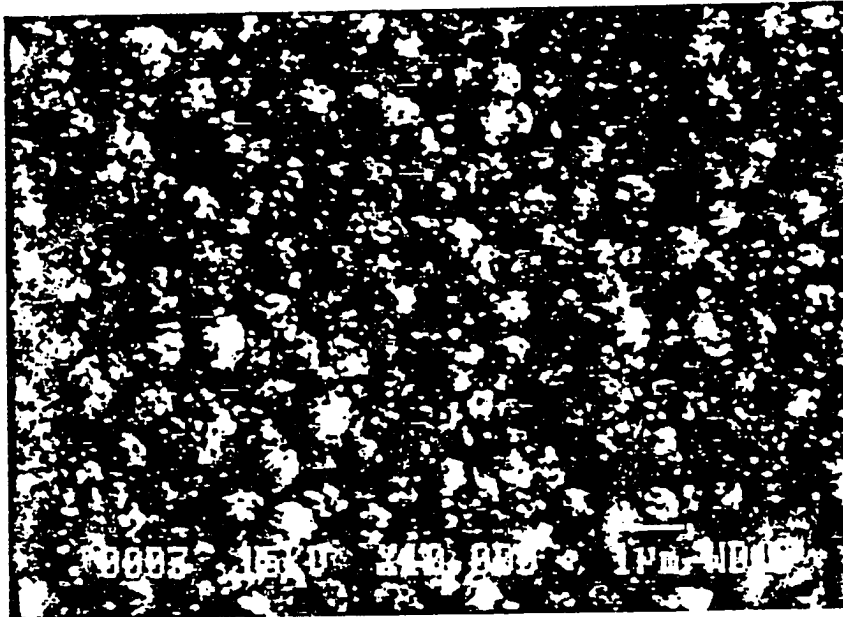Deposition solution: $[Bi^{3+}]/[Pb^{2+}]$ - 0.1

Figure 4C. Electron micrograph of normal Bi-PbO$_2$ film on Au substrate
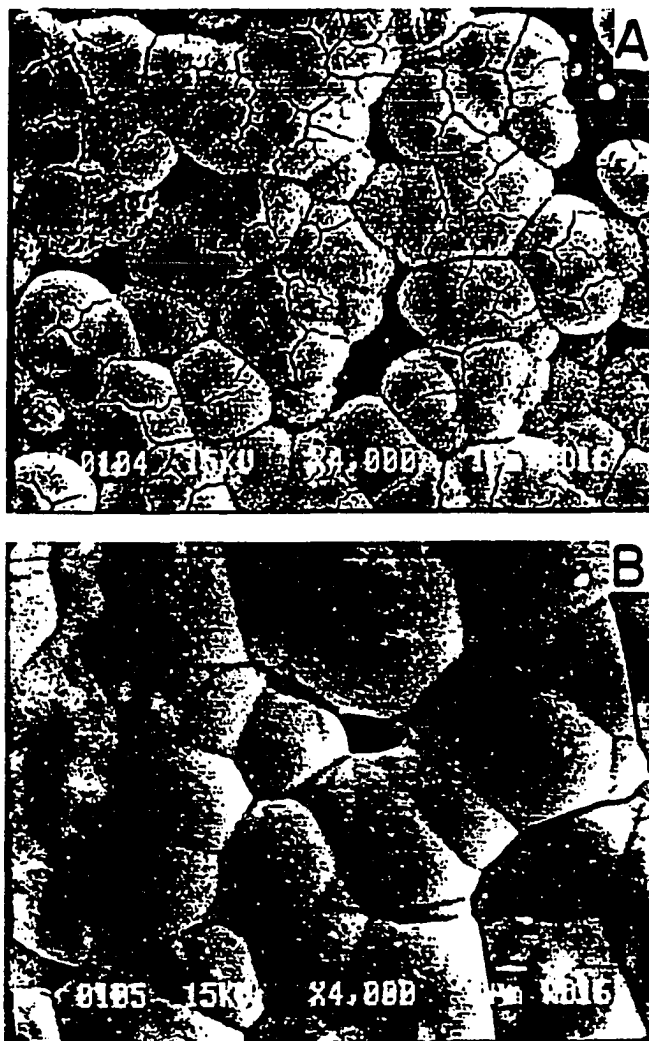
Deposition conditions: as given in Figure 4A&B

Figure 5. Electron micrographs of oxide films at Ti substrate

(A) ultra-thin Bi-PbO film,
(B) normal Bi-PbO$_2$ film
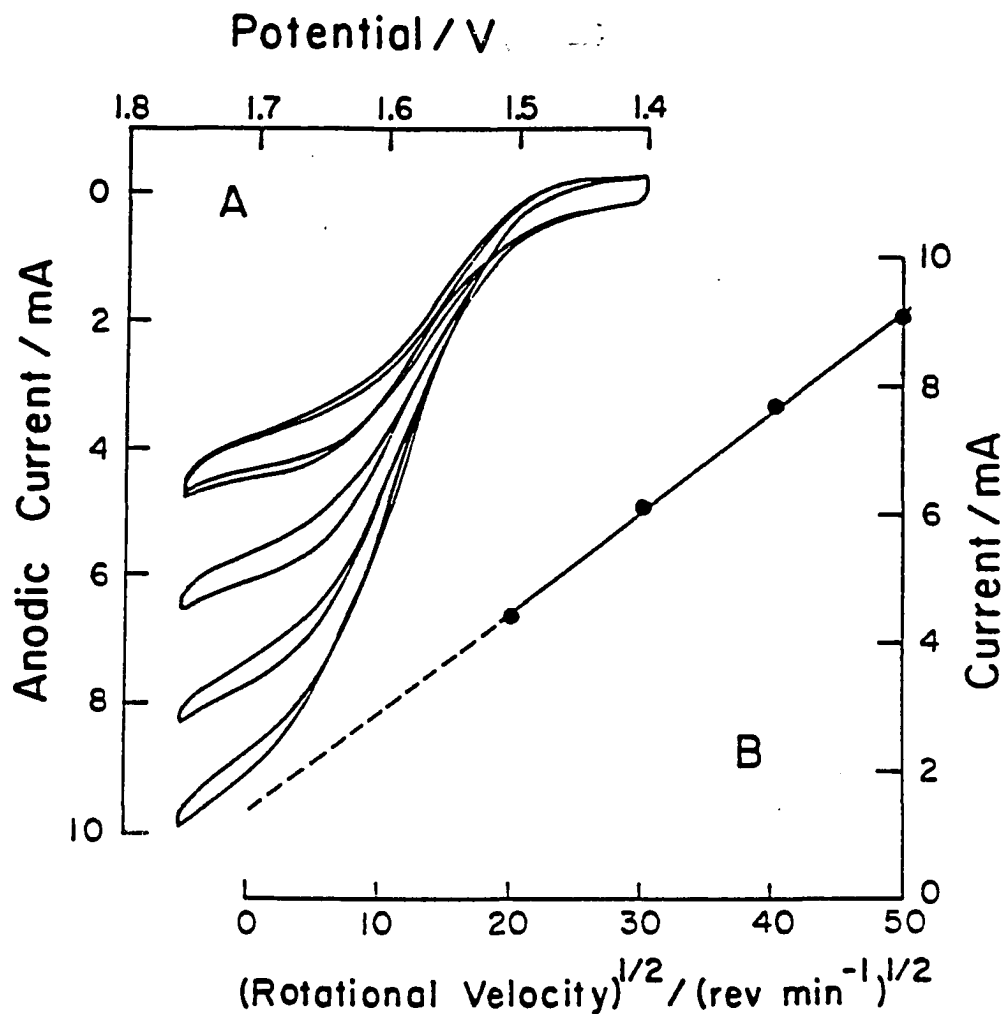
Deposition solution: $[Bi^{3+}]/[Pb^{2+}]$ = 0.1

Figure 6. Voltammetric responses of 10 mM DMSO at a Au RDE covered
by an ultra-thin film of $Bi\text{-}PbO_2$

(A) Effect of w (rev min^{-1}): (a) 400, (b) 900, (c) 1600,
(d) 2500

Conditions: 20 mV s^{-1}, 1.0 M $HClO_4$; electrode
deposited from $[Bi^{3+}]/[Pb^{2+}]$ = 0.1 solution

(B) Plot of current height at the negative scan 1.7 V in (A)
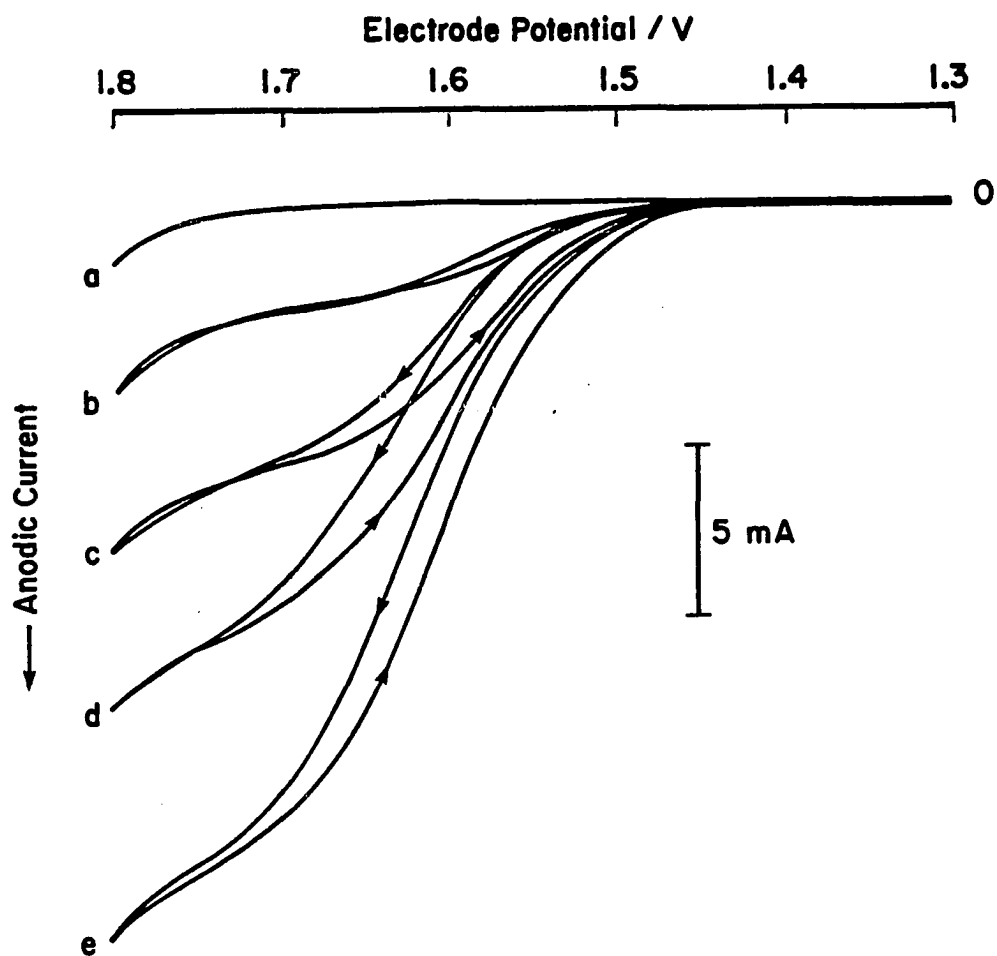vs. $w^{1/2}$

Figure 7. Voltammetric response of DMSO at ultra-thin Bi-PbO$_2$ film
electrode: effect of DMSO concentration

   DMSO concentration (mM):   (a) 0, (b) 10, (c) 20,
                                (d) 30, (e) 40
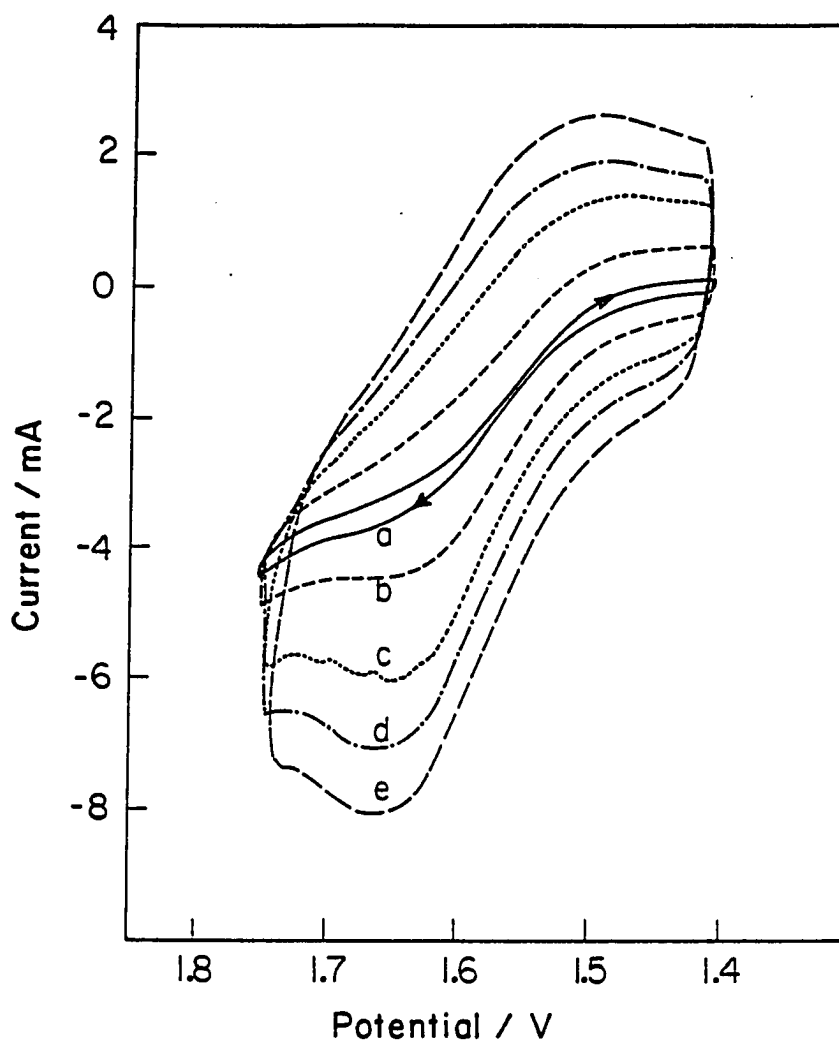
   Other conditions: as given in Figure 6

Figure 8. Effect of scan rate on the i-E curves of 10 mM DMSO at a Au RDE covered by an ultra-thin film of $Bi-PbO_2$

Conditions: 400 rev min^{-1}, 1.0 M $HClO_4$; electrode deposited from $[Bi^{3+}]/[Pb^{2+}]$ solution

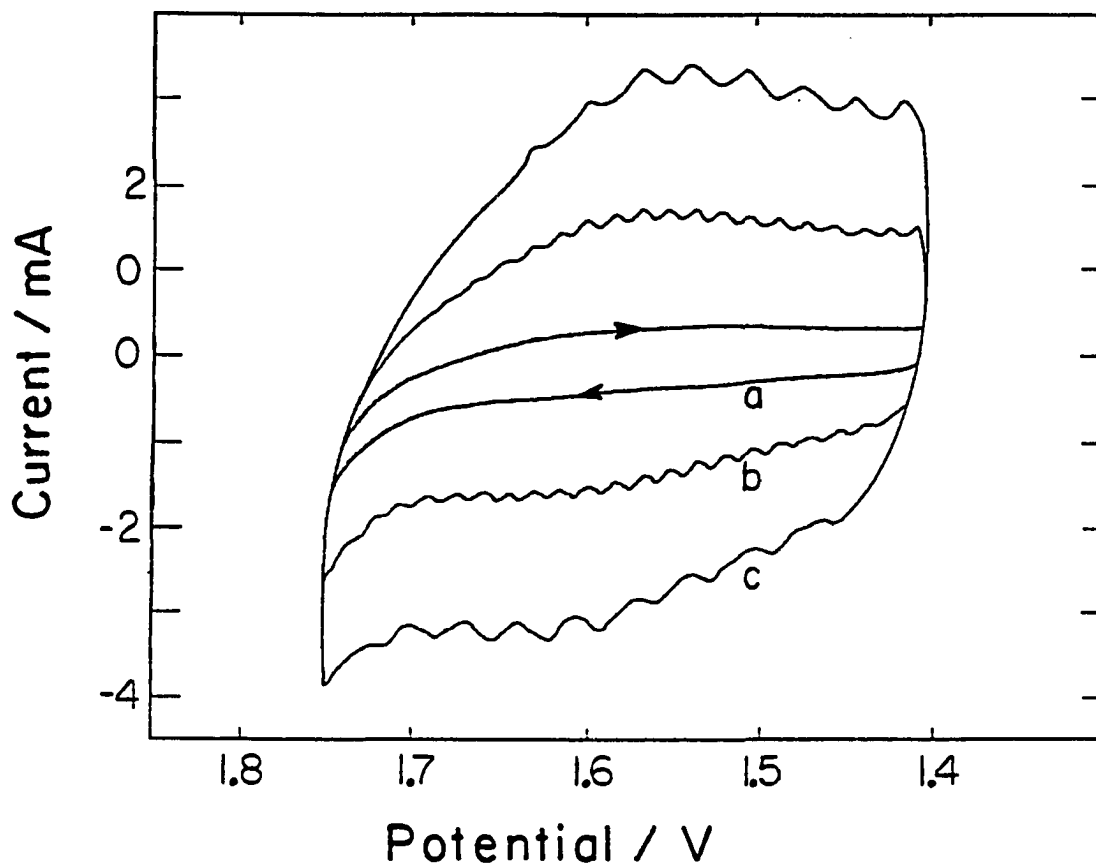Scan rate (mV s^{-1}): (a) 20, (b) 100, (c) 200, (d) 300, (e) 400

Figure 9. Effect of scan rate on the residual voltammetric response at
a Au RDE covered by an ultra-thin film of Bi-PbO$_2$

Conditions: as given in Figure 8

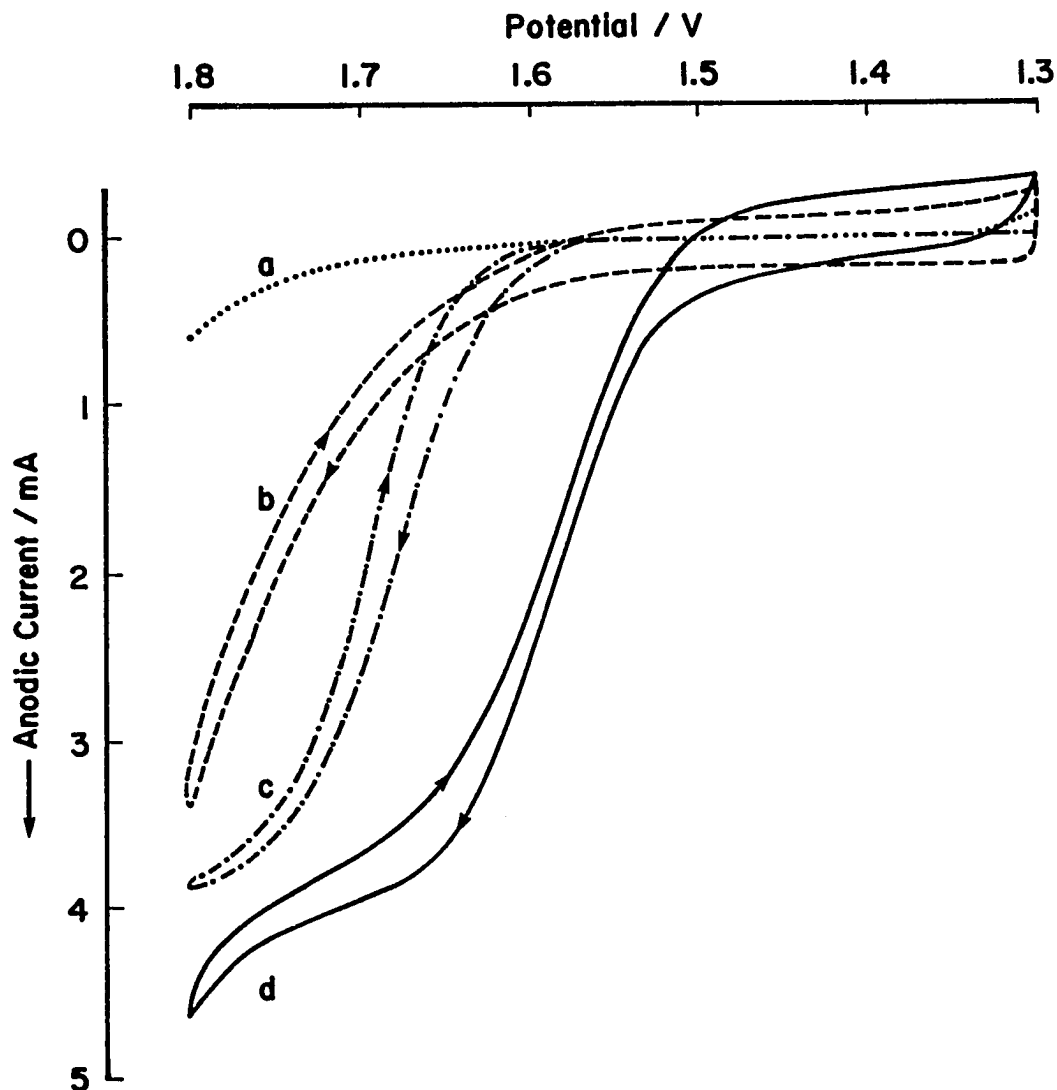Scan rate (mv s^{-1}): (a) 20, (b) 100, (c) 200

Figure 10.   Voltammetric responses of 10 mM DMSO at varied electrodes

Conditions: 20 mV s^{-1}, 400 rev min^{-1}, 10 mM DMSO

Au RDE covered by:
   (a) PbO$_2$ film,
   (b) PbO$_2$ film with 0.1 mM Bi^{3+} in the solution,
   (c) normal Bi-PbO$_2$ film; deposited from
        [Bi^{3+}]/[Pb^{2+}] = 0.1 solution,
   (d) ultra-thin Bi-PbO$_2$ film; deposited from the same
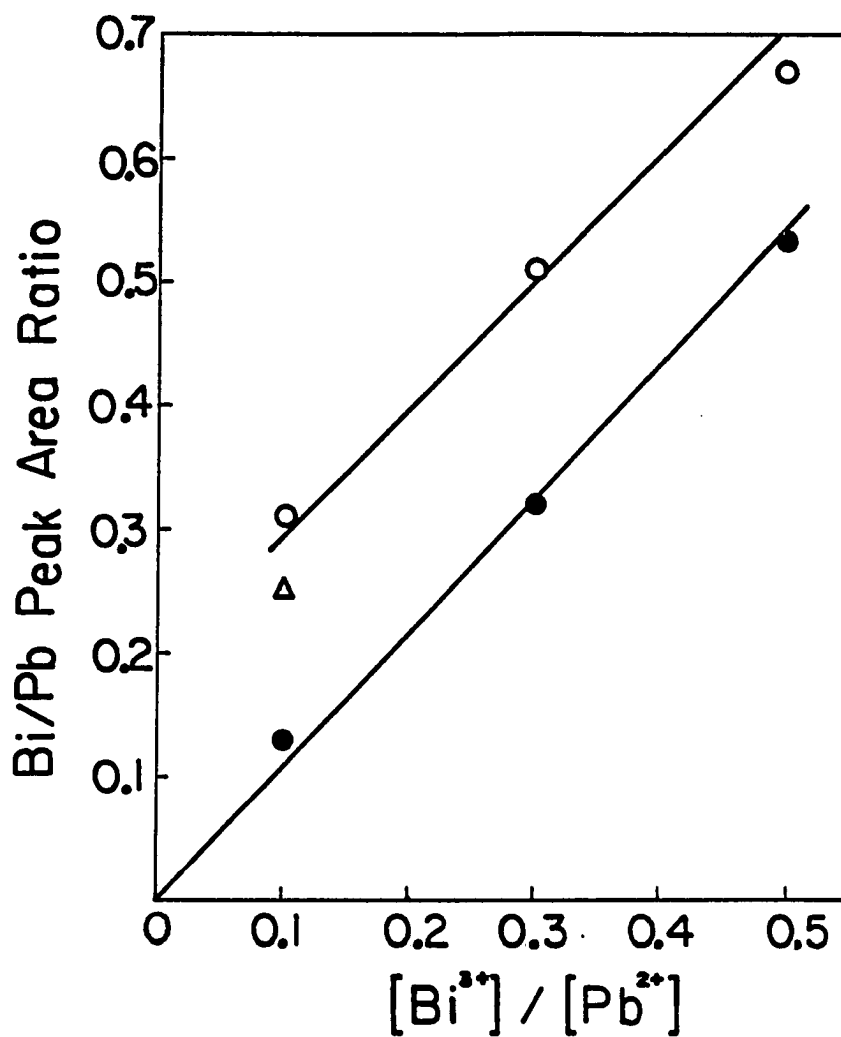   solution as given in (c)

Figure 11. Plot of Bi/Pb peak area ratio in the XPS data vs.
Bi/Pb concentration ratio

Curves: (O) ultra-thin Bi-PbO$_2$
          (●) normal Bi-PbO$_2$
          (▲) Bi^{3+}-adsorbed PbO$_2$, prepared by treating PbO$_2$
              electrode in 10 mM Bi^{3+} at 1.6 V for 10 min

VI. MISCELLANEOUS STUDIES

A. Electrolytic Conversion of Manganese(II) to Permanganate

in Acidic Media: An Ideal Reaction

for Demonstration of Electrocatalysis[1]

"Our knowledge can be symbolically represented by the area in a circle; what we don't know can represented by the area outside the circle. When our knowledge expands, our frontier line to the unknown world also expands."

-Unknown

---

[1]To be submitted to J. of Chem. Ed.

Introduction

Electrocatalytic reactions are of great importance in electrolysis, e.g., in the chloralkali and electrosynthesis industries, and as sensors in electroanalytical devices. However, electrocatalysis has not received much attention in chemical education in comparison with catalysis in general. No experiment or introduction article directly devoted to electrocatalysis has been published in This JOURNAL, while there have been an average of about six papers annually in recent years pertaining to chemical catalysis, e.g., Ref. 1.

Recently, electrocatalysis at chemically modified lead dioxide electrodes has been the subject of extensive research in our laboratory (2,3). It was discovered that the electrolytic oxidation of Mn^{2+} to MnO_4^- in acidic media proceeds readily by electrocatalysis at bismuth-modified PbO_2 electrodes. We believe that this reaction is ideal for demonstration of electrocatalysis for several reasons. First, the reaction is too slow to occur at any conventional anodes including Au, Pt, C, and pure PbO_2. Therefore, the catalytic effect at Bi-modified PbO_2 electrodes is quite obvious. Second, the product of the reaction MnO_4^- has an intense purple color and gives a strong visual evidence of the reaction. Third, the required chemicals and apparatus for this demonstration are very simple and inexpensive. Fourth, the oxidation product can be used as a strong oxidant (4) to illustrate the possible applications of electrocatalysis.

There are two types of Bi-modified PbO_2 electrodes: Bi-doped PbO_2 (2,3a) and Bi^{3+}-adsorbed PbO_2 (3d,c). In this article we describe the

procedures for electrolytic conversion of Mn^{2+} to MnO_4^- at Bi^{3+}-adsorbed PbO_2 electrodes as a demonstration experiment.

Experimental

Solutions   The following stock solutions are required: 100 ml of 10 mM $Mn(NO_3)_2$ in 1.0 M $HClO_4$, 10 ml of 10 mM $Bi(NO_3)_2$ in 1.0 M $HClO_4$, 100 of ml 20 mM $Pb(NO_3)_2$ in 0.1 M $HClO_4$, and 100 ml of 1:1 mixture of H_2O_2 (30%) and CH_3COOH (glacial).

Apparatus   Two graphite rod electrodes as the working electrode. Two Pt-wire counter electrodes. One saturated calomel electrode (SCE). Two 100-ml beakers as electrolysis cells. One potentiostat (can be substituted by battery). One 0.5-ml syringe.

Deposition of PbO_2 The graphite electrodes are first cleaned by immersion in the H_2O_2-CH_3COOH mixture, and then coated with PbO_2 by electrodeposition under these conditions (3a): E - 1.6 V vs. SCE in the 20 mM Pb^{2+} solution for 10 sec, then adjust to E - 1.55 V until the electrode is evenly covered by a PbO_2 film. Following completion of the experiment, the PbO_2 coating can be removed by treating the electrode with the H_2O_2-CH_3COOH solution.
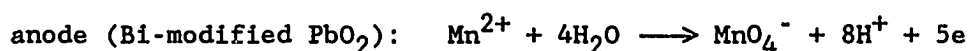
Procedures

Add 50 ml of the colorless Mn^{2+} solution to each of the two cells. Put the working, counter, and reference electrodes into one of the cells and connect them to potentiostat at E - 1.6 V. Observe if there is any color change in the solution over a 5-min period. There should be only a

very small evidence of MnO_4^- and with some suspended MnO_2 particles.

Add 0.5 ml of 10 mM Bi^{3+} solution to the second cell. Connect the electrodes. The solution should turn to a purple color immediately, with the intensity of the color increasing with electrolysis time.

Discussion

The electrode reactions can be written as follows:

anode (Bi-modified PbO_2): $\quad Mn^{2+} + 4H_2O \longrightarrow MnO_4^- + 8H^+ + 5e$

cathode: $\qquad\qquad\qquad\qquad 2H_2O + 2e \longrightarrow H_2 + 2OH^-$

It is obvious that the concentration ratio of Bi^{3+} (catalyst) and Mn^{2+} is 0.5:50 ≈ 1:100 in the electrolysis solution. Hence, the amount of catalyst needed for this highly catalytic effect is very low. It has been proved that the bismuth ions must first be adsorbed onto the PbO_2 surface in order to function as a catalyst (3c,d), which is the reason for the name, Bi^{3+}-adsorbed PbO_2. It is also true that this reaction only occurs at PbO_2 electrode (3c,d).

Many further experiments can be conducted based on this electrocatalytic reaction. For instances, this reaction can be used in coulometric titration with electrogenerated MnO_4^-. The electrogenerated MnO_4^- can also be used as oxidant in waste treatment, and many inorganic and organic reactions. Since only catalytic amount of Mn^{2+} is used, the Mn^{2+} waste can be kept minimum. The solubility of the MnO_4^- ions in organic phases can be enhanced by usage of phase transfer reagents (5). This experiment is also suitable for demonstration with a projector.

It should be pointed out that this experiment requires the use of

Pb^{2+} solution in the preparation procedure. Caution must be taken to handle the Pb^{2+} solution. The waste solution from the dissolution of used PbO_2 electrodes must not be drained through the sink. Special attention should also be paid to prepare the 1.0 M $HClO_4$ from concentrated $HClO_4$ (70%).

References

1. (a) Greco, F. A. J. Chem. Ed. 1986, 63, 382. (b) Frugoni, J. A. C.; Zepka, M.; Figueira, A. R.; Campos, A. S. J. Chem. Ed. 1986, 63, 549. (c) Copperthwaite, R. G.; Hutchings, G. J.; van der Riet, M. J. Chem. Ed. 1986, 63, 632.

2. (a) Austin, D. S.; Polta, J. A.; Polta, T. Z.; Tang, A. P.-C.; Cabelka, T. P.; Johnson, D. C. J. Electroanal. Chem. 1984, 168, 227. (b) Johnson, D. C.; Polta, J. A.; Polta, T. Z.; Newburger, G. G.; Johnson, J.; Tang, A. P.-C.; Yeo, I.-H.; Baur, J. J. Chem. Soc., Faraday Trans. 1 1986, 82, 1081. (c) Yeo, I.-H.; Johnson, D. C. J. Electrochem. Soc. 1987, 134, 1973. (d) Yeo, I.-H.; Kim, S.; Jacobson, R.; Johnson, D. C. J. Electrochem. Soc. in press. (e) Yeo, I.-H. Ph.D. Dissertation, Iowa State University, Ames, Iowa, 1987.

3. (a) Chang, H.; Johnson, D. C. J. Electrochem. Soc. 1987, 136, 17; Chapter II-A, this Dissertation. (b) Chang, H.; Johnson, D. C. ibid. 1987, 136, 23; Chapter II-B, This Dissertation. (c) Chang, H.; Johnson, D. C., in preparation; Chapter III-B, this Dissertation. (d) Chang, H.; Johnson, D. C., in preparation; Chapter III-A, this Dissertation. (e) Chang, H.; Johnson, D. C., in preparation; Chapter IV-A, this Dissertation.

4. (a) Steward, R. In "Oxidation in Organic Chemistry, Part A"; Wiberg, K. B., Ed.; Academic Press: New York, 1965; Chapter I, p. 1. (b) Lee, D. G. "The Oxidation of Organic Compounds by Permanganate Ion and Hexavalent Chromium"; Open Court Publishing Company: LaSalle, Illinois, 1980.

5. (a) Lee, D. G. In "Oxidation in Organic Chemistry, Part D"; Trahanvosky, W. S., Ed.; Academic Press: New York, 1982; Chapter II, p. 147. (b) Brown, K. C.; Chang, V. S.; Dar, F. H.; Lamb, S. E.; Lee, D. G. J. Chem. Ed. 1982, 59, 696.

B. Photocatalytic Production of Manganese Dioxide

   from Manganese(II) at Supported Lead Dioxide

"A philosopher is a person who knows less and less about
more and more, until he knows nothing about everything; a
scientist is a person who knows more and more about less
and less, until he knows everything about nothing."

-Unknown

Introduction

Many metal oxides are semiconductors. This is shown by the photocatalytic and photoelectrochemical reactions at these metal oxides (1). Recently, pure and modified lead dioxides (PbO_2) are used as anode materials in this laboratory for electrocatalysis of oxygen-transfer reactions (2,3). In order to understand the mechanism of electrocatalysis at these electrodes, the photocatalytic activities of these electrode materials are tested to determine whether these materials are semiconductors.

Experimental

A large area Pt screen was used as a support to the PbO_2 film which was electrodeposited under the optimal conditions (3a). A 60-ml cell was placed in a sealed box. Two bulbs were used: a normal bulb (25 W) and an ultraviolet bulb (100 W). Electrolysis was conducted with a Pt wire counter electrode, a saturated calomel reference electrode (Fisher Scientific, Incorporated), a three-apartment cell, and a model RDE4 potentiostat (Pine Instruments, Grove City, Pennsylvania).

All chemicals were of reagent grade. Water was distilled followed by purification in a Barnstead NANOpure II system (Boston, Massachusetts).

Results and discussion

The model reaction studied is the oxidation of Mn^{2+} in 1.0 M $HClO_4$ whose product can be MnO_2 or MnO_4^- depending on the efficiency of catalysis, as indicated below

$$Mn^{2+} \xrightarrow{\quad [1] \quad} MnO_2 \xrightarrow{\quad [2] \quad} MnO_4^-$$
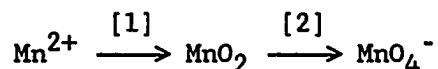
Both reactions are very slow at conventional electrodes (3c,d).

Therefore, the catalytic effects of the material modification and

illumination can be monitored easily by the observation of the oxidation

product, i.e., the brown MnO_2 particles or the purple MnO_4^-.

It was found that MnO_2 was produced at PbO_2 under open-circuit

condition with illumination of light, which indicates the photocatalytic

activity of pure PbO_2. The generation of MnO_2 was recorded as a function

of the existence of Bi^{3+} in solution, material, light source, and heating

effect. The results are listed in Table 1.

Addition of Bi^{3+} to the solution did not affect the photocatalytic

reaction (compare No. 1 and No. 2 in Table 1). It is known from our

previous experiment (3d) that Mn^{2+} is oxidized to MnO_4^- at Bi^{3+}-adsorbed

PbO_2 electrode. The difference between the electrocatalysis and

photocatalysis at Bi^{3+}-adsorbed PbO_2 surface suggests that the mechanisms

for the catalysis are different.

The photocatalytic reaction was not affected by the change of light

source from ultra-violet light to white light (see No. 2 and No. 3 in

Table 1). More detailed work on the dependence of the photocatalysis on

the wavelength requires the use of wavelenghth-selective light sources.

Very few amount of MnO_2 was observed under the shining of room light (No.

4), which indicates that the intensity of light is a factor in the

photocatalysis.

The illumination of light on the cell generated heat and increased

Table 1. Generation of MnO_2 generated by photocatalysis at supported PbO_2 in 10 mM Mn^{2+}, 1.0 M $HClO_4$

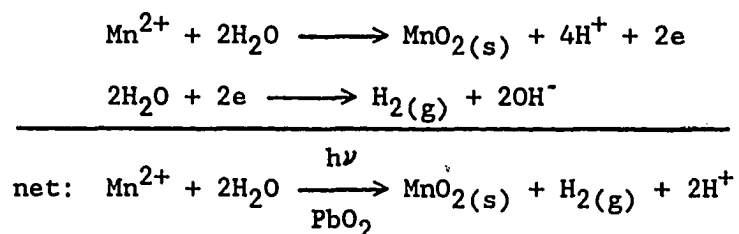| no.	$[Bi^{3+}]$	electrode	light	heating	generation of MnO_2
1	10 µM	PbO_2/Pt	UV	resulted from the light	yes
2	none	"	"	"	yes
3	"	"	visible	"	yes
4	"	"	room light	none	a
5	"	"	none	direct heating	b
6	"	Pt	UV	resulted from the light	no

[a]Very small amount.

[b]Small amount.

the solution temperature, which might have an impact on the photocatalysis. It was observed that a small amount of MnO_2 was generated by direct heating of the Mn^{2+} solution in the presence of PbO_2 (No. 5 in Table 1), which did not occur without PbO_2. This result suggests that heating can assist the generation of MnO_2, but is not solely responsible for the observed effect.

Removal of PbO_2 coating on the Pt resulted the loss of photocatalytic activity (see No. 6 in Table 1), which means that the photocatalytic reaction is related to the properties of PbO_2.

A gaseous product also was observed at the PbO_2 surface during the photocatalytic production of MnO_2. Since it must be a cathodic process in opposition to the oxidation of Mn^{2+}, the gaseous product is concluded as hydrogen (H_2) produced by the reduction of water.

In summary of the above, it is concluded that MnO_2 is generated from Mn^{2+} via a heat assisted photocatalytic reaction at PbO_2 surface, which can be symbolized as follows:

$$Mn^{2+} + 2H_2O \longrightarrow MnO_2{}_{(s)} + 4H^+ + 2e$$

$$2H_2O + 2e \longrightarrow H_2{}_{(g)} + 2OH^-$$

$$\text{net: } Mn^{2+} + 2H_2O \xrightarrow[PbO_2]{h\nu} MnO_2{}_{(s)} + H_2{}_{(g)} + 2H^+$$

This photocatalytic reaction can be explained by that PbO_2 is a degenerate semiconductor with a very small energy gap of ca. 0.4 eV (4). After the absorption of light, some potential differences are established at different positions of the PbO_2 surface, which yields local cells at

the surface. The low potential sites serve as the localized cathode for H_2 evolution and the sites with high potential serve as the anodes for MnO_2 production. The oxidation product is determined by the energy gap of the semiconductor. Since the energy gap is very small, the oxidation can only proceed to MnO_2 but not MnO_4^-. For the same reason, this photocatalytic reaction can occur even under visible light.

It also was observed that the oxidation of Mn^{2+} at pure and modified PbO_2 electrodes at 1.6 V was not affected by the shining of light. This result further proves that the mechanisms of electrocatalysis and photocatalysis at PbO_2 are different.

References

1. (a) Bard, A. J. In "Proceedings of the R. A. Welch Foundation Conf. Chem. Research"; XXVII, 1984; Chapter IV, p. 95. (b) Teichner, S. J.; Formenti, M. In "Photoelectrochemistry, Photocatalysis, and Photoreactions"; Schiavello, M., Ed.; Reidel: Dordrecht, 1985; p. 457. (c) Cunningham, J. In "Surface and Near-Surface Chemistry of Oxide Materials"; Nowotny, J.; Dufour, L.-C., Eds.; Elsevier: Amsterdam, 1988.

2. (a) Johnson, D. C.; Polta, J. P.; Polta, T. Z.; Newburger, G. G.; Johnson, J.; Tang, A. P.-C.; Yeo, I.-H.; Baur, J. J. Chem. Soc., Faraday Trans. 1 1986, 82, 1081. (b) Yeo, I.-H.; Johnson, D. C. J. Electrochem. Soc. 1987, 134, 1973. (c) Yeo, I.-H.; Kim, S.; Jacobson, R.; Johnson, D. C. J. Electrochem. Soc. in press. (d) Yeo, I.-H.; Ph.D. Dissertation, Iowa State University, Ames, Iowa, 1987.

3. (a) Chang, H.; Johnson, D. C. J. Electrochem. Soc. 1989, 136, 17; Chapter II-A, this Dissertation. (b) Chang, H.; Johnson, D. C. J. Electrochem. Soc. 1989, 136, 23; Chapter II-B, this Dissertation. (c) Chang, H.; Johnson, D. C., in preparation; Chapter III-B, this Dissertation. (d) Chang, H.; Johnson, D. C.,in preparation; Chapter III-A, this Dissertation.

4. (a) Pavlov, D. In "Power Sources for Electric Vehicles"; McNicol, B. D.; Rand, D. A. J., Eds.; Elsevier: New York, 1984; pp. 111. (b) Mindt, W. J. Electrochem. Soc. 1969, 116, 1076.

VII. GENERAL SUMMARY

The major discoveries described in this dissertation are summarized below in correlation with the considerations in Chapter I-A.

Intermediate product for deposition and electrocatalysis at in-situ deposited PbO_2

Soluble Pb(IV) species are concluded to be generated, along with adsorbed Pb(IV) species, as intermediate products during the electrodeposition of PbO_2 in acidic media (1,2). The unstable Pb(IV) species, possibly associated with oxygen, can be used as an oxidation catalyst for some anodic oxygen-transfer reactions at in-situ deposited PbO_2 electrodes. The use of the in-situ deposited results in longer electrode lifetime than observed for pre-deposited PbO_2 (3).

Methods for chemical modification of PbO_2 surface

Modification of PbO_2 by co-deposition A number of inorganic anions and cations can be incorporated into the PbO_2 matrix when they are present in the Pb^{2+} plating bath (4-5). This co-deposition, or electrochemical doping process, produces mixed-oxide films that behave differently from pure PbO_2. Some catalytic activities for O-t reactions were found at PbO_2 electrodes doped with Bi^{3+}, As(III), and Cl^-.

The Bi ions exposed at the surface of the Bi-doped PbO_2 can function as catalytic sites which are evenly distributed and spatially separated, as shown by EDS elemental mapping (4). This result is consistent with the proposed mechanism as shown in Figure 2 in Chapter I-A. The Bi-doped PbO_2 has higher electrochemical stability and wider voltammetric window

than the pure PbO_2, probably due to the decreased alkalinity of the mixed oxide.

Modification of PbO_2 by adsorption   Several ionic species, e.g., Bi^{3+}, As(V) (or As(III)), and Cl^-, can be adsorbed into the surface of PbO_2 as catalysts (5), because of the ion exchange or complexation ability of the PbO_2 surface. The adsorption method of modification has several advantages over the co-deposition method.

First, the adsorption method is more suitable for mechanistic studies. For instance, the surface concentration of Bi^{3+} at the surface of Bi^{3+}-adsorbed PbO_2 can be controlled easily by varying the bulk concentration of Bi^{3+}. A half-wave potential for the electrocatalytic oxidation reactions can be measured accurately at the Bi-adsorbed PbO_2.

Second, the co-deposition method has separate procedures for electrode preparation and testing, so is tedious and time-consuming for catalyst screening. The matter of screening is much improved with the adsorption method for which the two procedures are combined. Hence, a ˙large number of species can be tested in a short period of time, especially if the flow-injection technique also is used (3,5b).

Mechanism of Electrocatalysis at Chemically Modified PbO_2

The mechanism of oxygen-transfer mediation described in Chapter I-A is supported by many experimental results.

Correlation between O-transfer reaction and oxygen evolution   The relationship between anodic O-transfer and oxygen evolution as illustrated by Figure 1 in Chapter I-A is supported by results of the

studies of anodic deposition of PbO_2 (1) and Bi-doped PbO_2 (4), and the electrocatalytic oxidation of Mn^{2+} at in-situ deposited PbO_2 (3). The deposition of the oxides occurs only in a potential region close to oxygen evolution. It is concluded that there must be enough OH species accumulated at the electrode surface, indicated by the oxygen-evolution background, to have perceptable rate of oxide nucleation.

The slight decrease of oxygen-evolution overpotential at the Bi-PbO_2 electrodes with increase in Bi coverage, as predicted in Chapter I-A, was proved for both Bi-doped PbO_2 (4) and Bi^{3+}-adsorbed PbO_2 (5a).

Effect of catalyst coverage   The catalytic current for the oxidation of DMSO at Bi^{3+}-adsorbed PbO_2 electrode increases first with $[Bi^{3+}]$ at low values (5a), which is consistent with the kinetic analysis for partially covered electrodes. The mass-transport-limited values of current can be maintained only in an optimal range of $[Bi^{3+}]$. The current decreases if the $[Bi^{3+}]$ is above the optimal range due to a high value of Bi^{3+} surface coverage. This result is as predicted in Chapter 1

The catalytic activity of As(V)-adsorbed PbO_2 electrode, however, does not decrease even if the [As(V)] or [As(III)] is very high, probably because the adsorption behavior of As(V) is different from that of Bi^{3+} (5b). It is speculated that Bi^{3+} can be adsorbed more easily on PbO_2 than As(V) because of the similarity between Bi^{3+} and Pb^{4+}, so a high coverage of Bi^{3+} at PbO_2 can be built up easily.

Variation of analytes   Strong activity and high current efficiency at the modified PbO_2 electrodes were observed for many practically important electrolytic processes, besides the model reactions, e.g., oxidation of Cr(III) to chromic acid and of benzene to benzoquinone.

The same $E_{1/2}$ value was obtained at the Bi^{3+}-adsorbed PbO_2 electrode for a large variety of O-t reactions (5b), despite the large difference in their standard potentials. This result is consistent with the prediction in Chapter I-A. It is concluded that this $E_{1/2}$ value is associated with the discharge of water to generate the adsorbed OH species at the catalytic sites of the modified electrode surface.

Variation of catalysts   The $E_{1/2}$ values are almost the same for Bi^{3+} and As(V) (or As(III)), while the E° values for the Bi^{3+}/Bi^{5+} and As(III)/As(V) couples are far apart, at ca. 1.8 and 0.32 V vs. SCE, respectively. Therefore, it is concluded that the electrocatalysis at the modified PbO_2 electrodes does not occur via electron-transfer mediation but via oxygen-transfer mediation, and the catalyst at the electrode surface does not have to undergo any redox process. However, the electrocatalytic activity of Cl^-- and Ag^+-modified PbO_2 electrodes are lower than that of the Bi^{3+}- and As(V)-modified PbO_2, which is concluded to be due to the difference in the affinity of the catalysts to hydroxide radicals.

Use of modified PbO$_2$ to modify other solid electrodes

Modified PbO$_2$ films can be used to modify other conventional, inert solid electrodes (6). Consecutive deposition and stripping of Bi-doped PbO$_2$ at Au, Pt, GC, and Ti produced ultra-thin films of the mixed oxides on the substrates (6). The ultra-thin Bi-PbO$_2$ film-covered electrodes have higher electrochemical stability and catalytic activity than the thicker, normal film electrodes, due to an enhanced surface concentration of Bi.

Deposition of smooth, non-porous PbO$_2$ film with low residual signal

In order to use the pure and modified PbO$_2$ film electrodes in electroanalytical devices, the residual signal at the electrode should be as small as possible. A capacity residual current was observed to be proportional to the surface roughness or porosity of the PbO$_2$ film (4). A smooth, reflective, and compact PbO$_2$ film can be deposited on Au and Pt substrates under the optimized conditions (1). Electron microgrph showed that the surface of this PbO$_2$ film was smooth on a micrometer scale (6a). The residual current at this PbO$_2$ film was very small (4), which was also true after modification by Bi^{3+} adsorption (6a). As shown by XRD, the PbO$_2$ film deposited in this way has a small crystalline size (6b), due to a very fast rate of nucleation and growth.

References

1. Chang, H.; Johnson, D. C. J. Electrochem. Soc. 1989, 136, 17; Chapter II-A, this Dissertation.

2. Chang, H.; Johnson, D. C. J. Electrochem. Soc. 1989, 136, 23; Chapter II-B, this Dissertation.

3. Chang, H.; Johnson, D. C., in preparation; Chapter III-A, this Dissertation.

4. Chang, H.; Johnson, D. C. In preparation; Chapter III-B, this Dissertation.

5. (a) Chang, H.; Johnson, D. C., in preparation; Chapter IV-A, this Dissertation. (b) Chang, H.; Johnson, D. C., in preparation; Chapter IV-B, this Dissertation.

6. (a) Chang, H.; Johnson, D. C., in preparation; Chapter V-A, this Dissertation. (b) Chang, H.; Johnson, D. C., in preparation; Chapter V-B, this Dissertation.

VIII. SUGGESTIONS FOR FURTHER STUDIES

Answers to the questions in the present research always lead to many new questions for studies in the future.

Applications of chemically modified PbO$_2$ electrodes

The most important application of the modified PbO$_2$ electrodes is predicted to be in the area of large-scale electrolysis, e.g., electrosynthesis. Further studies are needed for up-scaling of the electrolytic processes already tested. Many more O-t reactions also can be studied.

Another application will be in the area of electrochemical transducers. Substances whose oxidation reactions are too slow at conventional electrodes can be detected at these new catalytic electrodes.

Mechanism of oxygen-transfer mediation

The mechanism of electrocatalysis at the modified PbO$_2$ electrodes is of fundamental importance. To further prove the mechanism of O-t mediation, some in-situ analytical methods, e.g., electron-spin resonance (ESR), infrared spectroscopy, scanning tunneling microscopy (STM), and Raman spectroscopy, can be used to monitor the changes of the electrode surface during the electrolysis. Kinetic analysis with digital simulation can be used to verify the mechanism with kinetic data.

Much information concerning the mechanism can also be obtained by a better understanding of the causes for the differences in catalytic activity among the Bi-doped, Bi-adsorbed, and Bi-doped ultra-thin-film

PbO_2 electrodes. It remains as a question whether the surface lead and oxygen species participate in the electrocatalysis.

Studies also can be conducted to understand more about the kinetics and mechanism of the adsorption of ionic species at the PbO_2 electrode, including a direct measurement of the surface concentration of the catalyst with surface analytical techniques.

Photocatalysis

The photocatalytic phenomenon at the supported PbO_2 can be the subject of future study, including a quantitative measurement of the rate of the photocatalytic reaction and the conductivity of the PbO_2 film as a function of preparation conditions. More reactions can be studied beside the oxidation of Mn^{2+} to MnO_2. It is expected that the conductivity of the PbO_2 will be changed by doping with bismuth, so will the photocatalytic activity. Attention also can be paid to the photoelectrochemical reactions at the pure and modified PbO_2 electrodes. These results will yield information for comparison of electrochemical and photocatalytic O-t reactions.

IX. ACKNOWLEDGMENT